ANALYSIS AND DESIGN OF LAMINATED VENEER LUMBER BEAMS WITH HOLES

A thesis submitted as partial fulfilment of

the requirements for the degree of

Doctor of Philosophy in

Civil Engineering

by

Manoochehr Ardalany

Supervised by:

Prof. Andy Buchanan

Assoc. Prof. Massimo Fragiacomo

Dr. Bruce Deam

Assoc. Prof. Peter Moss

Department of Civil and Natural Resources Engineering

University of Canterbury

Christchurch, New Zealand

UC
UNIVERSITY OF CANTERBURY
Te Whare Wānanga o Waitaha
CHRISTCHURCH NEW ZEALAND

September 2012

Abstract

Timber has experienced new interest as a building material in recent times. Although traditionally in New Zealand it has been the main choice for residential construction, with recently introduced engineered wood products like Laminated Veneer Lumber (LVL), the use of timber has developed to other sectors like commercial, industrial, and multi-story buildings. The application of timber in office and commercial buildings poses some challenges with requirements for long span timber beams yet with holes to pass services. The current construction practice with timber is not properly suited for the aforementioned types of structures.

There has been significant progress in designing timber structures since the introduction of timber codes like NZ3603-Timber Structures Standard; however, there are still a number of problems such as holes in beams not being addressed in the code. Experimental and numerical investigation is required to address the problem properly.

In Europe, there have been a few attempts to address the problem of cutting holes and strength reduction because of holes/penetrations in glulam beams. However, LVL has not received much attention due to smaller production and use. While other researchers are focusing on glulam beams with holes, this research is targeting LVL beams with holes. This thesis extends existing knowledge on LVL beams with holes and reinforcement around the holes through experimental tests and numerical analysis.

An experimental program on LVL specimens has been performed to indicate the material properties of interest that will be used in the analysis and design chapters through whole of the thesis. A wide-ranging experimental program was also performed on beams with holes, and beams with reinforcement around the holes. The experimental program pushes forward existing methods of testing by measuring the load in the reinforcement.

Analysis of LVL beams with holes using Linear Elastic Fracture Mechanics (LEFM) and Nonlinear Fracture Mechanics (NLFM) has been performed and compared with experimental results. Two dimensional finite element models (2D) and three-dimensional finite element models (3D) are incorporated in ABAQUS and have been used for analysis of beams with holes and reinforcement around the holes.

The theory of a beam on an elastic foundation is applied to beams with holes. Analytical formulations are developed capable of predicting the cracking load (load associated with crack initiation). For loads smaller than the cracking load, no reinforcement will be required for the holes. Larger holes need reinforcing and a truss model is proposed for derivation of analytical formulations for the tensile load predictions around holes.

It is concluded that the numerical and analytical models presented in this thesis are a sound basis for analysis and design of LVL beams with holes and for the design of reinforcement around the holes. However, future research is required to further verify and improve these prediction models.

Acknowledgements

There are so many that have contributed to this body of research, in so many ways, that it is difficult to know where to begin. I will start by acknowledging the entire Department of Civil and Natural Resources Engineering of the University of Canterbury, New Zealand.

Specifically, I would like to thank my supervisors: Prof. Andy Buchanan, Assoc. Prof. Massimo Fragiacomo, Dr. Bruce Deam, Prof. Keith Crews, and special thanks to Assoc. Prof. Peter Moss that helped a lot in finalizing the thesis with his smart way of solving problems.

Other academic staffs from the department that have guided my research include Assoc. Prof. Stefano Pampanin, Prof. Athol Carr, Dr. David Carradine, Assoc. Prof. Misko Cubrinovski, Assoc. Prof. Greg MacRae, Dr. Brendon Bradley, Dr. Alessandro Palermo, Dr. Elizabeth Bowman, and Prof. Roger Nokes. Thank you for your guidance.

Special thanks to postgraduate students: Wouter van Beerschoten, Dennis Pau, Vindo Sadashiva, Javad Arefi, Mostafa Nayyerlo, Arun Puthanpuria, Umut Akguzal, Daniel Morder, and many others who are hard to remember.

To staff and lab technicians: Elizabeth Ackerman, Alan Joliffe, Louise Barton, Alan Poynter, John Maley, Peter Coursey, Russel McConchie, Stuart Toase and many other good technicians in Structural Lab that helped a lot with experimental set up and testing. Thank you for your patience and efforts.

To past postgraduate students: Dr. David Yeoh, Dr. Umut Akgusel, Dr. Mike Newcombe, and Dr. Asif Iqbal, thank you for all the time spent deliberating and your friendship.

I acknowledge contributions from researchers outside the University of Canterbury that have contributed: Dr. Simon Aicher from Stuttgart University, Prof. Bob Leicester from CSIRO, Australia, Dr. Joergen Jensen from University of Auckland, Prof. Per Johan Gustafsson from University of Lund, Sweden, Dr. Stephen Franke from University of Auckland, Dr. Bettina Franke from University of Auckland, Prof. Pierre Quenneville, from University of Auckland, Dr. Thomas Bogensperger from Graz University of Technology, Austria, Dr. Robert Finch from Structural Timber Innovation Company (STIC), New Zealand, Dr. Marco Ballerini from the University of Treneto, Italy, and postgraduate student Robert Jockwer from ETH, Zurich, Swiss.

The financial support of the Structural Timber Innovation Company (STIC), University of Canterbury (UC) doctoral scholarship, Department of Civil Engineering scholarship, and the European IRSES travel fund, enriched my research by allowing me to attend several national and international conferences.

I would like to extend my deep appreciation to Assoc. Prof. Hooshang Dabbagh from University of Kordestan, Iran who encouraged me to follow a PhD program.

Finally, I would like to thank my family, especially my mother and father, whom tolerated of not seeing me for about four years, my brother Shahram whom made me hopeful through my university study. My wife Nazanin whom pushed me forward to finish my PhD studies on time. I have always felt your love and support in my heart.

List of publications

During the course of this research, a number of publications have been made, which are based on the work presented in this thesis. They are listed here for reference:

Journal papers

Ardalany, M., Deam, B. and Fragiacomo, M. (2012). "Experimental results of fracture energy and fracture toughness evaluation of Radiata Pine Laminated Veneer Lumber (LVL) in mode I (opening)." Journal of Materials and Structures RILEM 45(8): 1189-1205.

Ardalany, M., Deam, B., Fragiacomo, M. and Carradine, D. (2012). "Experimental and numerical analysis of hole placement in depth of Laminated Veneer Lumber (LVL) beams." Australian Journal of Structural Engineering (AJSE): 1-11 (Accepted).

Ardalany, M., Fragiacomo, M., Deam, B. and Crews, K. (2012). "Analytical cracking load estimation of Laminated Veneer Lumber (LVL) beams with holes." Journal of Holz als Roh- und Werkstoff (Accepted).

Ardalany, M., Fragiacomo, M., Moss, P. and Deam, B. (2012). "A new model for tensile load prediction in the reinforcement around the holes in shear dominant areas in Laminated Veneer Lumber (LVL) beams." Journal of Materials and Structures RILEM (Accepted): 1-32.

Ardalany, M., Carradine, D., Fragiacomo, M. and Deam, B. (2012). "Experimental tests on Laminated Veneer Lumber (LVL) beams with holes and different methods of reinforcement of the holes", Journal of Structures and Buildings (under review).

Conference papers

Ardalany, M., Fragiacomo, M., Deam, B. and Buchanan, A. (2012), "Design of reinforcement around holes in Laminated Veneer Lumber (LVL) beams", World Conference on Timber Engineering (WCTE 2012), P. Quenneville, Auckland, New Zealand 1: 539-547.

Ardalany, M., Deam, B., Fragiacomo, M. and Crews, K. (2010). "Tension perpendicular to grain strength of wood, Laminated Veneer Lumber (LVL) and Cross banded LVL (LVL-C)." 21st Australasian Conference on the Mechanics of Structures and Materials: 891- 896.

Ardalany, M., Deam, B. and Fragiacomo, M. (2010). "Numerical investigation of the load carrying capacity of Laminated Veneer Lumber (LVL) joists with holes", World Conference on Timber Engineering (WCTE 2010). Riva del Garda, Italy.

Table of contents

List of figures

List of tables

List of notation

This section lists an overview of symbols frequently used through this thesis. In addition, each symbol is explained where it is first mentioned.

Latin capitals

A	Area
A_1	Area of a section of a beam above a crack surface
A_2	Area of a section of a beam below a crack surface
B	Thickness of a body
C	Compliance
C	Distance of the farthest horizontal edge from neutral axis of the beam
C	Support dimension
D	Scalar damage variable
D	Parameter
D_v	Scalar viscous damage variable
$\mathrm{D_c}$	Distance of a centre of a hole from the upper edge of the beam
E	Modulus of elasticity of an isotropic material
E_i	Modulus of elasticity in i direction ($i = 1,2,3$)
$F_{t,90,d}$	Design tensile force perpendicular to the grain

F_R	Resistance tensile force
F_V	Shear force in the section
$F_{t,V,d}$	Design tensile force due to shear
$F_{t,M,d}$	Design tensile force due to moment
F_u	Failure load
G_I	Energy release rate in mode (I)
G_{II}	Energy release rate in mode (II)
$G_{ij}\ (i,j = 1,2,3, i \neq j)$	Shear modulus in plane with normal of i and in the j direction
$G_{ij}\ (i,j = x,y,z, i \neq j)$	Shear modulus in plane with normal of i and in the j direction
G_f	Fracture energy
G_{If}	Fracture energy in mode I (opening)
G_{IIf}	Fracture energy in mode II (shearing)
G_c	Critical energy release rate
G_{Ic}	Critical energy release rate in mode I
G_{IIc}	Critical energy release rate in mode II
I	Moment of the inertia
J	J- integral
K	Magnification factor in design of plywood reinforcement
K	Stiffness of spring in a beam on an elastic foundation theory
K_s	Coefficient of the stiffness amplification in a beam on an elastic foundation theory
K_I	Stress intensity factor in mode I
K_c	Fracture toughness

K_{Ic}	Fracture toughness in mode I
K_{II}	Stress intensity factor in mode II
K_{IIc}	Fracture toughness in mode II
L	Length of a beam
L_{ad}	Embedment length of a screw
L_{bd}	Embedment length of a screw
L_c	Distance of the centre of the hole from end of the beam
M_0	Moment at $x = 0$
M_t	Total resistance moment of the beam section for pure bending
M_{cr}	Moment resistance of the section
M_L	Local moment
N	Normal force
P	Shear force
P_0	Shear at $x = 0$
P_t	Total shear resistance of the beam section for pure shear
P_{cr}	Shear resistance of the section for pure shear
R	Ratio of the hole diameter to beam depth
$R_{1,k}$	Characteristic pull out resistance in vertical direction
$R_{ax,k}$	Characteristic axial resistance in vertical direction
$R_{ax,d}$	Design axial resistance in vertical direction
S	Distance of the nearest edge of the hole from the face of the support
S	Shear
T	Tensile load in the Truss model

T	Traction in cohesive elements
V_i	Shear force in the i direction
X	Horizontal axis of coordinate system
X_0	Crack length
Y	Yielding stress in the Dugdale model
Y	Axis of coordinate system
Z	Axis of coordinate system

Latin lower case

a	Crack length
a_r	Length
$a_{1,c}$	Distance of a screw from surface of a beam
$a_{2,c}$	Distance of a screw from nearest edge of a hole
b	Breadth of a beam
b_h	Larger side of a rectangular hole
d_r	Outer diameter of a screw
e	Eccentricity of a hole centre relative to neutral axis of the beam
f_t	Tensile strength
f_v	Shear strength
$f_{v,d}$	Design shear strength
$f_{v,k}$	Characteristic shear strength
$f_{1,k}$	Withdrawal strength in vertical direction
$f_{c,0,LVL}$	Compressive strength of LVL in the grain direction

$f_{t,0,LVL}$	Tensile strength of LVL in the grain direction
h	Depth of a beam
h_d	Diameter of a hole
h_{cr}	Height of a potion of a beam above potential crack surface
h_{ef}	Effective height
k	Parameter
k_I	Stress intensity factor in mode I for unit loading
k_{II}	Stress intensity factor in mode II for unit loading
k_{mod}	Material modification factor to account for DOL and moisture
k_n	Factor introduced in the draft of Eurocode 5
l	Chord length in Truss model
l_{ef}	Effective length
l_{cr}	Clear distance between reinforcement around the holes
m	Parameter
m_ω	Mass at moisture content of ω %
n	Parameter
m_{dry}	Dry weight of a timber specimen
r	Distance from the crack tip
s	Fracture process length
t	time
v_ω	Volume at a moisture content of ω %
w_x	Displacement in vertical direction at x
x	Horizontal distance from centre of the hole

y	Vertical distance from neutral axis of a beam

Greek

α	Angle
β	Correction factor in design tensile load in Truss model
β_i $(i = 1,2,3,4)$	Parameters of mixed mode fracture criteria
γ_m	Material modification factor
δ_c	Displacement corresponding to cracking
δ_e	Displacement corresponding to final separation
δ_i	Displacement in i direction $(i = n, s, t)$
ε	Strain vector
ε_i $(i = 1,2.3)$	Strain in i direction
θ	Angle
θ	Work per unit area
κ_2	Factor applied for calculation of the shear stresses in the sharp corners of the holes
λ	Parameter in beam on an elastic foundation theory
μ	Utilization factor in design of plywood in Swedish glulam handbook
μ	Average of the data in normal stress distribution
μ_v	Viscosity factor in cohesive crack model
ν_{ij} $(i, j = 1,2,3, i \neq j)$	Poison's ratio of orthotropic material
ν	Poison's ratio of isotropic material
ξ	Correction factor in Truss Model
ρ_ω	Timber density at moisture content of ω %

σ	Standard deviation in normal stress distribution
σ	Stress
$\sigma_i \ (i = 1,2,3)$	Stress in i direction
σ_a, σ_b	Normal stresses in the points of 'a' and 'b'
σ_M	Stress due to bending moment
σ_N	Stress due to axial load
τ	Shear stress
$\tau_{ij} \ (i, j = 1,2,3, i \neq j)$	Shear stress in plane with normal of i and in the direction of j
ω	Moisture content
ψ	Parameter

Miscellaneous

ΔW	Change of elastic energy of the body
$\Delta \Gamma$	Work

1 Introduction and literature review

1.1 Introduction

Structural timber beams with holes and reinforcement around the holes is the subject of this thesis. This chapter serves as an introduction. The importance of the study is highlighted. In addition, the research methodology, objectives, scope of the research and the outline of the thesis are presented. The chapter includes a comprehensive literature review summarizing previous works.

1.2 Background

Wood is one of the oldest and best-known structural materials much appreciated for environmental impact. Wood is a desirable material for construction because it requires less energy to produce a usable end product than do other materials (Green 2001). Uses of wood as construction material over decades has increased through introduction of engineered wood products like glue laminated timber (glulam) and Laminated Veneer Lumber (LVL).

LVL as an engineered wood product is more homogenous than sawn timber. The process of laminating in LVL smears imperfections and delivers more uniform properties for a specific direction. In normal LVL, all of the veneers are lined up in one direction, leading to excellent performance in the grain direction at the expense of properties perpendicular to grain.

According to Leicester et al. (1968), applying Linear Elastic Fracture Mechanics to occurrence of the butt joints in laminates provides a good explanation for improved strength properties of LVL. Assuming that the butt-joint can be regarded as a crack, application of conventional LEFM indicates that there is a size effect associated with thickness of butt joint laminates on tension strength of the LVL: the thinner the laminates, the greater the fracture strength. This size effect indicates that for LVL with laminates as a thin as a few millimetres, the tension strength in the grain direction of LVL containing butt-joints should be almost as good as the strength of clear wood itself.

Like wood, LVL is strong in the direction parallel to grain, but when exposed to perpendicular to grain stresses it shows poor behaviour, and may develop cracks (Figure 1.1); hence special attention should be given to this when designing structures especially connections, notches, and holes that considerably increase the tensile stresses perpendicular to the grain.

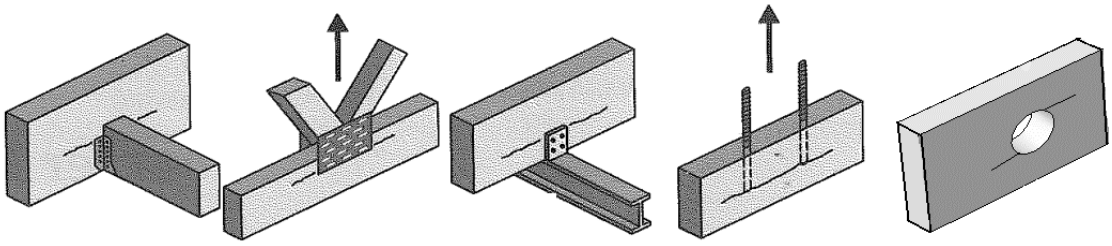

Figure 1.1. Crack propagation because of tensile forces perpendicular to the grain (Schoenmakers 2010)

Holes due to services can significantly affect the strength and stiffness of timber beams. Crack initiation and propagation around the holes diminishes the failure load of the beam to a fraction of the load associated to the beam without a hole (Figure 1.2).

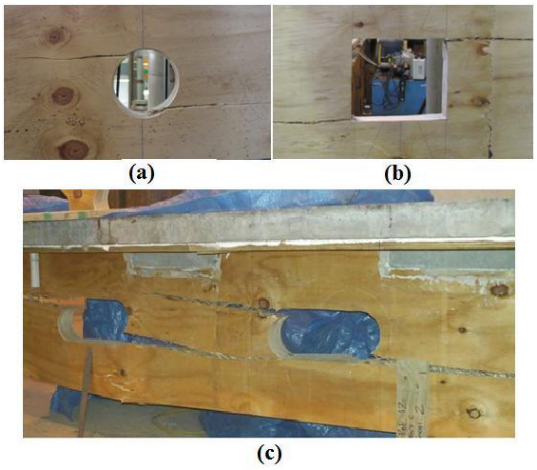

Figure 1.2. Crack initiation and propagation around holes: (a) circular, (b) rectangular, (c) in timber-concrete composite beam

The tensile stress perpendicular to grain around holes in beams in pure moment, and pure shear is presented in Figure 1.3 (a) and Figure 1.3 (b) respectively. Regions with positive sign are under tension, and other regions are under compression. The tensile stress occurs because of the hole, and the low tensile strength of LVL can result in crack formation. Other failure modes such as failure of the beam around the edge of the hole are also possible.

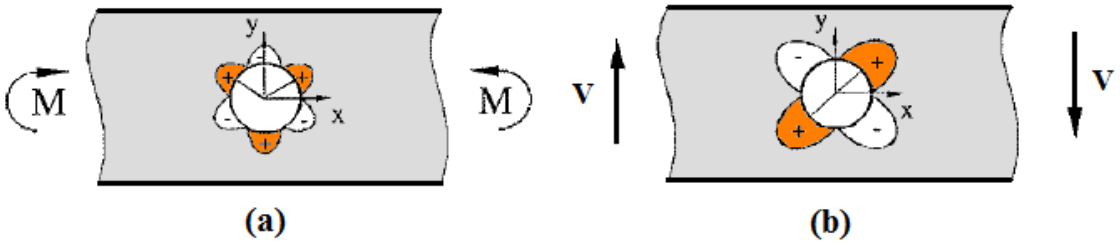

Figure 1.3. Tensile stress perpendicular to grain: (a) pure moment, (b) pure shear (Aicher et al. 2002)

Holes in the web of the beams can be reinforced to improve the behaviour, and to avoid crack propagation. Alternative reinforcement options such as plywood, screws, epoxied rods, brackets, and punched nailed plates exist that improve the beam behaviour. Unfortunately, because of the complex interaction between reinforcement and LVL, and

the complex stress field around the holes, little is known about the working mechanism of the reinforcement.

1.3 Motivation for the research

The New Zealand timber design code (NZS 3603 1993) does not report any solution regarding holes, and reinforcing methods of holes in LVL, glulam or sawn timber beams.

On an international scale, there are few design methods for holes in timber beams, and most of the works (if not all) are focused on glulam beams (such as (Aicher et al. 2009) and (Aicher et al. 2000)). There has not been enough research to discuss fracture of LVL beams with holes and methods of reinforcement around the holes. Little is known about fracture properties of LVL as well as tensile perpendicular to grain strength properties.

The research has been done because of lack of information on capacity reduction of LVL beam due to holes, and reinforcement methods of the holes to recover capacity. The Selection of an appropriate reinforcement type and design of the reinforcement required experimental and analytical investigations to be carried out.

1.4 General literature review on timber

The following is a general literature review on beams with holes and more specific literature on each particular topic is presented in its respective chapter. It should be mentioned that throughout this thesis for easier reference, the word “hole” refers to circular hole and for other types of holes; the shape of the hole has been mentioned such as rectangular hole or square hole.

Wood as a natural material is made of tubes that are formed close to each other (Figure 1.4 (a)). Wood can be characterized as a natural, anisotropic, hygroscopic, and heterogeneous material with low density. Its physical and mechanical properties can be conceptualized at many scales (Smith et al. 2003b). Three main directions of Longitudinal (L), Tangential (T), and Radial (R) are representative for the grain

direction, the perpendicular to grain direction and a second perpendicular to grain direction that coincides with the X, Y and Z respectively (Figure 1.4 (b)).

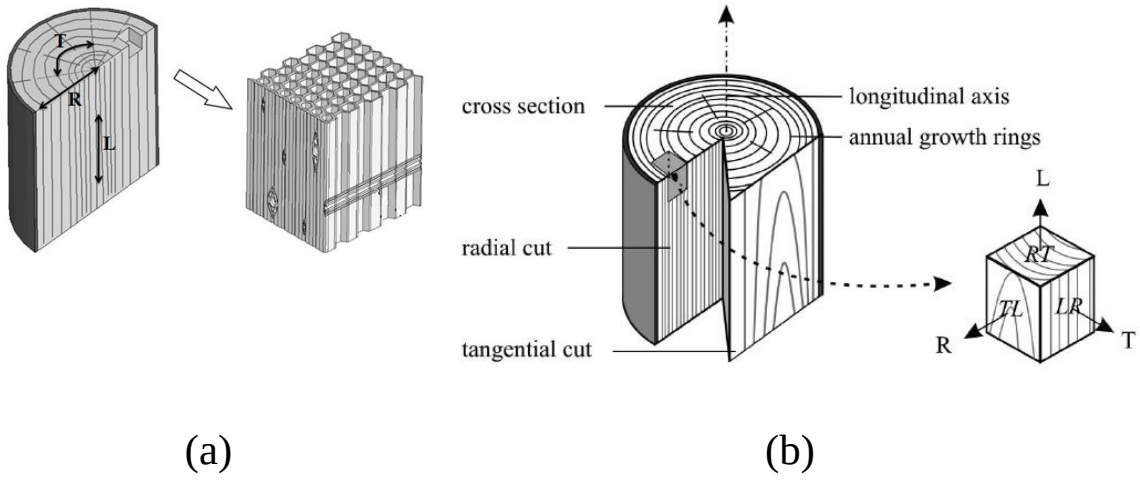

Figure 1.4. (a) Microscopic structure of wood, (b) three main directions in wood

A key factor supporting use of wood is that many wood-composite materials like LVL are being introduced to the market. In the process of LVL production, big logs of wood are fed into the peeler machine to make 3 to 4 mm thick veneers followed by drying of the veneer to remove extra water. Cutting long veneer to smaller ones and grading them completes the next step. Finally, gluing, pressing, and cutting finish the production process. The steps of LVL production are presented in Figure 1.5 (b) and three main directions of LVL are presented in Figure 1.5 (a).

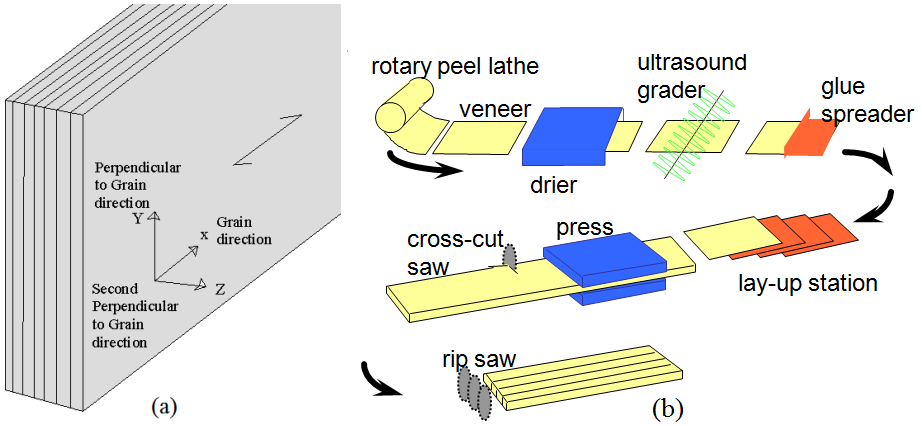

Figure 1.5. (a) Three main direction in LVL, (b) steps of LVL production (Buchanan 2007)

In LVL, the grain direction corresponds to L, first perpendicular to grain T, and the second perpendicular to grain R direction. LVL is widely used in New Zealand, especially in multi-story buildings where post-tensioning has been introduced lately. Figure 1.6 shows application of LVL in shear walls, columns, and beams.

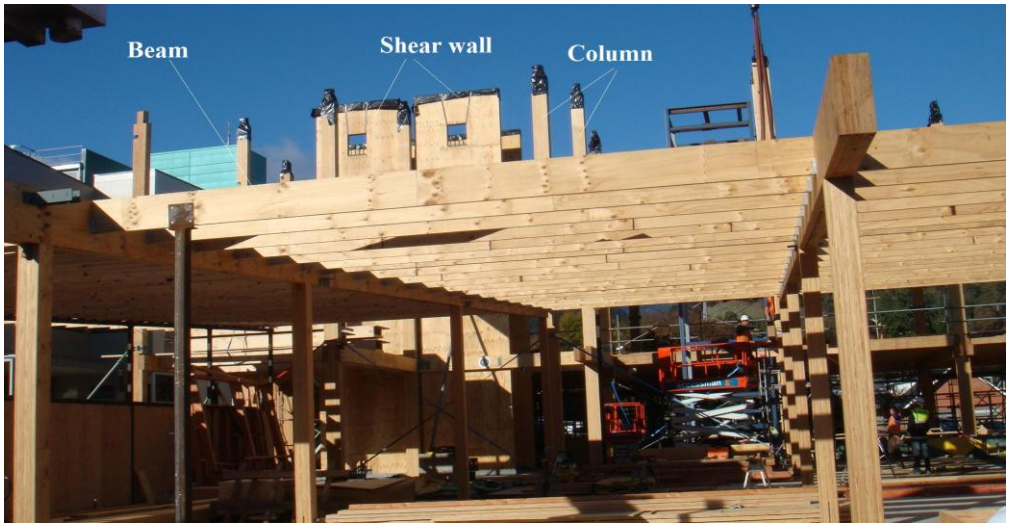

Figure 1.6. Use of LVL in shear walls, columns and beams (NMIT building Nelson, NEW ZEALAND)

1.5 Review of recent investigations

Over the last few decades, there has been some research on timber beams with holes and reinforcement around the holes. In general, efforts have been focused toward two main issues viz.: (i) analysis of beams with holes, (ii) reinforcing of the holes. Analysis can be divided again into two main groups of "before cracking", and "after cracking" with reinforcement mainly used to control crack propagation. The main analytical methods and types of reinforcement around the holes will be discussed in the following sections.

1.6 Analysis of timber beam with holes

Analysis of a timber beam with a hole is rather complicated due to the complexity of the stress distribution around the holes and the orthotropic nature of wood. The stress field around the holes varies from tension to compression (Zhu et al. 2005).

Danielsson (2007) presented a survey of methods used mainly in Europe for analysis of glulam beams with holes. The primary research on beams with holes was mainly concentrated on using the theory of elasticity with complex functions such as Penttala (in Finnish, adopted from (Danielsson 2007)) that used plate theory with complex functions to determine the state of stress around the holes.

Johannesson (1983) used three methods; "shear stress method", "Navier-beam method" and "exact-stress method". The shear stress method is an empirical method that compares the shear stress and fictitious shear strength obtained from experiments. The effect of the bending is not considered and the method yields a rough estimation of the cracking load.

The Navier-beam method has been formulated in an attempt to develop hand calculations. The basic idea is that hoop stress at the hole boundary can be calculated and compared with the corresponding strength value. Plane stress is assumed and normal stress on the stress plane varies linearly.

Exact-stress distribution could be obtained with different methods viz.: (i) closed form analytical formulation, (ii) Finite Element Method (FEM), and (iii) Boundary Element Method (BEM).

According to Johannesson (1983), the analytical formulation can be obtained for some simple cases like infinite plates with holes. Infinite here means the dimension of the hole relative to plate dimensions is small. The method is well described by Lekhnitskii (1963). However, the method has limited value for beams with finite boundaries and through a comparison with FEM results, it was concluded that closed form solution (analytical formulation) may not be used for derivation of a design method for glulam beams with holes because of its poor predictions of the failure loads (Johannesson 1983).

The boundary Element Method (BEM) is similar to FEM. By use of fundamental solutions for stress field and the displacement field in a homogenous body, it is necessary to specify boundary conditions. Thus, it is unnecessary to divide the interior of the body into finite elements. Only the boundary has to be discretized.

Recently finite element and fracture mechanics methods have received more attention because of vast applicability of the methods for analysis of beams with holes and

advancement in computer programming for analysis. In the following, the literature on application of the finite element method and fracture mechanics is presented in more details.

1.6.1 Finite element method

The Finite Element Method (FEM) is based on the assumption that a complex domain can be discretized to simpler domains and represented by simpler finite sized elements. The domain for using FEM is relatively vast. It can be used for the domains in continuum mechanics and for a variety of materials such as isotropic and orthotropic materials (Smith et al. 2003b). In the past, FEM application in beams with holes was limited to load associated with crack initiation (Johannesson 1983) because FEM mainly suffer from inability to propagate a crack that is necessary for failure load predictions of members capable of crack formation such as beams with holes and notched beams. However, new research such as that by Guan et al. (2009) has added capability for crack propagation in FEM. In most cases, model re-meshing will be necessary in the process of crack propagation. The process of re-meshing is rather time consuming, and for large models is not feasible with small processors.

A subroutine for crack propagation and failure load prediction of Oriented Strand Board (OSB) timber beams with holes was programmed by Guan et al. (2004) in ABAQUS. The subroutine yielded results in good agreement with the experiments. The subroutine was checking the elements surrounding the hole and putting the relative stiffness of the yielded element to zero. The beam was re-meshed and the analysis was followed toward crack propagation. Meshing about the hole was relatively finer than the other parts. The analysis procedure is costly because of re-meshing.

In Guan et al. (2004), the cracking was evaluated by Improved Tsai-Hill criterion. Tsai-Hill is defined in Equation (1.1).

$$\left(\frac{\sigma_L}{X}\right)^2 - \left(\frac{\sigma_L\sigma_T}{X}\right)^2 + \left(\frac{\sigma_T}{Y}\right)^2 + \left(\frac{\sigma_{LT}}{S}\right)^2 + \left(\frac{2\sigma_L|\sigma_{LT}|}{5XS}\right) + \left(\frac{2\sigma_T|\sigma_{LT}|}{5YS}\right) = 1 \qquad (1.1)$$

where σ_L, σ_T are normal stresses along the longitudinal and in the transverse directions respectively; X, Y are tensile or compressive strengths along the two directions respectively; σ_{LT} and S are shear stress and strength respectively.

Although the current model propagates cracking, it cannot deal with fast crack growth that causes brittle failure. Interface elements (cohesive elements) are another capability recently added to the finite element to allow for crack propagation. The method has been successfully used for the analysis of dowel connections loaded perpendicular to grain (e.g. Franke et al. (2011)). The cohesive elements will be discussed in detail in chapter 5.

1.6.2 Fracture mechanics analysis

Fracture of quasi-brittle materials like wood at the microscopic level is associated with the development of micro cracking in the crack tip vicinity. The existence of a damage zone around the crack tip is well known. In this area, from a study by Vasic et al. (2002a), micro cracks are being formed as result of randomness of the interfacial cohesive strength within and between the tracheids. Every tube of the wood structure is called a tracheid (Romanowicz et al. 2008). In the loading process, existing micro-cracks and flaws may grow and join to each other. This eventually forms defects in the body of the beam followed by gradual softening of the member under loading and receiving more deflection.

Fracture mechanics mainly deals with cracks and fracture of the cracked members. Among fracture mechanics models, application of the Linear Elastic Fracture Mechanics (LEFM) to timber structures is traditionally followed because of the apparent brittleness of wood (Vasic et al. 2002b), and because of its simplicity in application to timber structures. LEFM are frequently used for the failure load predictions of the beams with holes, notches, and connections (Leicester 1971; Gustafsson 1993b; Aicher et al. 1995; Gustafsson et al. 1999; Ballerini et al. 2001; Leicester 2006; Ballerini et al. 2007; Aicher et al. 2009; Danielsson 2009).

The work of Sih et al. (1965) is basic for the application of fracture mechanics to anisotropic materials like wood containing a crack. Stress intensity factors (K) are

evaluated and compared with fracture toughness (K_c) values. Fracture toughness is the ability of material containing a crack to resist fracture.

Following on from the Australian Timber Engineering Code (AS 1720-1975) with direct application of LEFM, application of LEFM to timber structure codes was proposed by Ranta-Maunus (1990), who states: "Traditionally the stress concentrations around holes and notches have been calculated by the use of theory of elasticity. However, the peak value of stress is related to the radius of curvature, and with small values of radius the peak stress values do not directly indicate the potential for failure. In principle, the application of fracture mechanics is natural in cases where a high stress peak occurring in a small volume is the case of fracture." He also mentions potential applications of LEFM including: (i) holes in beams, (ii) hangings, (iii) cambered beams, (iv) nail driving, and (v) drying checks.

The use of LEFM on glulam beams with holes has been carried out by several researchers. Aicher et al. (1995) used fracture mechanics for failure load predictions of glulam beams with holes. An imaginary discontinuity in the form of a crack was introduced into the model, and the stress intensity factors were calculated. The reason behind the use of the so called "Hypothetic Crack Model" is well explained by Aicher (1996): "Fracture mechanics and the K-concept can be employed in a straight forward deterministic manner to structures with distinct single or multiple macro cracks of defined dimensions. However, in most structures no macro crack singularities exists in the perfect case, for instance in the case of beams with round holes or with rectangular openings the singularities here are confined to the imperfect state of the structures with stochastically distributed defects (flaws) on a micro level due to local stress concentration which have grown, agglomerated and eventually localized into macro cracks. In case if wood, flaw growth, agglomeration and macro crack formation can mutually cause stresses resulting due to gravity loads and from climate caused eigen-stresses. The sizes and to a lesser extent the locations of the macro cracks, to be investigated by fracture mechanics, are unknown this leads to the probabilistic nature of the problem. A suitable way to examine and design such structures is the hypothetic crack approach where the load carrying capacity is traced depending on one or several extending hypothetic macro cracks."

Aicher et al. (1995) suggested the use of a crack length of 25-50 mm for large structures, and a crack length of 20 mm for large structure and small holes. For small structures with depth of 95 mm, a crack length of 2-7 mm for small and large holes may be used. The work was limited to glulam beams and no more extension for other material was performed. The hole diameter to beam depth ratio for the aforementioned values of crack length were not exactly defined.

Gustafsson (1993b) proposed the use of the initial crack method and mean stress method to generalize LEFM and to overcome its shortcomings for the analysis of notched members. Plane stress was also assumed for development of a series of formulations for crack length calculations. The generalized LEFM will be discussed in detail in chapter 4.

1.7 Failure mechanisms

An appropriate design method should prevent all failure mechanisms by using suitable reinforcement or applying limitations to the design approaches. Several different failure mechanisms could occur around holes in timber beams. Some possible failure mechanisms for circular and rectangular holes are defined below.

1.7.1 Failure mechanisms for rectangular holes

The Swedish glulam handbook (Hallström 1996) defines four different types of failure mechanisms for rectangular holes in the beams viz.: (a) failure due to tension perpendicular to grain, (b) failure at mid-span of the beam due to global bending moment, (c) failure due to global bending moment acting at the hole location, and (d) failure due to local bending moment in the upper and lower lever arms of the holes. Failure mechanisms for rectangular holes are presented in Figure 1.7.

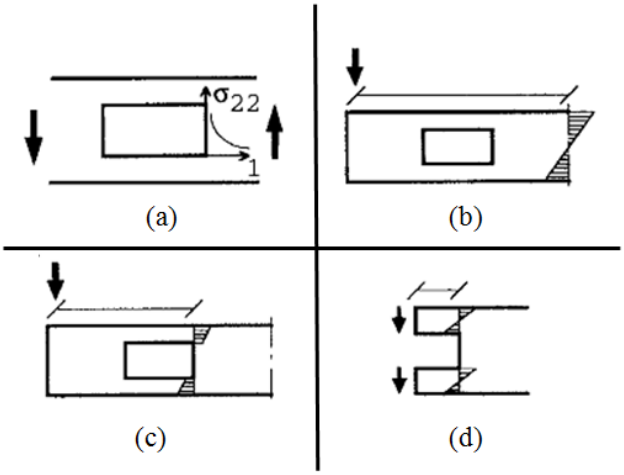

Figure 1.7. Illustration of theoretical failure modes for beams with rectangular holes (Hallström 1996): (a) failure due to tension perpendicular to grain, (b) failure due to global moment, (c) failure due to increased tension/compression at the hole location (d) failure due to local bending moment at the hole location

1.7.2 Failure mechanisms for circular holes

Similar to mechanisms of failure for rectangular holes, the Swedish glulam handbook (Hallström 1996) defines three failure mechanisms for circular holes that are presented in Figure 1.8.

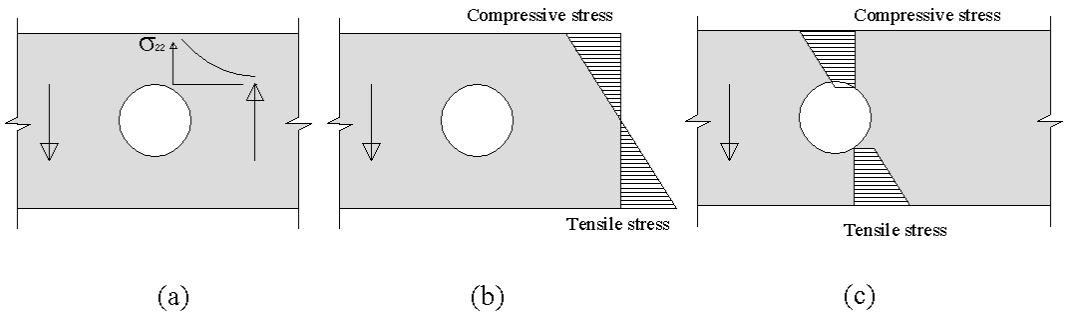

Figure 1.8. Failure mechanisms around circular holes: (a) crack propagation failure, (b) mid-span failure, (c) failure at the edge of hole

Again, case (a), failure due to tension perpendicular to the grain at the hole edge that cause crack initiation and propagation, case (b) shows the failure at the mid-span due to global moment in the section, finally, case (c) presents the failure mode at the hole edge because of the increased compression and tension in the section.

1.8 Design of holes without reinforcement

Few codes/handbooks give recommendations for designing of timber beams with holes. Design recommendations are discussed in the following sections.

1.8.1 Design according to draft of Eurocode 5

LEFM based method for design of the beams with holes was introduced in the draft of Eurocode 5 (2004). The formulation is adopted from the works of Gustafsson (1993b). The model assumes the beam with a rectangular hole to be regarded as an end notched beam with a sharp edge, and the circular one is also end-notched beam with the slope of 1:1 as shown in Figure 1.9.

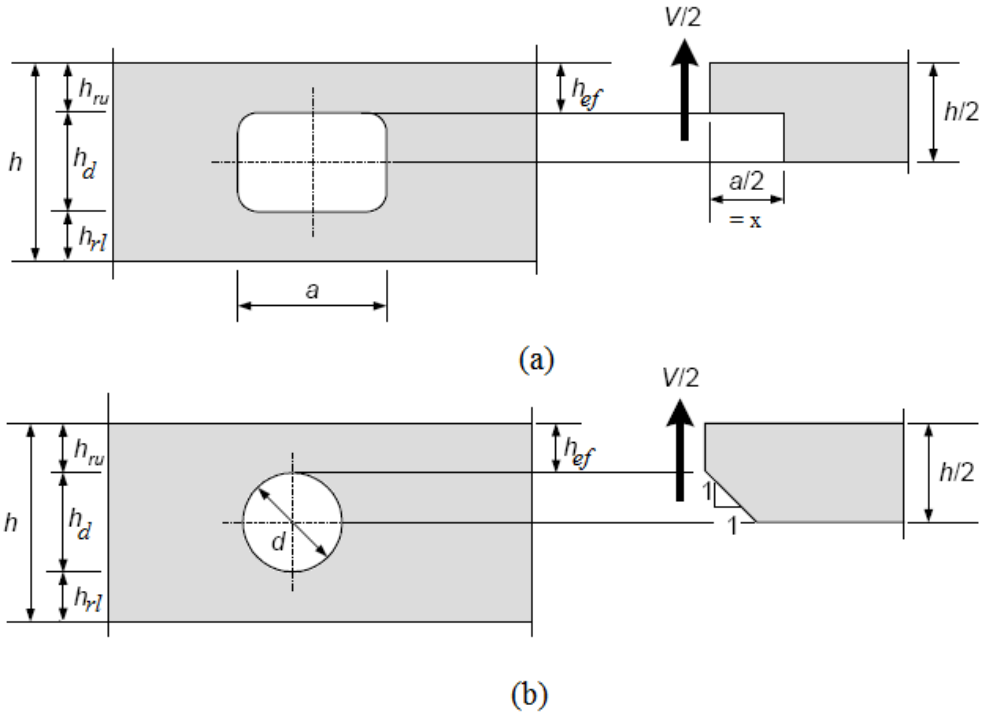

Figure 1.9. Beam with hole: (a) rectangular hole, (b) circular hole (Eurocode 5 2004)

The design equation uses comparison of the design shear stress (τ_d) with the design shear strength ($f_{v,d}$). The LEFM is hidden in the factors applied to the resistance side of the equations, namely the fracture energy of the material.

$$\frac{\tau_d}{K_v f_{v,d}} \leq 1 \tag{1.2}$$

$$\tau_d = \frac{1.5\, V_d}{b\, h_{ef}} \tag{1.3}$$

$$K_v = \text{Min}(\,1,\ \frac{k_n(1+\frac{1.1\, i^{1.5}}{\sqrt{h^*}})}{\sqrt{h^*}(\sqrt{\alpha(1-\alpha)}+0.8\,\frac{x}{h^*}\sqrt{(\frac{1}{\alpha}-\alpha^2)}}) \text{ for rectangular hole} \tag{1.4}$$

$$\mathrm{K_v} = \min(\,1, \frac{k_n}{\sqrt{\alpha(1-\alpha)}} \times \frac{1+\frac{1.1}{\sqrt{h^*}}}{\sqrt{h^*}}) \text{ for circular hole} \tag{1.5}$$

where $\mathrm{k_n} = 5$ for solid timber, 4.5 for LVL, and 6.5 for glulam, 'i' is notch inclination, h^* is taken equal to the half of the beam depth, $\alpha = h_{ef}/h^*$, other factors are defined in Figure 1.9. In the expanding of the formulations, only mode I (opening mode) of fracture has been regarded.

Predictions of the method were found to be non-conservative when compared with the experimental results (Aicher et al. 2002), and later this design approach was withdrawn from draft of Eurocode 5. A comparison of the predictions with experimental results is presented in Figure 1.10.

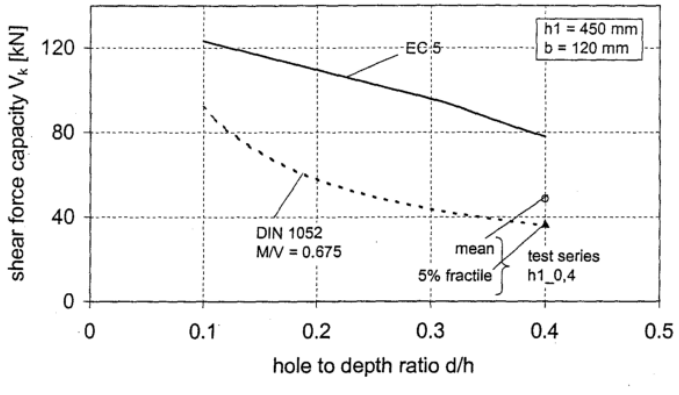

Figure 1.10. Comparison of the predictions with Eurocode 5, German design code DIN 1052, and experimental results for the tested beams of breadth 120 mm and total depth of 450 mm (Aicher et al. 2002).

1.8.2 Design according to an empirical formulation

This is an empirical method mentioned in the Swedish glulam handbook (Carling 2001) for glulam beams with breadth larger than 90 mm. The method considers the controlling of shear and moment for the net cross section at the hole while reducing the shear strength of the beam with hole ($f_{v,red}$). The shear in the section is divided between the upper and lower portion of the beam (h_u, h_l) according to their stiffness to form V_u and V_l as shown in Figure 1.11.

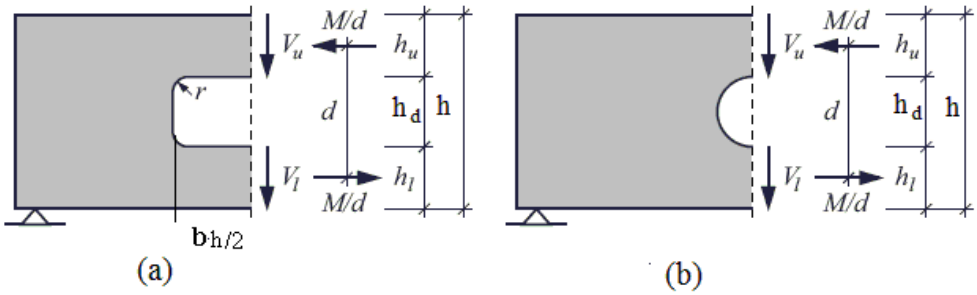

Figure 1.11. Beam with hole parameters for empirical method: (a) rectangular holes, (b) circular holes (Danielsson 2007)

The following controls have to be performed:

$$\tau = \frac{1.5\,V_i}{bh_i} \leq f_{v,red} \qquad \text{where index } i = u \text{ or } l \tag{1.6}$$

$$f_{v,red} = k_{vol} k_{hole} f_v \tag{1.7}$$

$$k_{vol} = \left(\frac{b}{90}\right)^{0.2} \quad \text{for } 90 \leq b \leq 215\ mm \tag{1.8}$$

$$k_{hole} = \begin{cases} 1 - 555(\frac{D}{h})^3 \text{ for } D/h \leq 0.1 \\ \frac{1.62}{(1.8 + \frac{D}{h})^2} \text{ for } D/h > 0.1 \end{cases} \quad (1.9)$$

where $D = \sqrt{b_h^2 + h_d^2}$ for rectangular holes, and $D = h_d$ for circular holes. In addition, for rectangular holes, extra bending moment due to the shear force should be considered, and if there are less than four lamellae, the shear capacity should be decreased by 25 %.

Through a comparison of experiments on glulam beams with design predicted values, Danielsson (2007) concluded that the empirical method underestimates the capacity of experimental beams for all of the rectangular holes. The empirical limitation in the formulation makes its application limited for other materials like LVL, and beams with breadth less than 90 mm.

1.8.3 Design according to Swiss code

The Swiss code for timber structures (adopted from (Danielsson 2007)) suggests a similar approach to the draft of Eurocode 5 for designing of the holes in glulam beams. The end-notched beam approach is suggested for designing of holes. Assuming f_v is the allowed shear stress; Equation (1.10) is advised for design control.

$$\tau = \frac{1.5V_d}{bh_{ef}} \leq f_{v,red} \quad (1.10)$$

where $f_{v,red}$ is reduced shear strength calculated as:

$$f_{v,red} = k_{red} f_v \quad (1.11)$$

k_{red} is a parameter equal to 1 for compression perpendicular to the grain, and for tension perpendicular to the grain is defined as:

$$k_{red} = \sqrt{\frac{h_{ef}}{h}\left(\frac{\Delta h_0}{\Delta h_{ef}}\right)} \leq 1 \qquad (1.12)$$

where Δh_0 is set equal to 45 mm.

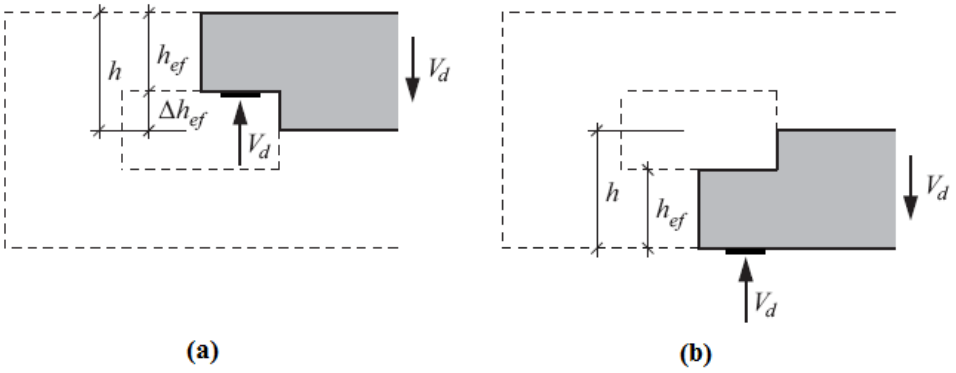

Figure 1.12. Notations of the Swiss code: (a) for tension perpendicular to grain, (b) for compression perpendicular to grain (Danielsson 2007)

1.8.4 Design according to DIN 1052

DIN 1052 (2008) applies to holes greater than 50 mm diameter. Unreinforced hole diameters to beam depths are limited in the code to 0.15. Some geometry conditions are included in the code viz.: (i) maximum hole diameter to beam depth equal to 0.4, and (ii) distance of the hole from centre of the support should be greater than $0.5h$. Rectangular holes should have rounded corners with greater than 15 mm radius. Holes that can be used without reinforcement are limited to service class 1 and 2. Service class 3 always needs reinforcing. Service class 1 covers indoor heated conditions, service class 2 is indoor unheated or outdoor protected conditions, and finally service class 3 is characterised mainly by outdoor conditions with possible contact with water (Eurocode 5 2004). The main design equation is defined as:

$$F_{t,90,d} \leq 0.5 b f_{t,90,d} l_{t,90} \qquad (1.13)$$

where $f_{t,90,d}$ is the design tensile strength perpendicular to grain, $l_{t,90}$ is defined as:

$$l_{t,90} = 0.5(h_d + h) \text{ for rectangular holes}$$
$$l_{t,90} = 0.353h_d + 0.5h \text{ for circular holes} \quad (1.14)$$

The parameters are defined in Figure 1.13.

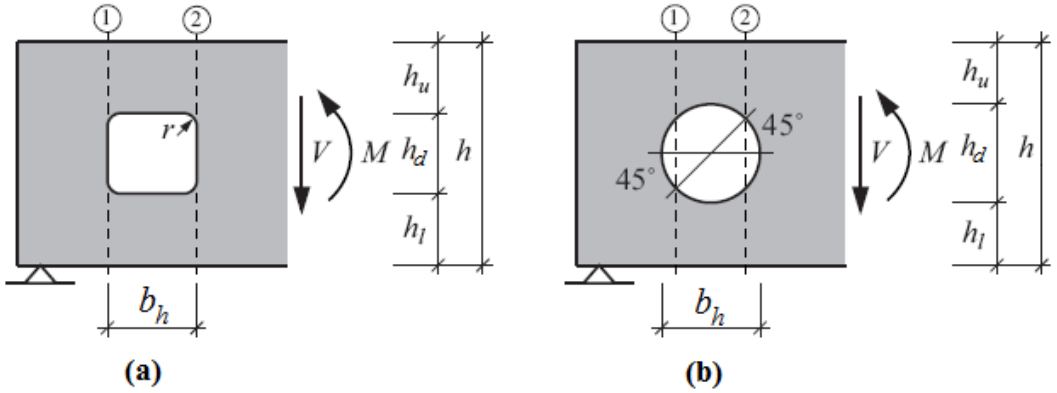

Figure 1.13. Beam with hole notations: (a) for rectangular holes, (b) for circular holes (Danielsson 2007)

Size effect in Eq. (1.13) is implemented by the factor of $(\min(1, (\frac{450}{h})^{0.5}))$, namely left hand side of Eq. (1.13).

Design tensile force perpendicular to the grain direction ($F_{t,90,d}$) has two contributions from shear and moment defined as:

$$F_{t,90,d} = F_{t,V,d} + F_{t,M,d} \quad (1.15)$$

The tensile force due to shear ($F_{t,V,d}$) and moment ($F_{t,M,d}$) is defined as:

$$F_{t,V,d} = \frac{V_d x}{4h}(3 - \frac{x^2}{h^2}) \quad (1.16)$$

V_d denotes design value of shear force in section (1) and (2) in Figure 1.13 and x is defined as:

$$\begin{aligned} x &= h_d \text{ for rectangular holes} \\ x &= 0.7h_d \text{ for circular holes} \end{aligned} \tag{1.17}$$

$F_{t,M,d}$ is tensile load due to the moment defined as:

$$\mathrm{F_{t,M,d}} = 0.008\,\frac{\mathrm{M_d}}{\mathrm{h_r}} \tag{1.18}$$

h_r is defined as:

$$\begin{aligned} h_r &= \min(h_u, h_l) \text{ for rectangular holes} \\ h_r &= \min(h_u + 0.15h_d\,, h_l + 0.15h_d) \text{ for circular holes} \end{aligned} \tag{1.19}$$

Equation (1.18) has been derived based on numerical analysis of glulam beams with holes. The formulation is independent of h_d/h and needs its application to be verified for other materials. More background of Equations (1.16) and (1.17) is presented in chapter 7.

DIN 1052 (2008) specify that the design has to be verified for each crack-prone location. This implies that the verification in case of predominant moment action has to be performed at partly different locations as compared to predominant shear locations (Aicher et al. 2001,2004; Aicher et al. 2007).

1.9 Reinforcements around holes

Reinforcement of timber beams with holes is an option to recover the capacity of the beam. The goal of the reinforcing is to recover the capacity of the beam with a hole so that it can carry the load equal to a beam without a hole. Different reinforcement methods have been used viz.: (i) glass fibre, (ii) screws, (iii) glued in rods, and (iv) plywood, Hallström (1996) used glass fibre reinforced holes in glue laminated timber beams (glulam) for a series of tests with circular and rectangular holes and concluded

that significant increase of the strength was achieved for rectangular and circular holes but it was higher for circular holes. Plywood for reinforcement of the defects was used by Szabo (1977). Aicher et al. (2009) used self-tapping screws, and glued in steel rods for reinforcing of glulam beams with holes in a comprehensive series of experiments. Aicher concluded that self-tapping screws, and epoxied in rods caused significant strength recovery. Maximum of 64 % of increasing shear capacity was reported in comparison to the un-reinforced beam with a hole.

1.9.1 Swedish glulam handbook

The Swedish glulam handbook (Carling 2001) has adopted the procedure of DIN 1052 for design of the plywood around holes except for limiting the maximum hole diameter to 0.5 of beam depth. The required thickness of plywood is dependent on the utilisation factor μ defined in Equation (1.20).

$$\mu = (\frac{1.5V}{bh})/f_v \tag{1.20}$$

Based on this utilization factor, the thickness values reported in Table 1.1 are required for plywood.

Table 1.1 Required thickness of plywood

Utilization factor (μ)	Plywood thickness on each side
0	0.05b
1/3	0.18b
2/3	0.25b
1	0.33b

For screw reinforcement design, the maximum hole diameter is limited to 0.35 of beam depth. The screw should be designed for tensile force in the reinforcement (F_t) as defined in Equation (1.21).

$$F_t = 0.5V[3(\frac{h-h_d}{h})^2 - 2(\frac{h-h_d}{h})^3] \quad (1.21)$$

The value of F_t should be smaller than the resistance tensile force in the screw (F_R):

$$F_t \leq F_R \quad (1.22)$$

The design tensile load as shown by Equation (1.21) does not include any contribution from the moment, and effect of the moment on the produced tensile load is zero. Further background on the formulation was not found.

1.9.2 DIN 1052

DIN 1052 suggests reinforcement around holes in glulam beams to recover capacity of the beam. The code advises two formulations for the tensile load predictions in glulam beams with holes viz.: (i) tensile force perpendicular to grain because of shear, and (ii) tensile force perpendicular to grain because of moment. The driving equation for design is Equation (1.15). Other controls like screw withdrawal is necessary.

It should be mentioned that hole diameter to beam depth of 0.3 is the limitation for screw reinforcing in DIN 1052 and the limitation for plywood reinforcing is 0.4.

1.10 Objectives of the thesis

The overall objective of this study is to develop a method of analysis and design of LVL beams with holes and reinforcement. The study has the following specific objectives:

- To determine experimentally how significant holes affect the strength of LVL beams.
- To determine experimentally effective reinforcement methods for LVL beams with holes, and the limitations of each type of reinforcement.
- To perform numerical analysis on LVL beams with holes and reinforcement around the holes.

- To better understand the working mechanism of reinforcement around holes in controlling stresses.
- To calculate the load associated with the cracking in LVL beams with holes.
- To develop a design method for unreinforced beams, and for beams with different types of reinforcement.

1.11 Scope of the research

There are many unknowns about the behaviour of LVL beams with holes. The current study will be focused on the effects of holes on the total behaviour of beams while designing for holes, and possible reinforcing of them for improving the mechanical behaviour will be also of interest.

The scope of this work is limited to:

- Static loading (not dynamic, hydroscopic or thermal loadings).
- Standard LVL (not cross-banded LVL).
- Straight beams (not curved or pre-cambered beams).
- Simply supported beams (not continuous, not cantilever).
- Short-term behaviour (as long term is overly complex).
- Rectangular and circular openings (the most common shapes).
- The scope of this study does not extend to instability arising from the flexural buckling of a beam.

1.12 Organization of the thesis

The thesis consists of 9 chapters as follows:

Chapter 1 includes introduction, literature review, and a state of the art for design of beams with the holes and reinforcement.

Chapter 2 presents material properties obtained through an experimental program on LVL specimens.

This chapter presents the preliminary work of this thesis. It presents experimental results on LVL for material properties. Elastic material properties, tensile strength perpendicular to the grain, fracture properties in mode I (opening mode), and screw withdrawal tests are presented. The result of this chapter has been used in chapter 3, 4, 5, 6, 7, 8 and 9.

Chapter 3 presents a comprehensive experimental program on LVL beams with holes, and reinforcement around holes. The results of the experimental program on LVL beams with holes and results of reinforcing of the LVL beams with holes are presented.

This chapter presents the experiments on LVL beams with holes and reinforcement around holes. Different shapes of holes with a variety of the diameters were tested. Reinforcement of the holes was also performed using plywood, steel brackets, self-tapping screws and epoxied-in rods. The result of this chapter has been used in chapter 4, 5, 6, 7, 8 and 9.

Chapter 4 uses Linear Elastic Fracture Mechanics (LEFM) for failure load predictions of LVL beams with holes.

This chapter presents a numerical model based on Linear Elastic Fracture Mechanics (LEFM). LEFM has been applied to LVL beams with holes and their failure load has been predicted. Effect of the hole eccentricity relative to neutral axis and effect of distance of the holes from supports on capacity has been investigated. The result of this chapter has been used in chapters 8, and 9.

Chapter 5 presents cohesive elements (interface elements), and the use of them for modelling crack initiation and propagation in LVL beams with holes. The chapter also address the working mechanism of reinforcement around holes.

This chapter presents a numerical model based on nonlinear fracture mechanics for load prediction of LVL beams with holes. 3D models of this chapter have been expanded by adding reinforcement. Effect of screw and plywood has been investigated by looking at the cohesive layer. The results of this chapter have been used in chapters 8 and 9.

Chapter 6 present a series of formulations developed for prediction of cracking load of LVL beams with holes.

This chapter presents an analytical model for predicting the cracking load of LVL beams with holes. The theory for a beam on an elastic foundation was applied to the LVL beam, and three formulations were derived. The formulation accuracy is compared against experimental data of LVL and showed good predictions. The result of this chapter has been used in chapters 8 and 9.

Chapter 7 presents a series of formulations for design tensile load prediction using a Truss Model. The chapter includes a detailed comparison of experimental, analytical, and numerical prediction.

This chapter presents a series of formulation for tensile load prediction in reinforcement around the holes in LVL beams. Different cases of hole shapes are investigated. Correction factor for larger depth of beams; and also for the eccentricity of the hole relative to neutral axis of beam is presented. The results of this chapter have been used in chapters 8 and 9.

Chapter 8 presents a design method for LVL beams with holes and possible reinforcement. The chapter uses the data in previous chapters to provide a design method. Designing for screws, glued in rods and plywood are also presented.

This chapter presents a design method for LVL beams with holes. Design of screws, epoxied in rod, and plywood is a part of this chapter. Recommendation regarding maximum and minimum hole size, hole location along beam, and hole location in depth of beams is also included. Finally, the chapter includes worked examples on reinforcement design around the holes. This chapter uses the results of the other chapters.

Chapter 9 gives conclusions of the study followed by the recommendations for future research.

1.13 Summary

The chapter presented the research background, literature review on beams with holes, methods of analysis, design of timber beams with holes, and reinforcement design around the holes. The chapter also highlighted motivations and objectives for the thesis.

2 Material properties

This chapter presents the preliminary work of this thesis. It presents experimental results on LVL for material properties. Elastic material properties, tensile strength perpendicular to the grain, fracture properties in mode I (opening mode), and screw withdrawal tests are presented. The results of this chapter have been used in chapter 2, 3, 4, 5, 6, 7, 8, and 9.

The majority of this chapter has been re-produced from the following papers:

Ardalany, M., Deam, B. and Fragiacomo, M. (2012). "Experimental results of fracture energy and fracture toughness evaluation of Radiata Pine Laminated Veneer Lumber (LVL) in mode I (opening)." Journal of Materials and Structures RILEM 45(8): 1189-1205.

Ardalany, M., Deam, B., Fragiacomo, M. and Crews, K. (2010). "Tension perpendicular to grain strength of wood, Laminated Veneer Lumber (LVL) and Cross banded LVL (LVL-C)." 21st Australasian Conference on the Mechanics of Structures and Materials: 891- 896.

2.1 Introduction

Material properties of LVL are necessary for finite element and fracture mechanic analyses. New Zealand LVL mainly is produced out of Radiata pine with density varying from 550 to 620 kg/m^3. The process of the laminating and gluing of LVL changes its material properties from sawn timber Radiata pine.

Material properties of New Zealand Laminated Veneer Lumber (LVL) for research purposes are not available. Most existing data are from manufacturers focusing on design values such as bending strength of LVL, compression strength in the grain

direction, tension strength in the grain direction, shear strength in the grain direction, compression in perpendicular to the grain direction, and modulus of rigidity in the grain direction summarized in Table 2.1 (Buchanan 2007).

Table 2.1 Characteristic strength and stiffness values of LVL by manufacturer brand (Buchanan 2007)

Brand	Bending strength (MPa)	Compression strength (MPa)	Tension strength (MPa)	Shear strength (MPa)	Compression strength perpendicular to grain (MPa)	Modulus of elasticity in bending (GPa)	Modulus of rigidity (MPa)
CHH hySPAN	48	45	33	5.3	12	13.2	660
Nelson Pine LVL	48	45	30	6.0	12	10.7	535

Elastic material properties, strength properties like tensile strength of LVL in perpendicular to the grain direction, screw withdrawal strength, and fracture properties are required for the analysis of the beams with holes. The current chapter summarizes the main material properties of LVL that are frequently used in the subsequent chapters.

2.2 Physical properties

Timber density is an important physical parameter since it correlates to most mechanical properties. The amount of the water obviously contributes to the mass of a wood sample. The timber density is highly affected by moisture, and it is usually presented at specified moisture content.

2.2.1 Timber density

Timber density $\rho_\omega$at a given moisture content ω can be calculated by Equation (2.1).

$$\rho_\omega = \frac{m_\omega}{V_\omega} \tag{2.1}$$

where m_ω denotes mass at moisture content of ω, and $V_\omega$is the corresponding volume.

To allow comparison of a standardized moisture content (i.e. 12 %) obtained in chamber, following transformation equations for softwood is advised by Kollmann (1951) (adopted from (Schoenmakers 2010)).

$$\rho_{12} = 10^3 \rho_0 \frac{112}{10^5 + 0.85\rho_0\omega} \tag{2.2}$$

$$\rho_0 = \frac{10^5 \rho_\omega}{-0.85\omega\rho_\omega + 10^5 + 10^3\omega} \tag{2.3}$$

where ρ_0 and ρ_{12} denote the timber density in 0 % and 12 % moisture content, respectively. The density of LVL is approximately equivalent to the density of the timber species used to manufacture the product.

2.2.2 Moisture content

Equation (2.4) gives the moisture content of a given sample:

$$\omega = \frac{(m_\omega - m_{dry})}{V_\omega}.100\% \tag{2.4}$$

where m_ω and m_{dry} denote the measured mass at given moisture content and oven dried mass of specimen respectively. According to Buchanan (2007), LVL leaves the factory with moisture content in the range of 8 % to 15 %.

2.3 Mechanical properties

Timber is an anisotropic material with different behaviour in tension and compression in different directions. In a simplified form, orthotropic elasticity is assumed for timber (Dias et al. 2007).

2.3.1 Orthotropic elasticity

The constitutive relationship for three-dimensional orthotropic linear elasticity is given by Equation (2.5).

$$\begin{Bmatrix} \varepsilon_{11} \\ \varepsilon_{22} \\ \varepsilon_{33} \\ 2\varepsilon_{23} \\ 2\varepsilon_{13} \\ 2\varepsilon_{12} \end{Bmatrix} = \begin{bmatrix} \frac{1}{E_{11}} & \frac{-\nu_{21}}{E_{22}} & \frac{-\nu_{31}}{E_{33}} & 0 & 0 & 0 \\ \frac{-\nu_{12}}{E_{11}} & \frac{1}{E_{22}} & \frac{-\nu_{32}}{E_{33}} & 0 & 0 & 0 \\ \frac{-\nu_{13}}{E_{11}} & \frac{-\nu_{23}}{E_{22}} & \frac{1}{E_{33}} & 0 & 0 & 0 \\ 0 & 0 & 0 & \frac{1}{G_{23}} & 0 & 0 \\ 0 & 0 & 0 & 0 & \frac{1}{G_{13}} & 0 \\ 0 & 0 & 0 & 0 & 0 & \frac{1}{G_{12}} \end{bmatrix} \begin{Bmatrix} \sigma_{11} \\ \sigma_{22} \\ \sigma_{33} \\ \tau_{23} \\ \tau_{13} \\ \tau_{12} \end{Bmatrix} \tag{2.5}$$

where E_{ii} $(i = 1,2,3)$ denotes the moduli of elasticity, G_{ij} $(i,j = 1,2,3, i \neq j)$ the modulus of rigidity, ν_{ij} $(i,j = 1,2,3, i \neq j)$ the Poisons' ratios, and finally ε_{ij} $(i,j = 1,2,3)$ strain components. Equation (2.5) could be re-written as below:

$$\{\varepsilon\} = [c]\{\sigma\} \tag{2.6}$$

$$\{\sigma\} = [D]\{\varepsilon\} \tag{2.7}$$

$$[D] = \begin{bmatrix} \frac{E_{11}(1-\nu_{23}\nu_{32})}{\psi} & \frac{E_{22}(\nu_{12}+\nu_{32}\nu_{13})}{\psi} & \frac{E_{33}(\nu_{13}+\nu_{12}\nu_{23})}{\psi} & 0 & 0 & 0 \\ \frac{E_{22}(\nu_{12}+\nu_{32}\nu_{13})}{\psi} & \frac{E_{22}(1-\nu_{13}\nu_{31})}{\psi} & \frac{E_{33}(\nu_{23}+\nu_{21}\nu_{13})}{\psi} & 0 & 0 & 0 \\ \frac{E_{33}(\nu_{13}+\nu_{12}\nu_{23})}{\psi} & \frac{E_{33}(\nu_{23}+\nu_{21}\nu_{13})}{\psi} & \frac{E_{33}(1-\nu_{12}\nu_{21})}{\psi} & 0 & 0 & 0 \\ 0 & 0 & 0 & G_{23} & 0 & 0 \\ 0 & 0 & 0 & 0 & G_{13} & 0 \\ 0 & 0 & 0 & 0 & 0 & G_{12} \end{bmatrix} \tag{2.8}$$

$$\psi = 1 - \nu_{12}\nu_{23} - \nu_{23}\nu_{32} - \nu_{31}\nu_{13} - 2\nu_{21}\nu_{32}\nu_{13} \tag{2.9}$$

The matrix [C] denotes the compliance matrix, and [D] is the stiffness matrix. Equation (2.10) also exists between Poisons' ratio and modulus of elasticity.

$$\nu_{ij} = \frac{E_{ii}}{E_{jj}}\nu_{ji}, (i,j = 1,2,3, i \neq j) \tag{2.10}$$

Dias et al. (2007) used nonlinear finite element analysis for modelling of the timber-concrete joints. In the elastic phase, the following assumptions for the material properties were made:

$$E_x = 30E_y = 30E_z \tag{2.11}$$

$$G_{xy} = G_{zx} = \frac{E_x + E_y}{2} \times \frac{1}{16} \tag{2.12}$$

$$G_{yz} = \frac{E_y + E_z}{2} \times \frac{1}{16} \tag{2.13}$$

E_x,E_y and E_z are the three modulus of elasticity in the three different main directions. G_{xy}, G_{zx}, G_{yz} are three shear modulus. Direction x is the direction parallel to the fibres, the other two principal directions are y and z. Direction y corresponds to perpendicular to the grain and parallel to the glue line (Tangential direction) and direction z is perpendicular to the grain and perpendicular to glue surface (Radial direction). It is worth mentioning that E_y and E_z values are very dependent on the measurement method (Madsen et al. 1992), and elastic properties of LVL can be different from clear wood because of production process. The process of laminating LVL, gluing and pressing can change elastic properties.

Although some design material properties like the modulus of elasticity in bending are available for LVL, other material properties like modulus of elasticity in compression in the three main directions, shear modulus, tensile strength perpendicular to the grain, and fracture properties for New Zealand LVL are not available.

2.3.2 Constitutive response

Timber is usually assumed to be elastic although it exhibits several nonlinearities like visco-elastic behaviour, creep and plasticity under certain loading conditions (Schoenmakers 2010). This implies that timber shows time-dependent material properties. Figure 2.1 (a) presents the results of tensile and compressive tests on clear wood specimens that show different material behaviours in tension and compression. Timber in compression shows plasticity while in tension it shows semi-brittle behaviour. The behaviour of timber for the numerical analysis in compression usually is idealized as elastic-plastic, and for tension is assumed linear up to failure of the beam. Figure 2.1 (a) shows the real behaviour of timber, and Figure 2.1 (b) shows the idealized behaviour for numerical analysis.

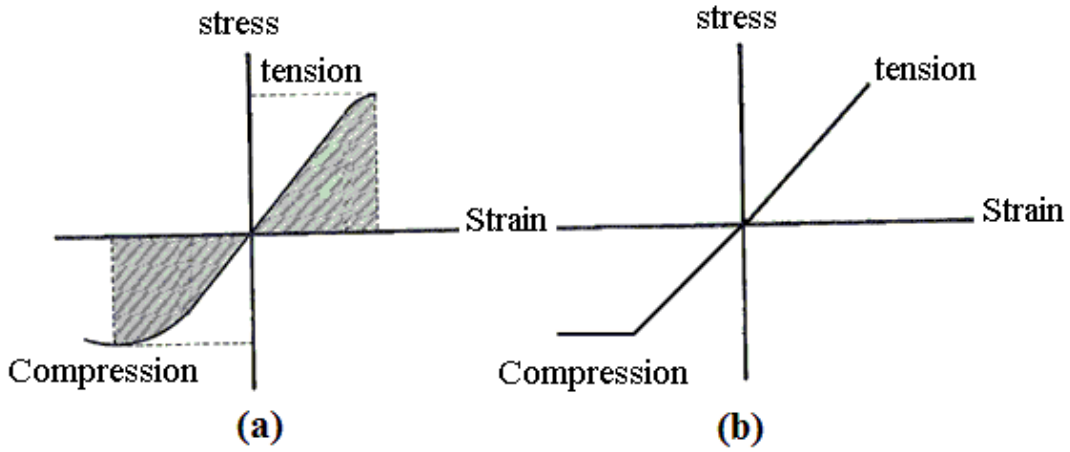

Figure 2.1. The behaviour of wood in compression and tension: (a) real, (b) idealized (Buchanan 2007).

2.4 Elastic properties of Laminated Veneer Lumber (LVL)

Elastic material properties of LVL are required for linear Finite Element (FE) modelling. Nine independent material properties of LVL are necessary for elastic modelling of wood. Selection of appropriate properties is vital for model accuracy and matching with experimental results. In this thesis, a combination of experiments and literature is used for the selection of appropriate material properties.

For orthotropic elastic modelling of LVL, nine independent material properties are required. These include three moduli of elasticity in main directions, three shear moduli, and three Poisson's ratios.

Three moduli of elasticity of LVL in the grain and perpendicular to the grain direction were obtained through experiments on LVL specimens. The modulus of elasticity in the third direction for LVL was indicated from previous work (Davies 2006). A picture of the experimental program for the modulus of elasticity in the grain and perpendicular to the grain direction is presented in Figure 2.2. The experimental setup was adopted from EN789 – Timber structures test methods - Determination of mechanical properties of wood based panels (European Committee for Standardization EN 789 2004).

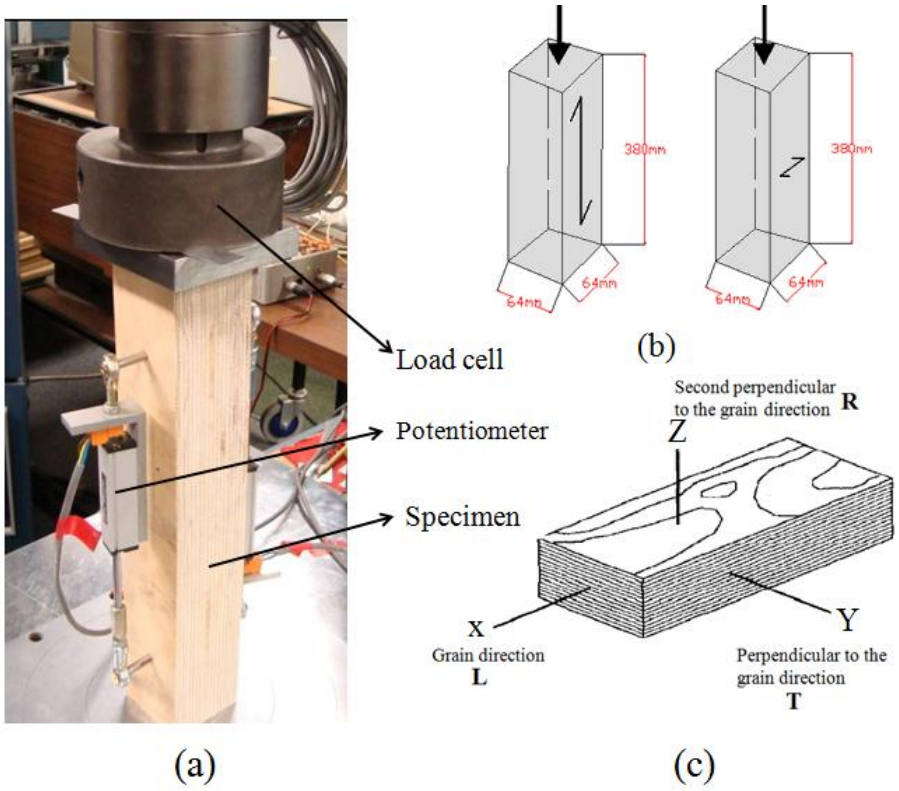

Figure 2.2. Experiments on modulus of elasticity of LVL: (a) experimental setup, (b) sketch of dimensions for modulus of elasticity testing, (c) principal directions in LVL

The shear modulus of LVL in the grain direction was obtained through limited experiments on LVL specimens. The shear modulus of LVL in the other directions was assumed as 1/16 of the average appropriate elastic material properties (Equations (2.11) to (2.13)). In the modelling, the effect of E_z and G_{yz} was not found critical on the results.

The elastic material properties for LVL was used in the modelling are presented in Table 2.2. The Poisson's ratio values were adopted from Schoenmakers (2010) for Oregon pine.

Table 2.2 Elastic material properties of LVL

E_x (MPa)	E_y (MPa)	E_z (MPa)	G_{xy} (MPa)	G_{yz} (MPa)	G_{zx} (MPa)	ν_{xy}	ν_{yz}	ν_{xz}
12000	485	280	600	24	600	0.38	0.51	0.51

2.5 Tensile strength perpendicular to the grain direction

In experiments on beams with holes, cracks start because of the low tensile strength perpendicular to the grain of LVL. An experimental program was planned for accurate estimation of the tensile strength of LVL. Tensile strength of LVL in the perpendicular to grain was indicated through tests on the dog-bone specimens. The specimens were tested according to ASTM D143-94 (2000) standard. The dimensions of the specimens and a picture of the experimental program are presented in the Figure 2.3.

Although the focus of the work was LVL, some tests were also performed on the LVL_C and radiata pine for comparison purposes. LVL_C is cross-banded LVL. In LVL all of the veneers are aligned in one direction while in the LVL_C, some of veneers are perpendicular to the direction of other veneers improving the tensile strength perpendicular to the grain. More experimental details could be found in Appendix 2.

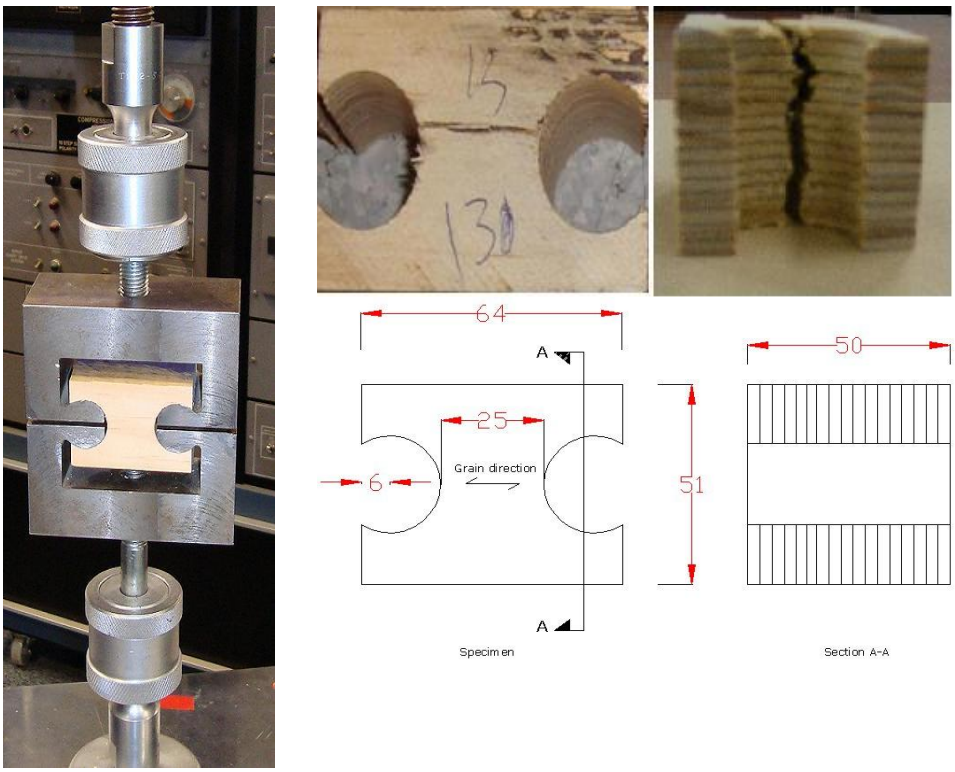

Figure 2.3. Experimental setup of tension tests perpendicular to the grain

The experimental program and the results of the experiments are presented in Table 2.3, and Table 2.4 respectively. LVL showed the average tensile strength perpendicular to grain of about 2 MPa with the coefficient of variation about 18 percent. The average tensile strength of sawn timber was about 3.9 MPa. Larger tensile strength perpendicular to grain for wood is also reported by Hummer et al. (2006).

Table 2.3. Experimental program for tension strength perpendicular to grain (Ardalany et al. 2010b)

Material (Radiata pine)	Number of Specimens	Thickness (mm)	Moisture content (%)	Number of veneers	
				Perpendicular	Parallel
LVL	57	50	9.3	0	16
LVL-C	30	35	11.7	2	8
Sawn Timber	30	50	11.0	-	-

Table 2.4. Results of the experimental program (Ardalany et al. 2010b)

Specimen	Selecting process	Average tensile strength (MPa)	Minimum tensile strength (MPa)	Coefficient of variation (%)	5th percentile of the values (MPa)
LVL	Random	2.021	1.152	18	1.434
LVL-C	Cut from one billet	7.540	5.827	10	6.495
Sawn timber	Random	3.887	2.662	23	3.018

Some size effect regarding tension perpendicular to grain may exist in the LVL. This needs further experimental tests and research to draw conclusion.

2.6 Fracture properties of LVL in Mode I (opening)

Fracture properties of LVL are necessary for analysis of the crack initiation, and propagation in the Linear Elastic Fracture Mechanics (LEFM) analysis around holes. An experimental program was carried out to indicate these parameters.

Experimental results of the fracture energy, fracture toughness, and calculated energy release rate values performed on the radiata pine, and Laminated Veneer Lumber (LVL) specimens are presented in Table 2.6, Table 2.7, and Table 2.8. A sketch of the experimental setup in Figure 2.4 (a), and a picture of the experiments is presented in Figure 2.4 (b).

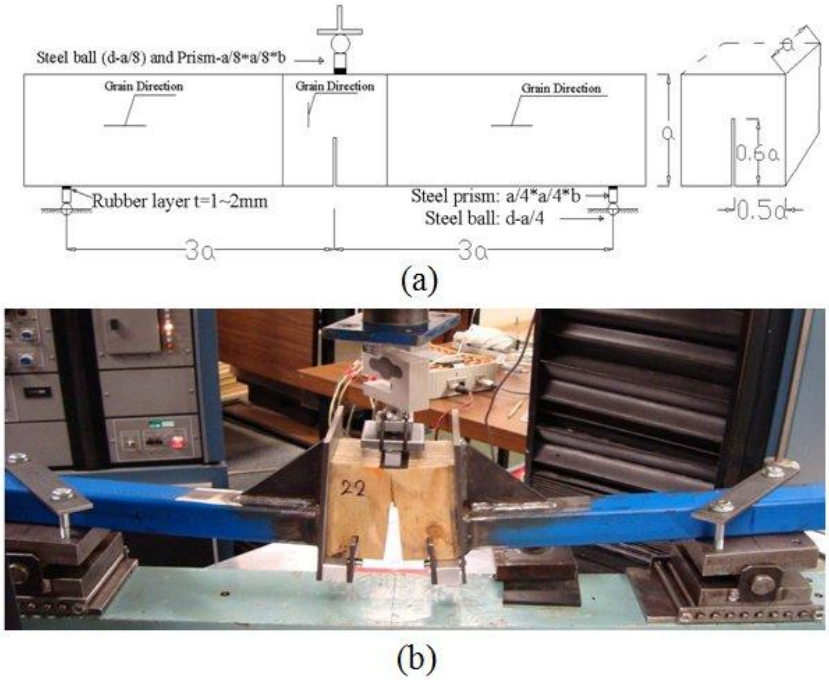

Figure 2.4. Specimen used for fracture energy and fracture toughness of wood in mode I: (a) sketch of model dimension (mm), (b) picture of experiment (Larsen et al. 1990)

The experimental program for indication fracture energy and fracture toughness values is included in Table 2.5. More experimental details could be found in Appendix 1 (Ardalany et al. 2012a).

Table 2.5. Experimental program for mode I fracture energy (Ardalany et al. 2012a)

Specimen Set	Material	Specimen Selection	Dimensions (mm)	Number of Specimens	Average Density $(\frac{kg}{m^3})$	Moisture content (%)
1	E10.7 LVL	Random	100×100×63	32	545	8
2	E10.7 LVL	single billet	100×100×63	11	555	8
3	E10.7 LVL	single billet	100×100×63	10	555	9
4	E10.7 LVL	single billet	200×200×63	10	555	8
5	E11 LVL	single billet	100×100×63	24	571	12
6	E10.7 LVL	Random	100×100×63	13	555	8
7	Sawn Radiata Pine	single stick	95×95×45	10	378	8
8	E10.7 LVL	Randomly selected	100×100×63	5	555	8

The results of the fracture energy of mode I for LVL and radiata pine are presented in Table 2.6. The data shows much higher values for LVL than sawn timber. In comparison, fracture energy of LVL is about four times than sawn timber. A comparison between results for 100 mm and 200 mm depth LVL specimen shows the size effect of about 33 % in the results.

Table 2.6. Results of fracture energy tests in mode I (G_{If}) (Ardalany et al. 2012a)

Specimen Set	Average Mode (I) Fracture Energy (N/mm)	Coefficient of Variation (%)	5th percentile of the values (N/mm)	Minimum fracture energy (N/mm)	Maximum fracture energy (N/mm)
1	1.3032	37	0.7056	0.7071	2.5310
2	1.1954	16	0.9588	0.9588	1.4436
3	1.2636	16	1.0298	0.9966	1.526
4	1.6773	18	1.2879	1.1668	2.0653
5	1.6081	32	1.0902	1.0881	2.0381
6	1.2063	30	0.7216	0.8149	1.8671
7	0.3816	17	0.2941	0.2831	0.4717

The results of the fracture toughness tests of LVL and sawn timber radiata pine are presented in Table 2.7.

Table 2.7. Results of the fracture toughness tests in mode I (K_{Ic}) (Ardalany et al. 2012a)

Set Number	Average Mode (I) Fracture Toughness ($MPa\sqrt{m}$)	Coefficient of Variation (%)	5th percentile of the values ($MPa\sqrt{m}$)	Minimum fracture toughness values ($MPa\sqrt{m}$)	Maximum fracture toughness values ($MPa\sqrt{m}$)
1	0.4512	12	0.3739	0.3240	0.5270
2	0.4754	5	0.4438	0.4370	0.5200
3	0.4542	10	0.4076	0.4000	0.5320
4	0.5307	9	0.4677	0.4650	0.6180
5	0.4564	14	0.3675	0.3620	0.5800
6	0.4395	17	0.3589	0.3210	0.6277
7	0.2813	5	0.2623	0.2560	0.2980
8	0.4442	-	0.4029	0.4029	0.6

Also, calculated values of the critical energy release rate of LVL and radiata pine are presented in Table 2.8.

Table 2.8. Calculated values of the critical energy release rate (G_{Ic}) (Ardalany et al. 2012a)

Set number	Average Mode (I) Critical strain energy release rate (N/mm)	Coefficient of Variation (%)	5th percentile of the values ($MPa\sqrt{m}$)	Min of values (N/mm)	Max of values (N/mm)
1	0.1938	23	0.1314	0.1273	0.2571
2	0.2129	10	0.1851	0.1795	0.2541
3	0.1955	18	0.1562	0.1504	0.2660
4	0.2666	18	0.2056	0.2032	0.3590
5	0.1955	28	0.1269	0.1232	0.3162
6	0.1866	37	0.1222	0.1429	0.3703
7	0.1444	9	0.1254	0.1194	0.1618

LVL in the tension mode of fracture shows that its critical energy release rate (G_{IC}) is different from the fracture energy (G_{If}). This could be due to the softening after cracking in LVL (Ardalany et al. 2012a).

2.7 Withdrawal strength of SPAX screw

It may be necessary to use of the withdrawal strength of SPAX screw for design purposes. The withdraw strength for SPAX screws were calculated with the test specimens in three main directions of LVL namely longitudinal, tangential and radial directions. The screws were inserted to depths of 4, 8, 12 and 16 times than the screw diameters in LVL, and then pulled out by the testing machines. Experiments showed that the radial direction has the highest strength. Figure 2.5 (a) presents the experimental setup for withdrawal tests on SPAX screws of 8 mm diameter and a sketch of experimental testing is presented in Figure 2.5 (b).

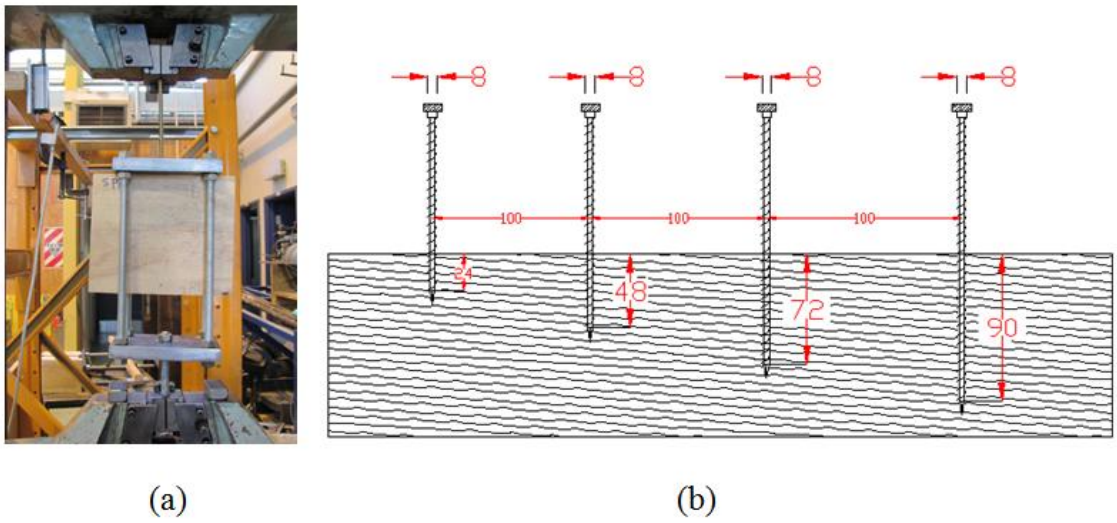

Figure 2.5. The experimental setup for the screw withdrawal tests: (a) real, (b) sketch of the test

Although only the tangential direction data is required for the screw reinforcement around the holes in LVL beams, the data of other directions are presented in Table 2.9 for comparison reasons. The tests performed with an 8 mm diameter SPAX screw that was later used for the reinforcing around the holes. The experiments showed different withdrawal strength for LVL in different directions.

Table 2.9. Screw withdrawal strength coefficients ($f_{(i=1,2,3),\mathrm{k}}$) in three main directions ($10^{-6} \times \rho^2$)

Material	Average strength (MPa)	Minimum strength (MPa)	Maximum strength (MPa)	5th percentile values (MPa)
Tangential (direction 1)	94	81	96	81
Radial (direction 2)	115	112	117	112
Longitudinal (direction 3)	69	56	81	60

The withdrawal strength coefficients are presented in terms of density of 550 kg/m^3 in Table 2.9. The withdrawal strength is calculated from Equation (2.14).

$$R_{\mathrm{i},k} = f_{\mathrm{i},k} \times d_{\mathrm{r}} \times l_{ef} \tag{2.14}$$

where l_{ef} is the effective length of screw inside LVL specimen, and d_r denotes the diameter of the screw. $R_{\mathrm{i},k}$ is characteristic pullout resistance for screw driven in i direction. For the screw withdrawal in tangential direction (direction 1) and for a screw having an angle of $45 \leq \alpha \leq 90$ between the screw axis and direction of the timber grain, Equation (2.15) is suggested for characteristic pull-out ($R_{\mathrm{ax},k}$) values (SPAX 2007).

$$R_{\mathrm{ax},k} = \frac{f_{1,k} \times d_{\mathrm{r}} \times l_{ef}}{\sin^2\alpha + \frac{4}{3}\cos^2\alpha} \tag{2.15}$$

According to the SPAX (2007), the values of $f_{1,k} = 80 \times 10^{-6}$ N/mm^2 is suggested for LVL that is in excellent match with experimentally indicated value of 81×10^{-6} N/mm^2.

2.8 Summary

This chapter presented some material properties of LVL such as modulus of elasticity in different directions, tensile strength perpendicular to the grain direction, fracture toughness, and fracture energy in mode I (opening) and withdrawal strength of screw obtained through experimental program on LVL specimens.

- In terms of material property, LVL is comparable with its counterpart sawn timber Radiata pine but with some differences. The laminating process improves some of the material properties like bending strength in the grain

direction at the cost of other properties such as tensile strength. Tensile strength of LVL perpendicular to the grain is about 2 MPa and sawn timber 3.9 MPa, the difference is roughly two times.

- The material properties that are presented in this chapter will be further incorporated into finite element models for the analysis of the beams with holes. The fracture properties will be also used in the fracture analyses. Finally, screw withdrawal strength will be intended for the designing of the reinforcement in the subsequent chapters.

- The fracture energy of LVL in perpendicular to grain direction is roughly four times the fracture energy of Sawn timber.

3 Experiments on LVL beams with holes and reinforcement around holes

This chapter presents the experiments on LVL beams with holes and reinforcement around the holes. Different shapes of holes with a variety of the diameters were tested. Reinforcement of the holes was also performed using plywood, steel brackets, self-tapping screws, and epoxied-in rods. The results of this chapter have been used in chapter 4, 5, 6, 7, 8, and 9.

The majority of this chapter has been re-produced from the following journal paper:

Ardalany, M., Carradine, D., Fragiacomo, M. and Deam, B. (2012). "Experimental tests on Laminated Veneer Lumber (LVL) beams with holes and different methods of reinforcement of the holes" Journal of Structures and Buildings (under review).

3.1 Introduction

The material properties of LVL were presented in chapter 2. In this chapter, experimental work on LVL beams with holes and reinforcement methods around the holes are presented. Different hole diameters to beam depths and location of the hole were tested experimentally. More experimental works on LVL beams reinforced with epoxy-grouted rods is presented in chapter 7.

In a simply supported beam without a hole, loaded at mid-span, the failure usually occurs due to high moment at mid-span. The failure usually starts by cracking of the tensile region and expands suddenly to the compression region. Introducing a large enough opening into a beam can change the failure mode to crack initiation and

propagation around the hole. The opening in a beam acts like a stress concentrator increasing tension perpendicular to grain stresses in a localized part of the beam. The tension perpendicular to grain strength of the timber materials is usually low compared to other directions (Ardalany et al. 2010b). When the tension stresses go beyond the strength of the material, the beam crack. Final failure of the beam occurs due to crack propagation around the hole (Figure 3.1).

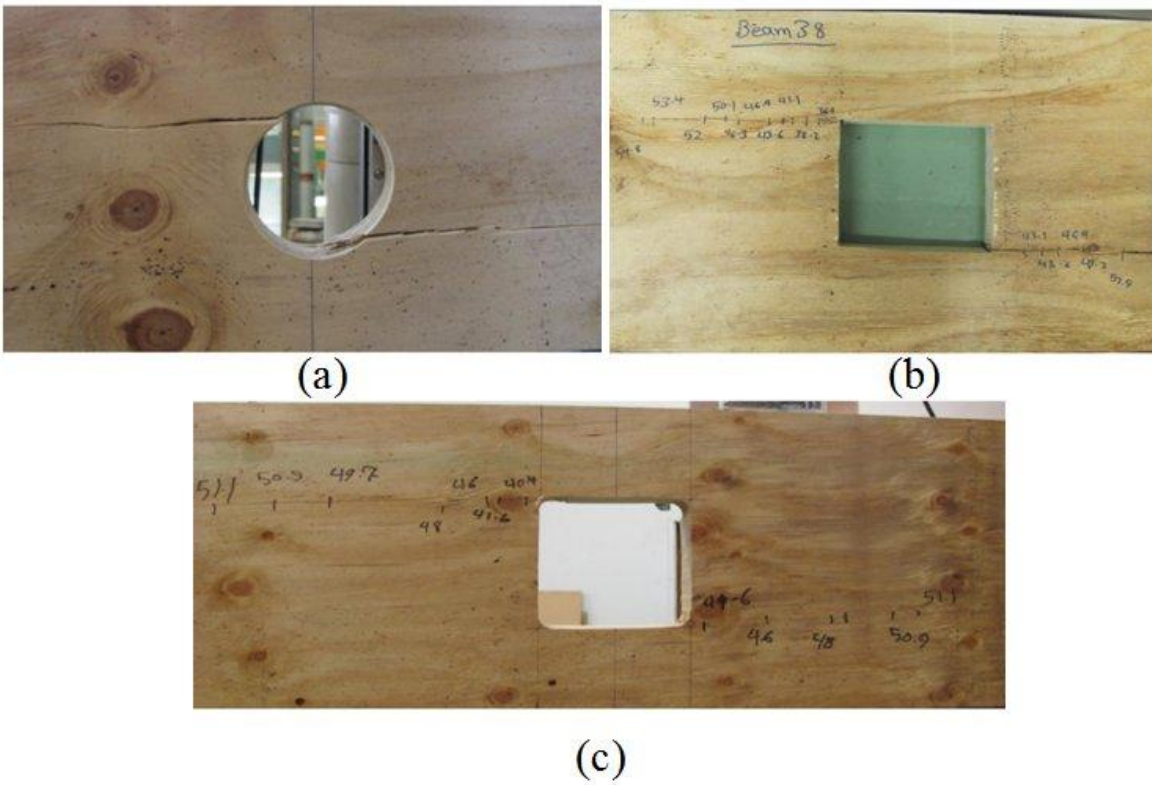

Figure 3.1. Crack formation around penetrations: (a) circular holes, (b) square holes with sharp corners, (c) square holes with rounded corners

Failure governed by crack initiation and propagation around holes occurs at much lower loads than predicted using full beam section properties. Research on methods for reinforcing holes is needed because in many practical situations holes will be required. When reinforcing a hole, the focus should be on avoiding crack initiation and propagation around holes, and restoring the original capacity of the beam. Restoring of the original capacity of the beam by providing reinforcement can be misleading because the load carrying capacity of a beam without a hole is not fixed due to the COV of the material strength. This means that by providing reinforcement around a hole, crack

initiation and propagation is avoided so other failure mechanisms such as mid-span failure due to maximum bending moment can occur prior to failing of the beam due to crack propagation.

Different methods for reinforcing timber beams have been proposed for glulam beams. Reinforcing with fully threaded screws and plywood is included in the current DIN 1052 German design code (DIN 1052 2008). Also, the use of a steel bracket, i.e. steel plates around a hole nailed to the beam (Figure 3.2 (e)), has been an alternative for reinforcing available in the New Zealand market. While using screws is more favourable for architects, other options like plywood can provide viable solutions for engineers, and builders also are interested in the "off the shelf" steel brackets. Screws can be installed and hidden from sight, glued plywood sheets provide a good bond with the beam, and steel brackets are easy to install. Figure 3.2 presents different methods for reinforcing beams.

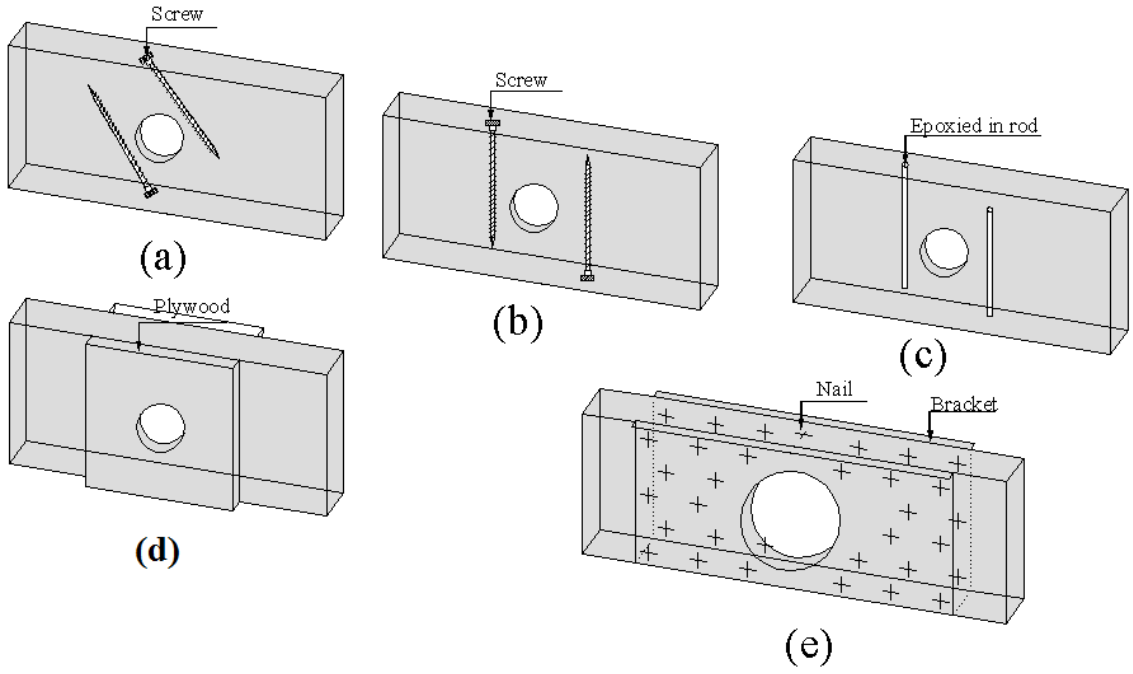

Figure 3.2. Sketch of different types of reinforcing around holes in LVL beams: (a) inclined screws, (b) vertical screw, (c) epoxy grouted rod, (d) plywood, (e) steel bracket

Different shapes of holes can also be used depending on the services that pass through the beam. Although circular holes are the most common, rectangular penetrations also may be required for ventilation systems. Cutting a rectangular hole is relatively simple

if the curved edges are being used; however, sharp corners require more hand work for finishing.

This chapter reports a series of experiments on LVL beams with holes and reinforcement. The beams were with different sizes and shapes of the holes. Different options for reinforcement, and effectiveness of each reinforcement for diverse opening diameters was investigated.

3.2 Properties of experimental materials

Holes in LVL beams were experimentally evaluated, and reinforcing of these holes using fully threaded screws, epoxy grouted in steel rods, plywood and steel brackets were considered. Below are descriptions of the materials used for the beams and reinforcing of the holes.

3.2.1 Laminated Veneer Lumber (LVL)

LVL was provided by a local New Zealand producer and shipped in sizes of 8000×1200×45 mm to the lab for testing. Beams were cut to size and circular openings were cut with a hole saw mounted in a drill press (Figure 3.3 (a)). For cutting of rectangular holes with curved corners, four holes were cut at the corners of a square. A jigsaw was used to connect the holes. The procedure for sharp rectangular holes was the same except for creating a sharp edge where the cutting work was finished using a jigsaw.

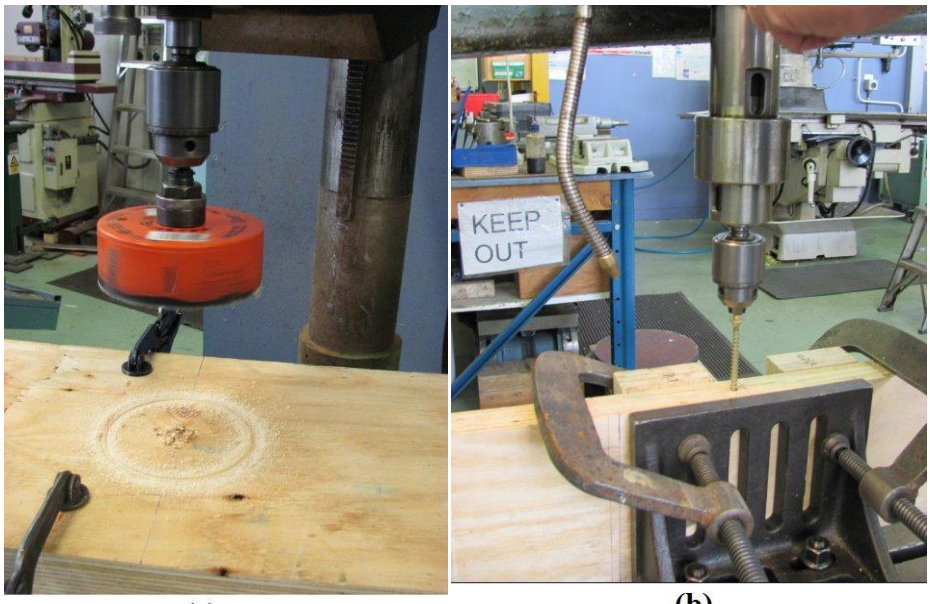

Figure 3.3. (a) Cutting hole in a beam, (b) drilling screw in LVL

LVL beams with different aspect ratios, hole locations, and sizes were tested for the experimental program. The length to depth ratio of the specimens, diameter of holes, and different methods of reinforcements were varied to study the reduced strength. The effectiveness of different kinds of reinforcements for varied breadth of beams was also checked, including some experiments performed with thicker beams to check the efficiency of reinforcement. The LVL used in the experiment had a published modulus of elasticity in bending of 10.7 GPa and was produced from Radiata Pine grown in New Zealand. The material had an average density of $573\ \mathrm{kg/m^3}$ which was obtained by testing some pieces of the LVL. The materials were stored and tested under ambient laboratory conditions. The moisture content of the material during the test varied between 8 to 10 %, which was assessed by oven drying small portions of the tested beams according to ASTM D4442-92 (2000). The LVL had an average tension perpendicular to grain strength of 2 MPa that was obtained through tests on small specimens (chapter 2). The published tension strength of the LVL in the grain direction was 33 MPa (Buchanan 2007). Other material properties for the LVL are presented in Table 3.1.

Table 3.1. Characteristics material properties of LVL (Buchanan 2007)

Modulus of elasticity in bending (GPa)	Bending strength (MPa)	Shear strength (MPa)	Compression Perpendicular to grain (MPa)	Shear Modulus (MPa)
10.7	48	6	12	485~535

3.2.2 Screws

In the case of screws as reinforcement around holes, screws should not yield, or withdraw, and should effectively transfer tensile stresses at possible crack planes. The withdrawal strength of screws can be controlled by embedment length and screws should satisfy other criteria such as diameter and distance from the edges to prevent of splitting of surrounding wood.

Fully threaded self-drilling SPAX screws were used for reinforcing around holes in LVL. SPAX screws are made of steel with the characteristic yield moment of 20 kNmm for 8 mm diameter (from manufacturer data). Figure 3.4 (a) shows different parts of the fully threaded SPAX screw. In the experiments, screws were inserted into the beams in two formats viz.: (i) inclined (Figure 3.2 (a)) and (ii) vertical (Figure 3.2 (b)). The inclined format may be used in the cases that the embedment length for the screw is not enough and there could be screw withdrawal. The embedment length for the screw is shown in Figure 3.4 (b).

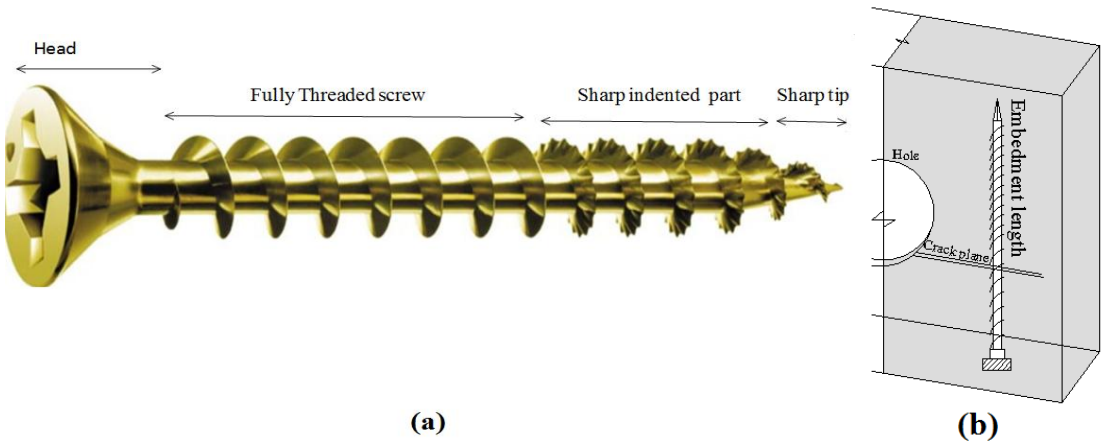

Figure 3.4. (a) Different parts of SPAX screws, (b) embedment length

In the experiments, screws were driven into beam by a drilling machine as shown in Figure 3.3 (b).

3.2.3 Epoxy grouted steel rods

Epoxy grouted steel rods are another reinforcement option. Two formats of the rod placement were considered in the experiments, one going through the beam (Figure 3.5 (a)), and the other having only one of the rods cutting the tensile edge (Figure 3.5 (b)). Fully threaded steel rods with modulus of elasticity of 210 GPa, and characteristics yielding strength of 400 MPa were used with an average thread diameter of 5.7 mm and root diameter of 5.28 mm. Rods were placed and epoxy grouted into 11 mm diameter holes in the LVL. The epoxy was selected from HILTI products with trade brand of HIT-RE-500-SD.

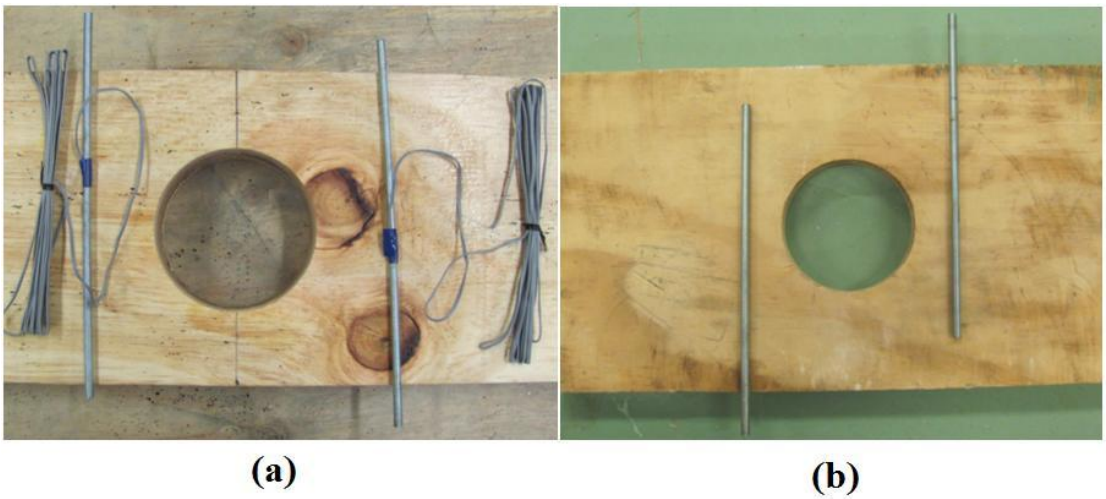

Figure 3.5. Two methods of rods placement using epoxy in LVL beams: (a) rods passing right through the beam, (b) rods stopping short at one end

3.2.4 Plywood

Plywood is a good option to transfer shear forces near holes in beams. Plywood can be glued and nailed on both sides of the beam, and there is a reasonably uniform bonding pressure between the plywood and the beam. Nailing of plywood to beam ensures uniform pressure on the connection. Plywood prevents stress concentrations at a single

point because it distributes stress over a larger area. Therefore, the opening size that can be reinforced by the plywood is greater than one that can be reinforced using screws. Although plywood has many advantages, it suffers from a few disadvantages concerning aesthetics. Plywood is attached on the outer faces of beams that can be visually distracting for architects and building occupants.

In the experiments conducted, plywood was also used for reinforcing holes in LVL beams. A local New Zealand producer from local Radiata Pine provided the plywood. The plywood had three veneers with average overall thickness of 8.8 mm. The details of the plywood layers thicknesses are presented in Figure 3.6. The stress grade of the plywood was F8, and its material properties adopted from AS/NZ 2269 (2004). Table 3.2 presents characteristic material properties of plywood used in the experimental program.

Table 3.2. Characteristic material properties of plywood (AS/NZ 2269 2004)

Stress class	Bending strength (MPa)	Tension strength (MPa)	Panel shear strength (MPa)	Modulus of elasticity (GPa)	Modulus of rigidity (MPa)
F8	25	15	4.7	9.1	455

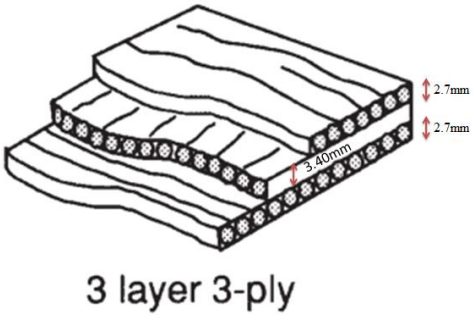

Figure 3.6. Details of the plywood used to reinforce holes in LVL beams

In the experiments, plywood was glued to the beams to improve the tension perpendicular to grain and shear strength of the beam locally. In order to create a good bond between plywood and beam, the glued plywood was also nailed to the beam, which avoided the need for clamping. The gluing of plywood to the LVL is effectively similar to the producing of cross banded LVL, where not all of the veneers are aligned in one direction, but some of the veneers are rotated 90°, a method that greatly increases the tensile strength of the LVL perpendicular to the grain (Hummer et al. 2006) and

improves its mechanical properties in the perpendicular direction. Cross-banded LVL is also less susceptible to cupping and is more dimensionally stable when exposed to moisture.

3.2.5 Steel bracket

Another option for reinforcing holes in timber beams is using a manufactured 1.16 mm thick steel bracket (available in New Zealand market) installed using nails as shown in Figure 3.7. Simple installation of the bracket is an advantage, while a deficiency is that the bond between steel and timber is not continuous, therefore cracks can initiate and propagate. Like plywood, the brackets may also not be very favourable for architects. Because the bracket is nailed to the beams, the shear is transferred by the nails from beam to bracket.

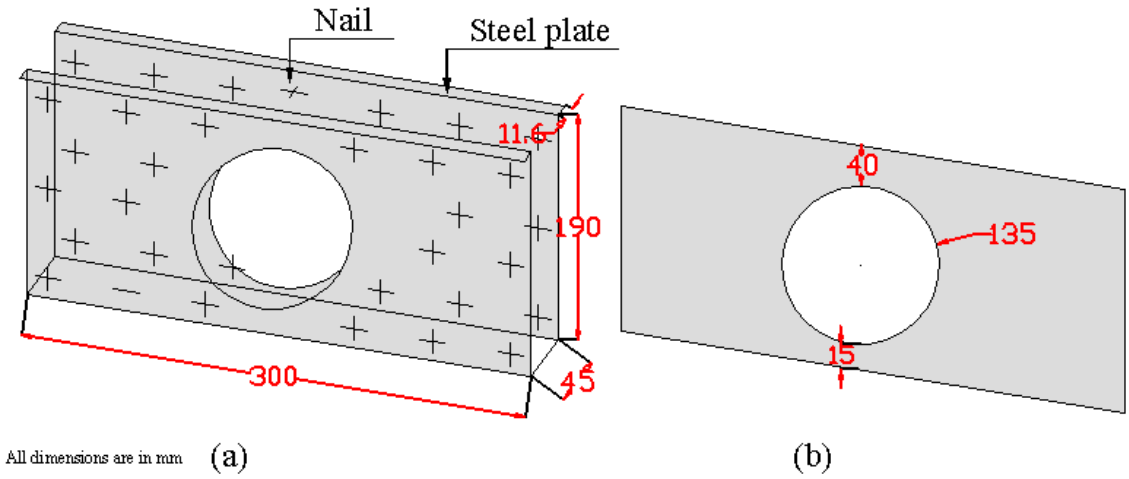

Figure 3.7. Steel bracket dimensions for beam of 190 mm depth: (a) 3D configuration, (b) dimensions of the hole

3.3 Experimental setup

Experiments were performed on simply supported beams using centre loading (Figure 3.8 (a)) and double-point loading (Figure 3.8 (b)) tests with a constant loading rate of 2 mm/minute. Applied load was measured using a load cell with an accuracy of $\pm$0.1 kN. For three-point bending (centre loading), load was applied to the beam via a ball and

socket joint on top of a steel plate (200×90×40 mm) to avoid timber crushing. For four-point bending, load was applied using a beam distributing the load equally between two socket joints. The edges of the plate were curved (10 mm radius) to transfer the load uniformly to the beam without having stress concentrations at the edges. Roller supports that can slide during loading were also used in the experiments. The test setup followed AS/NZS 4063 Characterization of Structural Timber (AS/NZS 4063 Part.2 2010). Two guiders were fabricated and installed on the supports to avoid possible lateral buckling of beams.

In the experiments, three Linear Variable Differential Transducers (LVDTs) with an accuracy of ± 0.1 mm were used for measuring deformations at supports and mid-span. At the end of the experiments, the average support deflection was also subtracted from mid-span deflection in order to remove the effects of the supports on the results. Based on the experimental observations, crushing of LVL at the support was not an issue to be considered.

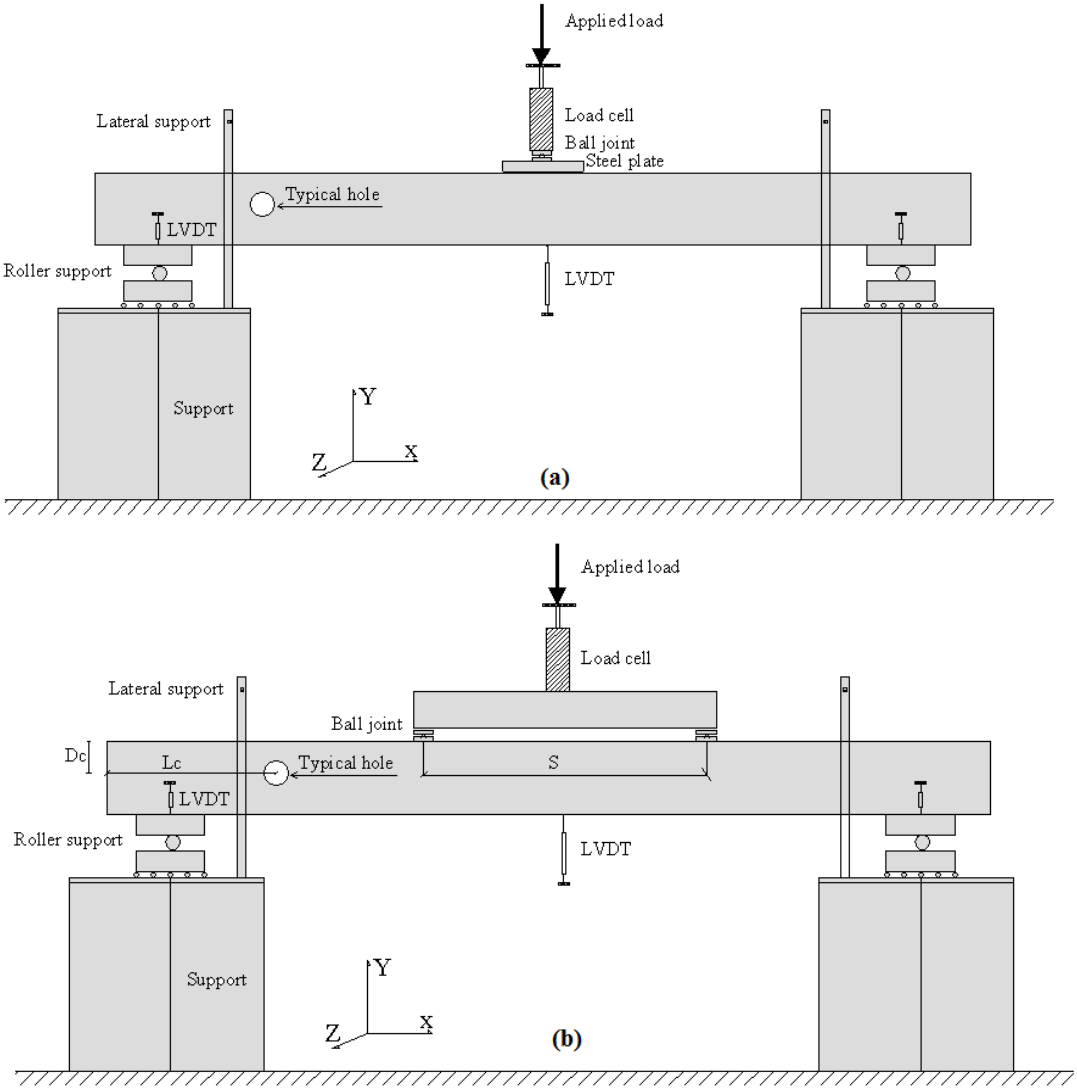

Figure 3.8. Schematic drawing of experimental setup: (a) 3-point, (b) 4-point bending tests

It was desired that holes be placed far from the supports and local loads, because the results may be affected by induced stresses (discussed more in chapter 4). The planned experimental program is presented in Table 3.3. The experiments included beams without holes, with holes, holes with reinforcement by screws, holes with plywood reinforcement, and finally holes with bracket reinforcement. The 'number of tests' in the table indicates that for an example 3 beams of the same type were tested during the experimental program. The loading type '3' refers to the centre loading (Figure 3.8 (a)) and loading type '4' refers to double point loading (Figure 3.8 (b)) and finally, 'estimated' in the table means that the values were obtained through calculations.

Table 3.3. Planned experimental program

#	Number of tests	Dimensions (mm)	Diameter (mm)	L_c (mm)	Reinforcement	Load type	Hole shape	S (mm)
1	2	1400×190×45	no hole	-	-	3	circle	-
2	2	1400×190×45	80	300	no	3	circle	-
3	2	1400×190×45	100	300	no	3	circle	-
4	2	1400×190×45	120	300	no	3	circle	-
5	2	1400×190×45	80	300	steel bracket	3	circle	-
6	2	1400×190×45	100	300	steel bracket	3	circle	-
7	2	1400×190×45	120	300	steel bracket	3	circle	-
8	2	1500×200×45	no hole	-	-	3	-	-
9	2	1500×200×45	50	400	no	3	circle	-
10	2	1500×200×45	65	400	no	3	circle	-
11	3	1500×200×45	80	400	no	3	circle	-
12	3	1500×200×45	100	400	no	3	circle	-
13	3	1500×200×45	80	400	plywood on both sides	3	circle	-
14	3	1500×200×45	80	400	plywood on one side	3	circle	-
15	3	1500×200×45	80	400	two screws	3	circle	-
16	3	1500×200×45	80	400	inclined screws	3	circle	-
17	2	2000×200×45	no hole	-	-	3	circle	-
18	2	2000×200×45	80	400	no	3	circle	-
19	2	2000×200×45	100	400	no	3	circle	-
20	2	2000×200×45	80	400	epoxy in rod	3	circle	-
21	2	2000×200×45	80	400	epoxy in rod	4	circle	500
22	2	2000×200×45	65	400	epoxy in rod	4	circle	500
23	2	2100×300×45	no hole	-	-	3	circle	-
24	2	2100×300×45	50	550	no	3	circle	-
25	2	2100×300×45	80	550	no	3	circle	-
26	2	2100×300×45	120	550	no	3	circle	-
27	2	2100×300×45	150	550	no	3	circle	-
28	3	2100×300×45	120	550	two screws	3	circle	-
29	3	2100×300×45	120	550	plywood on both sides	3	circle	-
30	3	2100×300×45	120	550	inclined screws	3	circle	-
31	3	2100×300×45	120	550	epoxy in rod	3	circle	-
32	3	2100×300×45	150	550	two screws	3	circle	-
33	estimated	2450×300×90	no hole	-	-	-	-	-
34	3	2450×300×90	120	550	two plywood	3	circle	-
35	3	2450×300×90	120	550	two screws	3	circle	

#	Number of tests	Dimensions (mm)	Diameter (mm)	L_c (mm)	Reinforcement	Load type	Hole shape	S (mm)
36	estimated	2800×400×45	no hole	-	-	3	-	-
37	2	2800×400×45	160	550	no	3	circle	-
38	2	2800×400×45	160	550	no	3	square with circular edge	-
39	2	2800×400×45	160	550	no	3	square with sharp edge	-
40	2	2800×400×45	160	550	two screws	3	square with circular edge	-
41	estimated	2800×300×45	no hole	-	-	-	-	-
42	2	2800×300×45	120	575	no	4	circle	500
43	2	2800×300×45	120	575	two screws	4	circle	500
44	2	2800×300×45	120	575	two plywood	4	circle	500
45	2	2800×300×45	150	575	two plywood	4	circle	500
46	2	2800×300×45	95	575	epoxy in rod	4	circle	500
47	2	2800×300×45	120	575	epoxy in rod	4	circle	500
48	estimated	2850×400×45	no hole	-	-	-	-	-
49	2	2850×400×45	120	575	epoxy in rod	4	circle	500

Note: L_c is the distance of the hole centre from the vertical outer edge of beam, 'S' is distance between two loading points in case of double point bending (Figure 3.8) and finally diameter in the case of square hole shows the dimension of the square side.

Dimension of plywood in the case of 200 mm deep specimens was 200×200×8.8 mm and for the 300 mm deep specimens was 300×300×8.8 mm. Selection of plywood dimensions was dependent on opening size and beam size. The plywood had a height equal to the beam and thickness of plywood selected was the thinnest possible (three veneers) at the start of experiments to avoid extra reinforcement, which was found to be unnecessary.

Screw dimensions were a function of LVL thickness and beam depth. For 200 mm deep beams, 180 mm long screws were selected, and for 300 mm deep beams, 280 mm long screws were used, in both lengths having an average root diameter of 4.85 mm. The average screw diameter (root plus thread) was 8.20 mm. Screws were driven into the wood in such a way that that the heads were placed as close as to the line of possible cracks propagation surfaces (Figure 3.9).

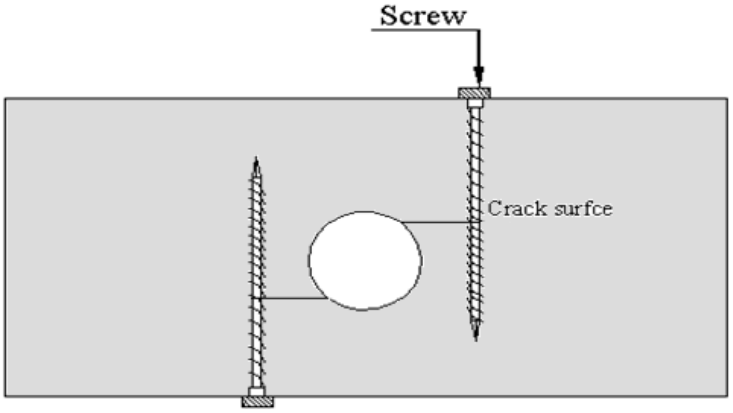

Figure 3.9. Driving of screws from both sides in beams

3.4 Experimental observations and results

Different experimental observation and conclusions are included in the following parts.

3.4.1 Beam with hole and without reinforcement

Experiments on beams were performed in a displacement driven testing machine. As load was applied, a linear load-deformation curve formed. With increasing load and deformation of the beams having large enough holes, the first crack formed at the interior (mid-breadth) edge of the hole (Figure 3.10 (a)) and propagated to the outer edges of the hole (Figure 3.10 (b)). The load associated with this phase is the cracking load. By propagating the crack toward the loading point and inducing more deformations in the beam, a crack also started and propagated on the other side of the hole. Following continued propagation of the cracks toward beam edges (Figure 3.10 (c)), when the critical length of the crack was reached, sudden shear fracture of the beams occurred at the failure load (Figure 3.11).

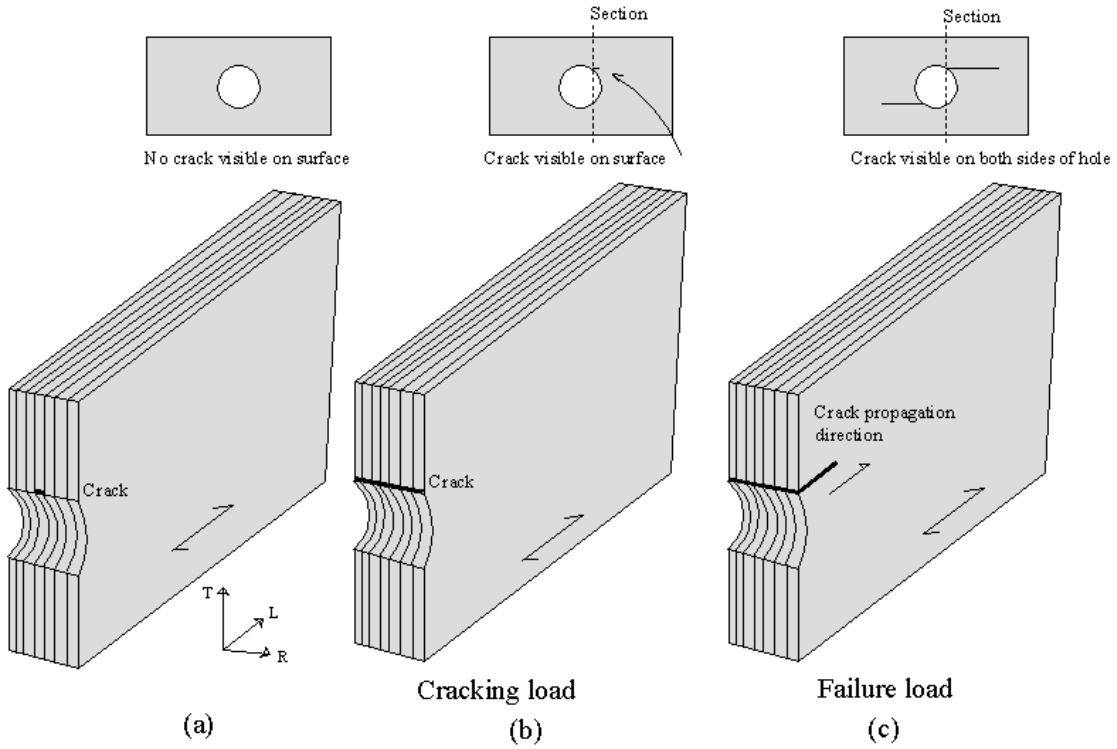

Figure 3.10. Different steps of crack initiation and propagation around holes: (a) crack at mid-breadth, (b) crack on the surface, (c) crack propagation along grain direction

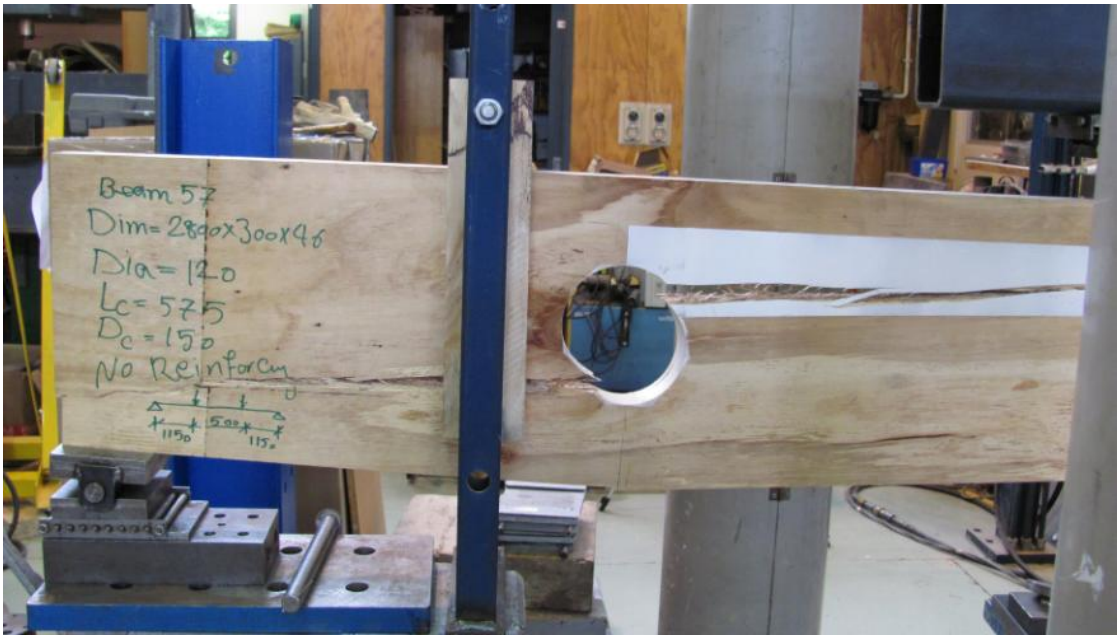

Figure 3.11. Shear failure of the beam with hole

Different failure modes occurred for different hole types and sizes. For small holes, the effect of the cut out was negligible and did not cause strength reductions in LVL beams. A limit of 50 mm diameter holes is reported by APA Report EWS-G535A (2010). Three-point bending tests on the 200 mm, and 300 mm deep specimens (Beams 9 and 24) also showed that the failure of the beams with 50 mm hole diameter occurred at mid-span. For the larger sizes of openings, crack initiation and propagation around the hole would direct the failure. Most of the experimental work focused on stopping crack propagation because it had more potential to be prevented by reinforcement.

In consideration of the shape of holes, tests were also performed using rectangular holes with sharp corners and curved corners. The radius of the curve was 15 mm. Limited number of experiments showed that the cracking load of the beam with sharp corners was about 10 % lower than the beam with rounded corners. This difference was understandable because with sharp corners stress concentrations occur.

Prediction of failure loads of beams with holes is rather complicated. An empirical relationship for the failure load prediction of unreinforced beams with the hole adopted from APA report (APA Report T2009L-30 2009) was used for failure load predictions. The relationship is a correction factor of $(1-(\frac{h-h_d}{h})^2)$ applied to the beam capacity without a hole, where h is the beam depth, and h_d is the diameter of the hole. The results of the comparison of ratio of the predicted load to the experimental load for different ratios of hole diameter to the beam depth are presented in Figure 3.12.

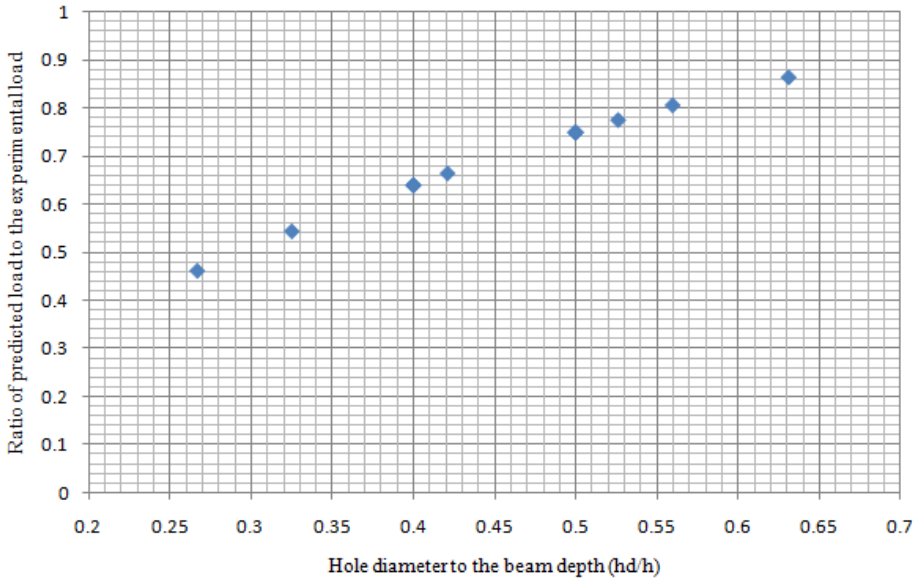

Figure 3.12. The results of the comparison of ratio of the predicted load to the experimental load for different ratios of hole diameter to the beam depth

3.4.2 Beam with hole and reinforcement

In order to avoid crack formation and propagation around the hole, different options for reinforcing were investigated. Reinforcing was performed using self-tapping screws, epoxy grouted rods, plywood and steel brackets. The reinforcement was used to redistribute the shear forces in the section, thereby avoiding crack formation and propagation.

The shear stress that cannot be transferred because of an opening is significant in beams with holes. A rough estimation of the moment and shear reduction based on first principles of engineering mechanics is presented in Figure 3.13. The graph for shear was obtained by integration of shear stresses over the area of the hole relative to the total shear in the section for different h_d/h values. Similarly, the graph for moment was obtained by integration of the stresses due to moment over hole depth. The resulting force was converted to moment and it was compared with total moment for different h_d/h values. The moment reduction for hole diameter to depth ratios of up 0.45 is less

than 10 % while for shear it is about 62%. This is because maximum shear stresses occur at the centre of the beam section while stresses due to moment are zero.

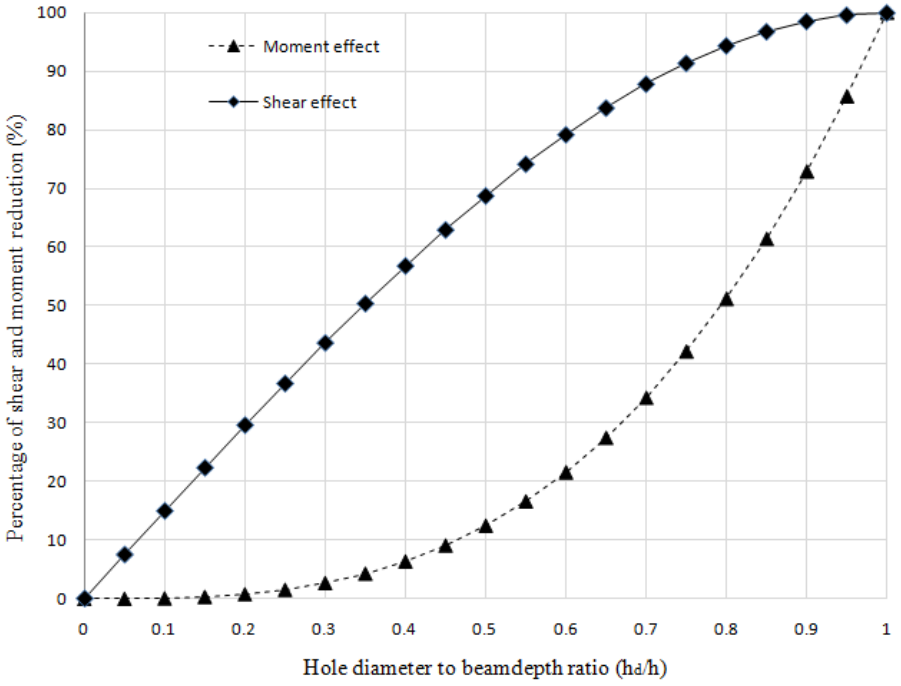

Figure 3.13. Effect of holes on shear and moment capacity of beams

3.4.3 Reinforcing using screws

Screw diameter was selected to avoid splitting of LVL. Some preliminary tests were performed to obtain a distance that would avoid splitting failures. For obtaining the critical distance of screws from the hole edge for LVL, several tests with 8 mm self-tapping screws were performed. For a distance greater than 30 mm from the edge, screws did not cause any visible splitting in the surface, so an edge distance of 30 mm was used. DIN 1052 (2008) used a distance between 2.5 to 4 times the screw diameter. The lengths of the screws were selected as just under the full depth of the beam.

The experiments on beams reinforced with two screws were performed for opening diameters up to 0.5 of the beam depth. During testing of beams with holes reinforced with two screws, as the load increased and reached critical values, cracks formed around the holes and gradually propagated toward the screws. When the crack reached a screw,

it was stopped from further propagation and the load increased. For the hole size of diameter less or equal to 0.4 of the beam depth, it caused failure at the mid-span in the high moment region of the beam. It seems that using screws delayed the crack propagation and the failure load was increased.

For hole size to beam depth equal to 0.5, the failure of the beam was governed by crack initiation starting from the tensile edge of the vertical hole created by the screw and right through the beam (Figure 3.14 (b)). Stress concentration in the screw as a result of hole, and weakening the beam section due to vertical hole for the screw in the tensile edge of the beam is the reason of this failure mode. Although driving a screw from the lower part of the beam is advantageous for providing the necessary embedment length at the other side of crack plane, it has a disadvantage of the possibility of beam failure starting from the edges of the screw hole.

In Figure 3.14, two cases of beams with reinforcement are presented. In Figure 3.14 (b), beam with h_d/h equal to 0.5 shows the fracture at the hole edge causing failure of the beam. The Figure 3.14 (a) is a beam with the h_d/h equal to 0.4 showing that cracks have propagated from the hole edge but stopped at the screw location. The failure of the left beam occurred at mid-span.

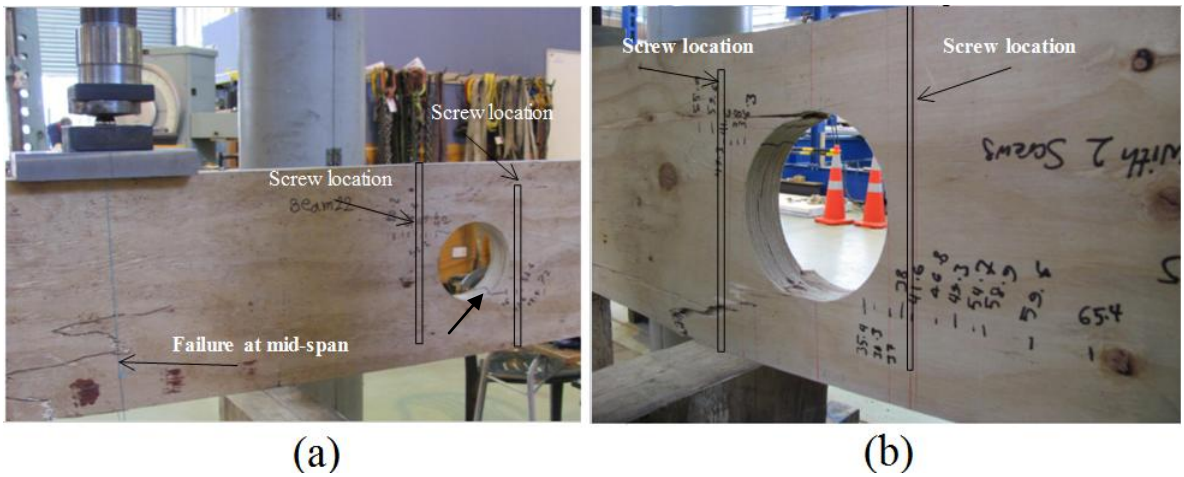

Figure 3.14. Different failure mechanisms in beams with holes: (a) mid span failure, (b) failure at hole edge

Some tests were also performed on beams reinforced with screws inserted at an angle of 45 degrees relative to the edge of beam, with a distance of 30 mm from the opening edge (Figure 3.15 (b)). Experiments were limited because the screws did not follow a

straight line. A comparison of typical results for beams without a hole, with a hole, and with inclined screws reinforcement is presented in Figure 3.15 (a). The main advantage of the inclined screws are providing the necessary embedment length and preventing screw withdrawal.

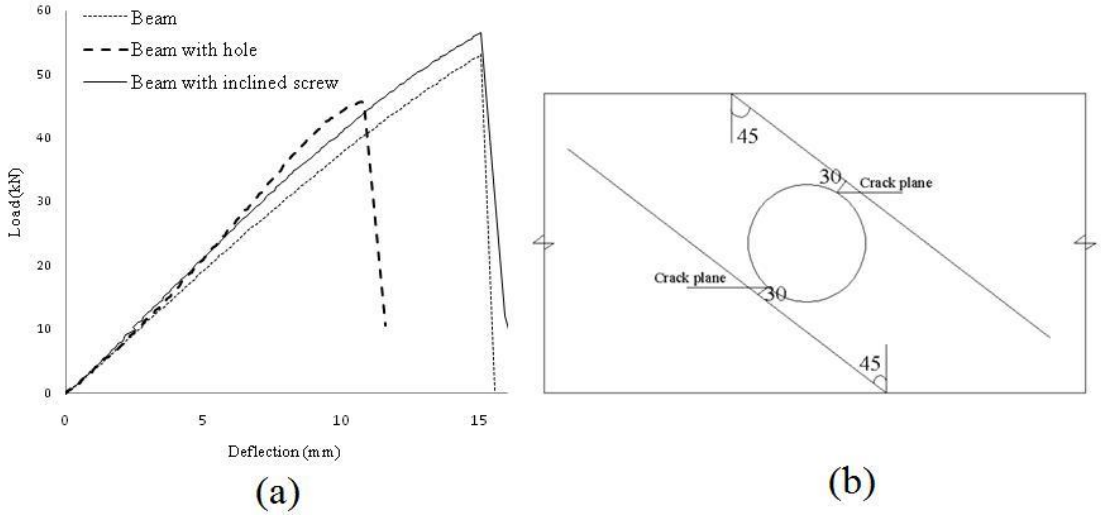

Figure 3.15. (a) Load-deflection plot at mid-span of the beams, (b) sketch of beam reinforced with inclined screws

The Swedish glulam Handbook (Carling 2001) also recommends driving screws on both sides for reinforcing of holes. The maximum hole diameter to beam depth ratio (h_d/h) is limited to 0.35, although experiments showed that screw reinforcing works well for holes up to 0.4 of beam depth.

3.4.4 Reinforcement using epoxy grouted steel rods

The working mechanism of the epoxy-grouted rod is similar to the screws. In the experiments, cracks started from the edge of the hole and stopped when at the rod. Depending on the length of the rod, and the ability to transfer tensile stresses, two failure types occurred. Figure 3.16 (a) shows the rod passing through the full depth of the beam, which failed because of tensile stresses propagated from the lower edge and passing through the depth of beam. The failure usually occurred in the rod far from the support. Figure 3.16 (b) shows a beam with a rod where only the left rod was protruding from the tensile edge of the beam. In this case, a steel plate of 45×100×1 mm was used and glued to the beam to avoid cracking of the tensile edge of the beam. The failure in

this case occurred at the mid-span of the beam. More experimental details and results are presented in chapter 7.

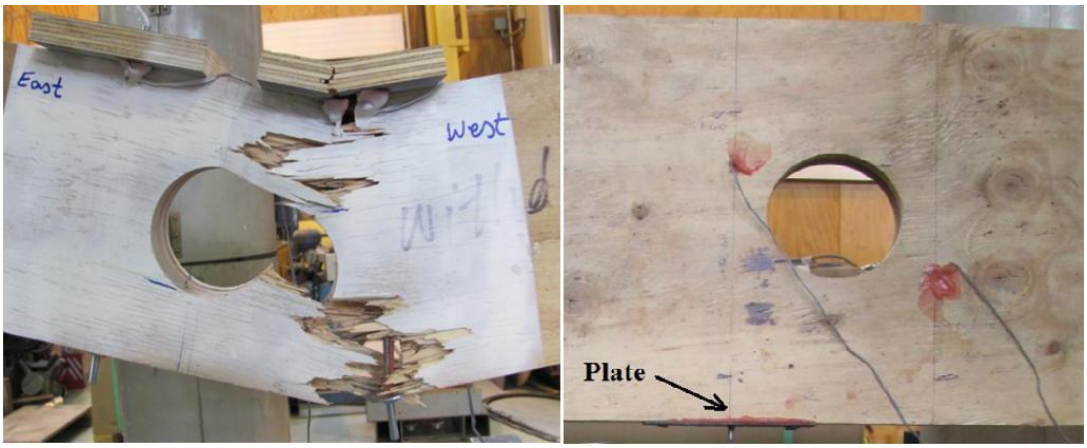

Figure 3.16. Beam failure reinforced with epoxied screw rod: (a) epoxy grouted rods fully through beam, (b) partially through beam

The results suggest that a vertical hole at the tensile edge may contribute to reducing the flexural resistance of the beam. This topic may future research for better understanding.

3.4.5 Reinforcing using plywood

Plywood was another alternative tested for reinforcing LVL beams. Plywood was glued and nailed to the surface of beams for an effective bond with the LVL. In the experiments, LVL with holes reinforced using plywood on both sides, and on one side was tested.

In the cases of plywood on both sides, it prevented crack propagation but could not stop crack formation. This is understandable because the crack usually starts at mid-breadth of the beam. In the experiments, failures of beams with a hole reinforced with plywood were governed by mid-span failures in the high moment area of the beams.

For beams reinforced with one plywood plate, cracks started to initiate at higher loads compared to beams without reinforcement. The crack initiated from the middle breadth of the beam toward the outer edge that was not reinforced. The crack propagated and

failure of the beam was governed by crack propagation. Figure 3.17 shows beams with holes reinforced with one layer and with two layers of plywood.

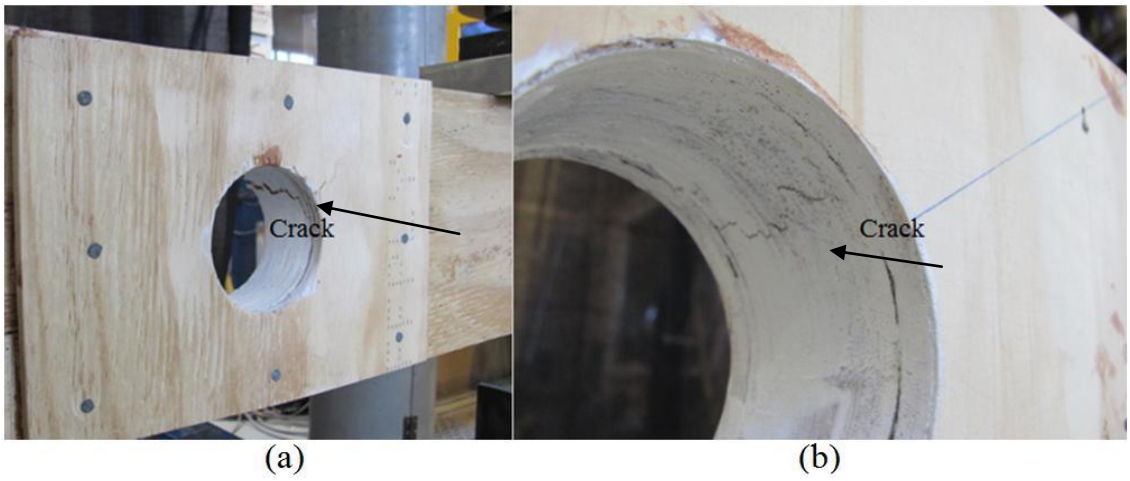

Figure 3.17. Reinforcing with plywood: (a) on one side only, (b) on both sides

A comparison of the typical load deflection for the beam with no hole, with a hole, with plywood reinforcement on one side and with plywood reinforcement on both sides is presented in Figure 3.18.

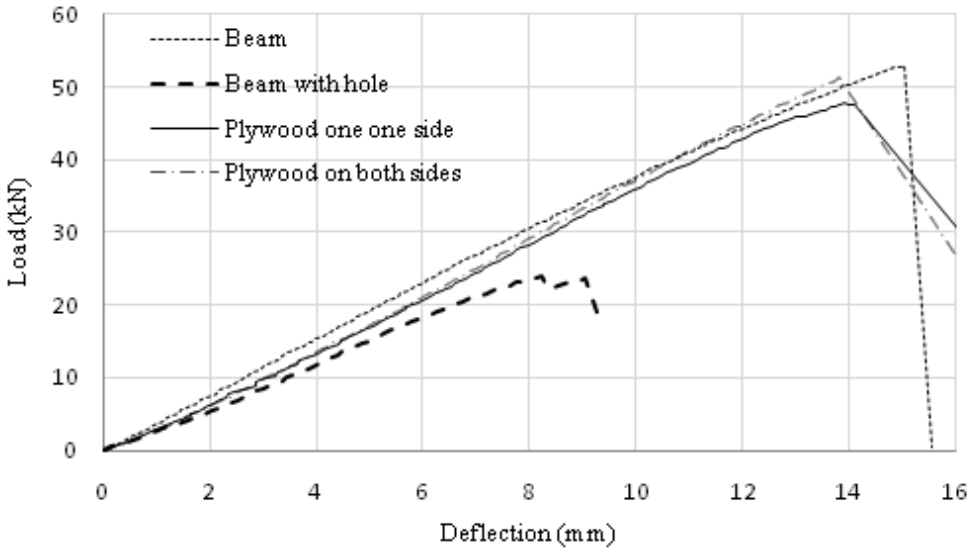

Figure 3.18. Comparison of load deflection curves at mid-span of the beams for different plywood reinforcement methods

3.4.6 Reinforcing using a steel bracket

A steel bracket is also an option for reinforcing holes in LVL beams for the New Zealand market. A bracket is a U shaped steel channel that is nailed to both sides of a beam. The nailing pattern on both sides of a beam coincides with each other. The term "Bracket" is adopted from manufacturer of the product. Brackets are produced for beam depths of 140 mm, 190 mm, 240 mm and 290 mm. Brackets for 190 mm deep beams were installed with 44 nails and tested with different hole sizes. Experiments showed that because the hole in the bracket is larger than the hole in the LVL, cracks could grow and move toward the bracket, which stopped continued crack propagation. For beams with smaller holes ($h_d/h \leq 0.4$), the failure was governed by mid-span failure, but for the case where ($h_d/h = 0.5$), the bracket caused stress concentrations around the nails/edges and failure started from the bracket expanding toward mid-span. For a larger hole ($h_d/h > 0.5$), failure was governed by crushing of wood in the bracket. Failure mechanisms for beams reinforced with brackets are presented in Figure 3.19.

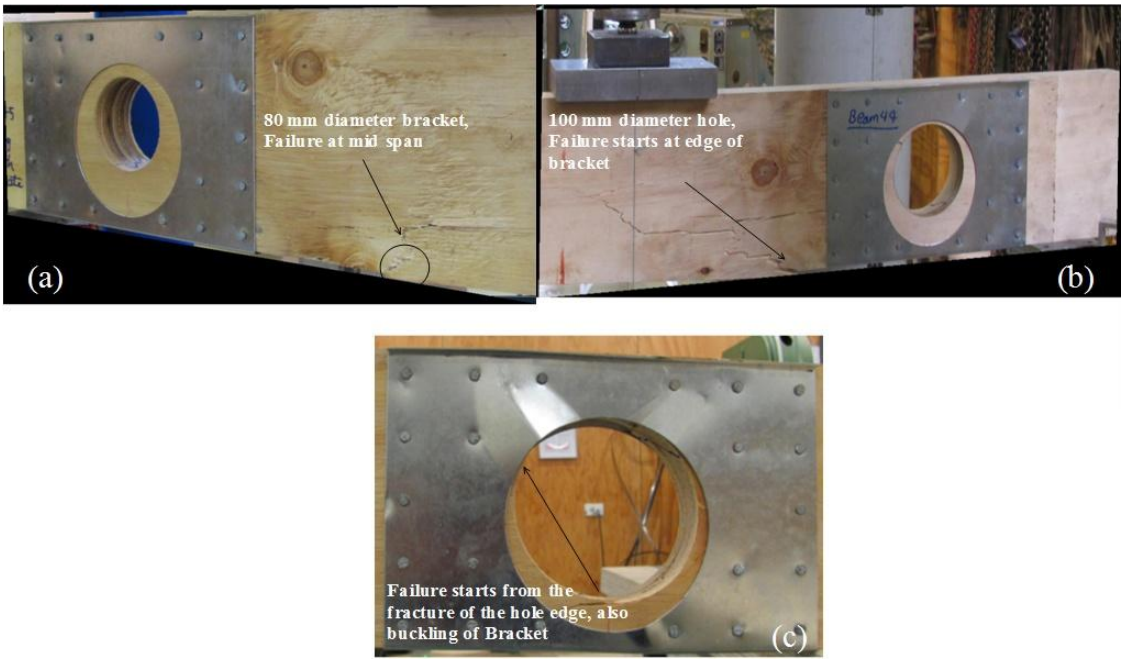

Figure 3.19. Different failure mechanisms of beams reinforced with brackets: (a) failure at mid span, (b) failure starting from the bracket, (c) failure of LVL in the bracket

Using ABAQUS (Habbitt et al. 2010b), a finite element model of a beam was created using orthotropic elastic material properties of LVL adopted from chapter 2 (Table 2.2). The modulus of elasticity of 210000 MPa and Poisson's ratio of 0.3 were used for modelling steel at the supports and loading point. The elastic analysis was performed with 10 kN load applied at mid-span using the geometry parameters presented in Figure 3.20 (a).

Figure 3.20 (b) shows that in the shear dominant parts of the beams, diagonal parts are going into tension (red part) and compression (blue part). The steel buckling can occur because of the compression fields (Figure 3.20 (c)). In addition, buckling occurred in two areas, which correlates well with the presented finite element analysis results. The buckling of the steel plate is a deficiency of brackets.

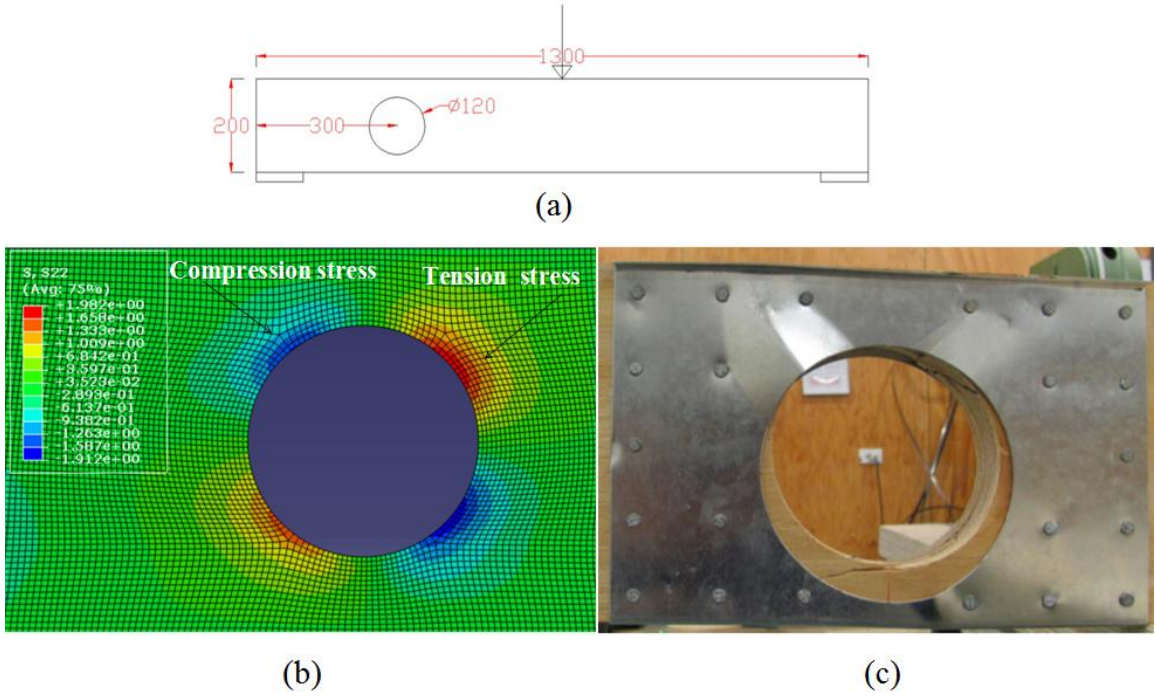

Figure 3.20. Finite element analysis of the beams with the holes: (a) sketch of the beam, (b) finite element analysis, (c) buckling of steel

The load-deflection curves for beams reinforced with brackets are presented in Figure 3.21. The improvement due to the bracket in the strength of the beam is clear. The effectiveness of the reinforcement for 100 mm hole diameter is higher (Figure 3.21 (d)) because the bracket is closer to the hole crack surface while in the 80 mm it is rather far

from the hole edge. More plastic deformations for a diameter of 120 mm is because of the wood crushing in the bracket

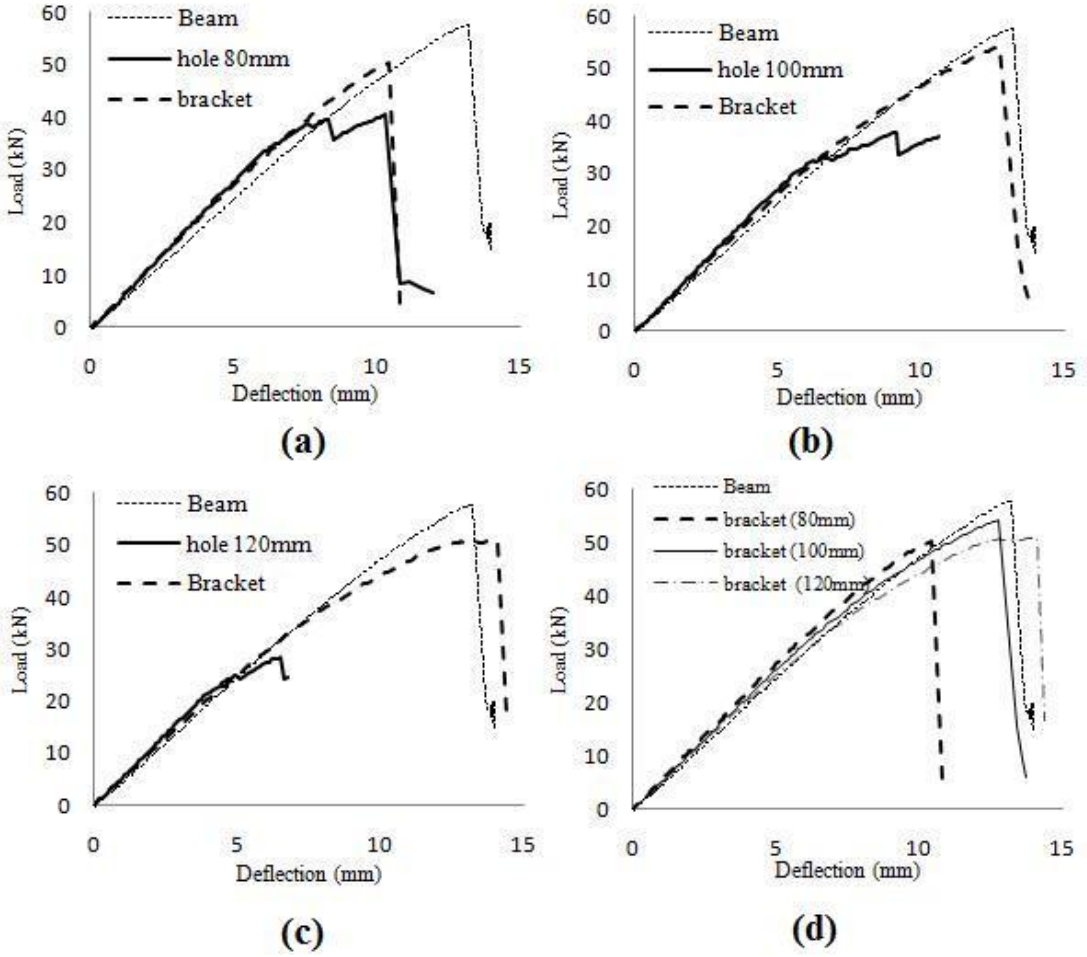

Figure 3.21. Load-deflection curves at mid-span of the beams using brackets: (a) 80 mm diameter hole, (b) 100 mm diameter hole, (c) 120 mm diameter hole, (d) a comparative plot of the different holes sizes

3.4.7 Reinforcement of thick LVL beam with hole

Another important reinforcing issue investigated was the effectiveness of plywood for use with thicker specimens. Reinforcement like plywood works well for thin specimens but for thicker specimens plywood may not work because it is attached to the outer surface of the beam. Therefore testing was conducted on two LVL beams (2450×300×45 mm) glued and screwed together to give a thickness of 90 mm to check the effectiveness of plywood reinforcement, as shown in Figure 3.22. Some experiments

were also performed on LVL beams reinforced with vertical screws for comparison purposes. For both types of reinforcement, experiments showed that the mode of the failure was a mid-span failure.

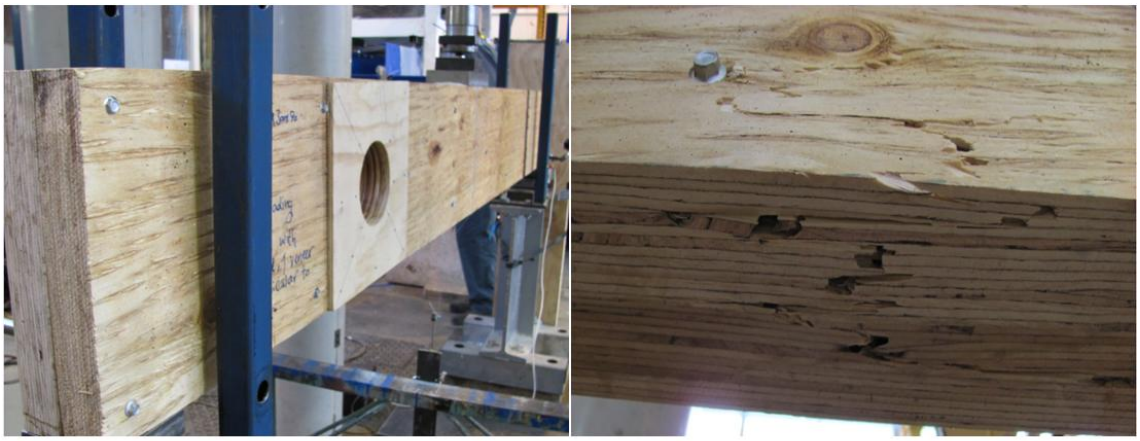

(a) (b)

Figure 3.22. Thick beam tests: (a) reinforced with plywood, (b) mid-span failure

3.5 Strain field around holes

It is rather complicated to obtain the strain field from experiments in a region using strain gauges because a strain gauge calculates average strain over a limited region of a beam. Image photogrammetry was used to obtain the strain field in beam number 37 adopted from Table 3.3. Figure 3.23 (a) presents a sketch of the experimental setup while Figure 3.23 (b) shows a picture of the experiment. The painting around the hole helps in the tracking of the particles.

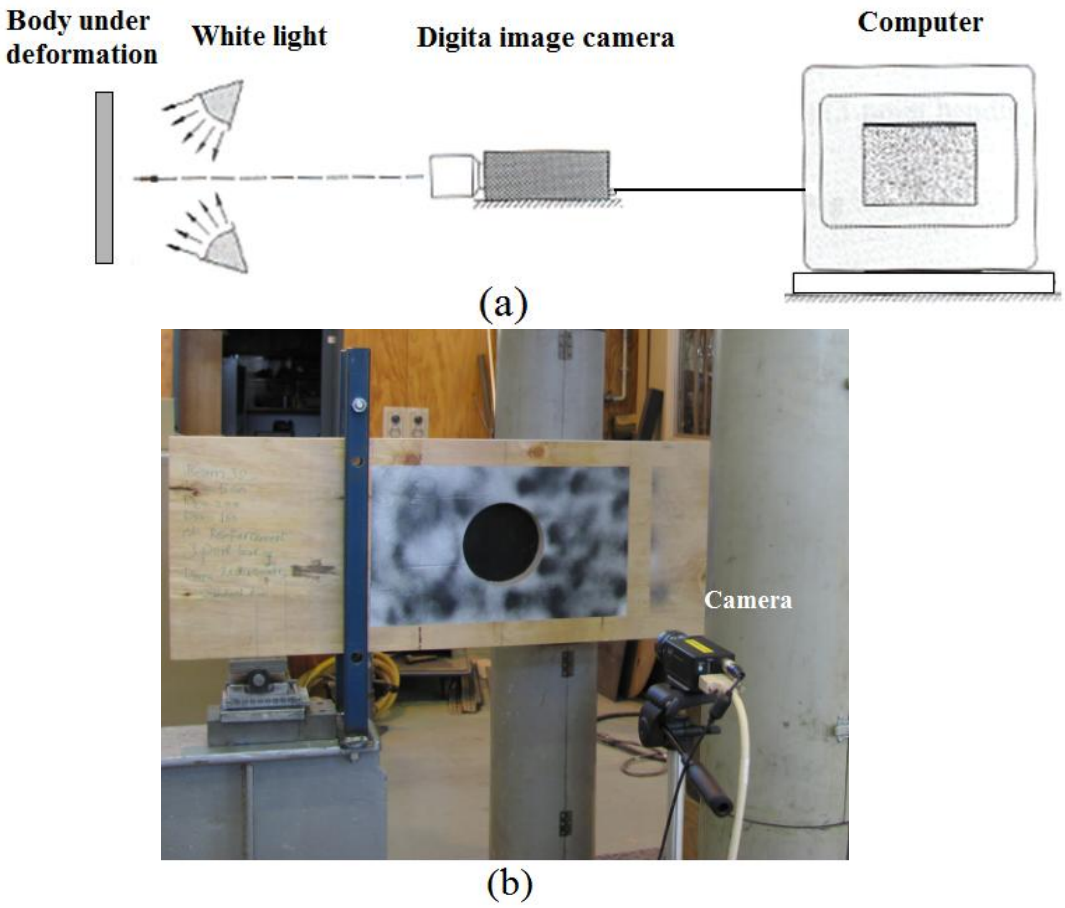

Figure 3.23. (a) Sketch of experimental set up of a image photogrammetric, (b) picture of experimental set up

Digital Image Correlation (DIC) as developed by Christopher (2006) was used for the analysis of the pictures taken by digital camera at a speed of 1 picture per second. Analysis of a small part of the beam as shown in Figure 3.24 (a) was investigated because cracking was propagating through that portion of the beam. The software uses a grid of points to track points in different pictures. Figure 3.24 (b) shows the grid. While the green colour shows the original position of the points, the red colour shows the deformed position of the point.

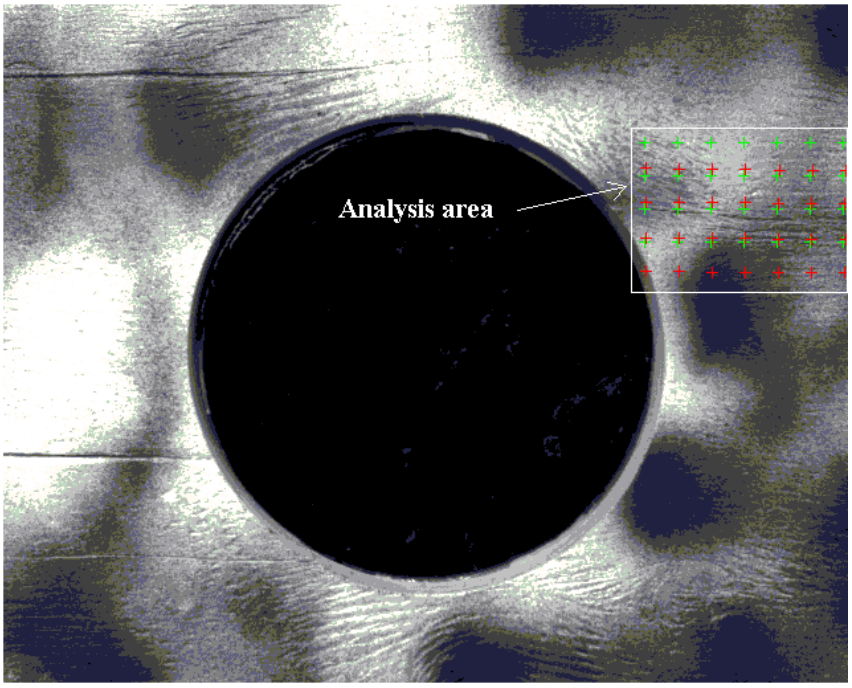

(a)

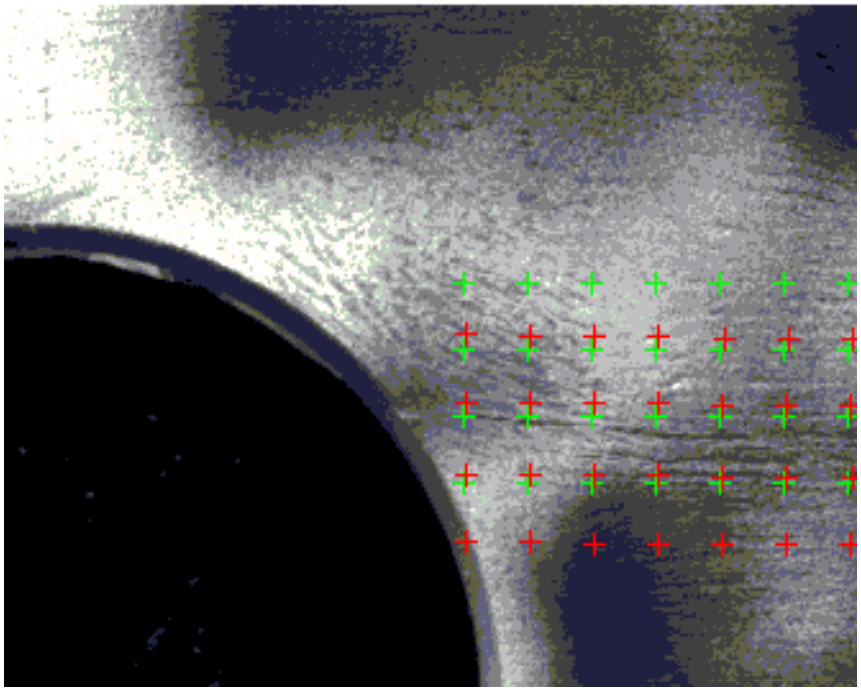

(b)

Figure 3.24. (a) Region under investigation, (b) grid used for the analysis

The predicted strains for different images using different grids are presented in Figure 3.25.

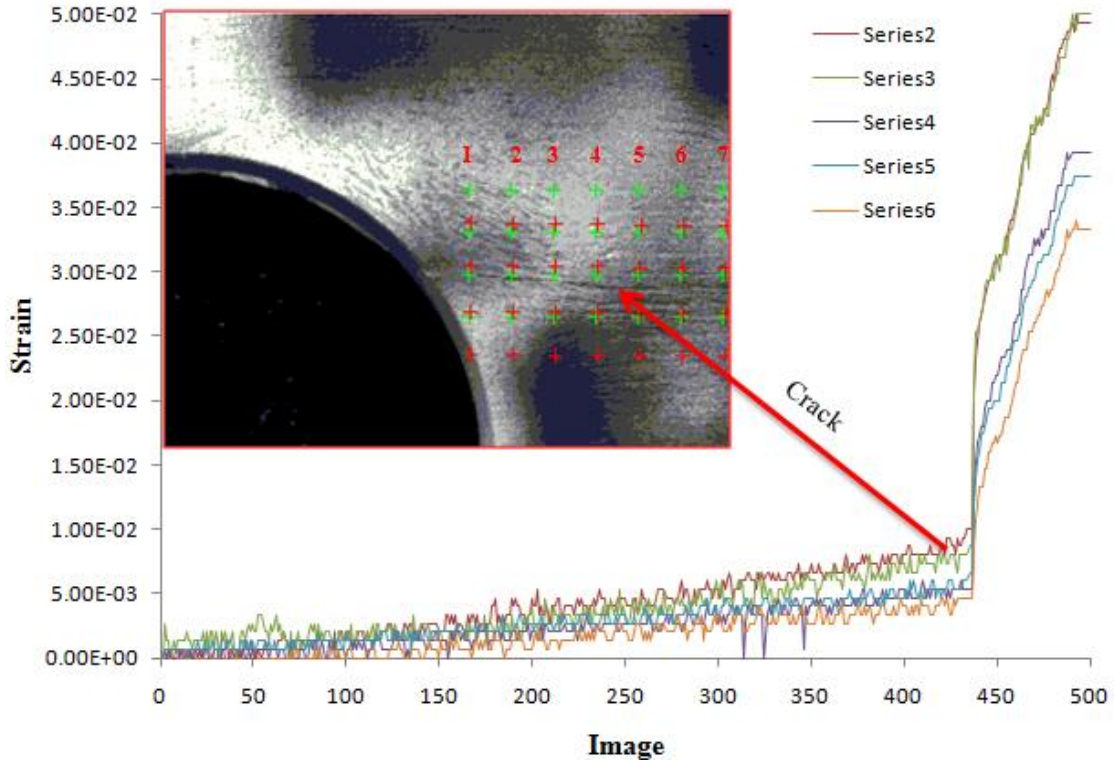

Figure 3.25. Increasing of strain in different images

The image shows that by gradually increasing the applied load on the beam, the strain surrounding the hole will increase. The beam cracked at a strain of 0.004 to 0.005 and then the strains increased rapidly. Comparing different series of data, the strain in grids closer to the hole edge during the loading process are higher than the strain at a farther distance. In the analysis, series 1 and series 7 of the grid shown in Figure 3.25 were deleted because they were mis-tracked by the software and caused unreasonable results.

3.6 Discussion

The results of the experimental program are presented in Table 3.4. In the table, cracking loads were recorded when cracks were observed on the surface of the beams and failure loads were the maximum load carried by beams.

Table 3.4. Experiments on beams with holes and reinforcement

Beam	Diameter (mm)	Reinforcement	Average cracking load (kN)	Average failure load (kN)	Failure description
1	no hole	-	-	57.8	-
2	80	no	30.0	40.5	crack propagation around the hole
3	100	no	24.0	36.9	crack propagation around the hole
4	120	no	20.0	28.5	crack propagation around the hole
5	80	steel bracket	43.7	50.3	mid span failure
6	100	steel bracket	35.3	54.0	failure from steel edge to centre
7	120	steel bracket	35.2	50.9	failure at the hole edge
8	no hole	-	-	53.1	mid span failure
9	50	no	-	50.5	mid span failure
10	65	no	30.0	48.0	crack propagated around the hole
11	80	no	24.9	39.4	crack propagation around the hole
12	100	no	20.7	30.6	crack propagation around the hole
13	80	plywood on both sides	41.0	54.4	mid span failure
14	80	plywood on one side	34.0	49.7	crack propagation around the hole
15	80	two screws	29.2	44.9	mid span failure
16	80	inclined screws	42.0	56.6	mid span failure
17	no hole	-	-	42.9	mid span failure
18	80	no	20.8	28.7	crack propagation around the hole
19	100	no	20.5	28.3	crack propagation around the hole
20	80	epoxy in rod	-	37.0	hole edge failure
21	80	epoxy in rod	32.5	47.0	mid span failure
22	65	epoxy in rod	40.8	46.7	mid span failure
23	no hole	-	-	69.3	mid span failure
24	50	no	-	74.0	mid span failure
25	80	no	53.0	57.3	crack propagation around the hole
26	120	no	38.5	55.9	crack propagation around the hole
27	150	no	34.1	40.3	crack propagation around the hole
28	120	two screws	44.0	76.3	mid span failure
29	120	plywood on both sides	45.7	72.2	mid span failure
30	120	inclined screws	45.6	66.2	mid span failure
31	120	epoxy in rod	42.5	77.0	mid span failure
32	150	two screws	31.0	65.0	hole edge fracture

Beam	Diameter (mm)	Reinforcement	Average cracking load (kN)	Average failure load (kN)	Failure description
33	estimated	-	-	112.5	-
34	120	two plywood	-	119.0	mid span failure
35	120	two screws	79.0	128.5	mid span failure
36	estimated	-	-	80.0	-
37	160	no	55.0	67.3	crack propagation around the hole
38	160	no	40.0	51.5	crack propagation around the hole
39	160	no	36.1	48.7	crack propagation around the hole
40	160	two screws	47.0	82.9	mid span failure
41	estimated	-	-	70.0	-
42	120	no	38.0	46.7	crack propagation around hole
43	120	two screws	44.5	54.0	mid span failure
44	120	two plywood	56.0	67.0	mid span failure
45	150	two plywood	52.0	59.3	mid span failure
46	95	epoxy in rod	43.3	58.0	mid span failure
47	120	epoxy in rod	43.5	61.8	mid span failure
48	estimated	-	-	80.0	-
49	120	epoxy in rod	48.5	88.7	mid span failure

Load-deflection data of similar beams with a hole (Beam 26), a hole and screw reinforcement (Beam 28), a hole and inclined screw reinforcement (Beam 30), a hole and plywood reinforcement (Beam 29), and without hole (Beam 23) have been presented in Figure 3.26. It can be observed that slopes of the load-deflection curves of beam with a hole and a beam with a hole reinforced with screws are nearly the same, while the beam with plywood reinforcing is slightly higher. Also, the failure load of the beam with screws is higher than the beam without reinforcement and the beam reinforced with plywood exhibited the highest failure load. However, this result could be questioned and attributed to the Coefficient of Variation (COV) of the material but the effectiveness of the reinforcement in the recovering of beam capacity is clear. The difference between the curves seems logical because the failure of the beam with a hole and without reinforcement was governed by crack initiation near the hole, while the failure of beams with reinforcement was governed by mid-span failure. For beams with reinforcement by screws, cracks can also form and propagate until they reach the screws, but for beams reinforced with plywood cracks usually could not propagate.

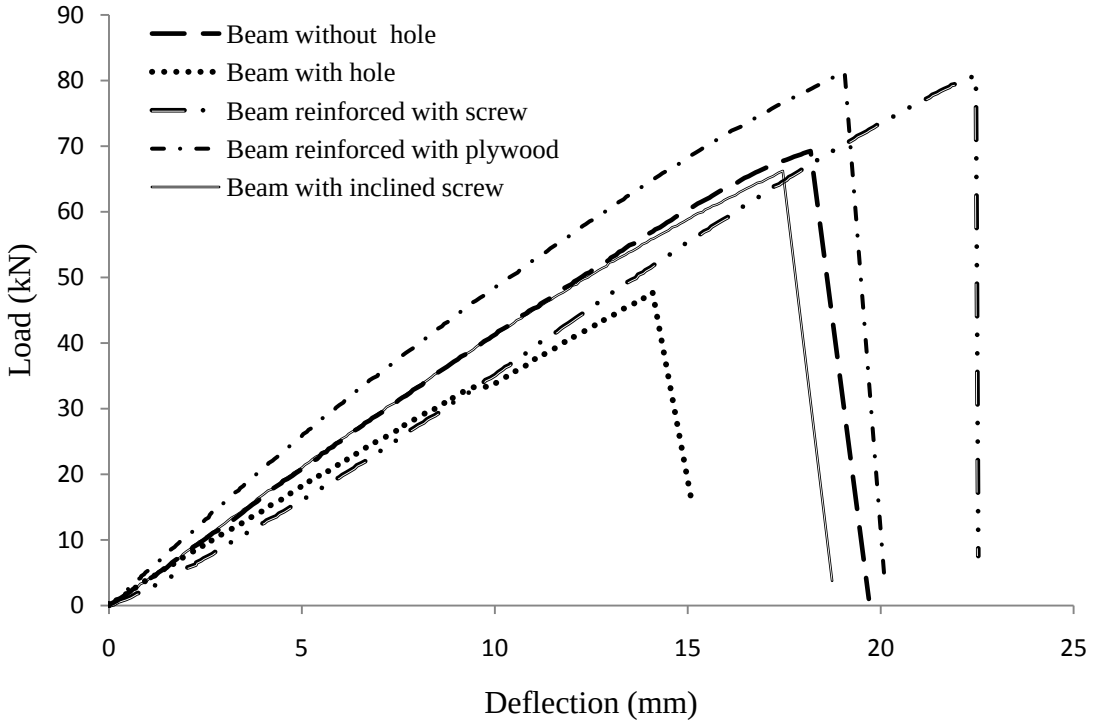

Figure 3.26.Comparison of different cases of reinforcement around holes in LVL beams at the mid-span of the beam

A comparison of the cracking load with the failure load for beams of 2100×300×45 mm shows that the cracking load for holes of 80 mm, 120 mm, and 150 mm diameter is about 76%, 56%, and 49% of the final failure load of beam without a hole respectively.

From a comparison of the failure load of a beam 2100×300×45 mm with a hole and with beam without hole, a maximum reduction of 42% in the strength for the beam with hole diameter of 150 mm could be observed for 300 mm depth specimens. The reduction is about 19 % for hole diameter of 120 mm and the reduction is about 17% for an 80 mm diameter hole.

3.7 Summary

An experimental program was performed on Laminated Veneer Lumber (LVL) beams with holes. The effect of holes on the strength reduction of the LVL beams was experimentally investigated with hole size, location and shape considered as variables in the experiments. Five methods of reinforcement were considered, namely vertical screws, inclined screws, epoxy grouted rods, plywood, and steel brackets. The effectiveness of reinforcement was dependent on bonding to the LVL and mechanism of stress distribution around the holes. Reinforcement like glued plywood created a good bond with LVL. The connection in the case of bracket was not complete and allowed the steel plate to buckle. The following results were determined based on the previously described experimental program and data analyses:

- While the effect of 50 mm diameter holes on the beam capacity reduction was negligible, holes of larger diameters ranging from 0.3 to 0.6 of beam depth reduced the final capacity from 10 to 52% (a comparison with beam without hole).

- A comparison between the cracking load and the failure load (for a beam of 300 mm depth) of the unreinforced beams with the holes shows that the failure load of the beam is typically 8 to 46 % higher than the cracking load.

- Reinforcements like screws, epoxy grouted rod, brackets and plywood could not prevent crack initiation but was effective at limiting crack propagation.

- Fully threaded screws were an effective method of reinforcement for LVL beams with holes having a diameter to beam depth ratio of less than 0.4. This limit for glulam in DIN 1052 is 0.3, and for glulam in the Swedish glulam design handbook (Carling 2001) is 0.35.

- Limited experimental tests showed that inclined screws are also a successful method for controlling crack propagation around holes and the failure mode of the reinforced beams was mid-span. However, control of screws driving in a straight line is difficult.

- Epoxy grouted rods are as effective as screw reinforcement. The vertical hole for the reinforcing should be avoided on the tensile edge of the beam, or be additionally reinforced by some alternate method (e.g. steel plate).

- Plywood is a promising way of reinforcing LVL beams with the holes. Plywood can restore the failure mode of the beam to that of a beam with no hole. Plywood can effectively prevent crack propagation for large holes. Glue bonding of plywood reinforcement is critical. Plywood plates should be glued on both sides of beams. Gluing on just one side is not very effective in restoring the failure mode of the beam. Gluing makes it possible for internal forces to flow around holes by alternative routes. In the experiments, use of plywood for holes up to 0.5 of the beam depth prevented crack propagation; the full beam capacity was recovered.

- In the experiments, plywood and screw reinforcement also worked well for LVL beams up to 90 mm thick.

- Although manufactured steel bracket can improve the failure load of a beam, steel bracket has potential for buckling due to compression stress field around the hole and not continuous connection with the beam.

- A comparison between different methods of reinforcement shows greater effectiveness of the reinforcement with the plywood in comparison to the other methods, although due to aesthetic constraints, this method may not be feasible in all situations.

- Photogrammetry of a beam with hole shows that the beam cracks at a strain of 0.004 to 0.005 and then strains increase rapidly.

In this chapter, experiments on LVL beams with the holes and reinforcements presented. In the next chapter, an analysis method using Linear Elastic Fracture Mechanics (LEFM) for the failure load predictions of LVL beams with the holes is presented.

4 Analysis of beams with holes using Linear Elastic Fracture Mechanics (LEFM)

This chapter presents an analysis method based on Linear Elastic Fracture Mechanics (LEFM) for failure load prediction of Laminated Veneer Lumber (LVL) beams with holes. The results of this chapter have been used in chapters 8 and 9.The use of presented numerical model is limited to this chapter.

The majority of this chapter has been re-produced from the following papers:

Ardalany M, Deam B, Fragiacomo M, Carradine D (2012)" Experimental and numerical analysis of hole placement in depth of laminated veneer lumber (LVL) beams" (Accepted). Australian Journal of Structural Engineering (AJSE):1-11

Ardalany M, Deam B, Fragiacomo M (2010) Numerical investigation of the load carrying capacity of Laminated Veneer Lumber (LVL) joists with holes. Paper presented at the World Conference on Timber Engineering, WCTE2010, Riva del Garda, Italy.

4.1 Introduction

In Chapter 2, the material properties of Laminated Veneer Lumber (LVL) were presented. Chapter 3 covered the experiments on the LVL beams with holes. The data from these two chapters will be used in the current chapter for analysis of beams with holes.

Openings are often required to allow services to pass through timber beams. Their presence, location and size relative to the beam depth influences the beam strength (Guan et al. 2009). In extreme loading conditions, cracks will develop around the holes and propagate, causing beam failure at much lower loads than would be expected in the absence of any holes as shown in chapter 3. The normal beam design procedures are therefore unable to predict the load carrying capacity of timber beams with penetration holes. Fracture mechanics methods are required to predict crack failure, and propagation of cracks in beams with penetrations. The strength computed using fracture mechanics provides a conservative estimate (lower bound) of the ultimate beam strength (Patton-Mallory et al. 1987).

Different models can be applied viz.: (i) Linear Elastic Fracture Mechanics (LEFM), (ii) Finite Area Theory, and (iii) Fictitious Crack Model (or cohesive layer). There are a number of methods available from fracture mechanics for crack analyses such as:

- Stress Intensity Factor (SIF) approach
- Energy Balance approach
- Strip-yield model according to Dugdale (1960)
- Cohesive crack model according to Barenblatt (Hillerborg et al. 1976)

In the Stress Intensity Factor (SIF) approach, the stresses near the crack tip are studied. These stresses theoretically approach infinity at the crack tip ($r \to 0, \sigma = \frac{K}{\sqrt{2\pi r}} \to \infty$), where K is the SIF and is a coefficient. K is dependent upon the load, the crack dimension, beam geometry and constitutive law of the material. When K reaches the critical (K_c) value the crack propagates. The SIF method has been implemented in finite element analyses; the method could not explain the crack formation but can predict failure load.

In the Energy Balance approach, energy release rate (G) also termed crack extension force is the released energy at infinitesimal crack extension which is absorbed in the form of new surface formation. On the resistance side, (G_c) is the material resistance which under ideal conditions (linear elastic, fully brittle) is two times the surface energy. The crack propagates when the energy release rate (G) is greater than crack propagation energy ($G \geq G_c$).

In the Dugdale model (Dugdale 1960), it is assumed that there is a plastic zone near the crack tip where the stresses are equal to the yielding stress of the material. The Barenblatt model (adopted from (Hillerborg et al. 1976)) is similar to that of Dugdale except for a small difference in the stresses that are assumed to vary with deformation.

A cracked body can be loaded in any individual or combination, of the three displacement modes as shown in Figure 4.1. Mode I (opening) is caused by tensile load whereas mode II (shearing) and mode III (tearing) are caused by shearing loads as shown (Norman 2009). In beams with holes a combination of mode I and mode II occurs, so the potential cracks in the beams are subject to local opening and shearing stresses (Ranta-Maunus 1990).

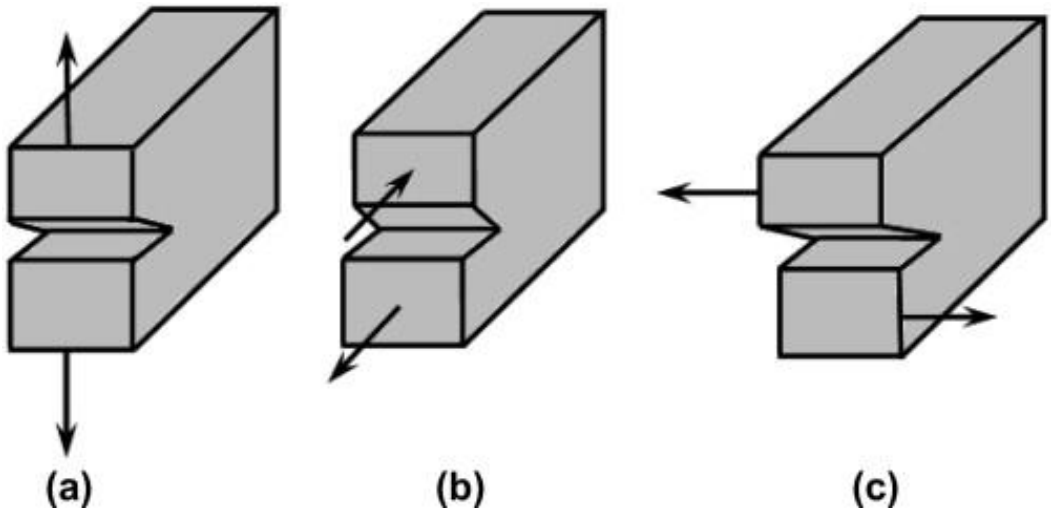

Figure 4.1. The basic modes of crack propagation: (a) opening, (b) shearing, (c) tearing

4.2 Linear Elastic Fracture Mechanics (LEFM)

Fundamental fracture mechanics were first described by Griffith (1921). In the case of sharp notches and stress concentrators, conventional stress criteria should not apply and fracture mechanics techniques should be used. There are essentially two methods used in LEFM analysis to describe crack formation/propagation viz.: (i) Stress Intensity Factor (SIF) approach and, (ii) Energy balance approach (Ardalany et al. 2010a). If only mode I (opening) is assumed then the stress in a plane of a crack can be written as Equation (4.1):

$$\sigma = \frac{K_I}{\sqrt{2\pi r}} \tag{4.1}$$

where r is the distance from the crack tip, and K_I is stress intensity factor. For an infinitely large plate with a crack length of $2a$ under a tension stress of σ perpendicular to the crack orientation, the stress intensity factor is:

$$K_I = \sigma\sqrt{\pi a} \tag{4.2}$$

For other geometries and loading, a geometry coefficient f is added.

$$K_I = \sigma\sqrt{\pi a} f \tag{4.3}$$

Irwin (1958) introduced K_{Ic} for the critical value of the SIF, and introduced the following failure criterion.

$$K_I = K_{Ic} \tag{4.4}$$

Griffith (1921) proposed an energy approach for the unstable failure resulting from a crack. He did his work using glass. Griffith noticed that when an existing crack of Δa expands whilst at the same time the points where the energy are applied do not move, the elastic energy of the body decreases. This change of elastic energy of the body (ΔW) is defined in Equation (4.5).

$$\Delta W = -G_I B \Delta a \tag{4.5}$$

where $G_I$the strain energy release rate, and B is the thickness of the plate.

As the crack grows, the atomic layers at the crack tip are torn apart. This implies that work is carried out, and if the work per unit new area is termed θ, it implies that the following work has been performed on the system:

$$\Delta\Gamma = 2\theta B\Delta a \tag{4.6}$$

In addition, the crack will propagate if the total energy in the body is unchanged or reduced, i.e.:

$$\Delta W + \Delta\Gamma \leq 0 \tag{4.7}$$

So, the following relation could be obtained:

$$G_I = 2\theta \tag{4.8}$$

Finally, Griffith found:

$$\sigma = \sqrt{\frac{GE}{\pi a}} \tag{4.9}$$

This by re-arrangement implies:

$$K_I = \sqrt{G_I E} \tag{4.10}$$

Moreover, in the critical case:

$$G_I = G_{Ic} \tag{4.11}$$

The above are derived with the assumption of isotropic material properties. However, for orthotropic materials, it is important that this effect is included.

SIF method can be used to study the stresses near the crack tip. In beams with holes, due to the mixed mode fracture at the crack tip, closed form solutions are difficult to formulate. Some formulations (e.g. (Riipola 1995)) require complex calculus and are only available for limited crack lengths, loading conditions and boundary conditions.

Another popular and general method for SIF calculations takes advantage of the elastic Finite Element Method (FEM). FEMs are well developed and have fewer limitations on the boundary and loading conditions.

4.3 Evolution of SIFs in mixed mode problems

The values of the SIFs are critical to the prediction of the failure load of beams with holes. Two methods are incorporated in ABAQUS (Habbitt et al. 2010b) which is a suite of software applications for finite element analysis, for the stress intensity factor calculation. The first is the displacement extrapolation technique and the second is the virtual crack closure integral method.

The displacement extrapolation technique calculates the SIFs using the horizontal and vertical displacements at the crack tip by a method proposed by Chen et al. (1993). This derivation comes from Sih et al. (1965). It is shown that if this crack is aligned with one of the main directions at the crack tip, the stress and the displacement fields are similar to those of an isotropic material. It can be expressed as the sum of three independent modes. The virtual crack closure integral calculates the values of energy release rates. The calculated energy is for unit crack closure. The values of the SIFs can be calculated from the relationship between the SIFs and the energy release rate.

It is well known that the values calculated from the Energy Approach provide better predictions than displacement extrapolation methods. However, the recent literature (Guinea et al. 2000) introduces a collapsed rectangular 8-node quarter point elements around the crack tip for the SIF calculations that gives improved predictions (Figure 4.2). Figure 4.2 (b) presents the collapsed elements. This will be discussed more in the next part.

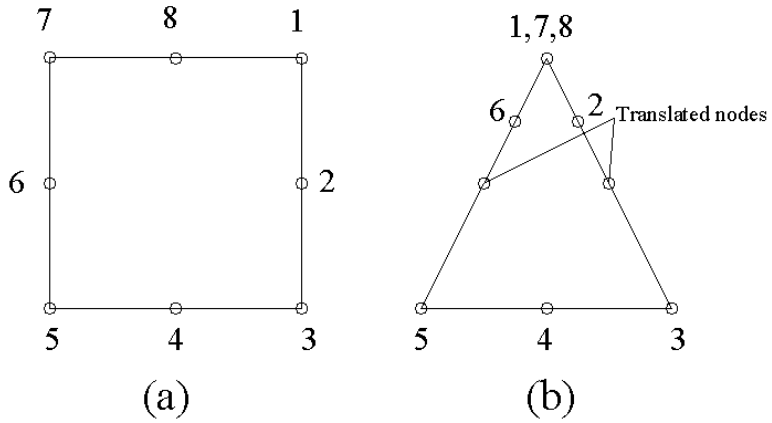

Figure 4.2. (a) Plane quadratic element, (b) collapsed quarter point element

4.4 Finite element modelling

Finite element modelling of wood is a significant challenge. Assuming a homogenous material for modelling of wood is necessary to simplify the analysis. Wood may be described as an orthotropic material for its elastic deformation which requires twelve constants to describe it, nine of which are independent, including three moduli of elasticity, three shear moduli, and six Poison's ratios (3 independent) in the elastic region (Green 2001). However, the nine constants decrease to four independent values in 2D modelling.

Finite Element Modelling (FEM) of the beams with holes was implemented in the ABAQUS package (Habbitt et al. 2010b). The procedure is summarized as follows:

- Orthotropic elastic modelling and analysis of a LVL beam with a hole in order to obtain the most probable location of crack initiation, which is the point with the highest stress concentration. The direction of crack propagation for wood will be in the grain direction.

- Hypothetic cracks with different lengths are introduced into the model. The 'seam' option of ABAQUS is used for the crack modelling, where a 'seam' is a crack that can open if loaded. The model is analysed under unit loading.

- After re-meshing and re-analysis the SIFs at the crack tip in modes I and II are obtained. Fine meshing is used near the crack tip along with special elements

(collapsed quarter point elements) because the software uses rings of elements for the calculation of the SIFs in opening and shearing modes.

- Hypothetic crack length in the model is calculated from the point stress criterion approach that was presented by Gustafsson (1993b)
- Use an appropriate mixed mode fracture criterion, the failure load of the LVL beam with hole is calculated. Here, the failure load using different mixed mode fracture criteria (Jernkvist 2001a,b; Romanowicz et al. 2008) are calculated as well for comparison purposes.
- In order to simplify modelling, plane stress is assumed for the beam. The finite element model used is a 2D orthotropic model with shell elements loaded at the mid-span. The material properties for modelling of the LVL adopted from chapter 2.

The steel plates forming the supports, and under the loading points were assumed to behave as linear elastic with the modulus of elasticity of 210000 MPa and Poisson's ratio of 0.3.

Meshing of the model was performed with special care. The crack tip was modelled with a ring of triangular collapsed quarter point elements, with five degrees of freedom in each node (S8R5). The region around the crack tip was modelled with eight node doubly curved thick shell elements (S8R). To improve the accuracy of the predictions, the middle node of the elements close to the hypothetic crack tip was moved to half of its way closest to crack tip to create a singularity of $1/\sqrt{r}$ (Figure 4.3 (b)). Theory shows that for linearly elastic conditions, stresses near the crack tip are proportional to $1/\sqrt{r}$. Although, the normal elements cannot represent the $1/\sqrt{r}$ singularity, they can be used to obtain stress intensity factors (Cook 2002). According to Henshell et al. (1975) and Barsoum (1976) the theoretical stress or strain singularity of $1/\sqrt{r}$ can be obtained exactly by moving the mid-side nodes of the elements surrounding the crack tip to the 1/4 positions (Lin et al. 1999) and hence the stress intensities could be calculated using the Equation (4.12):

$$K = \frac{E}{4(1-\nu^2)}\sqrt{\frac{2\pi}{r_{0.25}}}u_{z(0.25)} \tag{4.12}$$

In Equation (4.12), K is the stress intensity factor, E is the modulus of elasticity, ν is the Poison's ratio, and $r_{0.25}$ is a quarter of the distance of the element from the crack tip. The vertical displacement $u_{z(0.25)}$ is shown in Figure 4.3 .

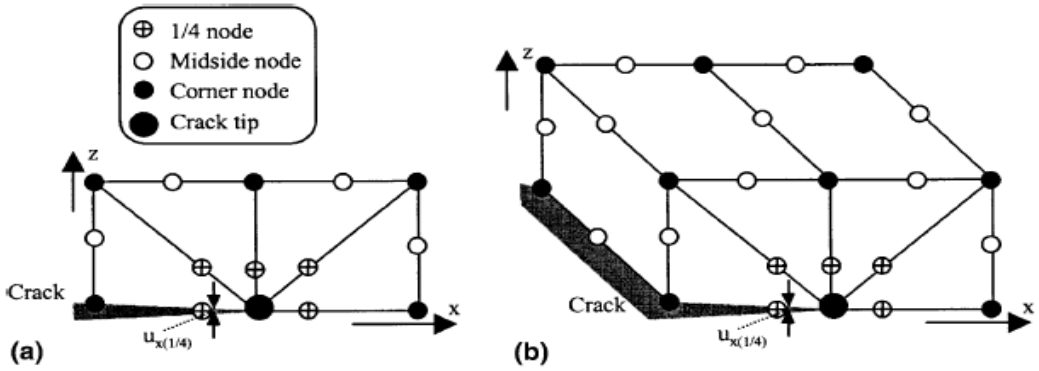

Figure 4.3. Meshing around crack tip and vertical displacement $u_{z(0.25)}$: (a) 2D, (b) 3D (Lin et al. 1999)

The rings used by ABAQUS need to be of uniform size, otherwise the calculated stress intensities will not converge using either ring. In the calculations of the stress intensity factors, usually the first few contour integrals, which are based on few first mesh rings, should be ignored because they are very close to the hypothetic crack tip and may yield quite unreliable values. The rings of elements have been presented in Figure 4.4.

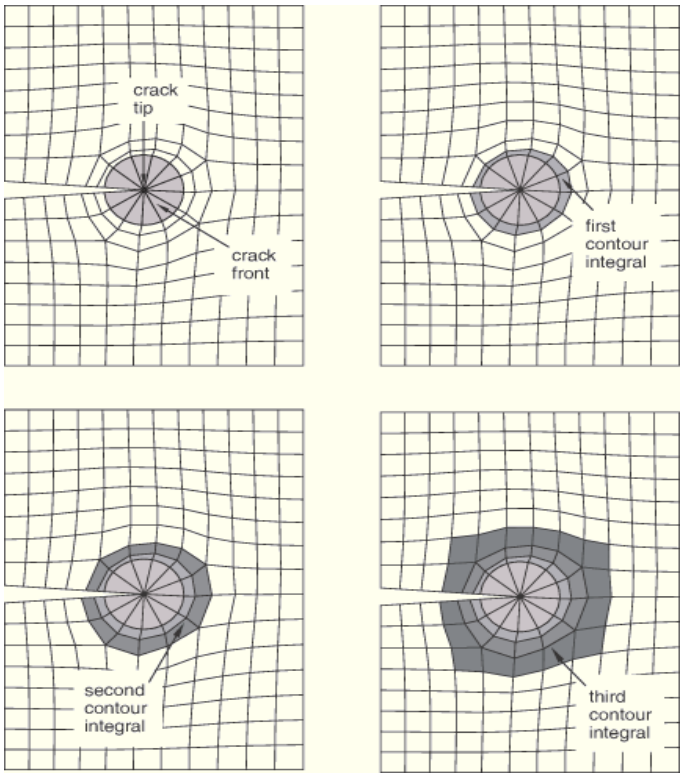

Figure 4.4. Rings of elements used for the calculations of the stress intensity factors (Habbitt et al. 2010b)

The software for calculation of SIFs automatically detects the crack tip, recognizes the first ring of elements surrounding it, and then continues adding other rings depending upon the number of the output requested contours.

4.5 Mixed mode fracture criteria

When a beam with a notch or a hole is subjected to bending, two fracture modes usually exist at the crack tip, namely opening and shearing. In other words, a combination of opening and shearing of the crack tip will simultaneously occur and govern the fracture of the whole system. Wu (1967) suggested a mixed mode fracture criterion for failure load prediction. Wu's mixed mode fracture is a general fracture criterion for anisotropic composite materials (Smith et al. 2003a).

The proposed fracture criterion is defined as below:

$$(\frac{K_I}{K_{IC}}) + (\frac{K_{II}}{K_{IIc}})^2 = 1 \qquad (4.13)$$

$$K_I = k_I \times F_u \quad (4.14)$$

$$K_{II} = k_{II} \times F_u \quad (4.15)$$

where K_I is stress intensity factor of LVL in mode I (opening), K_{II} stress intensity factor of LVL in mode II (shearing), K_{IC} fracture toughness of LVL in mode I, K_{IIC} fracture toughness of LVL in mode II, k_I, k_{II} SIFs in modes I and II respectively obtained in the case of a beam under unit loading, and finally F_u is failure load.

Figure 4.5 provides graphical representation of the mixed mode fracture criterion. The plot represents a fracture envelope for an arbitrary fracture mode. If the specimen goes into pure mode I or mode II, there will be no interaction and the fracture envelope will be a straight line.

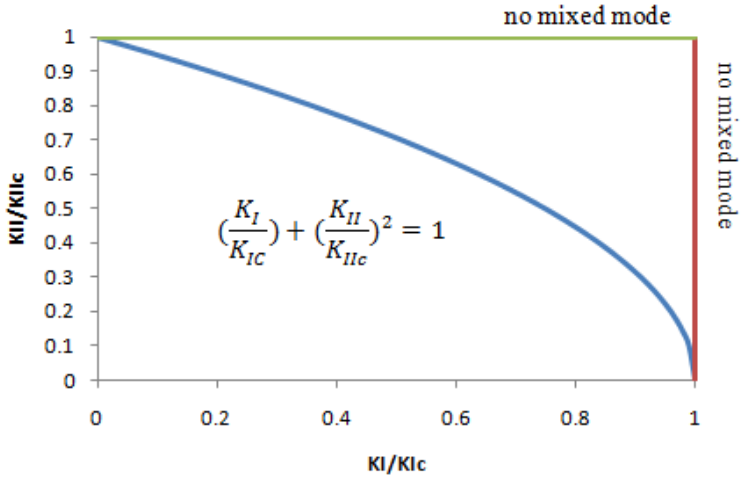

Figure 4.5. Wu's mixed mode fracture criterion

By inserting Equation (4.14) and (4.15) in the Equation (4.13), the following equation is obtained:

$$(\frac{k_I \times F_u}{K_{Ic}}) + (\frac{k_{II} \times F_u}{K_{IIc}})^2 = 1 \quad (4.16)$$

By solving Equation (4.16), F_u can be calculated. With the assumption of the crack oriented along the wood fibres, another mixed mode fracture criterion based on the strain energy release rate could be obtained (Jernkvist 2001a; Romanowicz et al. 2008):

$$K_I{}^2 + \beta_1 K_{II}{}^2 - K_{Ic}{}^2 = 0 \tag{4.17}$$

In Equation (4.17) β_1 is defined as below:

$$\beta_1 = (\frac{K_{Ic}}{K_{IIc}})^2 \tag{4.18}$$

If Equation (4.17) is divided by $K_{Ic}{}^2$, and using the definition of β_1 as defined in Equation (4.18), Equation (4.17) becomes:

$$(\frac{K_I}{K_{IC}})^2 + (\frac{K_{II}}{K_{IIc}})^2 = 1 \tag{4.19}$$

This equation is very similar to Wu's fracture criterion, which can be generalized as the following:

$$(\frac{K_I}{K_{IC}})^m + (\frac{K_{II}}{K_{IIc}})^n = 1 \tag{4.20}$$

where m, n are calibration factors, to be determined via experimental testing. Equation (4.20) is a general case of Equation (4.19) where $m = n = 2$. The ultimate load F_u can then be derived by substituting Equations (4.14) and (4.15) in Equation (4.19), viz.:

$$F_u = \sqrt{\frac{K_{Ic}{}^2}{(k_I{}^2 + k_{II}{}^2 \beta_1)}} \tag{4.21}$$

Fracture criteria expressed in different analytical forms can be obtained if the crack growth is assumed to be governed by the magnitude of near crack tip stresses rather than the strain energy (Jernkvist 2001a).

Another stress-based fracture criterion can be derived by assuming that fracture occurs when the maximum principal stresses at a distance (r) in front of the crack tip attain a critical value (Jernkvist 2001a):

$$\frac{1}{(\beta_3 + \sqrt{\beta_4})}\left(\beta_3 K_I + \sqrt{\beta_4 K_I{}^2 + K_{II}{}^2}\right) - K_{Ic} = 0 \tag{4.22}$$

In Equation (4.22) β_3 and β_4 are coefficients which depend solely on the elastic properties of the material. Such coefficients could also be obtained using analytical formulas (Romanowicz et al. 2008).

Using Equations (4.14) and (4.15), Equation (4.22) is re-written as:

$$F_u = \frac{K_{Ic}\left(\beta_3 + \sqrt{\beta_4}\right)}{\beta_3 k_I + \sqrt{\beta_4 {k_I}^2 + {k_{II}}^2}} \tag{4.23}$$

Previous studies in the literature indicated that the Wu is mixed mode yield criterion gives good predictions; consequently, Wu's criterion will be used in this thesis.

4.6 Hypothetic crack length calculations

Fracture mechanics studies analysis of mechanical failure developed by the separation of material due to cracking or the behaviour of an existing crack in the member. Theoretically, in LEFM the stress at the crack tip tends to infinity while exponentially decreasing along the crack length. Gustafsson (1993b) proposed two formulations for the hypothetic crack length calculations based on the Norris failure criterion (Norris 1962). Two sets of formulations, called the Mean Stress Criterion Approach and the Point Stress Criterion Approach are introduced in resulting hypothetic crack length calculations.

In the mean stress criterion approach, mean values of the tensile and shear forces are used in the Norris failure criterion. The length of the hypothetic crack is selected such that the Norris failure criterion $\left(\left(\frac{\sigma}{f_t}\right)^2 + \left(\frac{\tau}{f_v}\right)^2 = 1\right)$ gives values equal to the Wu's mixed mode criterion.

In the point stress criterion approach, the hypothetic crack length is calculated in such a way that it yields a failure load equal to the load predicted using a normal failure criterion. The hypothetic crack length predicted by the mean stress criterion approach is two times larger than the hypothetic crack length predicted by the point stress approach. In the point stress approach, the hypothetic crack length is calculated using the following equations.

$$2X_0 = \frac{2}{\pi}\frac{E_I G_{Ic}}{f_t^2}\frac{E_x}{E_y}\left(\frac{G_{IIc}}{G_{Ic}}\right)^2 \frac{1}{4k^2}\left(\sqrt{1+4k^2\sqrt{\frac{E_y}{E_x}}\frac{G_{Ic}}{G_{IIc}}}-1\right)^2\left(1+\frac{k^2}{\left(\frac{f_v}{f_t}\right)^2}\right) \quad (4.24)$$

$$\frac{1}{E_I} = \frac{1}{E_x}\sqrt{\frac{E_x}{2E_y}}\sqrt{\sqrt{\frac{E_x}{E_y}}+\frac{E_x}{2G_{xy}}-\nu_{yx}\frac{E_x}{E_y}} \quad (4.25)$$

$$\frac{1}{E_{II}} = \frac{1}{E_x}\sqrt{\frac{1}{2}}\sqrt{\sqrt{\frac{E_x}{E_y}}+\frac{E_x}{2G_{xy}}-\nu_{yx}\frac{E_x}{E_y}} \quad (4.26)$$

where, x_0 signifies the hypothetic crack length which is half of the hypothetic crack length obtained using the mean stress criterion method, f_v is the shear strength of the LVL in the crack plane, f_t is the tensile strength of the LVL in the perpendicular to grain direction, G_{Ic} and G_{IIc} are the critical energy release rate values in mode I and II respectively, k is the mixed mode ratio defined as K_{II}/K_I, and E_I and E_{II} are equivalent moduli of elasticity for orthotropic materials calculated from the above formulas. Also, the relationship between stress intensity factors and fracture energy can be expressed as below:

$$K_I = \sqrt{E_I G_I} \quad (4.27)$$

$$K_{II} = \sqrt{E_{II} G_{II}} \quad (4.28)$$

For the special case of pure mode I, the relationship of hypothetic crack length would be summarized as below:

$$2X_0 = \frac{2\,E_I G_{Ic}}{\pi\, f_t^2} \quad (4.29)$$

Also for pure mode II:

$$2X_0 = \frac{2\,E_{II}G_{IIc}}{\pi\,f_v^2} \tag{4.30}$$

4.7 Experimental data

Experimental data from chapter 3 Table 3.4 were used for the comparison of the model results with the experiments. The tests results on the beams with holes and without reinforcement were used for the predictions. In order to facilitate access to the data, a summary of data are re-presented in Table 4.1.

Table 4.1. Experiments on beams with holes

Beam	Dimension (mm)	Hole diameter (mm)	End distance (L_c) (mm)	Edge distance (D_c) (mm)	Experimental failure load (kN)
1	1400×190×45	80	300	95	40.5
2	1400×190×45	100	300	95	36.9
3	1400×190×45	120	300	95	28.5
4	1500×200×45	65	400	100	48
5	1500×200×45	80	400	100	39.4
6	1500×200×45	100	400	100	30.6
7	2000×200×45	80	400	100	28.7
8	2000×200×45	100	400	100	28.3
9	2100×300×45	80	550	150	57.3
10	2100×300×45	120	550	150	55.9
11	2100×300×45	150	550	150	40.3
12	2800×400×45	160	550	200	67.3

4.8 Results of finite element analysis

Finite element models have been developed for failure load prediction of the beams that were tested experimentally. The models were analysed under 1 kN loading. A hypothetic crack was introduced into the beam at the location of maximum normal stresses that is normal to the beam axis. The maximum normal stresses exist in four areas (two compressions and two tensions) around the holes for shear dominant regions

of beams. The normal stresses at the moment dominant area of the beam exists in six areas (three compressions and three tensions) around the holes. Figure 4.6 presents the normal stress field around the holes for the first beam of Table 4.1 (hole close to support (a)) and moment areas (Hole at mid-span, (b)).

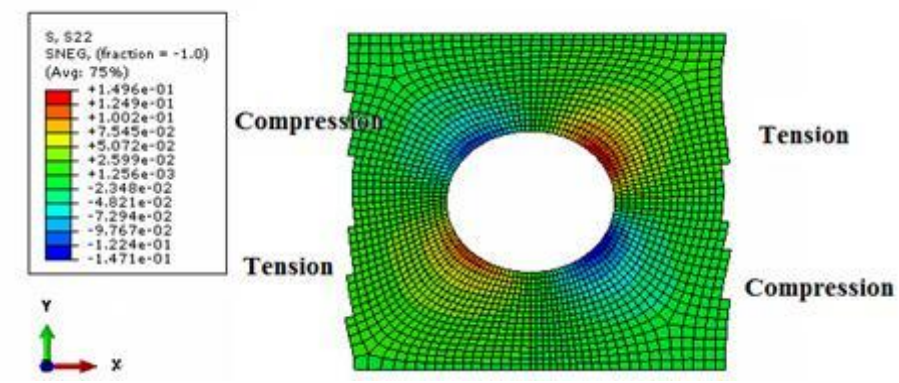

(a)

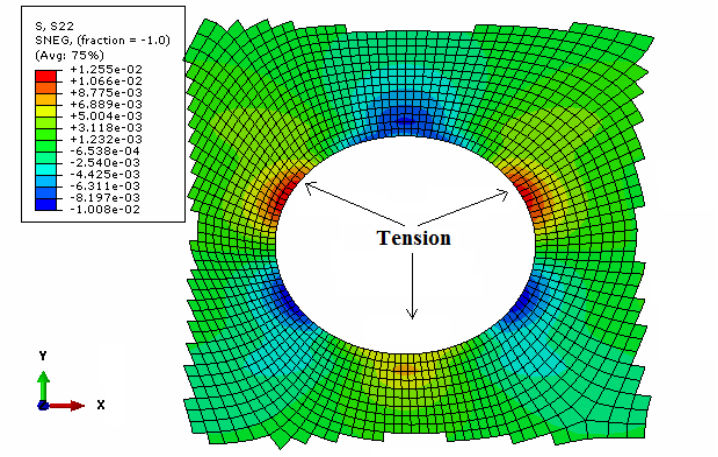

(b)

Figure 4.6. (a) Normal stress in shear area, (b) in moment area of beams

Using the model, the predicted loads for the beams with holes are presented in Table 4.2. The results are conservative for hypothetic crack length predicted by the initial crack criterion. The method in general underestimates the failure load (Gustafsson 1993a). This could be because of the softening after cracking in tension in LVL that is different from sawn timber. In sawn timber, the crack propagates easily when the body is pre-cracked while in LVL, some softening is observed and the crack does not

propagate very fast. When using a 2 mm hypothetic crack length, the failure load predictions provided results which correlate closely to the experimental values.

The failure load predictions are critically dependent upon the pre-crack length. The first beam in Table 4.1 was modelled with different hypothetic crack lengths and the failure load was calculated for each. The modelling showed that for a hypothetic crack length of 14.3 mm and greater, the failure load did not change very much and the predicted failure load was relatively constant (Figure 4.7 (a)). A comparison between stress intensity factors (Figure 4.7 (b)) also showed that for small hypothetic cracks the value of the effect of mode I is significant, and the mode II effect is relatively low. This implies that crack initiation is sensitive to the tensile strength of the wood. For larger hypothetic crack lengths, the effect of the shearing mode increases, implying that shear strength becomes a key factor.

Table 4.2. Failure load predictions

Beam	Hypothetic crack length calculation (mm)	Failure load based on Equation (4.13) (kN)	Hypothetic crack length calculation (mm)	Failure load based on Equation (4.13) (kN)	Experimental Failure Load (kN)
1	14.3	21.2	2	37.5	40.5
2	14.3	15.5	2	31.4	36.9
3	14.3	12.3	2	22	28.4
4	14.3	24	2	41	48
5	14.3	20.1	2	39	39.4
6	14.3	16.7	2	34	30.6
7	14.3	15.9	2	30	28.6
8	14.3	14.5	2	27	28.3
9	14.3	35.5	2	63	57.3
10	14.3	26.6	2	50	55.9
11	14.3	25.5	2	50	40.3
12	14.3	36.9	2	73	67.3

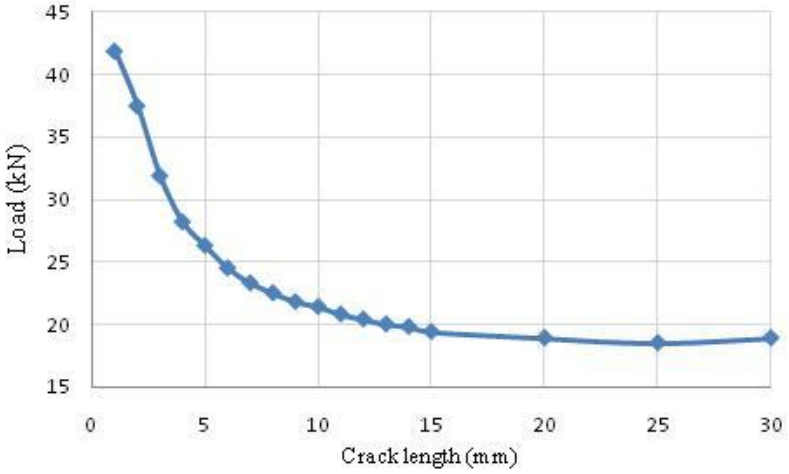

(a)

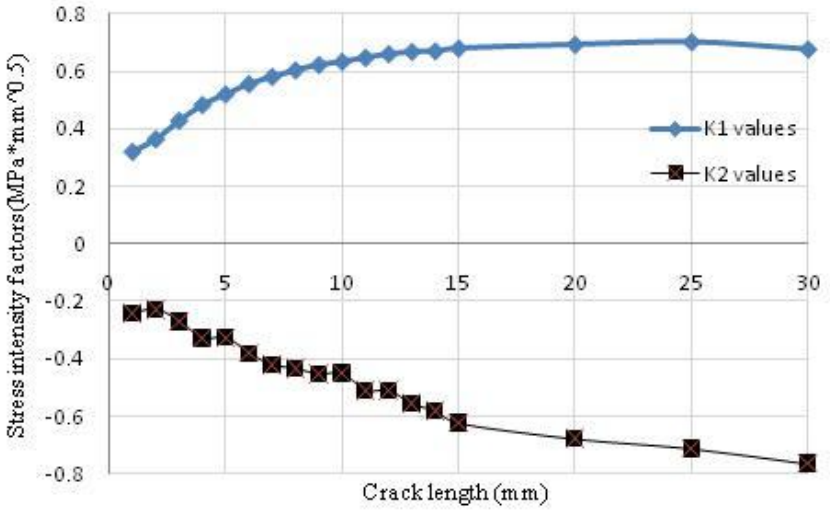

(b)

Figure 4.7. (a) Predicted failure load for different hypothetic crack length, (b) change of SIFs in mode I and II for different hypothetic crack length

4.9 Change of the Stress Intensity Factor

It was considered that variation of the SIF along the beam axis could provide useful information for studying the holes. In this step, a series of finite element models for the first beam in Table 4.1 were developed. The location of the hole along the beams axis

was gradually shifted at increments of 25 mm from the beam end and the SIFs at the crack tip calculated using the model. Two cases of loading i.e. three-point and uniformly distributed loading were investigated.

Figure 4.8 and Figure 4.9 show the results of the calculated SIFs. The model was analysed under 10 kN loading at mid-span for the case of centre loading and 1 kN/m for uniformly distributed loading. The curves have three areas of interest. At approximately 240 mm from the beam end (about 200 mm from the support of the beam), the rate of increase of SIF declines significantly and the curve flattens out indicating that the SIF only increases slightly for holes located between approximately 240 mm from the beam end, and support to the mid-span (where the concentrated load is applied). It is important to note that the 200 mm is equal to the depth of the beam. As the hole location shifts further from the beam end support and approaches the mid-span, the SIF rapidly declines, implying the failure load increases again.

The fact that SIFs decrease near the supports indicates that the beam portion containing a hole will be affected by the support. A hole placed close to the support will increase the chance of long term crushing of the wood and decreases shear resistance length of the beam. So, it is logical not to cut holes close to the supports. A distance equal to beam depth guarantees the hole is out of the possible crushing area.

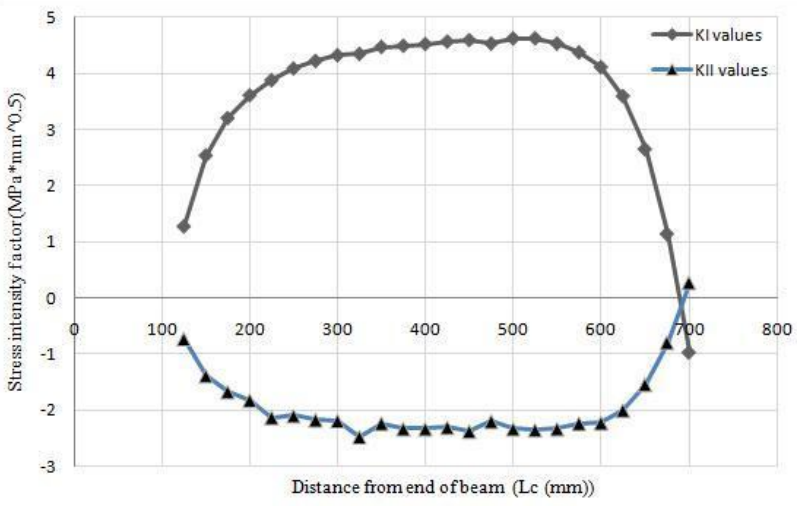

Figure 4.8. Change of SIFs along the beam for centre loading

Figure 4.9 shows the variation of the SIF for a 1 kN/m Uniformly Distributed Loading (UDL) case for the same beam. The SIF is increasing as the hole location shifts further away from the end supports. The SIF then decreases linearly as the hole moves toward the mid-span of beam. This implies that as the hole moves toward mid-span, the predicted failure load increases.

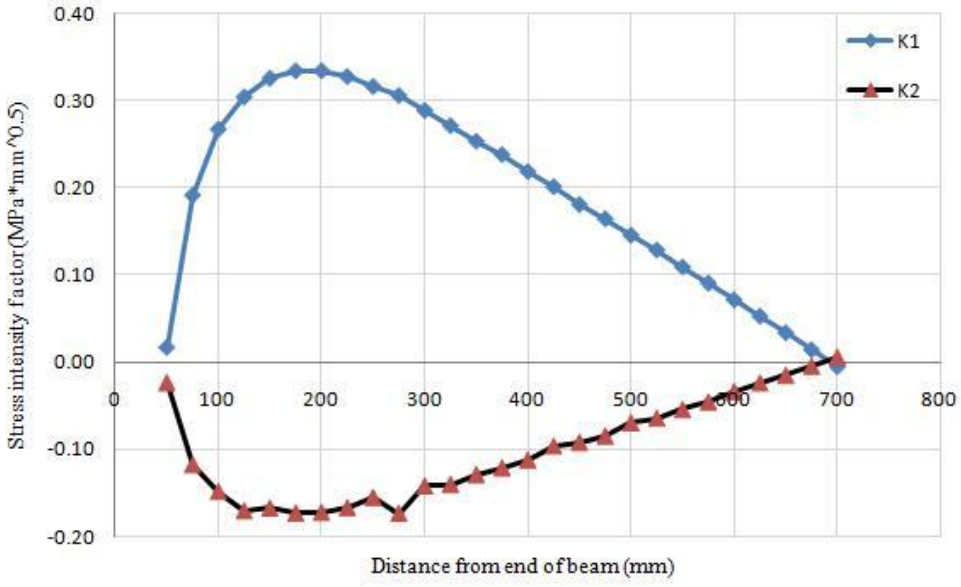

Figure 4.9. Change of SIFs along beam for uniformly distributed load

4.10 Location of crack initiation

The location of crack initiation in the hole is of considerable interest. Two theories assessed are (i) point of maximum principal stress, and (ii) point of maximum normal stress in the perimeter of the hole. The maximum principal stress suggests that the crack will initiate at the point in the beam where the magnitude of the combined shear and normal stresses is greatest; where the principal stress is maximum. However, the maximum principal stress does not always lie on the plane perpendicular to the grain direction, and thus is not in good agreement with the experimental observation that cracks propagate in the grain directions. The maximum normal stress ignores the effect of shear stresses and assumes the crack will start only due to the tension perpendicular to grain.

A comparison of the failure load predictions using the first beam of Table 4.1 with a hole at the neutral axis using the maximum principal stress and maximum normal stress for different hypothetic crack length values is presented in Figure 4.10. The predictions are close to each other. In this thesis, the maximum normal stress criterion is used for the location of the crack initiation around the holes, except for Table 4.3 where the maximum principal stress is being used.

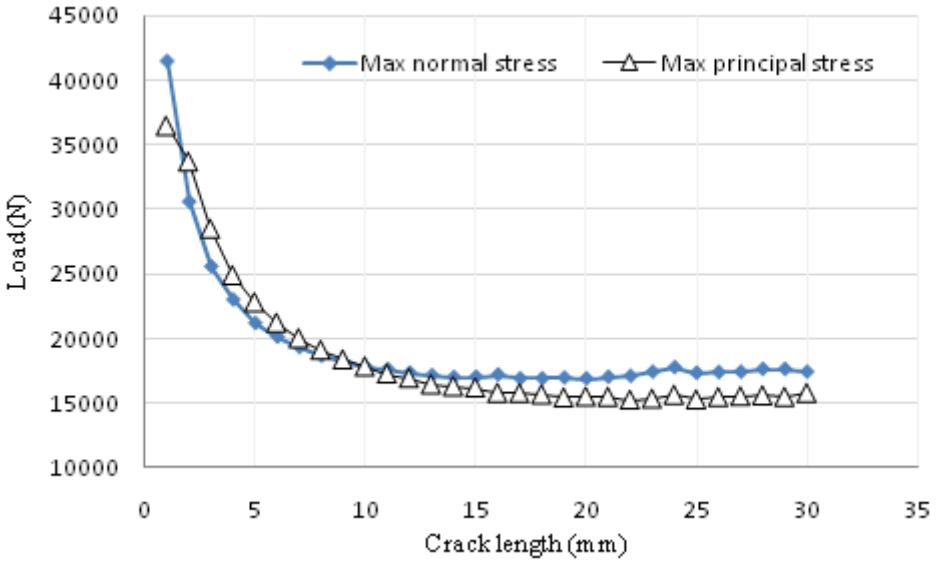

Figure 4.10. Comparison of predicted failure load using maximum principal stresses and maximum normal stress criterion.

4.11 Hole in depth of LVL beams

Location of holes in the depth of LVL beams could also be varied. Clearly, holes cannot pass very close to compressive or tensile edge of beams as this would cause failure of the beams at the hole location. A numerical-experimental model was defined to investigate the effect of small eccentricity on strength reduction of LVL beams. Again, using the finite element, the stress intensity factors were calculated along the beam for different hole positions in depth of LVL beams, namely 35 mm above, 35 mm below, and at the neutral axis for 1300×200×64 mm beam loaded at mid span under 1 kN. The hole of 70 mm was placed at a distance of 300 mm from the end of beam (Lc). A total of 70 elastic models were analyzed in ABAQUS to obtain the stress intensity factors.

The results of the analyses for different positions of the holes are presented in Figure 4.11.

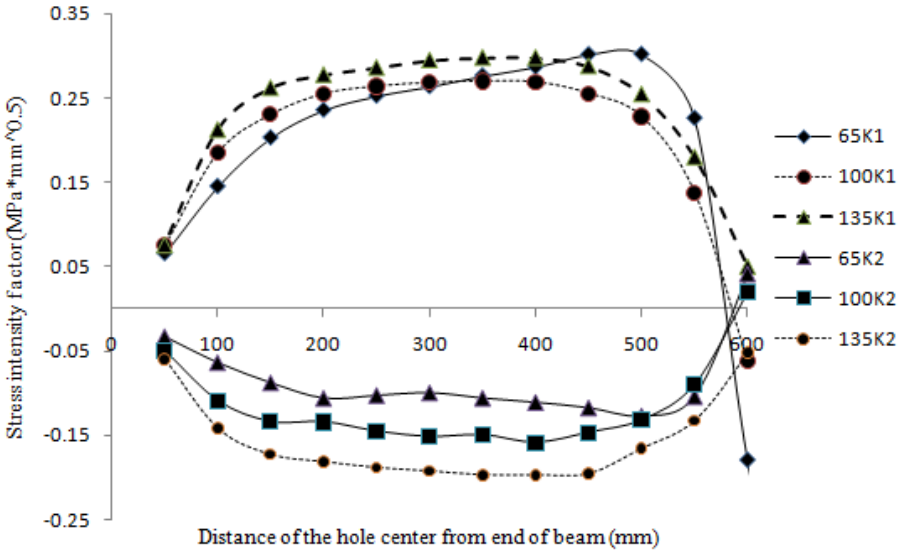

Figure 4.11. Variation of the stress intensity factors in mode I and II along the span for different location of hole along the depth of a beam loaded with a concentrated load

In Figure 4.11, for example, 65K1 shows a distance of the centre of the opening placement relative to the upper edge of the beam of 65 mm, and the curve shows the k_I values. Similarly, 65K2 stands for the distance of the hole centre relative to the upper edge of 65 mm, which presents k_{II} values. As the hole is moving downward, the stress intensity factors increase and this in turn decreases the load-carrying capacity of the beam. However, the change of the failure load for small eccentricities (here less than 17.5% of the depth) is small. The results of the stress intensity factors for the three locations of the openings at a distance of 300 mm from the support are presented in Table 4.3.

Table 4.3 Stress intensity factors for different hole positions at 300 mm from the support based on the maximum principal stress criterion (MPa$\sqrt{\text{mm}}$) and a hypothetic crack length of 2 mm

Hole location	Stress Intensity factors in mode (I) ($\times 10^{-3}$MPa$\sqrt{\text{mm}}$)	Stress Intensity factors in mode (II) ($\times 10^{-3}$MPa$\sqrt{\text{mm}}$)	Predicted failure load (kN)
Hole above neutral axis	0.2608	-0.1018	60.3
Hole at neutral axis	0.2663	-0.1549	58.5
Hole below neutral axis	0.2933	-0.1918	53.0

Figure 4.12 shows the results of a similar parametric study carried out for the same beam subjected to a uniformly distributed load of 1 N/mm. For clarity, only the stress intensity factors for the hole above and below the neutral axis are presented, the third case being intermediate. The curve shows that as the hole moves towards the compressed part of the section, the load-carrying capacity of the beam increases.

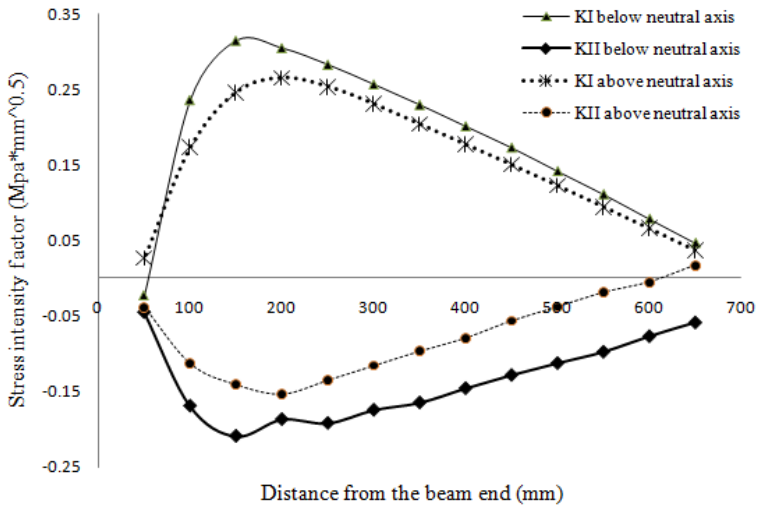

Figure 4.12. Variation of the stress intensity factors in mode I and II along the half span of beam for different locations of hole along the depth of a beam loaded with a uniformly distributed load

4.11.1 Experiments on beams with varying hole in depth

In order to verify the numerical results presented above, three sets of experiments were planned. The first set was performed with the centre of the hole located exactly on the

neutral axis of the beam. In the other two sets, the hole was located above and below the neutral axis. The hole location relative to the neutral axis, and the notation of the other geometrical parameters is displayed in Figure 4.13 .

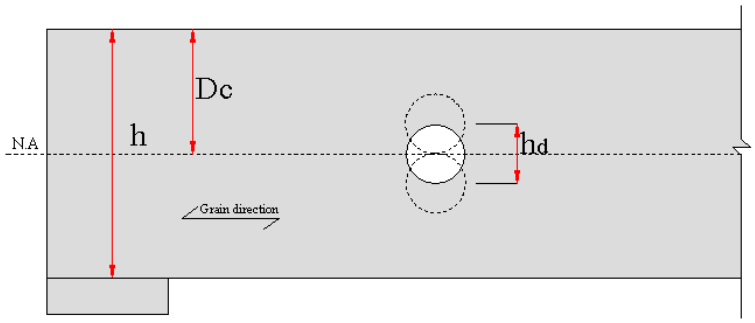

Figure 4.13. Notation of geometrical quantities for the hole location relative to the neutral axis

Table 4.4 summarizes the geometry of the beam, the hole location along the beam length, depth, and the number of the specimens tested in each set of the experiment.

Table 4.4 Geometry and hole locations of the beam in the experiments

Beam dimensions (mm)	Lc (mm)	Dc (mm)	Hole diameter (mm)	Number of specimens
1300 × 200 × 63	300	65	70	4
1300 × 200 × 63	300	100	70	4
1300 × 200 × 63	300	135	70	4

All of the beams were tested under three point bending. The testing set up was as reported in chapter 3 for the experimental program. Figure 4.14 (a) presents the experimental setup and Figure 4.14 (b) shows a picture of the tested beams.

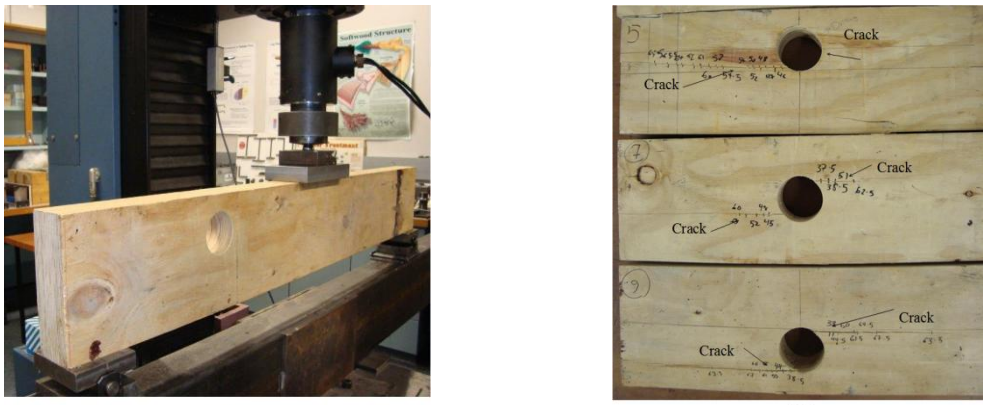

(a) (b)

Figure 4.14. (a) Experimental setup, (b) crack initiation and propagation around holes for different location along the depth

The cracking load similar to the experimental program was recorded when the crack was visible on the surface of the hole. The experimental cracking and failure loads, including statistics (maximum, minimum, average, and coefficients of variation) are reported in Table 4.5.

Table 4.5 Experimental cracking and failure loads

Hole location	Average Cracking load (kN)	Min Cracking load (kN)	Max Cracking load (kN)	COV Cracking load (%)	Failure load (kN)	Min Failure load (kN)	Max Failure load (kN)	COV (%)
above neutral axis	42.125	37.5	46	9	66.775	64	70.6	4
at neutral axis	39.125	35	45	11	59.375	57	64	5
below neutral axis	39.225	37	42.9	7	58.950	55.2	67.5	10

For small eccentricities of the hole with respect to the neutral axis (here 17.5% of the beam depth), experimental and numerical analyses showed that the failure load is not constant. The failure load slightly increases as the hole moves towards the compressive part of the section perhaps because the compressive stresses decrease the tensile stresses perpendicular to the grain around the hole. The difference of the calculated failure load

is however not very high, and is confirmed by the results of the experimental programme. Smaller differences were found when the hole moved towards the tensile edge of the beam. This could be due to the COV of the material and variations in the fracture properties of LVL in the crack area. The results of the failure load predictions from numerical analysis for the different hole positions along the depth of Figure 4.11 and along the length are presented in Figure 4.15. Again, the curves clearly show that the predicted loads are close to each other, and the predictions are relatively constant after a distance from the supports of about 150 mm to 200 mm.

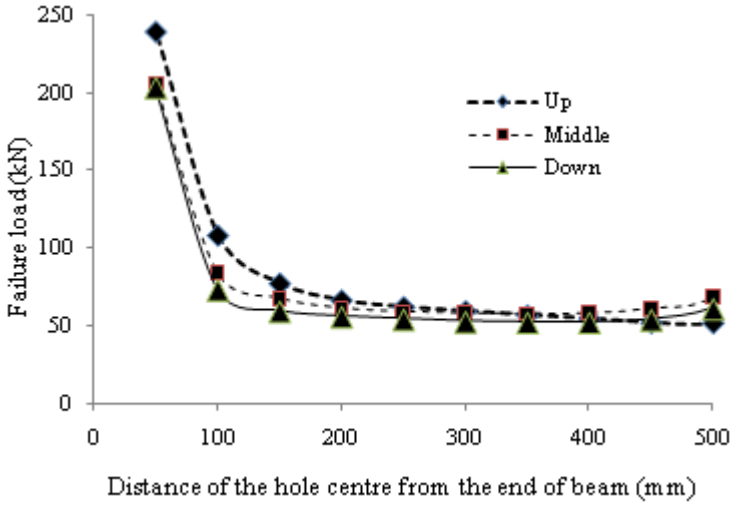

Figure 4.15. Predicted failure loads for different distances of the hole from the support and from different locations within the beam depth

4.12 Summary

In this chapter, Linear Elastic Fracture Mechanics (LEFM) was used for the failure load prediction of LVL beams with holes. Key outcomes of the study are presented below:

- The initial crack criterion approach provided conservative estimations of the failure load of LVL beams with holes. The predicted hypothetic crack length was 14.3 mm.
- Linear Elastic Fracture Mechanics (LEFM) can be used to predict the failure load of LVL beams with holes provided that an appropriate pre-crack length is

used. Analyses indicated that a hypothetic crack length of about 2 to 3 mm provided good predictions of the failure load for the range of the experimentally tested beams.

- A distance equal to beam depth, based on SIF analysis is proposed for the minimum distance of the hole centre from the support. This distance will decrease the probability of long term crushing of timber beams with holes at the supports.

- Maximum normal stress and maximum principal stress criterion yield similar results for the prediction of failure load.

- For small eccentricity of hole above neutral axis (17.5 % of beam depth), the failure load of the experimental beams slightly increased (about 10 %) and remained almost fixed for moving below the neutral axis.

- Decreasing of the SIFs for uniformly distributed loading points to increasing load as the hole moves toward mid-span of the beam.

The predicted failure load based on generalized LEFM is conservative and much dependent on the hypothetic crack length calculations. However, a more accurate method is to use Nonlinear Fracture Mechanics (NLFM) for the prediction of failure load. Chapter 5 gives more analysis for the failure load predictions of the beams with the holes. The cohesive element in ABAQUS will be incorporated with the aim of providing greater understanding of the behaviour of the crack layer. This model will be then used for the failure load predictions of the beams with reinforcement.

5 Analysis of beams with holes using cohesive elements

This chapter presents a numerical model based on nonlinear fracture mechanics for load prediction of Laminated Veneer Lumber (LVL) beams with holes. The model parameters, comparison of the model with experimental results, and the model results are discussed. The model is further developed by adding reinforcement. The results of this chapter have been used in chapter 8 and 9. The use of the presented numerical model is limited to this chapter.

5.1 Introduction

In the previous chapter, Linear Elastic Fracture Mechanics (LEFM) was used for the failure load prediction of LVL beams with holes. LEFM does not address the problem of crack initiation and propagation. In this chapter, interface elements with traction-separation law behaviour will be used for the failure load predictions, and more accurate investigation of the crack initiation and propagation in LVL beams with the holes. The chapter also includes modelling of LVL beams with the holes reinforced with screws and plywood.

Applications of LEFM theory to the fracture of wood has been significant, although LEFM does not quite account for all physical phenomena associated with wood fracture and has some limitations in its applications. Two basic limitations exist for using of LEFM viz.: (i) LEFM works well for the cases where a sharp-tip or a flaw exists in the solid body. (ii) LEFM gives results that are in good agreement with reality if the length of the initial crack or notch (pre-crack) is large as compared to the size of the Fracture

Process Zone (FPZ) and other dimension of the body. FPZ by definition is a damaged zone ahead of a traction-free crack (Wittmann et al. 1991).

The first limitation for LVL beams with holes in the previous chapter was discussed through assigning a crack to the model, so that crack tip computationally becomes located at the centre of gravity acting across the fracture region. The second limitation has been the subject of many researches. The degree to which toughening mechanisms affect fracture behaviour, determines whether LEFM is applicable or not to certain materials. This brings up the discussion of the fracture process zone comparisons with the structural size.

LEFM limitations in application and lack of inclusion of crack initiation and propagation push the analyses of the LVL beams with holes toward nonlinear methods. The quasi-brittle nature of LVL also supports that idea. Nonlinear fracture mechanics modelling of LVL beams with holes is a more efficient way for studying the crack initiation and propagation.

5.2 Nonlinear fracture mechanics

A number of the approaches such as that developed by Dugdale (1960) and Hillerborg et al. (1976) have been used for calculation the size of the fracture process zone. These approaches in turn have been used to develop predictive nonlinear fracture mechanics.

5.2.1 Dugdale (1960) model

Dugdale (1960) studied a slit of total length (2L) in a sheet loaded under uniform tensile stress (T) that yields over a length of 's'. The relationship between the effective crack length 'a' and the length of the plastic zone for the material with yielding strength of 'Y' according to Dugdale is stated in Equation (5.1).

$$\frac{s}{a} = 2sin\left(\frac{\pi}{4}\frac{T}{Y}\right) \tag{5.1}$$

The model assumes a plastic zone of length 's' ahead of the crack tip or notch, with closing stresses of 'Y'. Figure 5.1 shows the Dugdale model.

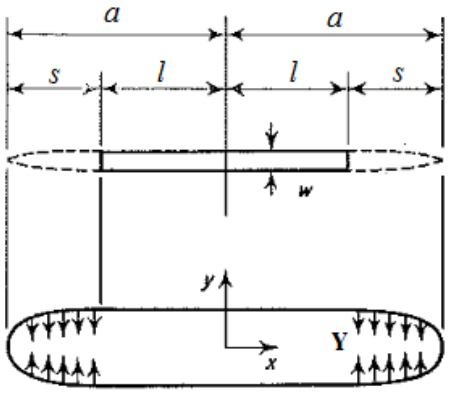

Figure 5.1. Crack tip stress distribution (Dugdale 1960)

5.2.2 **Hillerborg et al. (1976) model**

Hillerborg studied the fracture process zone in concrete. Similar to Dugdale, Hillerborg assumes a plastic zone ahead of the crack tip. The tip of the real crack is replaced with an equivalent crack containing closing stresses. The stresses at the crack tip correspond to the opening of the crack.

In the Hillerborg model, the crack is assumed to propagate when the tensile stresses at the crack tip reach the tensile strength of the material. When the crack opens, it is not assumed that stresses to fall to zero at once, but to decrease with increasing crack width. For the area of the crack (w) that its opening is less than w_1, the crack in reality corresponds to a micro-cracked zone with some remaining ligaments for stress transfer. As there is a stress to overcome in the opening of the crack, energy is absorbed. The amount of energy absorbed per unit crack area to widening the crack zone from zero to w_1, is called the critical energy release rate (G_f) as presented in Equation (5.2).

$$G_f = \int_0^{w_1} \sigma_w dw \tag{5.2}$$

where σ_w is stress that is assumed as a function of the crack opening.

Figure 5.2 (a) shows the variation of stresses at the crack tip for the cohesive model. Figure 5.2 (b) shows the curve of tensile stress reduction corresponding to crack width.

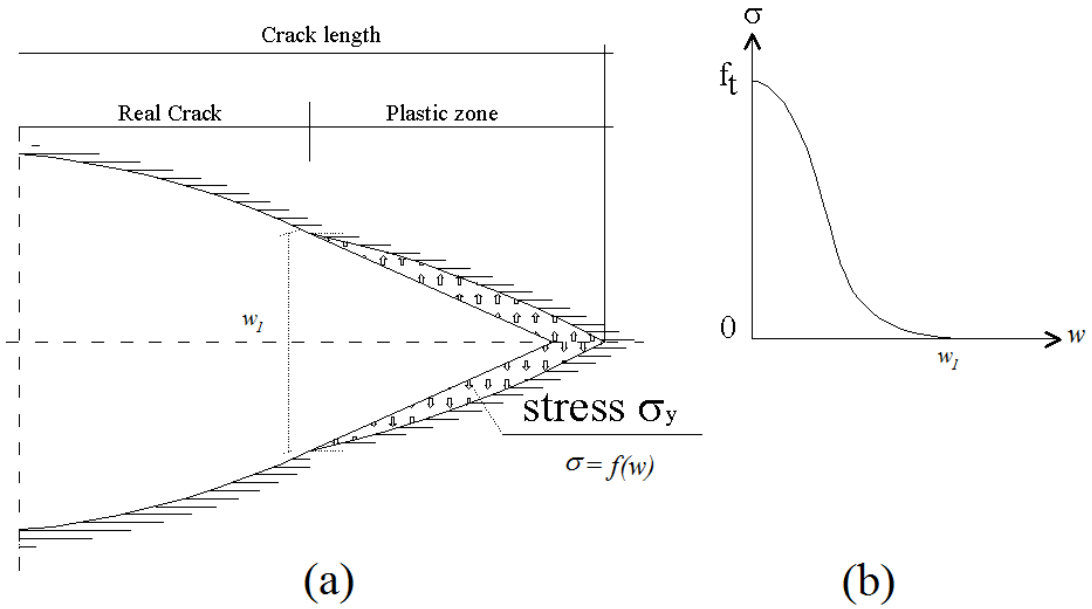

Figure 5.2. (a) Crack tip stresses in the cohesive model, (b) the stress reduction corresponding to crack width (Hillerborg et al. 1976)

The model of Hillerborg is similar to the Dugdale model; they both assume a plastic zone with closing stresses. The main difference in the Hillerborg and Dugdale models is the stress distribution at the fracture process zone. The Dugdale model assumes a certain length over which the stresses are equal to the yielding stress, while the Hillerborg model assumes a variation of the stresses.

The model of the Hillerborg et al. (1976) has different names such as: fictitious crack model, cohesive crack model, cohesive zone model or damage zone model (Hillerborg 1991) and since the introduction, the model has been applied to different materials such as ordinary concrete, fibre reinforced concrete, rock and wood. Gustafsson (1985) used the cohesive crack model for wood. Also, Bostrom (1992) applied the model with bilinear stress-softening behaviour to the wood. Since then the bilinear stress-softening model has been used to obtain load-displacement curves for wood. Applying the cohesive crack model seems appropriate to model fracture mechanisms in wood, since it enables quasi-brittle failure to be modelled (Schoenmakers 2010).

Usually an experiment is used for more description of the cohesive crack model. A prismatic specimen is loaded in tension. The prism does not have any crack or notch. Figure 5.3 (a) shows that the material starts to behave in the linear elastic range where the Hooks' law $(\sigma = E\varepsilon)$ is valid. Then, due to the mico-cracking a non-linear part forms that is due to the damage in the entire specimen. Finally, approaching the maximum load, a nonlinear softening occurs. This is due to the damage in a localized region of the specimen (possible failure surface). Before the peak load, the deformation is assumed uniformly distributed along the specimen. Therefore, elongation of the specimen due to loading is $\delta = l\varepsilon$. When the load reaches the maximum value, a localized fracture process zone is assumed to form. The total deformation in the specimen will be δ plus a local additional deformation called w.

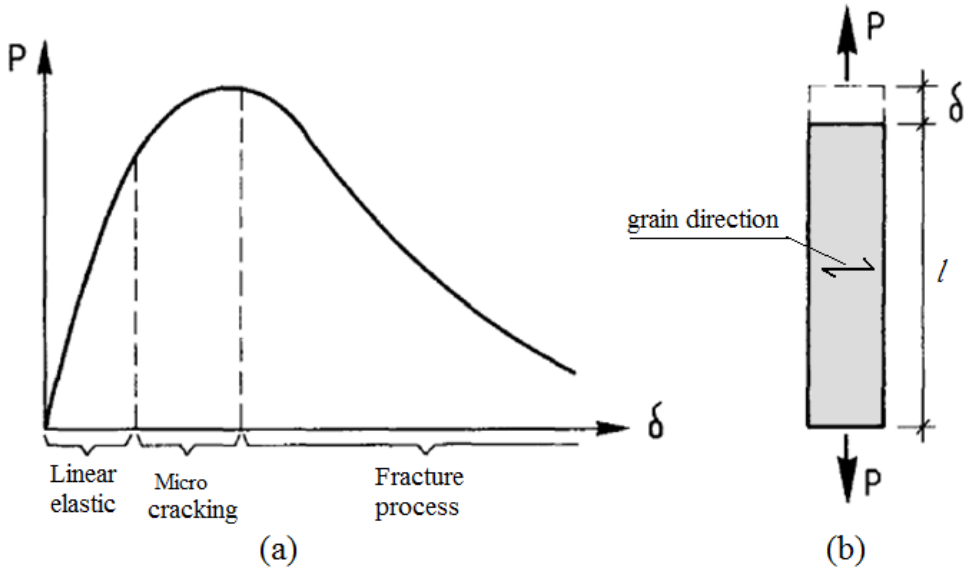

Figure 5.3. (a) Example of stress-deformation curve in tension perpendicular to the grain, (b) wood specimens loaded in tension perpendicular to the grain (Bostrom 1992)

Figure 5.4 explains the cohesive crack model assumptions. Part 'b' of the figure shows the possible crack area lumped over a small width (w) and the stress-deformation curve divided into two curves viz.: (i) one with stress-strain relation and (ii) the stress-separation curve. The model assumes two mechanical behaviours. For material outside the fracture process zone, the stress-strain relationship is assumed, and for the material

in the fracture process zone, the stress (traction) versus separation curve is used. This will be discussed more in the next parts.

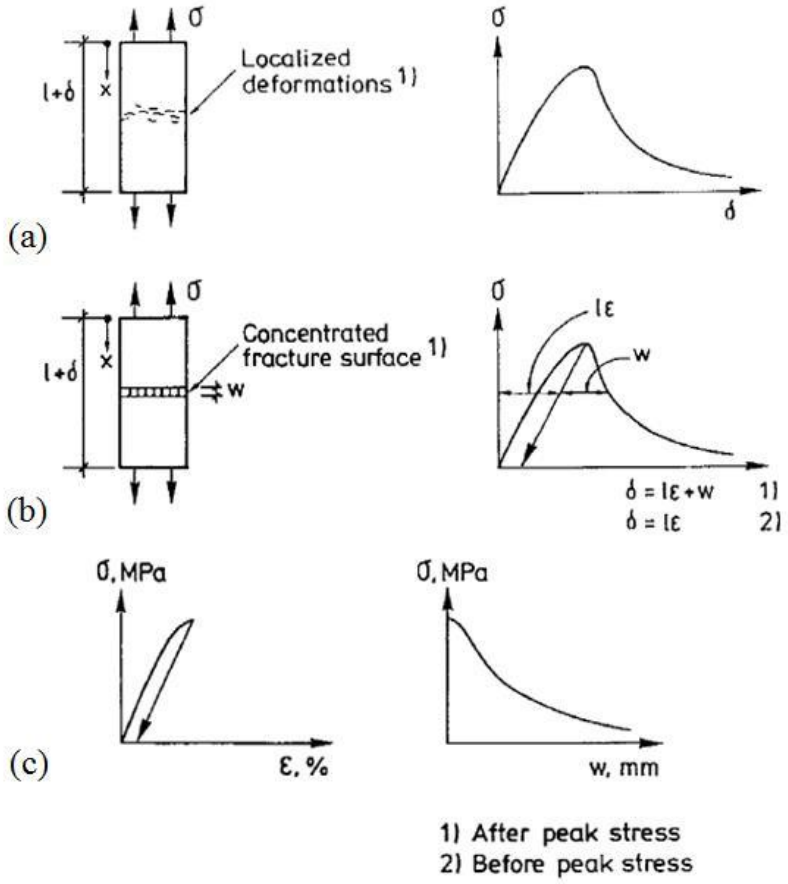

Figure 5.4. Tensile fracture main characteristics: (a) real structural behaviour, (b) model of structural behaviour, (c) model of material properties (Gustafsson 1985)

The load-deflection of the prism in Figure 5.4 is theoretically possible to obtain, although the experiment is complicated to follow for the case where wood is loaded in perpendicular to the grain direction due to the softening part of the curve. Stanzl-Tschegg et al. (1995) developed a wedge-splitting test to obtain the curve. The specimen has a cut at the middle and it is split apart by a wedge that pushes against two steel roller supports installed on the edges of the specimens (Figure 5.5). A sketch of the experimental set up is illustrated in Figure 5.5 (a) and a picture of the experiment is performed on spruce specimen is shown in Figure 5.5 (b).

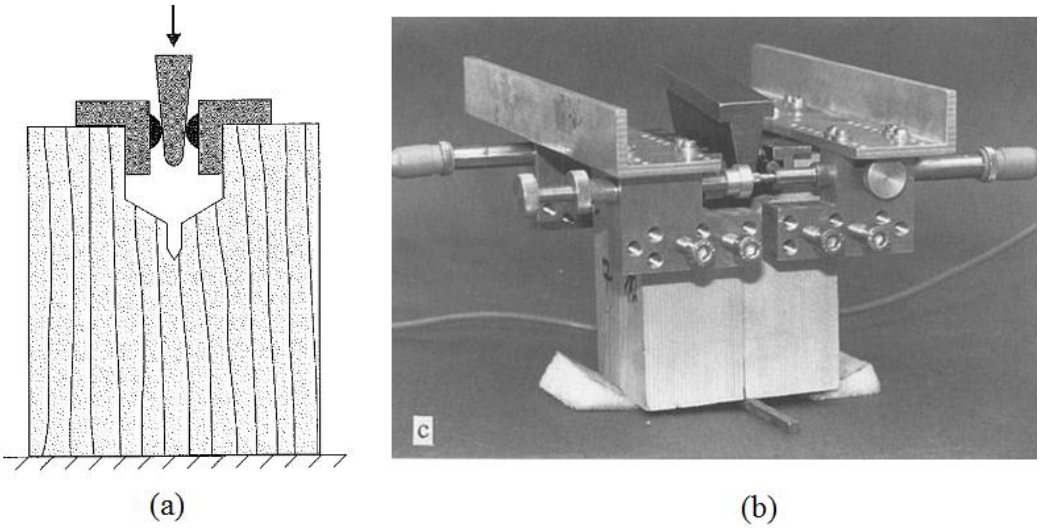

Figure 5.5. (a) Sketch of the wedge splitting specimens, (b) picture of the experimental set up (Stanzl-Tschegg et al. 1995)

Figure 5.6 shows a physical interpretation of the cohesive crack model. The stresses are increasing until it reaches its maximum values at the crack tip. Stresses behind the crack tip are decreasing relative to the crack tip (usually assumed linear) and some remaining ligaments transfer stresses in this region.

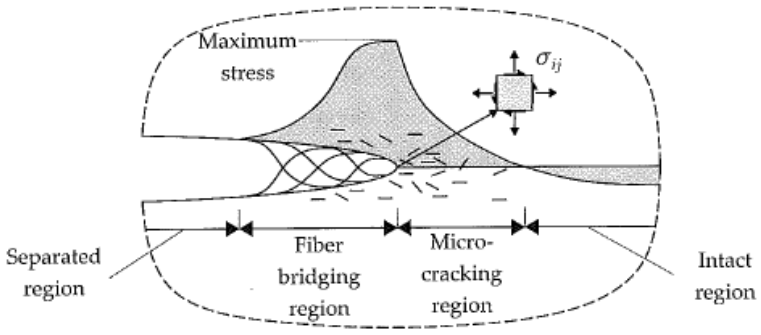

Figure 5.6. Physical interpretation of the crack propagation and cohesive zone model (Schoenmakers 2010)

Recent advances within fracture mechanics and Finite Element Methods (FEM) have now given us the possibility of analysing crack growth. While fracture mechanics gives basic rules for crack propagation, finite element methods enable the analyses to be performed for complicated geometries like beams with holes.

5.3 Cohesive elements in ABAQUS

The interface elements are specialised finite elements used to simulate crack initiation and propagation. Interface element behaviour is governed by a traction-separation curve relating to element traction (stress) to mode I (opening) and mode II (shearing) displacement. Despite timber exhibiting exponential softening behaviour, a bilinear curve is commonly used for this traction-separation curve (Harper et al. 2008). The linear softening of the traction-separation curve improves the convergence of the analyses. This could be noticed in Figure 5.7 (a). If an exponential curve is being used (Figure 5.7 (b)), the critical crack opening in certain cases may become excessive due to a fixed critical stress and fixed fracture energy. It is recognised that adopting linear instead of exponential softening affect the degradation rate (Schoenmakers 2010).

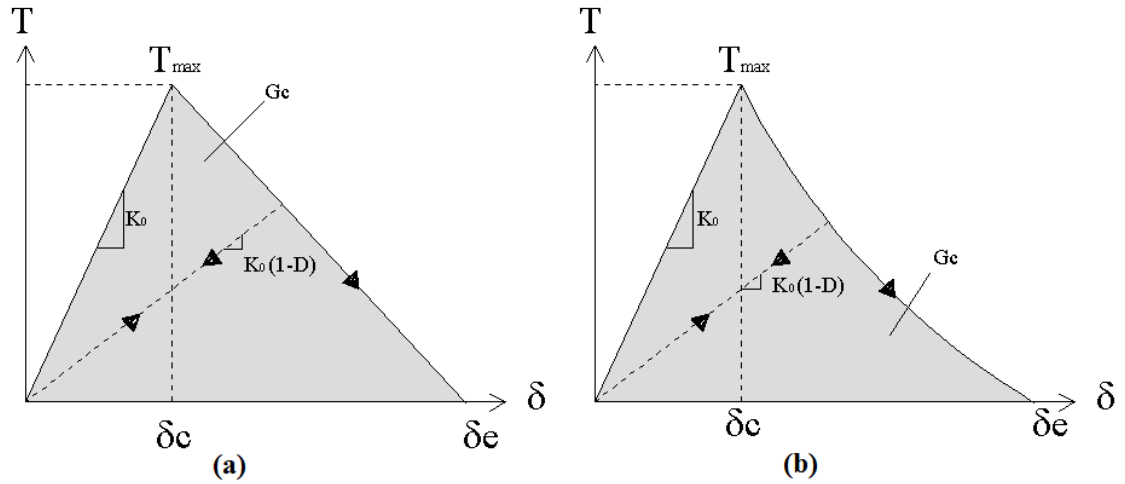

Figure 5.7. Response of cohesive element: (a) linear softening, (b) exponential softening

The bilinear curve of traction-separation consists of: (i) an initial elastic region showing the interfacial strength, (ii) a subsequent softening region until zero stress is reached. The total area under the curve is the fracture energy of the material. Equation (5.3) presents the scalar form of the traction-separation law. For deformations smaller than the deformation corresponding to the maximum strength of the material, the stiffness of the cohesive layer is constant while for the larger deformations, the stiffness of the cohesive layer decreases. Finally, for a deformation larger than the maximum value, the traction is set to zero.

$$T = \begin{cases} K\delta & \delta \le \delta_c \\ (1-D)K\delta & \delta_c < \delta < \delta_e \\ 0 & \delta \ge \delta_e \end{cases} \tag{5.3}$$

where T denotes the traction, δ deformation, and D is damage parameter changing from $D = 0$ (undamaged) to the $D = 1$ (fully damaged), defined as Equation (5.4).

$$D = \frac{\delta_e(\delta - \delta_c)}{\delta(\delta_e - \delta_c)} \tag{5.4}$$

The parameters δ_c and δ_e are defined in Figure 5.8 (b). δ_c presents the separation corresponding to damage initiation and δ_e is the final separation corresponding to the full fracture of the specimen.

Figure 5.8 (a) shows status of the cohesive layer elements due to the tensile stresses in the section. The elements surrounding the crack tip are yielded and the other elements either have their stiffness decreased or not depending on their distance from the crack tip.

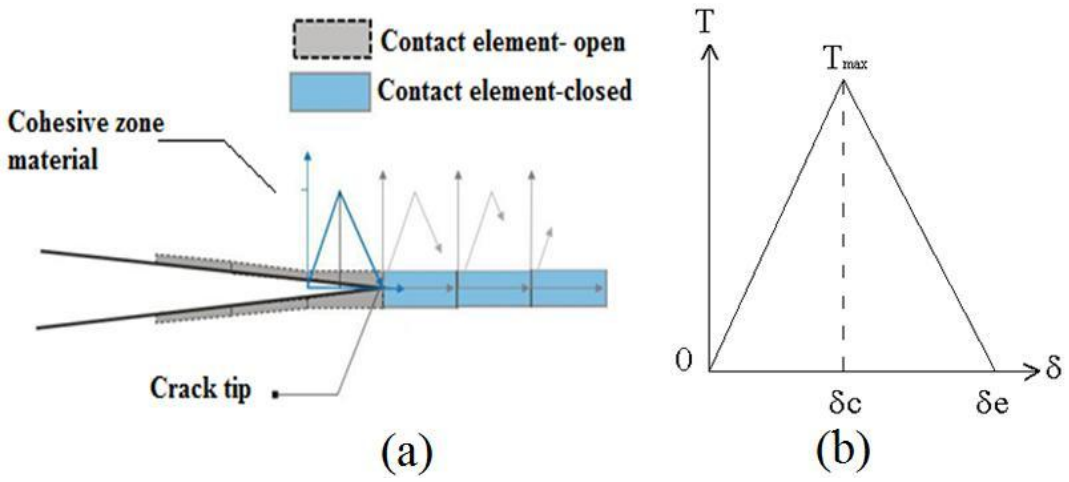

Figure 5.8. (a) Traction-separation in the cohesive layer, (b) bilinear curve of traction-separation

Damage initiation can be defined where the tensile stress or shear stress attains its maximum value. If the stress in the three main local directions (n, t, s) are σ_n, σ_t and σ_s and their relative material parameters are N_{max}, T_{max} and S_{max} , Equation (5.5) should be satisfied for damage initiation:

$$Max\left\{\frac{<\sigma_n>}{N_{max}}, \frac{\sigma_t}{T_{max}}, \frac{\sigma_s}{S_{max}}\right\} = 1 \qquad (5.5)$$

The damage evolution could be energy or displacement based. Different mixed mode fracture criteria can be used for the damage evolution (refer to chapter 4). In the case of a beam with a hole, at the crack tip usually mixed mode fracture occurs. Wu's mixed mode fracture criterion is a commonly used. The general form of the criterion is:

$$\left(\frac{G_I}{G_{Ic}}\right)^m + \left(\frac{G_{II}}{G_{IIc}}\right)^n = 1 \qquad (5.6)$$

where G_I and G_{II} are the fracture energies for mode I and II respectively, G_{Ic} and G_{IIc} are their critical energy release rate values, 'm' and 'n' denote the power of the equation. A comparison between different curves with different values of m and n is shown in Figure 5.9. $m = 0.5, n = 1$ is Wu's mixed mode failure criterion.

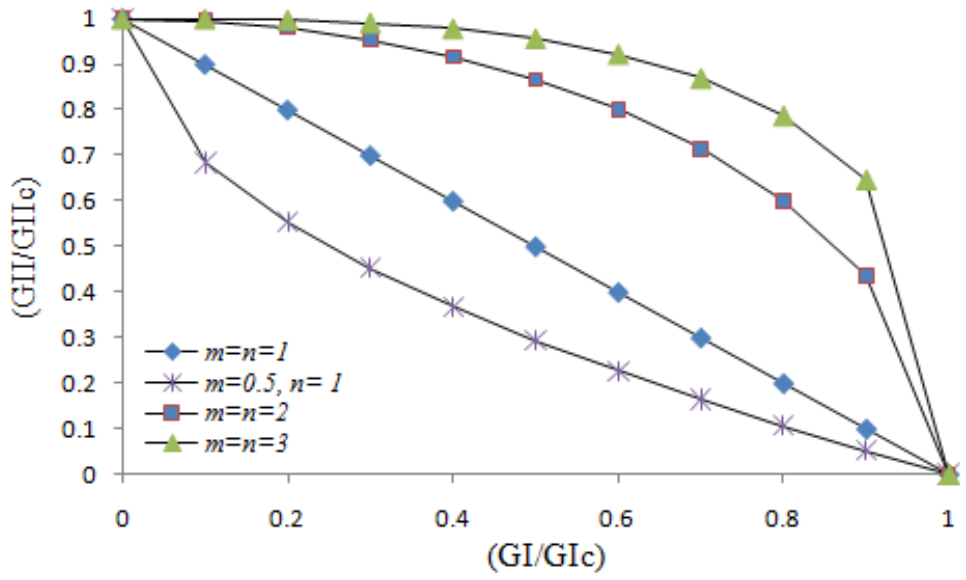

Figure 5.9. Damage evolution criteria

Since in ABAQUS, only values of m equal to n are allowed, therefore $m = n = 1$ is selected for the damage evolution. The procedure of modelling followed in ABAQUS and the results will be discussed in the following sections.

5.4 Solution procedure

The definition of the cohesive elements is based on progressive degraded stiffness. The change of the stiffness can cause severe convergence problems using the implicit solver of ABAQUS/Standard. ABAQUS (Habbitt et al. 2010a) suggests using viscous regularization of constitutive equations resulting in the tangent stiffness matrix of the softening material to be positive for small increments. The procedure is incorporated in the concrete damage plasticity model too. The regularized traction-separation law allows the stresses outside to be set. The regularization process involves using viscous stiffness degradation D_υ. The value is defined: $\frac{\partial}{\partial t} D_\upsilon = \frac{1}{\mu_\upsilon}\left(D - D_\upsilon\right)$, where μ_υ is a viscosity parameter and D calculated from the model (Habbitt et al. 2010a). According to ABAQUS, a smaller viscosity value in the model leads to more accurate results of the analyses. A schematic of the procedure is illustrated in Figure 5.10 .

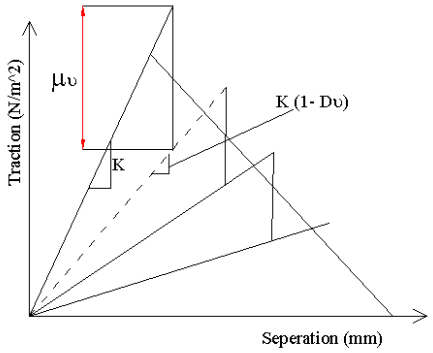

Figure 5.10. Schematic of viscous regularization (Schoenmakers 2010)

In order to obtain a stable value for μ_υ to use in the simulation, modelling of the beam with the hole was performed for several orders of magnitude of μ_υ changing from 0.1 to 0.0001. For beam 11 of the Table 3.3, the load-mid span deflection curves for different μ_υ values were modelled and compared to the experimental results in Figure 5.11. The modelling indicates that for $\mu_\upsilon = 0.1, 0.01$ the predicted load is considerably higher than experimental values while for $\mu_\upsilon = 0.001$ the prediction of the final load is closer to the experimental results. The value of $\mu_\upsilon = 0.0001$ yielded the best results in the simulations. In the later simulations $\mu_\upsilon = 0.001$ was used because using smaller values

for the viscosity considerably increases the number of iterations and takes much longer processing time. As an example, for $\mu_v = 0.1$ the number of iterations for solving is 33 and the value for $\mu_v = 0.0001$ is 256.

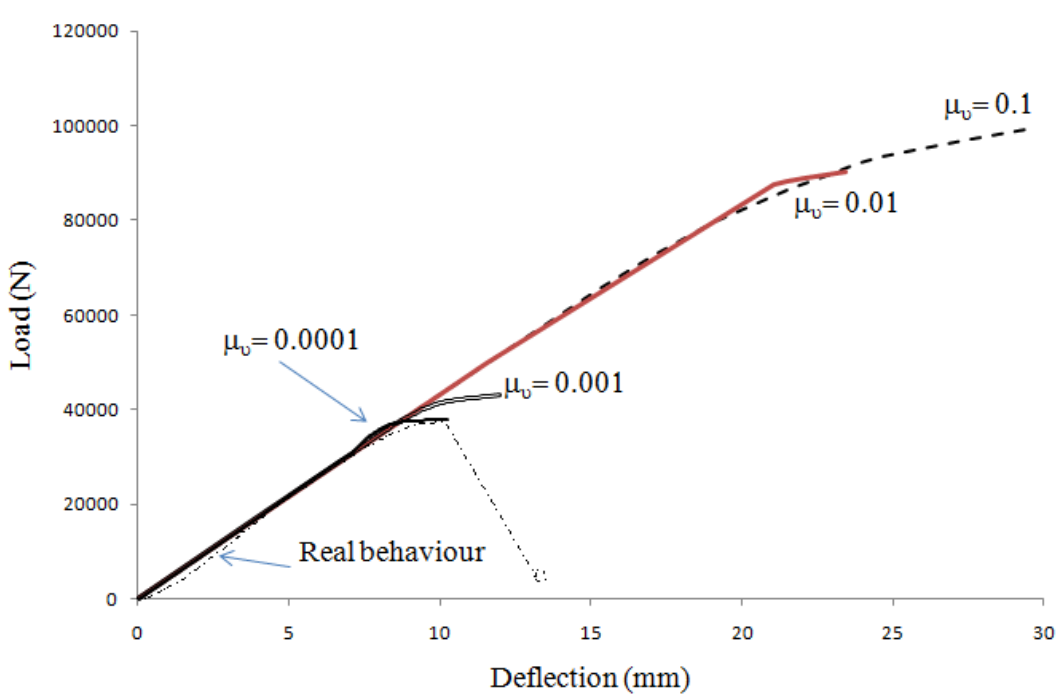

Figure 5.11. Load- deflection response for different viscosities

5.5 Modelling

Modelling of the experimentally tested LVL beams without reinforcement was first investigated to study the behaviour of the cohesive layer and possible calibration of the modelling with the experimental results. The calibrated model was further propagated by adding reinforcement to the model in the next steps. Three dimensional modelling (3D) of the beam with the hole was performed in ABAQUS software (Habbitt et al. 2010b). A 3D model was selected because reinforcement modelling such as screws and plywood was easier to follow. The steps of the modelling were:

- ***Elastic modelling***: Elastic 3D orthotropic modelling of the LVL beams with holes, and isotropic modelling of steel plates at the supports and loading points. Elastic analysis of the model was first performed to indicate the point

of maximum normal stress at the hole edge. A sketch of the elastic model is illustrated in Figure 5.12 (b).

- ***Material properties of LVL:*** Linear elastic orthotropic material properties were used for the material outside of the cohesive layer for the beam parts and isotropic material properties for the steel plates. The material properties of the LVL adopted from chapter 2 are presented in Table 5.1 .

Table 5.1 Material properties of LVL

E_x (MPa)	E_y (MPa)	E_z (MPa)	G_{xy} (MPa)	G_{yz} (MPa)	G_{xz} (MPa)	ν_{xy}	ν_{yz}	ν_{xz}
12000	485	280	600	24	600	0.3	0.3	0.3

- ***Loading, boundary conditions:*** The loading was applied to the steel plate at mid-span as in the experiments. Two steel plates were also used for the supports to mimic the test setup. The boundary conditions of the simply supported beam were applied to the model. The beam and steel plates were tied together to avoid any relative movement.

- ***Cohesive layer location:*** In the maximum normal stress location, a plane of cohesive elements in the grain direction with the normal perpendicular to the plane was introduced in the model. The cohesive layer was tied to the upper and lower part of the beam so there was full bond between the upper and lower parts.

- ***Behaviour of the cohesive layer:*** Traction-separation was selected as the governing behaviour of the cohesive layer. The damage initiation in the cohesive layer was defined as occurring when the tensile or shear stress in the layer reaches its maximum values, with the energy method (Equation (5.6)) being implemented for the damage evolution because the data of the energy values are available from the experiments. The softening was assumed as linear. The material properties of the cohesive layer will be further discussed in the following parts.

- ***Meshing of beam and the cohesive layer:*** Four-node linear tetrahedron (C3D4) and eight node linear brick elements (C38D) were used for meshing of

the beam around the cohesive layer. For meshing the cohesive layer, eight-node three-dimensional cohesive elements (COH3D8) were used. The reason for using different meshes was that for some of the modelling due to the complicated geometry, meshing with brick elements in ABAQUS was not possible; therefore, tetrahedron elements were used for the modelling. The purpose of the cohesive layer is to transfer the stresses from the upper part of the beam to the lower part. A mesh size of 20 mm was used for the elements of the beam from a sensitivity analysis using different mesh sizes. A smaller mesh size did not improve the results. According to the guideline of ABAQUS, one fourth of that selected mesh (here a little smaller mesh size of 4 mm) needed to be used for the cohesive layer.

- ***Parts and assembled models:*** Figure 5.12 (a) and Figure 5.12 (b) show the model setup for the analysis. The model is assembled from seven parts tied together. The cohesive layer is defined to provide a full connection between upper and lower parts of the beam. No slipping was allowed between the steel plates and the LVL beam at the supports and loading points.

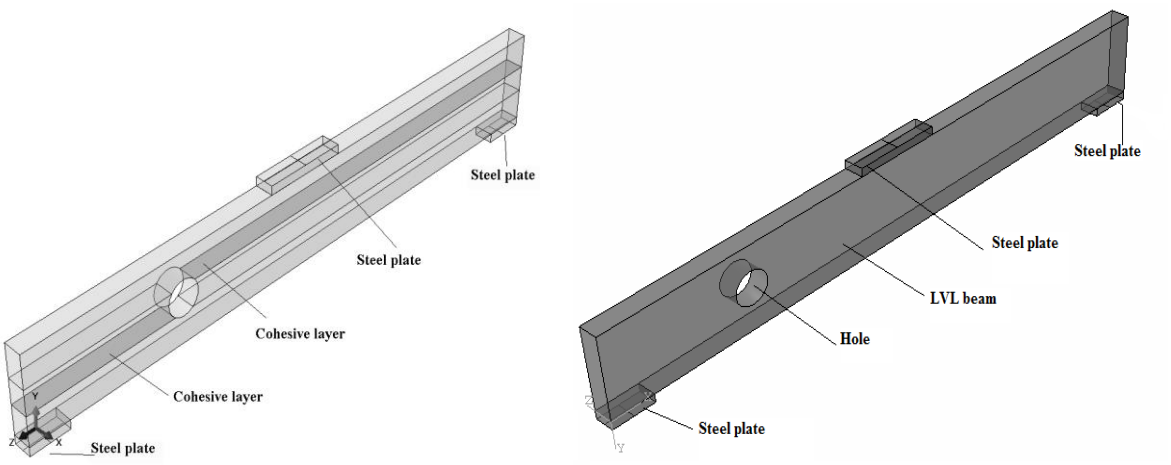

(a) (b)

Figure 5.12. Model setup for the analysis: (a) with cohesive layer, (b) without cohesive layer

5.5.1 Distribution of the stress along the breadth of LVL beams with holes

The results of the elastic analysis in terms of stress distribution around the hole on the beam 11 of the Table 3.3 are shown in Figure 5.13 while Figure 5.14 shows the distribution of the tensile stresses along the breadth of the beam in the location with maximum tensile stresses. The beam was analysed under a load of 30 kN. The tensile stress perpendicular to the grain was previously explained in chapter 4 for two-dimensional modelling. The 3D modelling gives the distribution of the tensile stresses across the thickness of the specimen. The model shows that, the tensile stresses at the mid-breadth of the specimens are slightly larger than other surrounding points. The difference across the breadth of the hole is however small. This implies that plane stress is valid and 2D modelling gives similar results to 3D modelling. This result is in good agreement with the experiments where the crack started always from mid-breadth of the specimens and expanded towards the outer edge of it.

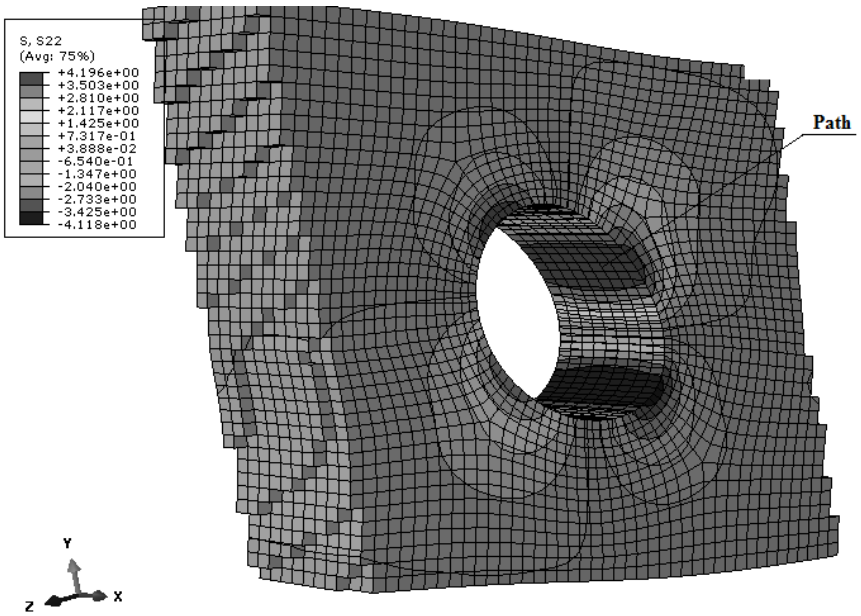

Figure 5.13. Result of the elastic analysis of beam 11 in Table 3.3

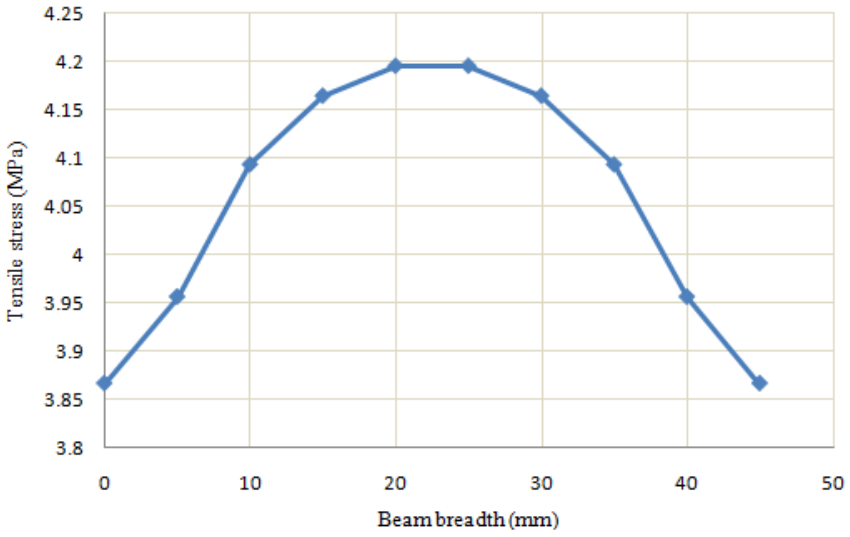

Figure 5.14. Tensile stress distribution across the breadth of the hole

5.5.2 Adjusting material properties of the cohesive layer

Calibration of the material parameters of the cohesive layer to the experimental test is important. The parameters of the cohesive layer (traction-separation behaviour) need to be addressed properly to obtain better estimation of the failure load. At the Lund Institute of Technology, complicated equipment has been developed for obtaining traction-separation behaviour of wood. The equipment loads specimens bi-axially, and it creates mixed mode testing. The measured tensile and shear movements δ_n and δ_s allow mixed mode behaviour (Figure 5.15 (a)). The glued notched timber specimen enables stable crack propagation as shown in Figure 5.15 (b) and Figure 5.15 (c). The curves refer to shear stress-displacement and tensile stress-displacement for spruce.

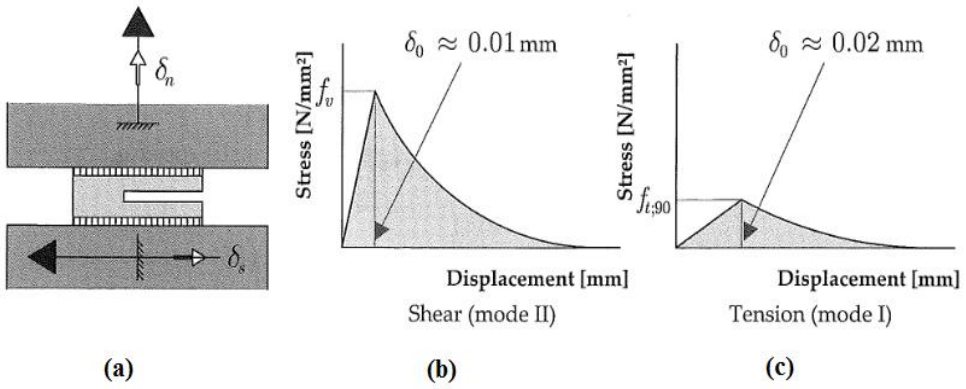

Figure 5.15. Experiment for traction-separation behaviour: (a) sketch of the test set up, (b) load-displacement relationship for shearing, (c) load-displacement for tensile load (Schoenmakers 2010)

Indication of the parameters of the cohesive layer in ABAQUS needs three elastic material properties for the cohesive layer, three strength properties including one tensile strength, two shear strength values for damage initiation and three fracture energy values for opening and shearing modes aimed at evaluation of the damage.

Elastic material properties: The initial stiffness of the cohesive elements defined in terms of the traction-separation curve does not represent a physically measurable quantity and it is treated as a penalty parameter. Ideally, the stiffness of the cohesive elements should be infinite so that they do not affect the overall compliance of the model before the damage initiation; however, finite values should be used in the context of the finite element method. Using guidelines provided by ABAQUS (Dassault-Systemes-Simulia-Corp. 2006), the stiffness of the cohesive layer for tension was selected to be equal to the surrounding material stiffness. The shear moduli (Table 5.2) without distinction between the two directions were assumed to be twice the corresponding material properties.

Damage initiation: Strength properties for damage initiation for tension perpendicular to grain were obtained through an experimental program on the materials presented in chapter 2, and repeated in Table 5.2. The shear strength property of LVL was adopted from Buchanan (2007).

Damage evolution: The damage evolution of cohesive elements in terms of the traction-separation curve is described as fracture energy of the interface. Selection of appropriate

fracture energy for the cohesive layer is important. LVL in the tension mode of fracture shows that its critical energy release rate (G_{IC}) is different from the fracture energy (G_{If}). This could be due to the softening after cracking in LVL (Ardalany et al. 2012a). Inserting the lower value of the critical energy release rate (G_{IC}) in the model under-estimates the experimental results, while G_{If} values over-estimates the failure load. So, a calibration of the model results with the experimental results was regarded as necessary to alleviate this discrepancy. Saved models were analyzed with different values of the fracture energy starting from the lower value G_{IC} to the higher values G_{If} with small increments of the fracture energy being used. Closer results to the experimental values were obtained with the fracture energy value of 0.70 N/mm which is about the average value of G_{IC} and G_{If}. Figure 5.16 shows a comparison of the load-deflection curves with different fracture properties of LVL. The shearing fracture energy values were adopted from Van der Put $G_{IIc} = 4G_{Ic} = 1.2$ N/mm (Van Der Put T.A.C 2011).

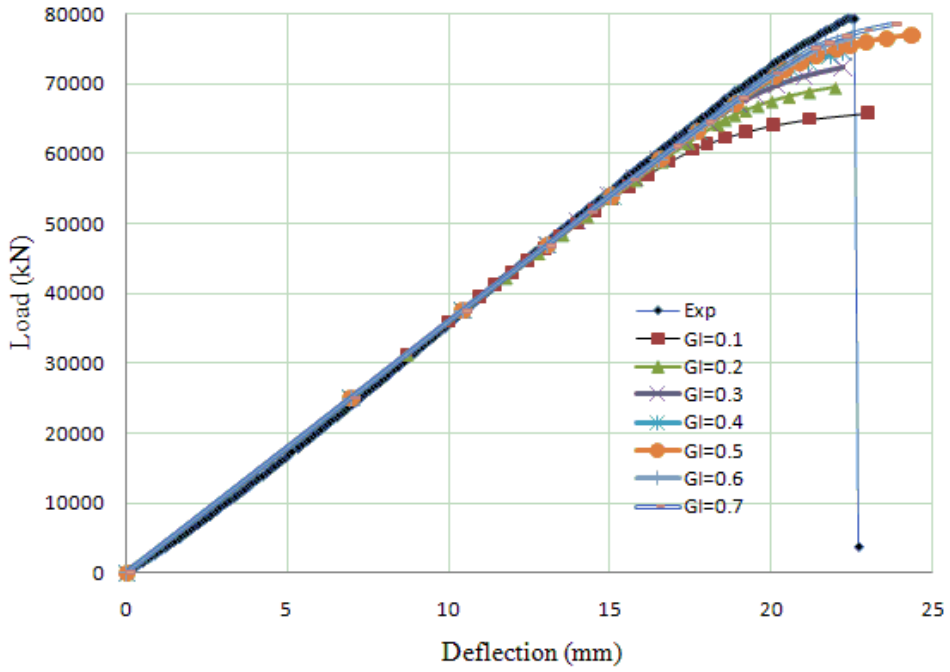

Figure 5.16. Load-deflection curves of beams with hole for different values of fracture energies

Table 5.2 summarizes the material properties used for the cohesive layer.

Table 5.2. Material properties of the cohesive layer

Elastic material properties	Modulus of elasticity (perpendicular to grain) = 485 MPa Shear modulus = 1200 MPa
Damage initiation	Tensile strength perpendicular to grain = 2 MPa Shear strength = 6.2 MPa
Damage evolution	Normal mode = 0.70 N/mm Shear mode = 1.2 N/mm

5.6 Model validation

Using cohesive elements requires some benchmark modelling; therefore, the experiments on 700×100×63 mm size specimens (Appendix 1) were modelled to investigate mode I (opening) of LVL fracture, and to compare with the experimental results. The parameters of Table 5.2 with the experimental fracture energy in mode I were used for the modelling.

Figure 5.17 shows the experimental/numerical comparison in terms of the load-deflection curve. Cohesive elements with mesh size of 2 mm were used between the arms where the crack should start to grow. The meshing outside of this region was coarser (15 mm). Riks analysis (a method to capture the behaviour after the instability) was used in the analysis, because the Newton method fails to converge in softening part of the curve.

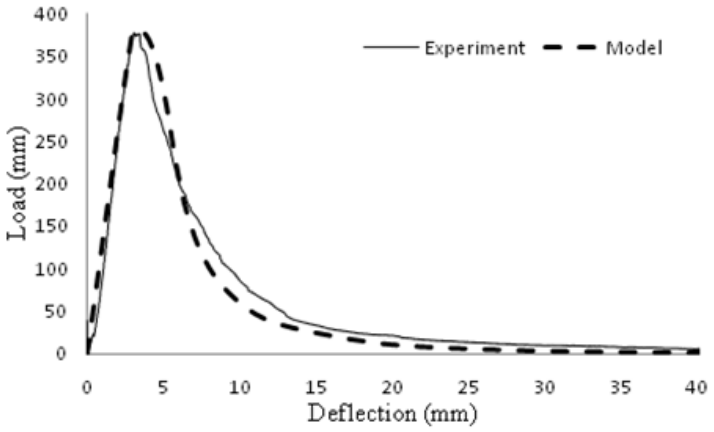

Figure 5.17. Experiments on mode I of LVL: (a) deformed specimen, (b) comparison of the experimental data with the numerical analysis

Another series of the numerical analysis was performed on the notched LVL beams, tested experimentally, and was used for comparison. The dimensions of the beam and arrangement of the cohesive layer is shown in Figure 5.18.

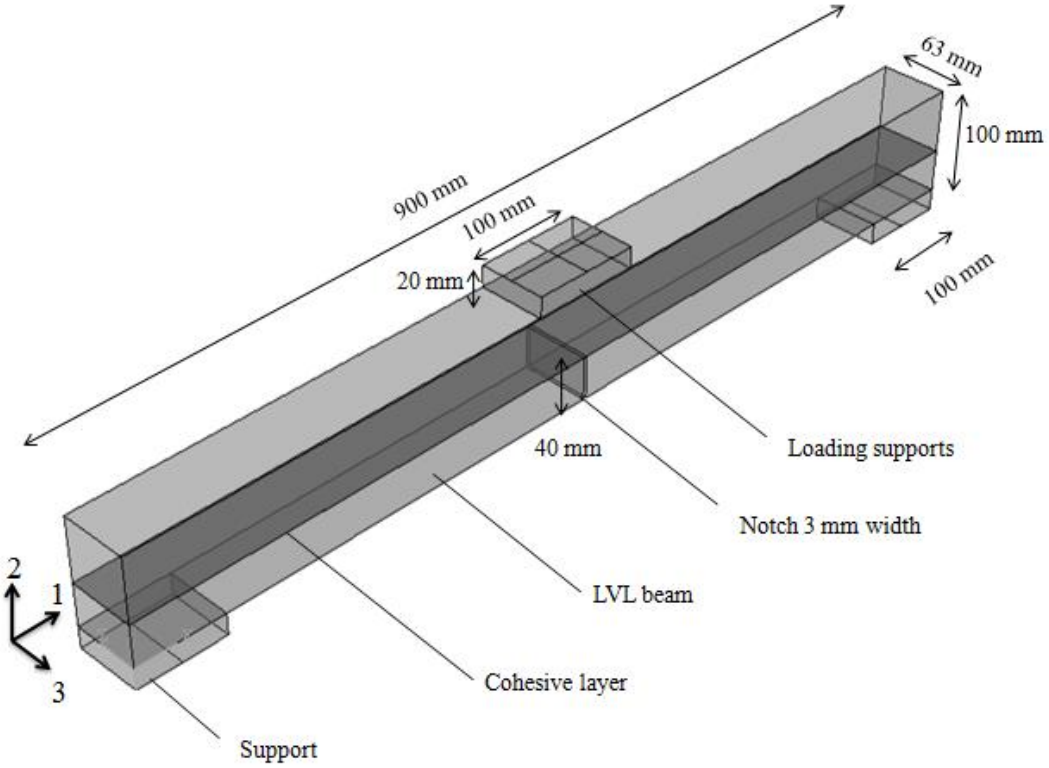

Figure 5.18. Notched LVL beam

A comparison of load-deflection at mid-span of the beam with the numerically predicted values is shown in Figure 5.19 (a) and a picture of the numerical model is shown in Figure 5.19 (b). The load-deflection from the finite element analysis is similar to the average of the experimental program. However, the numerical analysis does not have any yielding criterion and the calculation continues with higher deflections in the elastic body. A picture of the experiment is presented in Figure 5.19 (c).

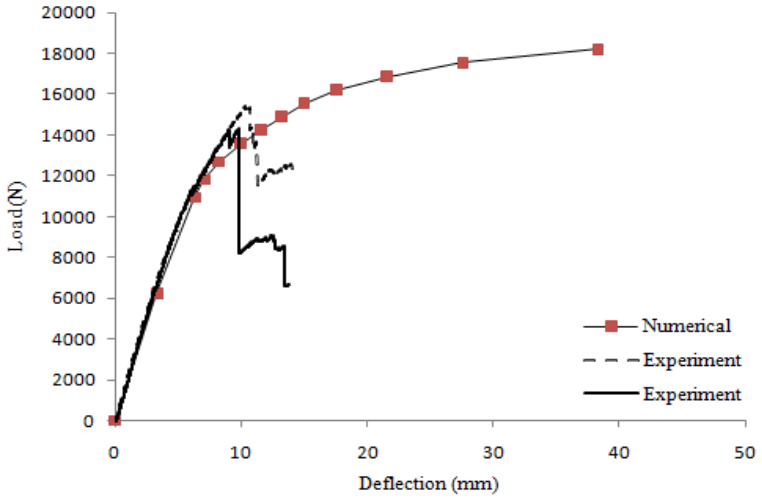

(a)

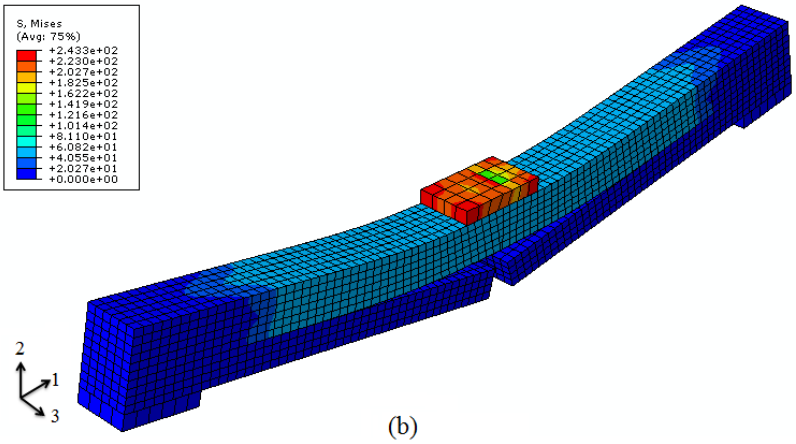

(b)

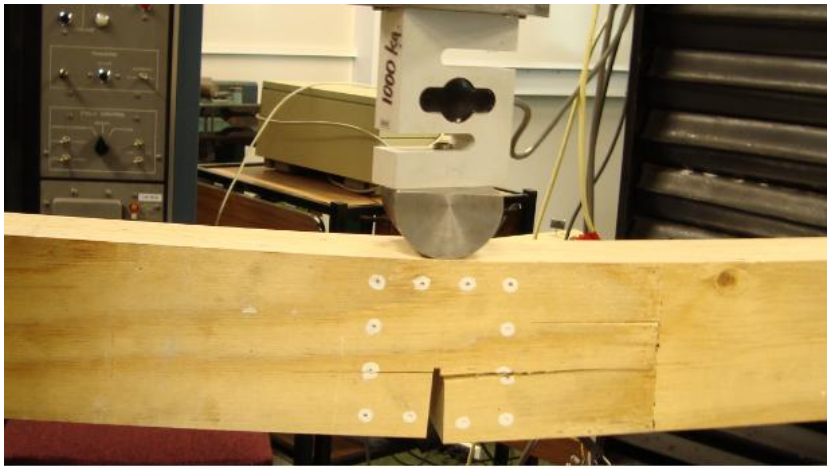

(c)

Figure 5.19. (a) Comparison of the load-deflection, (b) model of notched analyzed LVL beam, (c) experiment on LVL beam

5.7 Experimental verification

Comparison of the experimentally tested LVL beams with the numerical values was performed to investigate the accuracy of the numerical results and to study the behaviour of the fracture layer. In the following parts modelling of LVL beams with the holes, LVL beams with holes reinforced with screws and plywood are presented.

5.7.1 Modelling LVL beam with hole

Figure 5.20 (a) shows the model of a beam with hole (beam 4 in Table 5.3) where the crack propagated from the hole edge to the end of the beam. Meshing of the model has been removed for clear presentation. The loading history of the beam could be divided into four steps: Step (i), initial loading the model caused the tensile stress at the cohesive layer to increase while the shear stress in the layer was relatively low. Step (ii), by increasing the load, the tensile stress at the cohesive layer crack tip first reached the strength of the material, then the crack started to propagate. According to the bilinear model, crack propagation caused the stiffness to decrease and consequently the tensile stress at the crack tip to decrease. Step (iii), subsequent load increments caused additional reduction of the elements stiffness at the crack tip until the elements stiffness decreased to zero. At this stage, the element is removed from the model. This procedure is repeated for the other elements. Gradually, the amount of the shear stress at the other elements of the cohesive layer increased and reached its maximum value. Finally, the shear failure governed the failure of the beam at the end of the process. Step (iv), similar to the experiments, in the model, the cracks propagated from the edge of the hole towards the end of the beam and the shear failure governed the failure of the beam. The crack at the mid-span of the beam failed to propagate because of the concentrated load at mid-span. The element removal due to the tensile stress was gradual while shear crack propagation caused a series of elements of the cohesive layer to fail.

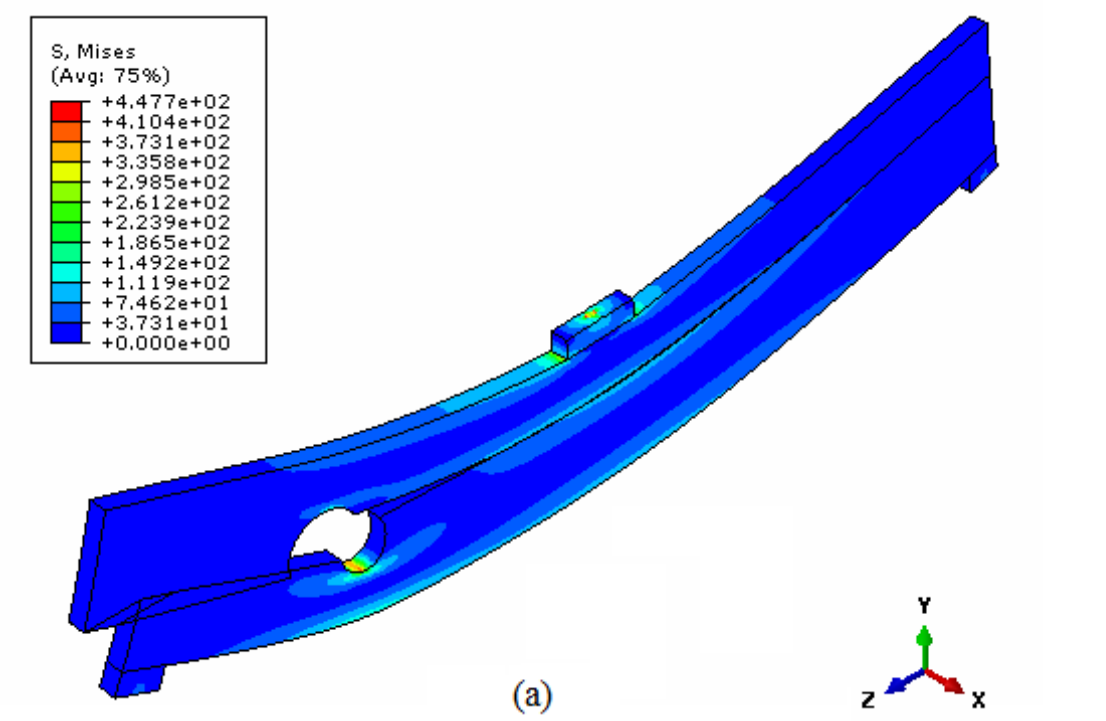

Figure 5.20. (a) Deformed shape of the model with cohesive layer at failure, (b) photo of the experiment

Figure 5.21 shows the successive contours of the tensile stresses layer for four load increments of beam 4 listed in Table 5.3. In the Figure 5.21 (a), the tensile stresses at the crack tip reached the maximum value. In the few next increments (Figure 5.21 (b)), the tensile stresses increased in few more elements. Now according to the bilinear

traction separation law, the following increment (Figure 5.21 (c)) caused the tensile stresses at the crack tip to decrease because according to the model, the stiffness of the layer now decreased. This was due to the increase in the element thickness because of crack opening. Finally, when the stiffness of that layer reaches zero, the elements surrounding the crack tip were removed from the model (Figure 5.21 (d)). Two rows of elements were removed from the model.

Figure 5.22 shows the contours of the shear stress change in the cohesive layer for the beam 4 of Table 5.3. The same increments that were used for the tensile stresses were selected for the shear contours. The first contour (Figure 5.22 (a)) shows that the shear stress in the layer is relatively low and the next increase (Figure 5.22 (b)) shows a moderate increase in the shear at the crack tip. In the third contour (Figure 5.22 (c)), the shear stress at a distance far from crack tip has increased considerably and finally (Figure 5.22 (d)) by increasing the load, the shear further increased in the cohesive layer. This corresponds to the element removal from the hole edge due to the tensile stresses.

Table 5.3 presents the results of failure load predictions for the beams that were experimentally tested. The predicted failure loads are close to the values obtained from the experiments.

Table 5.3. Comparison of the experimental result with numerical data

#	Dimension (mm)	Lc (mm)	Dc (mm)	Diameter (mm)	Experimental failure load (kN)	Numerical failure load (kN)
1	1500×200×45	400	100	80	39.4	39
2	2100×300×45	550	150	80	68.3	70.4
3	2100×300×45	550	150	120	55.9	60
4	2600×400×45	550	200	160	67.3	60

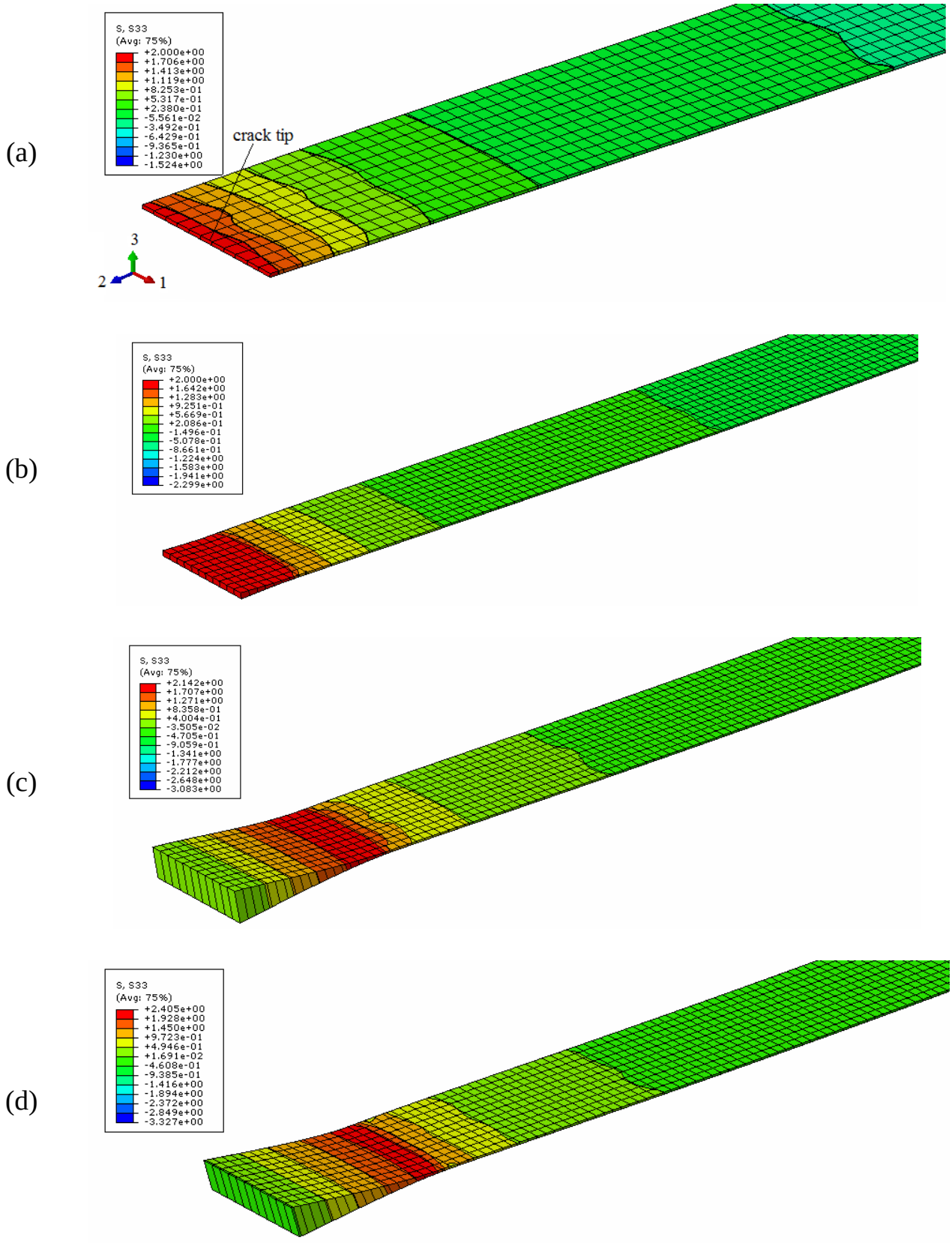

Figure 5.21. The contours of tensile stresses in the cohesive layer

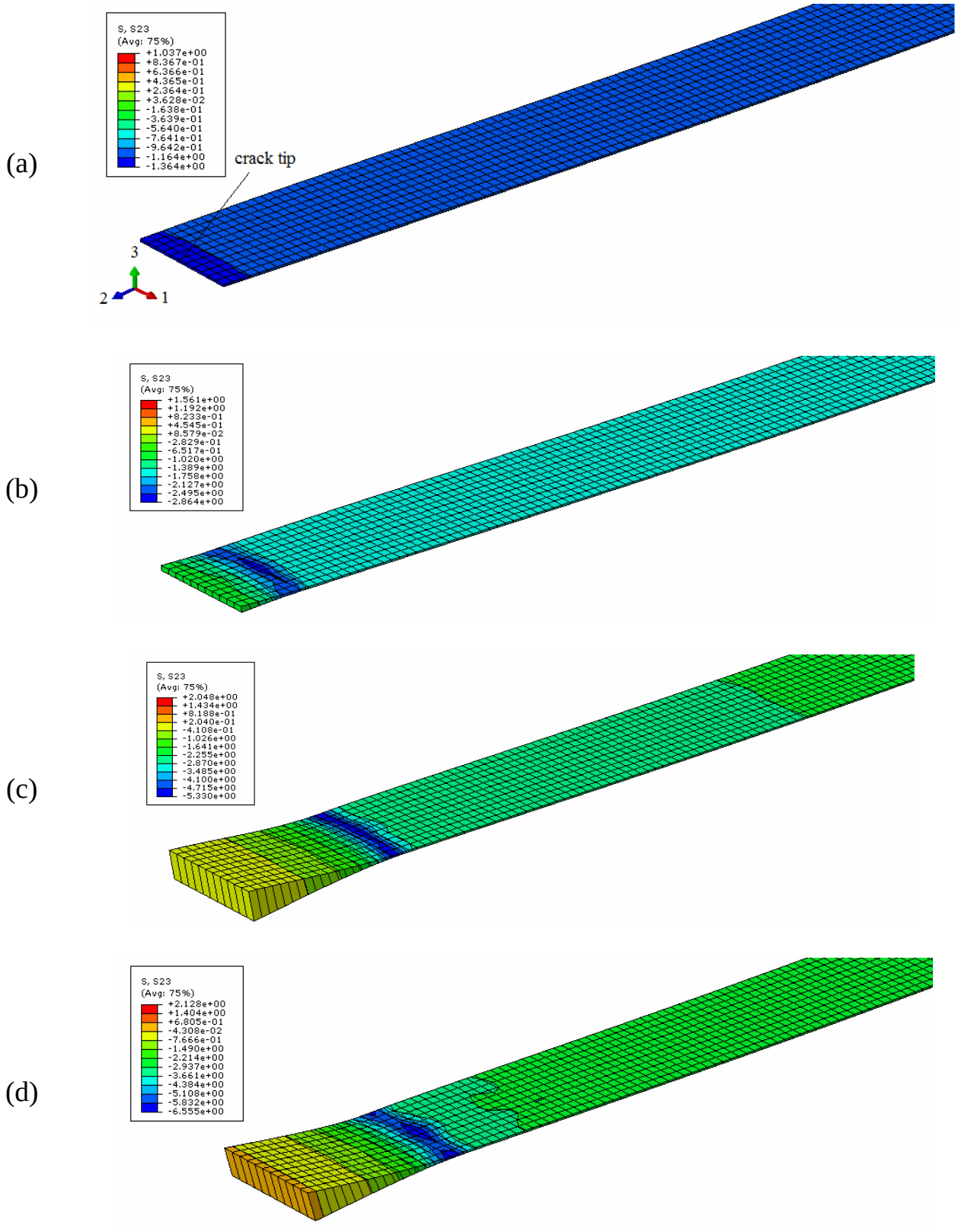

Figure 5.22. The contour of the shear stresses in the cohesive layer

5.8 Modelling of reinforcement

As indicated in chapter 3 in the experimental program, screws and plywood are two viable options for reinforcement of LVL beams with holes. The behaviour of screws and plywood in controlling the crack propagation is not clear. Cohesive elements help to obtain better understanding of the working mechanism of reinforcement because the behaviour of the fracture layer can be studied. For modelling purposes, two cases of reinforcement were considered viz.: (i) screws and (ii) plywood.

5.8.1 Screw reinforcing

The working mechanism of the screw for controlling crack propagation was studied through using cohesive elements. Beam 15 of Table 3.3 was used for the modelling. Table 5.4 presents the beam geometry for easier access while the corresponding model set up is shown in Figure 5.23.

Table 5.4. Model geometries

Dimension (mm)	Diameter (mm)	Lc (mm)	Dc (mm)	Reinforcement	Loading (kN)	Loading type
1500×200×45	80	400	100	two screws	44.9	centre loading

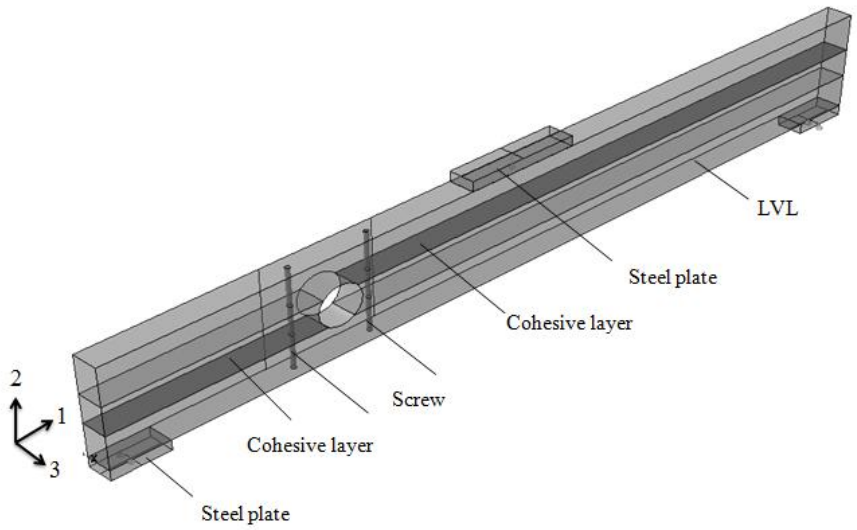

Figure 5.23. Reinforcement with screws

The figure shows two layers of cohesive elements (left and right as depicted in Figure 5.23) tied to the beam at two possible crack surfaces. The procedure of the modelling is such as the previous explained procedure with a difference that comes back to the screws. Two screws of 8 mm diameter are inserted vertically in the beam to mimic the behaviour of the screws. The centres of the screws have a distance of 30 mm from the nearest edge of the hole, the same as the experiments. Connection between the screws and the beam (vertical tube in the beam) is assumed perfect. A mesh size of 2 mm was used for the screws, while a 15 mm mesh size were used for the remainder of the beam. Figure 5.24 shows the right cohesive layer of Figure 5.23. The numbers as shown on the figure point to the row and they will be referred to in the next parts.

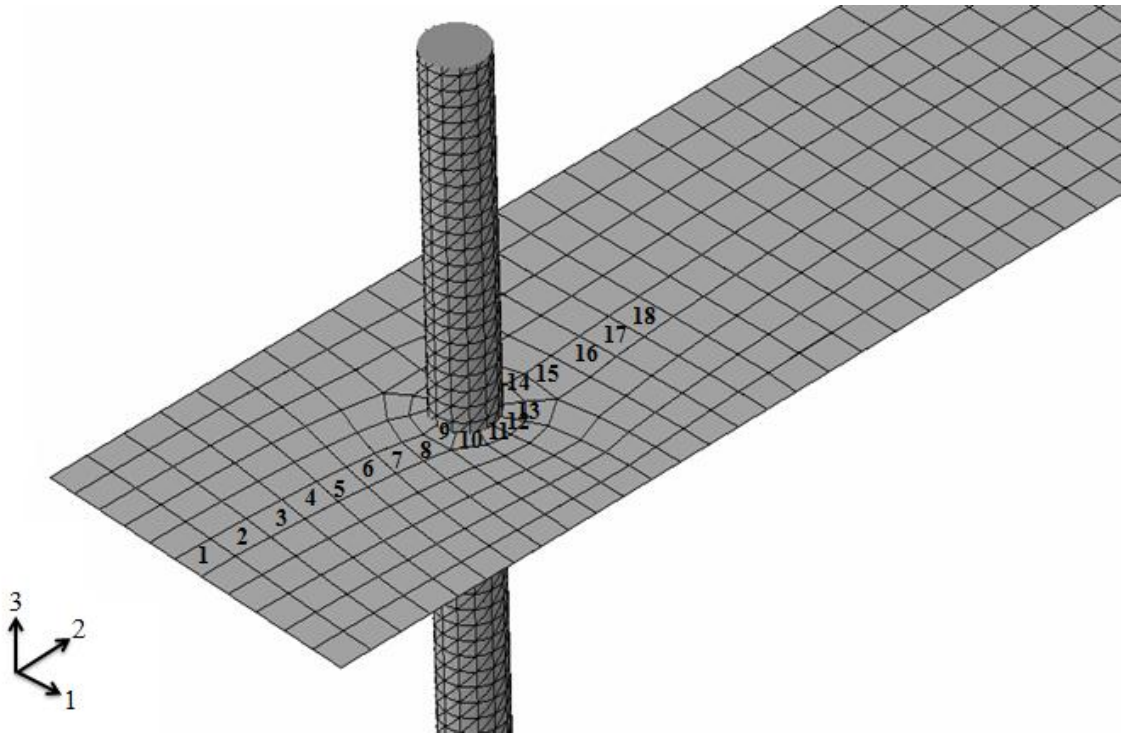

Figure 5.24. Cohesive layer elements

The procedure of crack initiation in a reinforced beam with screws is similar to the unreinforced one. The modelling indicates that as the tensile stresses at the hole edge (row 1 in Figure 5.24) increase and reach the tensile strength of the material (2 MPa), the elements farther along (e.g. row 2, 3 in Figure 5.24) will receive more deformations. Increasing the load causes the tensile stress at the hole edge elements (row 1 in Figure 5.24) to fall gradually and consequently reach maximum stress in the other elements

(row 2 and 3 in Figure 5.24). The procedure continues until the stress of the elements surrounding the reinforcement reaches their maximum values (Figure 5.25).

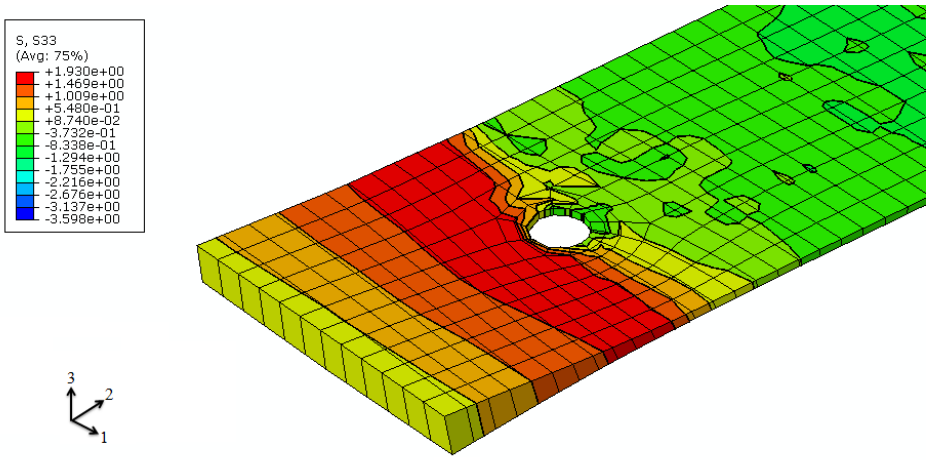

Figure 5.25. Normal stress increases around the screw

As the load increases, the tensile stresses at the other side of the screw (row14, 15, 16, 17, 18, 19 in Figure 5.24) do not increase anymore. This is due to the screw that controls the tensile stresses considerably. Now the shear stresses increase surrounding the screw (row 14, 15, 16, 17, 18, 19 in Figure 5.24) (Figure 5.26). If no other failure modes such as breakdown due to high moment at mid-span occur, increasing load may cause yielding of the screw and shear failure to start at the screw location.

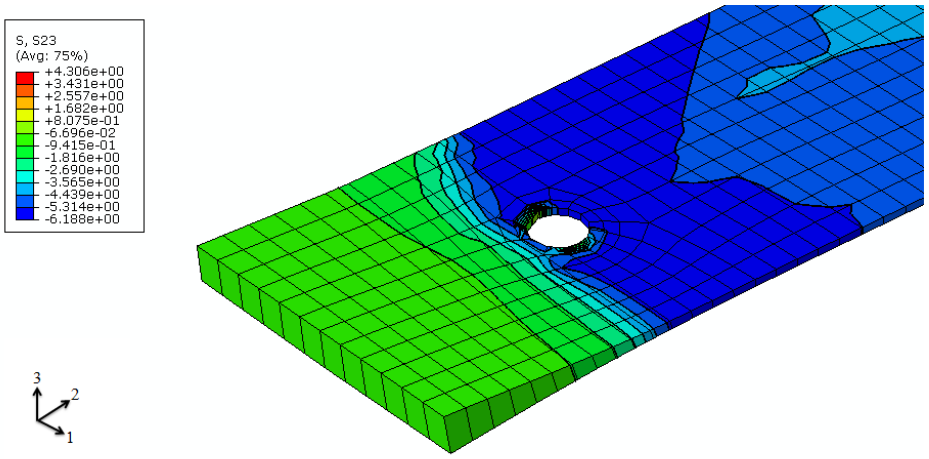

Figure 5.26. Shear stresses increase around the screw

5.8.2 Plywood reinforcement

Plywood is also an alternative for reinforcing of LVL beams with holes. Plywood creates a full bond with the surrounding beam. To look into the working mechanism of the plywood, beam 13 of Table 3.4 was modelled using the cohesive elements. The geometry of the beam is presented in Table 5.5 for easier access.

Table 5.5. Geometry of the beam with hole reinforced with plywood

Dimension (mm)	Diameter (mm)	Lc (mm)	Dc (mm)	Plywood dimensions (mm)	Loading type
1500×200×45	80	400	100	200×200×9	centre loading

In the modelling, plywood was assumed to have full bond with the LVL with elastic orthotropic material properties of the LVL. As in the experimental program, three veneers were defined for the plywood in the modelling, and material orientation was changed to match with the experimental program. The modelling procedure was the same as reinforcing with screws. Figure 5.27 shows the meshing and model parts. The meshing size of the beam was 20 mm, and 5 mm for plywood with linear four node tetrahedron elements (C3D4). The meshing of the cohesive layer was with eight node three-dimensional cohesive element (COH3D8) with the meshing size of 4 mm.

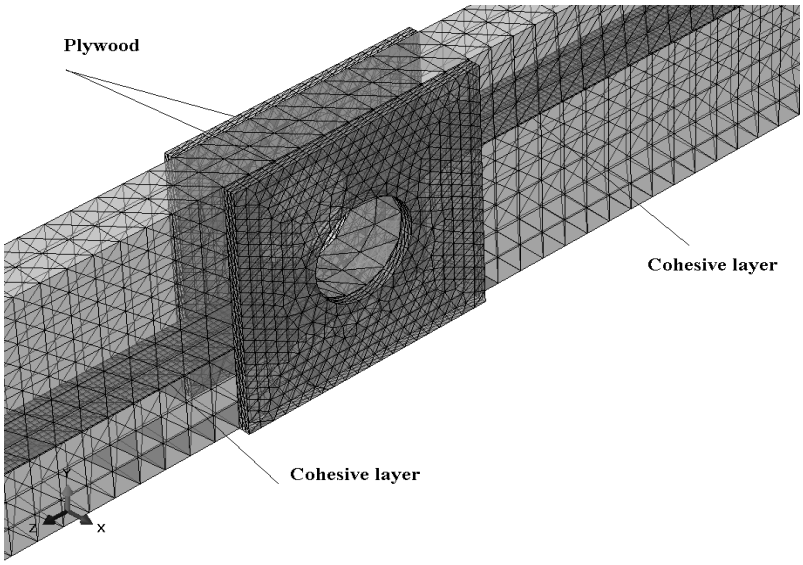

Figure 5.27. Reinforcement with plywood

The modelling indicates that as the load increases, the elements surrounding the opening edge at the mid-breadth reach the maximum tensile strength of the material. These are elements farther from the plywood surface. The plywood affects closer elements more than farther elements (Figure 5.28 (a)). Increasing the load, the shear stresses simultaneously are increasing in the layer. The maximum shear increases occur in elements that are not close to the hole edge (Figure 5.28 (b)). Again, if no failure mechanism such as a mid span failure due to high moment occurs, the failure is governed by opening of the crack at the hole edge at mid-breadth followed by its expansion to the outer edges and finally shear failure at the other elements in the layer. Since plywood has a dual action in controlling tensile stress and the shear stress, it can effectively recover the capacity of reinforced beams.

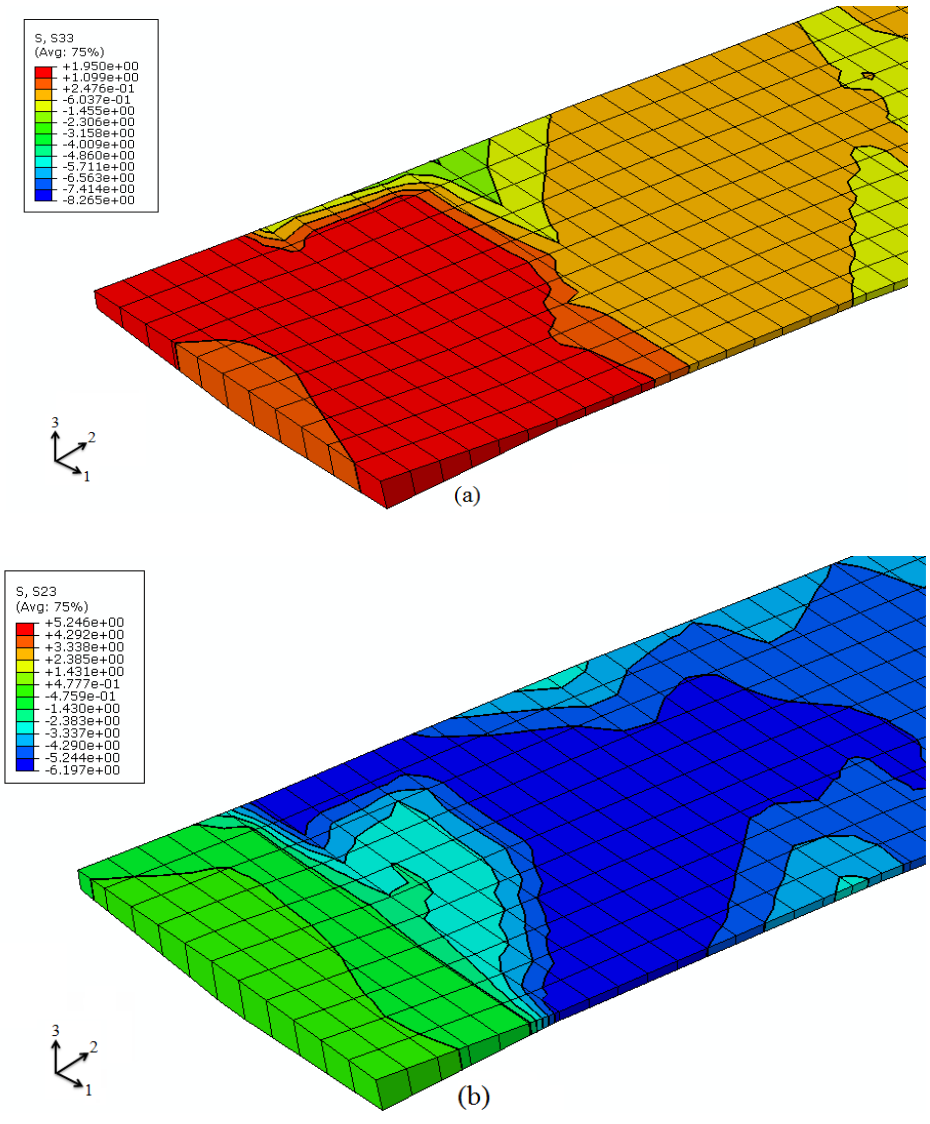

Figure 5.28. (a) Tensile stresses at the cohesive layer, (b) shear stress at the cohesive layer

5.9 Summary

This chapter used cohesive elements for failure load predictions of LVL beams with holes. The model was expanded by adding reinforcement to the model. The behaviour of the fracture layer was investigated. The key outcomes of the modelling are:

- Cohesive elements with traction-separation behaviour can be used for the failure load predictions of LVL beams with holes. The material properties of the cohesive layer are important parameters for the failure load predictions.
- Finite element analysis showed crack initiation begins with the elements surrounding the crack tip reaching the material strength. The tensile stresses cause the crack to start and the shear stress at the crack propagation becomes important.
- Plywood controls the tensile stress while it simultaneously increases the shear capacity of beam locally. Plywood because it controls shear stresses and also tensile stresses simultaneously is a good option for reinforcing thin members while for thick members screws is effective in controlling the tensile stresses
- Although reinforcement like screws can stop crack propagation, they simultaneously increase shear stress concentrations locally around the reinforcement. While the shear stress concentration around the screw is being transferred mainly by LVL, for the reinforcement by plywood, a mixture of plywood and LVL transfers the shear stresses.

The next chapter covers an analytical model for cracking load estimation of LVL beams with the holes.

6 Analytical predicting the cracking load

This chapter presents an analytical method for predicting the cracking load of LVL beams with holes. The theory for a beam on an elastic foundation was applied to the LVL beam, and three formulations were derived. The formulation accuracy is compared against experimental data of LVL and showed good predictions. The results of this chapter have been used in chapters 8 and 9.

The majority of this chapter has been re-produced from the following journal paper:

Ardalany M, Fragiacomo M, Deam B, and Crews K (2012) "Analytical cracking load estimation of Laminated Veneer Lumber (LVL) beams with holes (Accepted). Journal of Holz als Roh- und Werkstoff:1-12

6.1 Introduction

Chapter 2 presented material properties of LVL including fracture properties and tensile strength of LVL in the perpendicular to the grain direction. Chapter 3 covered experiments on LVL beams with holes and reinforcement methods for holes. Analysis of beams with holes using LEFM and the cohesive element were presented in chapters 4 and 5 respectively. Previous chapters were mainly experimental or numerical analysis toward failure load prediction. The current chapter is about the cracking load prediction of LVL beams with holes.

In the process of crack initiation and propagation around a hole, three phases have been reported in the literature from the crack formation to failure for glulam beams with holes (Danielsson 2007). Experiments in chapter 3 confirmed similar phases of crack

initiation and propagation for LVL beams with holes. In the first phase, a crack is formed at the mid-breadth of the beam around a hole, followed by the propagation to the surface of the beam during the second phase and by the crack propagation along the beam axis until the structural failure of the beam during the third phase. These phases are depicted in Figure 6.1.

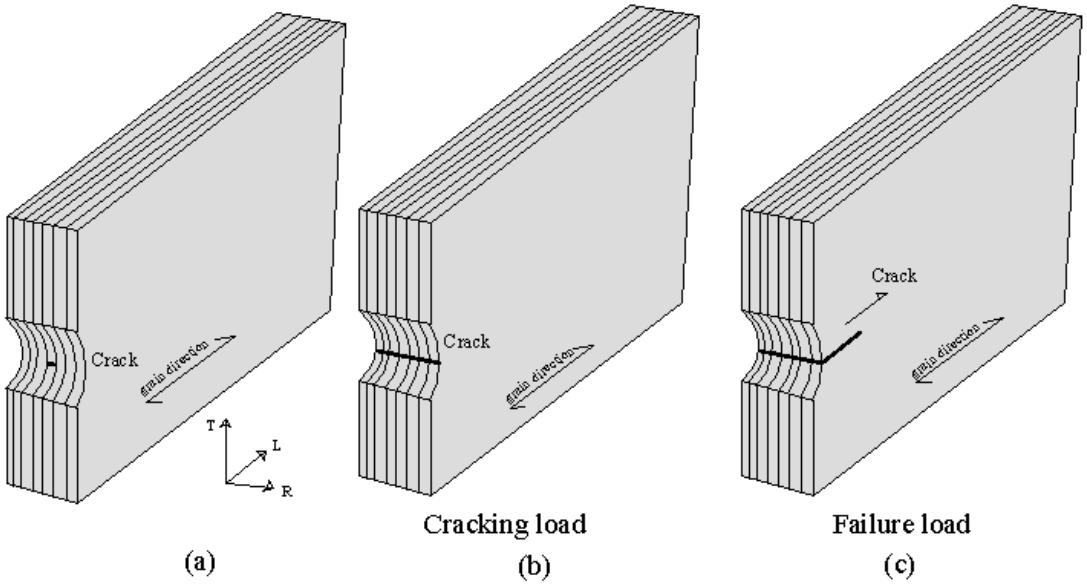

Figure 6.1. Different phases of crack initiation and propagation around the hole in LVL beams: (a) mid-breadth cracking, (b) crack reaches surface, (c) crack propagation along the grain direction

Predicting the cracking load is important because if the load that the beam is designed for is smaller than the cracking load, no further actions like reinforcement of the holes will be required in design. Such load prediction could also be incorporated into design codes to account for the tensile strength of timber perpendicular to the grain. Although extensive study has been carried out in this field, most of the research is concentrated on the failure load prediction, that is, the final load that the beam can carry (Figure 6.1(c)).

Up to now, no closed form solution exists in the literature that can effectively handle this problem. This chapter investigates the prediction of the cracking load for LVL beams with round and rectangular holes. Three cases of beams subjected to pure shear, pure bending moment, and a combination of them are considered. The derived

analytical formulas are compared with the results of experiments from chapter 3 showing good correlation.

6.2 Beam subjected to pure shear (moment is disregarded)

Consider a simply supported beam with a round hole located close to the support. The beam is loaded at mid span with a concentrated load. If the hole is large enough, as the experimental program in chapter 3 demonstrated, the cracks are likely to initiate and propagate around the hole because of the low tensile strength perpendicular to grain of LVL. Figure 6.3 shows the crack propagation around a hole in a specimen subjected to centre loading.

The cracks usually start in the point of the hole perimeter either with the maximum tensile stress perpendicular to grain (the maximum normal stress) or with the maximum principal stress. The maximum normal stress criterion is used by (Aicher et al. 1995) while the maximum principal stress criterion is used by Guan et al. (2004). From the finite element sensitivity analysis carried out in chapter 4, it was concluded that their differences in failure load predictions are small.

From a finite element analysis of a 1300×200×45 mm beam loaded at mid-span with a 30 kN concentrated load, it was found that the maximum normal stresses predicted the angle of the first crack formation at about 45 degrees (Figure 6.2) that matches fairly well with the experimental results. However, the maximum principal stress shows a 258 degrees angle from the horizontal axis. This is mainly pointing to the place where the second crack occurs in the beam (left side of the hole in Figure 6.3 (a)). However, the first maximum principal stress occurs at an angle of 60 degrees (Figure 6.2), which does not match very well with the experimental results.

Although the crack initiation location could change depending on the region where the hole is cut in the shear-dominated regions, it can be stated that cracks usually start at an angle of 45 degrees with respect to the beam axis (Figure 6.3 (c)). After formation, the crack propagates in the grain direction because of the highly anisotropic nature of wood and low tensile strength perpendicular to grain (Jernkvist 2001a,b).

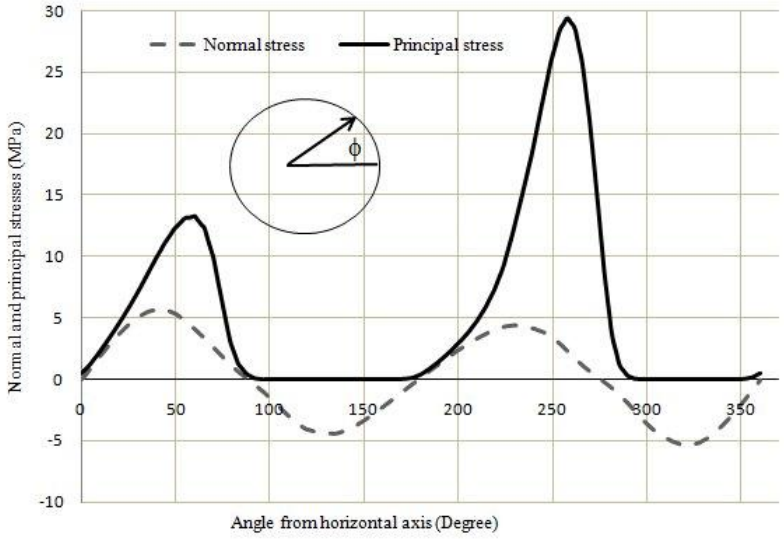

Figure 6.2. Variation of principal stresses and normal stresses with the angle from horizontal axis

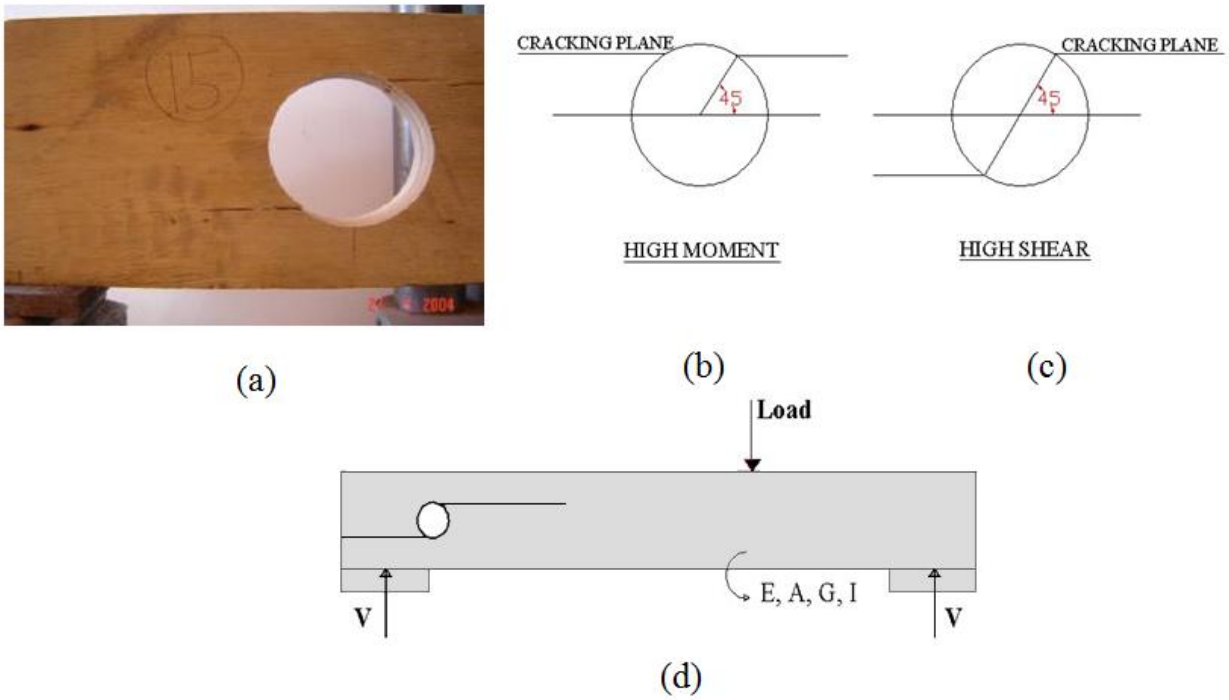

Figure 6.3. Crack initiation and propagation around the hole: (a) tested beam, (b) sketch of cracking in high moment area, (c) sketch of cracking in shear-dominant area, (d) sketch of the beam with hole

After crack formation, the crack separates the beam in two parts, which can be assumed to be connected with linear elastic springs ahead of the crack tip, where the springs schematize the cohesion force or glue for material interfaces in tension. With the formation of the first crack, the upper beam can be regarded as a beam on an elastic foundation, assuming the lower beam is infinitely stiff in bending (Kanninen 1973; Schoenmakers 2010). Figure 6.4 displays the beam on an elastic foundation schematization along with the crack propagation in a beam with a hole in a shear-dominated region, where 'a' signifies the crack length, P_0 and M_0 signify the shear force and bending moment of the beam in the cross-section at the hole location, 'x' is the abscissa of a cross-section measured from the point where the crack forms, and 'w' is the displacement in the vertical direction. The cracking surface is modelled as a spring with a specified stiffness. Assuming two separate beams in the crack region (Figure 6.4 (c)) is close to reality since according to Chan et al. (1974), and Pirzada et al. (2008), the parts of the beam near the hole can be treated as individual structural members, and analyzed using established structural mechanics methods.

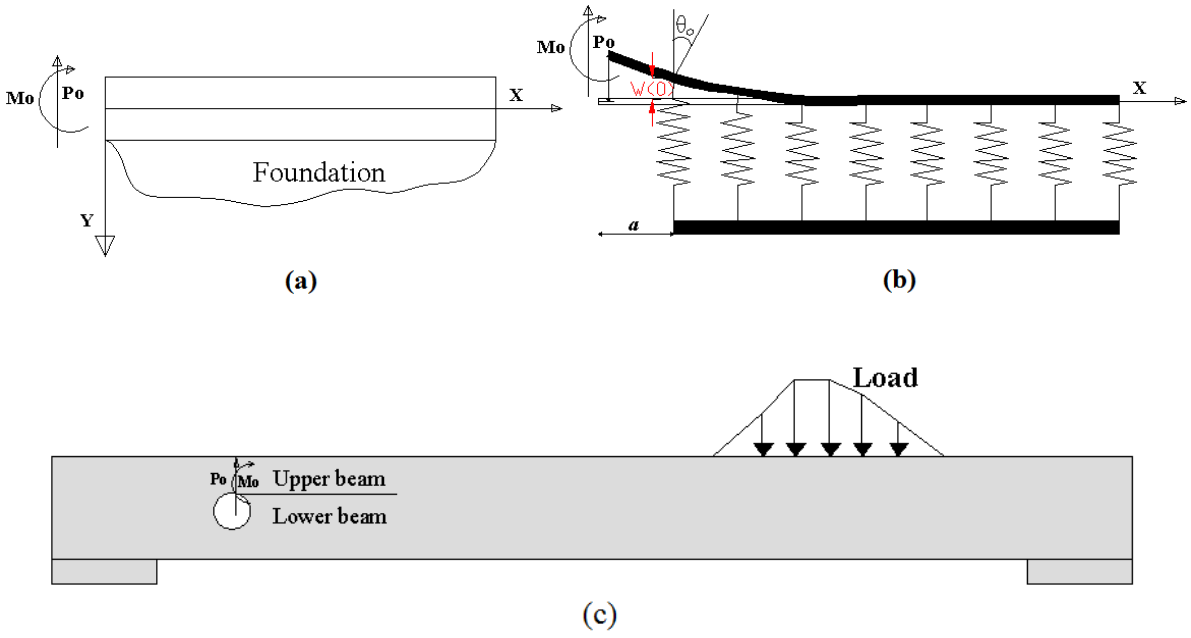

Figure 6.4. Model of beams on elastic foundation: (a) beam on foundation, (b) schematization of a beam on spring as elastic foundation, (c) crack around a round hole

Since stress concentration normally occurs at the hole perimeter at an angle close to 45 degrees with respect to the horizontal axis, it is assumed that the crack will form at that location and will propagate in the grain direction. After the cracking the upper part of the beam may considered as an elastic beam resting on Winkler springs connected to the lower beam part assumed as infinite stiff foundation (Figure 6.4 (b)). Such an assumption holds for the case where the upper beam is much smaller than the lower beam because the stiffness of the upper beam will be much lower than the lower beam. The model also does not include the shear springs in the layer.

The concept of a beam on an elastic foundation is then used for the analysis assuming that the fracture properties of wood apply to the springs, namely the stiffness of the Winkler springs is defined in terms of the tensile strength and fracture energy. If the deformation at $x = 0$ is denoted by $w_{x=0}$, according to the beam on elastic foundation theory the following formulation that accounts for the shear deformations in the beam section can be derived (Jensen et al. 2004):

$$w_{x=0} = \frac{-2}{Kb}(\beta P_{x=0} + \lambda^2 M_{x=0}) \tag{6.1}$$

$$\beta = \sqrt{\lambda^2 + \frac{3Kb}{10GA}} \tag{6.2}$$

$$\lambda^4 = \frac{Kb}{4EI} \tag{6.3}$$

$$\theta_{x=0} = -\frac{P_{x=0}}{2EI\lambda^2} - \frac{M_{x=0}}{\beta}\left(\frac{6\lambda^2}{5GA} + \frac{1}{EI}\right) \tag{6.4}$$

$$\sigma = -Kw(x) \tag{6.5}$$

In the above formulation, 'K' is the modulus of elasticity of the foundation (springs), 'E' is the modulus of elasticity of the beam in bending, 'b' is the breadth of the beam, 'G' is the shear modulus of the beam, 'A' is the cross-sectional area of the assumed beam, 'I' is the second moment of area of the assumed beam, ' σ' is the stress in the foundation (spring), which schematizes the tensile stress ahead of the crack tip, $w(x)$ is the deflection of the foundation, $\theta_{x=0}$ is the change in the angle of the rotation of the

beam on the elastic foundation . $M_{x=0}$ and $P_{x=0}$ are the moment and shear at that section of the beam. For pure shear in the beam, the above formulations will simplify as below:

$$w_{x=0} = \frac{-2}{Kb}(\beta P_{x=0}) \tag{6.6}$$

$$\theta_{x=0} = -\frac{P_{x=0}}{2EI\lambda^2} \tag{6.7}$$

The stress perpendicular to the grain ahead of the crack tip is obtained by inserting Equation (6.6) into Equation (6.5):

$$\sigma_{x=0} = \frac{2P_{x=0}}{b}\sqrt{\lambda^2 + \frac{3Kb}{10GA}} \tag{6.8}$$

At the time ($t = 0$) of the crack formation, $\sigma_{x=0} = f_t$ where f_t is the tensile strength of the material perpendicular to the grain at the crack tip. The above formulation can then be re-written as Equation (6.9), where P_{cr} is the critical value of the shear for the section of the beam most probable for crack initiation.

$$P_{cr} = \frac{bf_t}{\sqrt{4\lambda^2 + \frac{6}{5}\frac{Kb}{GA}}} \tag{6.9}$$

Equation (6.9) can be re-written in terms of the energy release rate in the opening mode. In fracture mechanics, G_I is a material property that usually denotes the release of elastic strain energy rate for unit area of crack propagation. The fracture energy is defined as the area below the stress – deflection curve (here tensile stress-deflection) and could be estimated by a triangular curve with constant stiffness '*K'*. Figure 6.5 shows a sketch of the experimental and idealized curves of stress-deflection for mode I fracture. The experimental curve is estimated with a triangle of the same area and with the same height.

$$G_I = \frac{1}{2}\frac{f_t^2}{K} \tag{6.10}$$

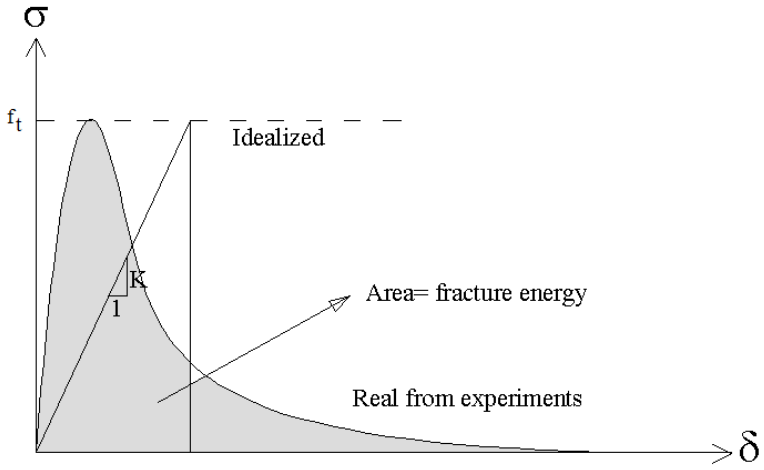

Figure 6.5. Linearized constitutive relation

In the critical case, the energy release rate is equal to the critical energy release rate ($G_I = G_{Ic}$) and in Linear Elastic Fracture Mechanics (LEFM) $G_{Ic} = G_{If}$, where G_{If} is the fracture energy of the LVL in mode I (opening). The above formulation can be rewritten as Equation (6.11):

$$P_{cr} = \frac{b\sqrt{2KG_{If}}}{\sqrt{4\lambda^2 + \frac{6}{5}\frac{Kb}{GA}}} \tag{6.11}$$

6.3 Beam subjected to pure bending moment

In the case of pure bending moment in a section of a beam, the upper portion of the beam can be assumed again as a beam on an elastic foundation. Similar to the aforementioned equations, using the beam on elastic foundation schematization, the following relationships can be obtained:

$$W_{x=0} = \frac{-2\lambda^2 M_{x=0}}{K_I b} \tag{6.12}$$

$$\theta_{x=0} = \frac{-M_0}{\beta}\left(\frac{6\lambda^2}{5GA}\right) \tag{6.13}$$

Again, the stress perpendicular to the grain ahead of the crack tip can be calculated as Equation (6.14):

$$\sigma_{x=0} = \frac{2\lambda^2 M_{x=0}}{b} \tag{6.14}$$

The critical moment in the section occurs when the stress in the section equates to the maximum tensile stress. So, Equation (6.15) can be obtained:

$$M_{cr} = \frac{f_t b}{2\lambda^2} \tag{6.15}$$

The calculated moment from Equation (6.15) is a local moment in the upper section of the beam. It will be added to the moments due to the axial load in the beam section and the moment in lower section of the beam (assumed equal) to yield the total moment.

Figure 6.6 shows the graphs of stress distribution for different stresses at the section A-A obtained from elastic finite element analysis on a LVL beam of dimension 2100×300×45 mm loaded at mid-span with concentrated load of 20 kN. A hole of 80 mm diameter at the end distance of 400 mm is made in the beam. The distribution of the stresses in all direction for both portions of the beam (upper and lower potion) is similar. Therefore, the main assumption of the equal moment for upper and lower section of the beams can be verified.

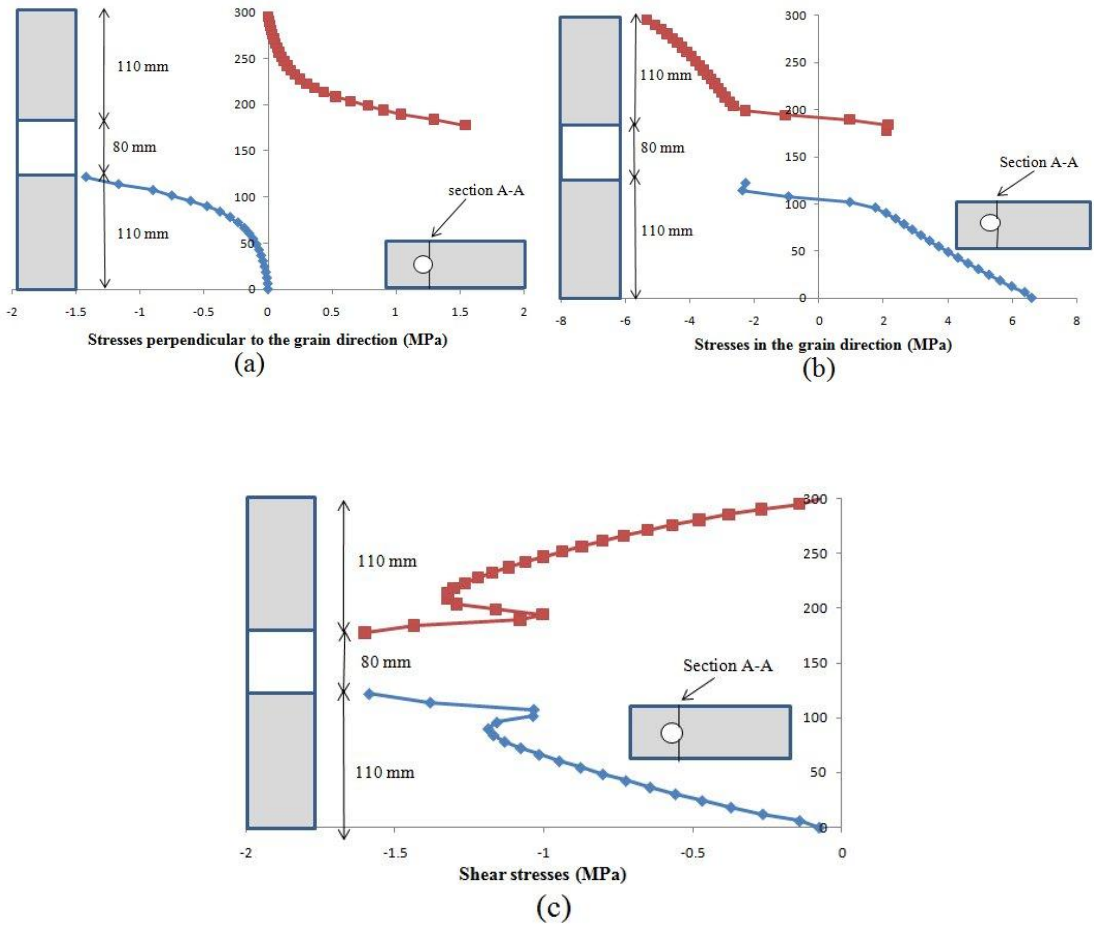

Figure 6.6. Stress distribution at beam depth at crack plane (section A-A): (a) stress perpendicular to beam axis, (b) stress in beam axis direction, (c) shear stress

Assuming that the distribution of the stresses due to the bending moment (M) at the upper portion of the beam is similar to trapezoid of BCDE as shown in Figure 6.7, the stress distribution can be divided to two cases viz.: (i) rectangular stress distribution (EBFI), and (ii) triangular stress distribution (OCF and OID). Using the symmetry of triangles (COF and OAG), σ_N that is axial stress as shown in Figure 6.7. is calculated as:

$$\sigma_N = \frac{\sigma_M(h_{cr} + h_d.cos(45))}{h_{cr}} \tag{6.16}$$

where σ_M denotes the stresses due to the bending moment of M_{cr} in the section, h_{cr} is the height of the upper portion of the beam. The compressive force N is the resultant force of the stresses over the section of the beam as shown in Equation (6.17).

$$N = b\sigma_M(h_{cr} + h_d \cos(45)) \tag{6.17}$$

Therefore, the total moment in the section of the beam (M_t), is calculated from Equation (6.18).

$$M_t = 2M_{cr} + b\sigma_M(h_{cr} + h_d \cos(45))(h - h_{cr}) \tag{6.18}$$

For rectangular holes, Equation (6.18) may be rewritten as Equation (6.19).

$$M_t = 2M_{cr} + b\sigma_M(h_{cr} + h_d)(h - h_{cr}) \tag{6.19}$$

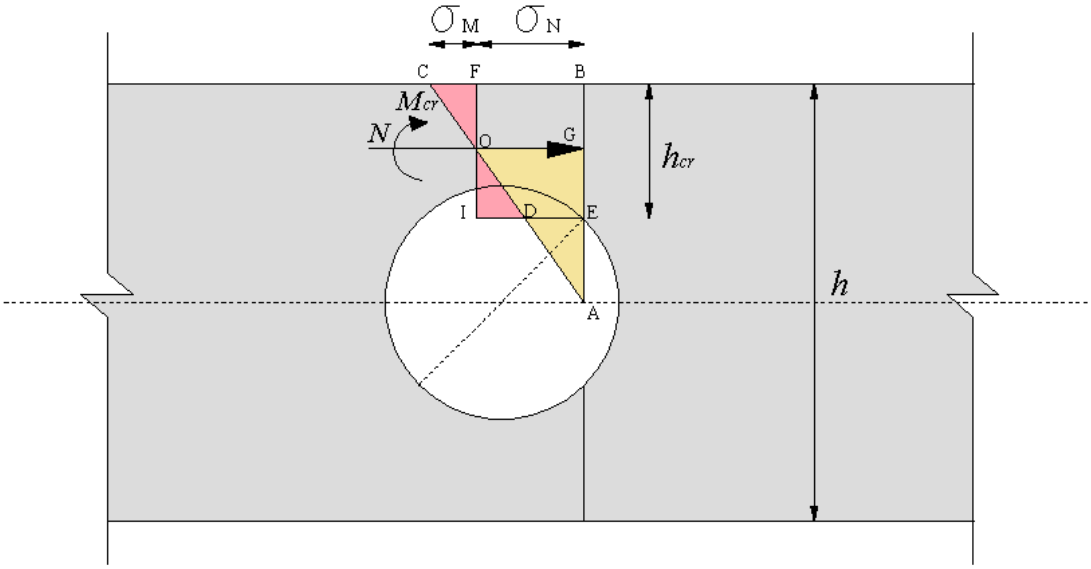

Figure 6.7. Sketch of the stress distribution due to the bending moment in the section

In Equations (6.18) and (6.19), σ_M is a function of M_{cr} that is dependent on material properties of wood.

6.4 Beam subjected to combined shear and bending moment

For a beam with a hole placed in a section of nonzero shear force and nonzero bending moment, the influence of both shear and moment will govern the failure load of the beam with the hole. Many combinations of the shear and moment in the beam section can be assumed for the cracking load predictions. The following empirical relationship may is suggested for the load predictions.

$$\frac{P}{P_t} + (\frac{M}{M_t})^2 = 1 \qquad (6.20)$$

where P_t and M_t are the total resisting shear and total resisting moment in that section of the beam.

6.5 Limitations of the formulations

The assumption of a beam on an elastic foundation is not valid for small hole sizes because the stiffness of the lower beam also contributes to the rotational and transverse stiffness of the upper beam. However, Jensen (2005) suggested a modification for the stiffness of the springs to account for the stiffness of the lower beam. K_s denotes an additional contribution to the foundation stiffness because of the deflection of the beam below the potential crack path. K_s is assumed as:

$$K_s = K(\frac{1-\alpha}{\alpha})^m \qquad (6.21)$$

where α signifies the ratio of the depth of upper beam to the total beam depth (h_{cr}/h) and m is a parameter to be determined empirically. Note that $m = 1$ corresponds to the $K_s/K = A_1/A_2$ and $m = 3$ corresponds to the $K_s/K = EI_1/EI_2$, where subscript 1 refers to the lower beam and 2 to the upper beam. In other words, one may increase the fracture energy (multiply by $(\frac{1}{1-\alpha})^m$) to account for the lower beam stiffness/deflection.

For very large holes, the formulation overestimates the shear capacity of the beam in the section because the main beam can be assumed as two separate solid beams connected by two small strips that may behave differently by fracture around the hole. However,

through some comparisons with the experimental results available for glulam in the literature, it was concluded that for $h_d/h \leq 0.5$ the results match well with the experimental available data.

6.6 Formulation application to square and rectangular holes

In the case of rectangular holes, again a combination of moment and shear force should be considered for the cracking load predictions of timber beams. The distribution of the normal stresses perpendicular to the grain in the case of a beam with a sharp corner square hole and rounded corner square hole (beams in Figure 6.8 (a) and (b)) are presented in Figure 6.9 (a) and (b), respectively.

Figure 6.9 (a) and (b) display the stress concentrations for the simply supported LVL beams with dimensions of 1300×200×45 mm displayed in Figure 6.8 (a) and (b) respectively. The beams were loaded with a 10 kN concentrated load applied at mid-span. The high stress concentration in the sharp and curved corner square hole imply the most probable location for crack initiation and propagation around the holes.

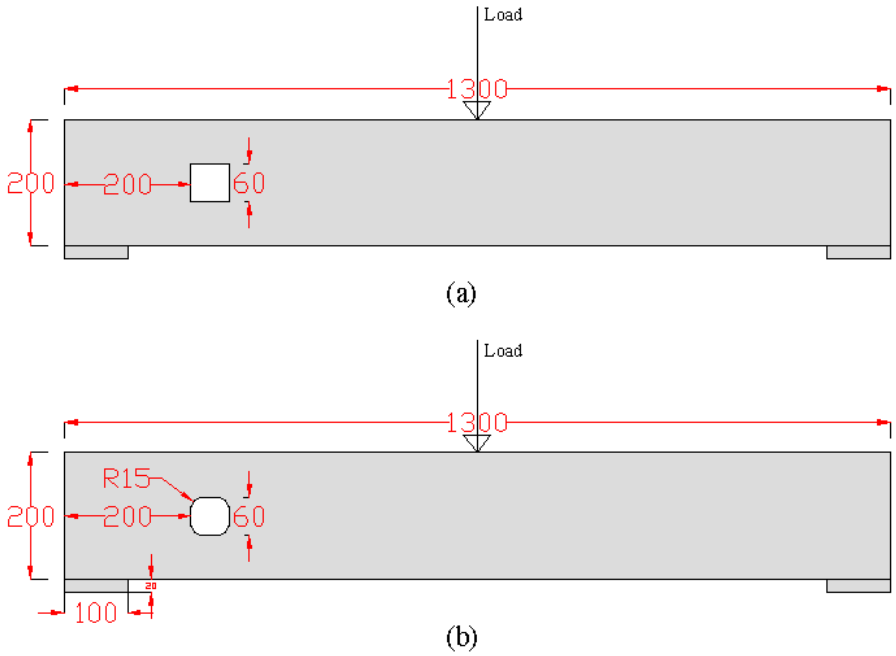

(dimensions in mm)

Figure 6.8. Geometry of LVL beam specimens with square holes: (a) sharp edges, (b) curved edges

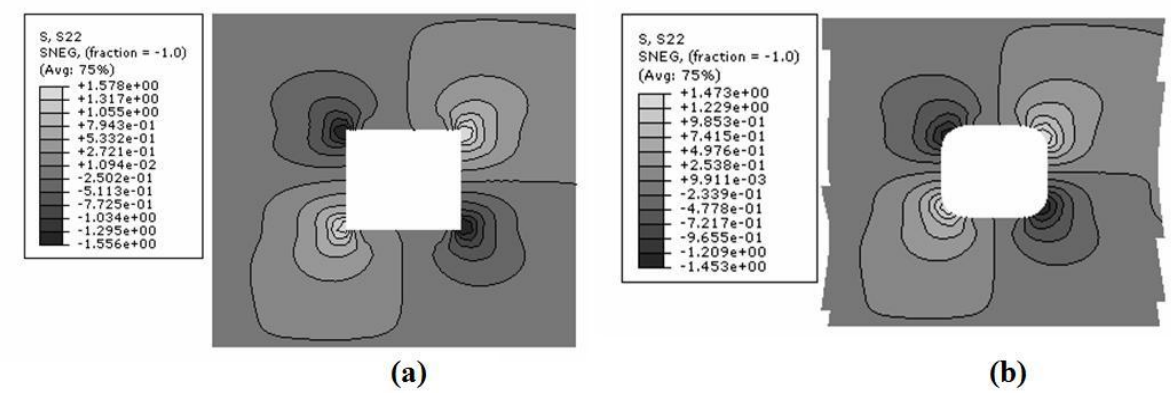

Figure 6.9. Distribution of stresses perpendicular to grain: (a) square hole with sharp edges, (b) square hole with rounded edges

In the case of a large enough rectangular/square hole, the crack starts exactly at the corner of the rectangular/square hole with a sharp edge and in the middle of the rounded corner in the case of the curved corner. Therefore, the formulation for holes presented before can be used also for rectangular holes with either type of corner (rounded and sharp) provided that revisions for the crack location are applied.

6.7 Experimental validation

In order to check the results of the formulation, a comparison of the predicted values with experimental values from chapter 3 was performed. A typical load - deflection data for the beam specimen 2100×300×45 mm with a 120 mm diameter circular hole is presented in Figure 6.10. The cracking load for this beam is 36 kN and the failure load is 42 kN. Small changes in the slope of the load-deflection curve can be seen in Figure 6.10 after the first crack formation. This indicates that the beam has undergone more deformation because of the crack formation.

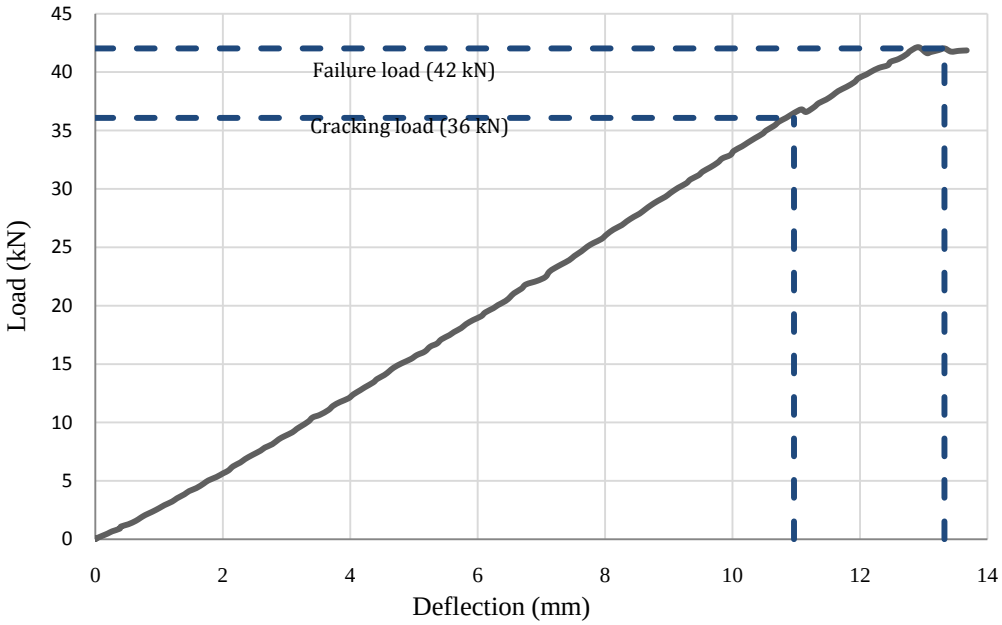

Figure 6.10.Typical load-deflection curve for a beam with the hole with cracking and failure load

An average tensile strength of 2 MPa for LVL, fracture energy of 1.15 N/mm and modulus of elasticity of 10.7 GPA were used for the calculations. These values were adopted from chapter 2. The dimensions of the specimens tested, including the hole diameter and the location, of the hole are summarized in Table 6.1 together with the results of the experiments and the predicted cracking loads. The holes were centred mainly at the neutral axis in the shear-dominated region, namely close to the supports.

Table 6.1. Comparison of predicted cracking loads and experimental results

Beam number	Dimensions (mm)	Hole diameter or side length (mm)	Hole centre distance from support (mm)	Average cracking load (kN)	Predicted cracking load (kN)	Error (%)
1	1400×200×63	70	250	37.9	40.0	-5
2	1400×190×45	80	250	30.0	26.2	15
3	1400×190×45	100	250	24.0	25.2	-5
4	1400×190×45	120	250	20.0	23.8	-16
5	1500×200×45	80	350	24.9	27.0	-8
6	1500×200×45	100	350	20.7	21.2	-2
7	2100×300×45	60	500	60.0	56.0	7
8	2100×300×45	80	500	53.0	54.0	-2
9	2100×300×45	120	500	38.5	35.6	8
10	2100×300×45	150	500	34.1	34.2	0
11	2800×400×45	160×160 rounded edge	500	40.0	37.0	8
12	2800×400×45	160×160 sharp edge	500	36.1	37.0	-2

As stated before, the predictions for the small holes are conservative because of the deviation from basic assumptions of beam on an elastic foundation. That assumes an infinite stiffness of the lower beam. It was found that for hole diameter smaller than 0.4 of beam depth, assuming $m = 2$ for LVL yields the best match with the experimental values. Therefore, in Table 6.1 for beams 7 and 8 the results are presented applying this assumption. The differences between the analytical predictions and the experimental results are low. Due to the uncertainty in material properties like tension perpendicular to grain, the size dependency of the fracture energy, and the fairly high coefficients of variation (COV), it is quite reasonable to assume that predictions are fairly accurate.

6.8 Discussion

The main assumption of the proposed formulation is that the behaviour of this type of structural element can be modelled as a portion of beam supported on an elastic foundation. Fracture properties of the wood are assigned to the possible fracture area (springs) and then the shear strength is calculated. The formulations presented in this

chapter lead to good predictions of the cracking load for beams with round and square holes.

The method yielded better answers for larger size holes because the assumption of a beam on an infinitely stiff foundation deviates from infinite stiff foundation for small sizes of openings. The stiffness of lower beam contributes to the beam deflection. However, by applying a modification factor to the calculations, the predictions are closer to the experimental values.

It is rather difficult to use literature for comparison purposes because the proposed formulation is sensitive to the fracture energy and tensile strength perpendicular to the grain. Small changes of these values can affect the predicted load considerably. However, with some assumptions, the formulation was also applied to the other test results in the literature that were all for glulam. The tensile strength perpendicular to grain of 3 MPa, fracture energy in mode I of 0.3 N/mm, and modulus of elasticity of 13700 MPa was used for predictions. These values were adopted from Gustafsson (1993b). However, for predictions of Pizio (1991) experiments with Class B of glulam, a tensile strength of 2 MPa with modulus of elasticity of 10000 MPa was assumed. The cracking load predictions for the glulam beams with the holes are presented in Table 6.2.

Table 6.2. Comparison with the literature

Reference	Number of tests	Dimensions (mm)	Distance of the hole centre from support (mm)	Hole Diameter (mm)	Experimental cracking load (kN)	Predicted cracking load (kN)	Error (%)
(Hofflin 2005)*	5	3150×450×120	675	90 (circle)	76.8	73.7	4
(Hofflin 2005)*	6	3150×450×120	675	135 (circle)	65.5	69.4	-6
(Hofflin 2005)*	4	3150×450×120	675	180 (circle)	47.6	44	8
(Hofflin 2005)*	5	6300×900×120	1350	180 (circle)	106.4	112	-5
(Hofflin 2005)*	6	6300×900×120	1350	270 (circle)	96.4	106.4	-9
(Hofflin 2005)*	6	6300×900×120	1350	360 (circle)	69.2	66.1	5
(Hallström 1996)*	5	4000×315×90	875	150 (circle)	24.5	25.6	-4
(Pizio 1991)*	2	1620×400×120	420	180×180 (square)	30.6	29.3	4
(Pizio 1991)*	2	1620×400×120	420	180×90 (rectangle)	54.9	49.4	11
(Pizio 1991)*	2	2320×400×120	700	10×180 (rectangle)	34	29.3	16
(Pizio 1991)*	2	2320×400×120	700	180×90 (rectangle)	54.2	49.4	10
(Pizio 1991)*	2	2320×400×120	700	180×180 (square)	26.8	29.3	-9
(Johannesson 1983)*	4	5000×495×88	1250	125 (circle)	51.9	50	4
(Johannesson 1983)*	4	5000×495×88	1250	125×125 (square)	40.4	45	-10
(Johannesson 1983)*	4	5000×495×88	1250	375×125 (rectangle)	37.7	45	-16
(Johannesson 1983)*	1	5000×400×140	900	600×200 (rectangle)	37.5	38	-1
(Johannesson 1983)*	2	5000×400×140	650	250 (circle)	29.6	34.6	-14
(Johannesson 1983)*	2	5000×500×90	650	250×250 (square)	26.8	28.2	-5
(Johannesson 1983)*	2	5000×500×90	1400	250 (circle)	30.7	33.2	-8
(Johannesson 1983)*	2	5000×500×90	1400	250×250 (square)	27	27.1	0
(Johannesson 1983)*	2	5000×500×90	300	250 (circle)	35.8	38.8	-8

*. Adopted from (Danielsson 2007)

For glulam beams with an opening diameter size smaller than 0.4 of the beam depth, $m = 2$ was assumed. This value was selected because it yielded the best match for different experiments on glulam. The predictions are relatively close to the experimental load.

The method does not seem to have any limitation if it is used for holes with eccentricity above the neutral axis of beam at different positions along the beam provided that a good estimation of the crack initiation location can be made and entered into the calculations.

6.9 Summary

This chapter provided a series of formulations for cracking load predictions of Laminated Veneer Lumber (LVL) beams with holes. The theory of a beam on an elastic foundation was applied and three formulations were derived. A summary is included below:

- A beam with a hole at the time of crack initiation ($t = 0$) can be assumed as a beam resting on Winkler springs as an elastic foundation. This requires that the lower beam assumed as an infinite stiff beam. Clearly this assumption works well for large hole sizes and for small diameter hole sizes the stiffness of the lower beam contributes to the deflection of the beam and will make the predictions conservative.

- Three formulations have been derived that are for the critical shear resistance in the section in case of pure shear, the critical moment resistance for the case of pure moment in the section of the beam, and finally a mixed mode formulation for combination of shear and moment in the section.

- The beam on an elastic foundation works well for hole diameters equal or larger than 0.4 of the beam depth ($h_d/h \geq 0.4$) to predict the cracking load of the beam. The model for a very large hole may overestimate the cracking load, however for $0.4 \leq h_d/h \leq 0.5$ the predictions matches well with the experimental results. For the hole diameters smaller than 0.4 of the beam depth ($h_d/h < 0.4$), the results of the model for cracking load predictions are mostly conservative.

- For small hole sizes ($h_d/h < 0.4$), their cracking load could be predicted by artificially changing the stiffness of the Winkler springs. A modification factor can be applied to improve predictions. The modification accounts for the stiffness of the lower beam.

- If the modification factor is ignored and the expanded formulations are used for the cracking load predictions of LVL beam with holes, the predicted loads for small hole sizes will be conservative, and for large hole sizes will be close to the experimental values.

- The expanded formulation was also applied to the glulam beams from the literature. The results are relatively close to experimental results.
- Reinforcement of the holes in LVL beams is necessary when the load on the beam is larger than the load predicted from the proposed formulation.

The presented formulation will be incorporated into the design method in chapter 8. The next chapter of the thesis will consider reinforcing of LVL beams with the holes for recovering their capacity. A new model for the tensile load prediction in the reinforcement is presented.

7 Tensile load in the reinforcement around holes

This chapter presents a series of formulation for tensile load prediction in reinforcement around the holes in LVL beams based on a truss model. Different cases of hole shapes are investigated. Correction factor for larger depth of beams; and also for the eccentricity of the hole relative to neutral axis of beam is presented. The results of this chapter have been used in chapter 8 and 9. The use of the presented numerical model is limited to this chapter.

The majority of this chapter has been re-produced from the following journal paper:

Ardalany M, Fragiacomo M, Moss P, Deam B (2012) A new model for tensile load prediction in the reinforcement around the holes in shear dominant areas in Laminated Veneer Lumber (LVL) beams. Journal of Materials and Structures RILEM (Accepted):1-32

7.1 Introduction

Chapter 4 and 5 covered analysis of beams with holes and reinforcement around the holes while chapter 6 presented an analytical formulation to estimate cracking load of LVL beams with holes. This chapter mainly is on tensile load prediction in reinforcements around the holes. The analytical model, experimental program, and the finite element analysis are incorporated to estimate the produced load due to the hole. The chapter also includes experimental results on measuring the tensile force in the reinforcement.

As shown in the experimental program (chapter 3), reinforcing around the hole in LVL beams can control or prevent the crack propagation. Design of reinforcement requires an estimation of the tensile load produced due to the shear and moment in the section of beam.

Little guidance is available in the literature to address the issue of designing a LVL beam with holes and reinforcement. Most of the research has been focused on glulam beams. DIN 1052 suggests two formulations for the tensile force predictions. The first is based on integration of the shear stresses that cannot be transferred over a section of the hole as shown in Figure 7.1, and the second one is mainly a calibration factor obtained from numerical analysis. The dependence of the formulation on the numerical analysis and the validity for other wood-based materials; however, need to be verified. To the best of the author's knowledge, there is no verification of the formulations for other engineered wood materials like LVL.

It would be useful if a simplified formulation based on mechanics principles that can be used by design engineers could be derived. The primary objective of the current study described herein was to develop a design load for the reinforcement around the holes. This objective was achieved by developing a simplified truss model to predict the tensile load due to shear and moment in the section. The validity of the formulation was checked against numerical and experimental results.

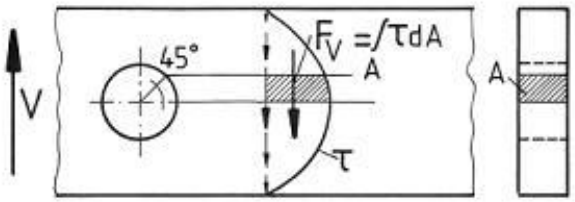

Figure 7.1. Integration area of the tensile force due to the shear in the section (Aicher et al. 1995)

7.2 Crack location

The presence of a hole affects the flow of stresses in a beam and the stress field at the hole edge varies from tension to compression (Guan et al. 2004). Figure 7.2 (a) shows

the stress field perpendicular to grain obtained through an elastic finite element model for a beam of dimensions 1300×200×45 mm loaded at mid-span with a 30 kN concentrated load. A hole of 80 mm diameter was cut at mid-depth of the beam and at the distance of 300 mm from the end edge of the beam, therefore in the high shear area of the beam. The top region and its diagonally opposite side are in tension, and the other regions are in compression. From the same model, the distribution of tensile stress perpendicular to the grain along a path parallel to the grain direction can be obtained. It can be observed that the tensile stress decreases exponentially with the distance from the edge of the hole (Figure 7.2 (b)). Integration of the tensile stresses yields the tensile force that the reinforcement should carry.

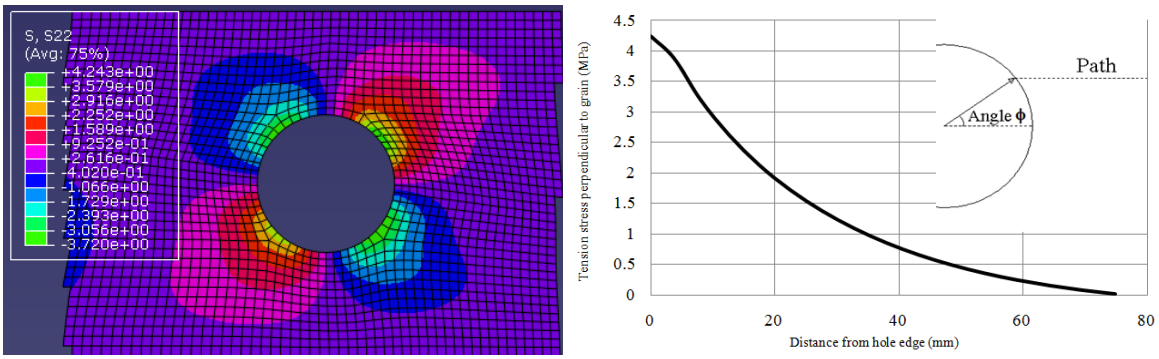

(a) (b)

Figure 7.2. (a) Perpendicular to grain tensile stress field around the hole, (b) exponentially decrease of the tensile stresses along a path parallel to the grain at an angle ϕ =40°

Since the tensile stress perpendicular to the grain may exceed the material strength, cracking could form around the hole at the location with the highest value of the tensile stress. The exact cracking location depends on several factors such as the amount of shear force and moment in the section of the beam, the hole location along the depth of the beam, and also the knot distribution in the section of the beam. The cracking is usually assumed to occur at 45 degrees angle relative to the horizontal beam axis in the high shear areas because there the tensile stresses reach their maximum values.

Figure 7.3 presents the variation of the stresses perpendicular to the grain along the perimeter of the hole for the aforementioned beam in the case of different hole diameters ranging from 60 to 100 mm. The maximum tensile stresses perpendicular to

grain occurred at an angle between 30 and 45 degrees depending on the geometry and on the hole diameter. More specifically, for the cases under investigation, the maximum tensile stress is attained at an angle of 44, 41, and 34 degrees for the hole diameters of 60, 80, and 100 mm, respectively.

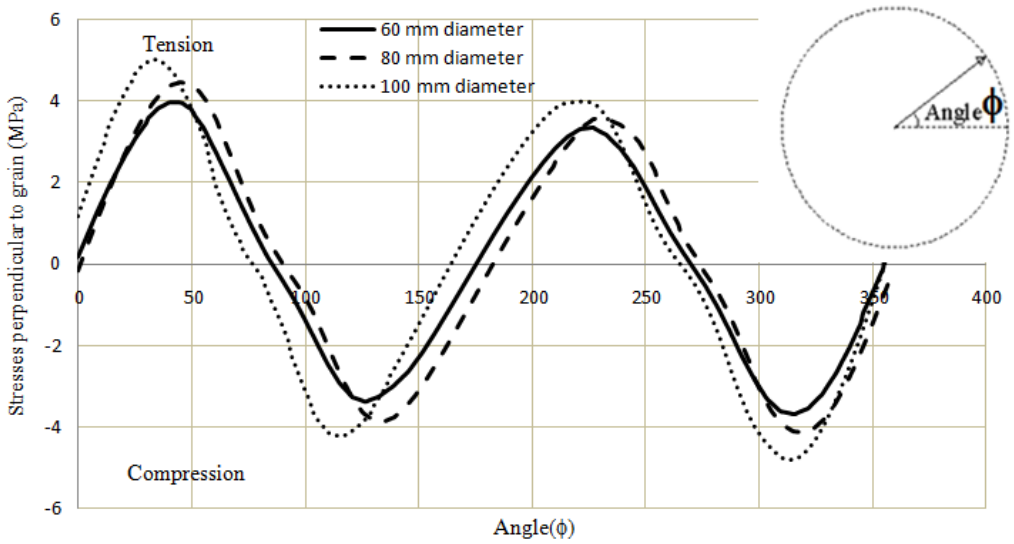

Figure 7.3. Variation of the stresses perpendicular to grain along the hole perimeter for different hole diameters

7.3 Tensile force due to shear

The aim of this section is to develop a simplified model to predict the tensile force induced in screw reinforcement by a hole. Introducing a hole into a beam reduces the resisting section; therefore, the remaining section and possible reinforcement should carry the stresses due to shear and moment in the section.

The main assumption of the proposed model is that the shear force and the bending moment due to the external load that cannot be transferred through the hole will be carried around the hole by truss action. This is somehow similar to the concept of water approaching an obstacle in fluid mechanics. The water bypasses the obstacle. This implies that compressive and tensile forces in the resisting truss mechanism around the hole will transfer the shear force in the section.

Assuming that in Figure 7.4 introducing a hole cuts the compressive inclined member, a truss mechanism is formed that transfers forces around the hole. The load path around the hole is presented in Figure 7.4 showing the compressive and tensile members in the truss.

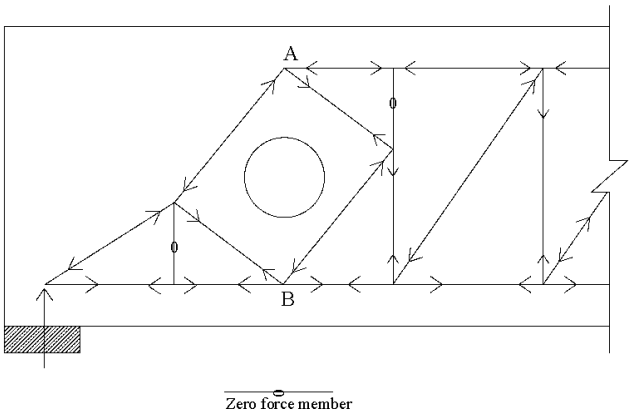

Figure 7.4. Truss model around a hole in a beam shows load path

By integrating the shear stresses that cannot be resisted in the centre of the hole (Figure 7.5), and by transforming the resultant shear force to a tensile force in the member, the design tensile forces due to the shear in the section can be calculated.

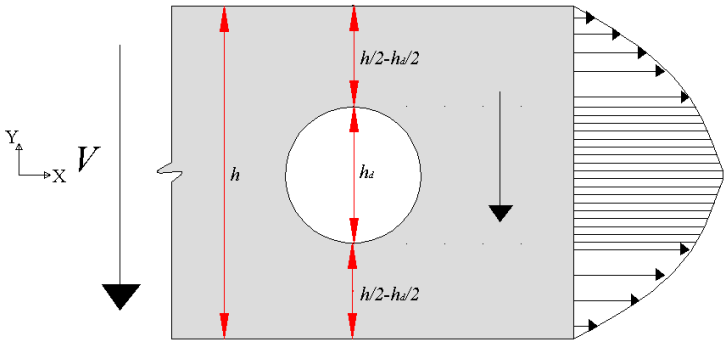

Figure 7.5. Distribution of the shear stresses over the hole

From the basics of structural mechanics, the shear stress in a section of a rectangular beam is:

$$\tau = \frac{6V}{bh^3}\left(\frac{h^2}{4} - y^2\right) \tag{7.1}$$

Integration of the shear stresses over the hole diameter gives the shear force that cannot be transferred as:

$$F_V = \int_{-\frac{h_d}{2}}^{\frac{h_d}{2}} \tau b dy \tag{7.2}$$

$$F_V = \frac{V\, h_d(3h^2 - h_d^2)}{2\, h^3} \tag{7.3}$$

The shear force that cannot be transferred due to the hole is converted to the tensile force that is calculated using the equilibrium of the node A in the truss shown in Figure 7.4. By applying the model, the Equation (7.4) is derived for the tensile force perpendicular to the grain ($F_{t,v}$) in a beam with a hole:

$$F_{t,v} = \frac{\sqrt{2}}{8h^3} V\, h_d(3h^2 - h_d^2) \tag{7.4}$$

where V signifies the shear force in the centre of the hole, h the depth of the beam, y the vertical distance from the horizontal axis, h_d the hole diameter, b the breadth of the beam, F_V the resultant shear force that cannot be transferred at the centre of the hole and, finally by defining parameter R as presented in Equation (7.5), the tensile force due to the shear ($F_{t,v}$) in the section of the beam given by Equation (7.6).

$$R = \frac{h_d}{h} \tag{7.5}$$

$$F_{t,v} = \frac{\sqrt{2}}{8} V(3R - R^3) \tag{7.6}$$

The produced tensile force due to shear in Equation (7.6) is dependent on the ratio of the hole diameter to beam depth (h_d/h) and the shear force (V) in the section of the beam.

7.4 Tensile force due to bending moment

The effect of the bending moment on the tensile force is also understandable and it needs a robust model to estimate it. Previously DIN 1052 (2008) used a formulation to account for the moment effect in the section of a beam with a hole. The formulation is based on the results of a numerical finite element calculation on glulam beams for a limited range of hole diameters to depth ratios. The formulation does not include any term of h_d/h. Equation (7.7) presents the formulation:

$$F_{t,M} = 0.008\frac{M}{h_r} \tag{7.7}$$

where M is the moment in the section of the beam, and h_r for circular holes centred at the neutral axis of the beam is given by:

$$h_r = 0.5h - 0.35h_d \tag{7.8}$$

Figure 7.6 presents a similar truss model for the calculation of the tensile force due to moment in the section. The model assumes that a couple of forces produced by the local moment due to the hole is carried out through a truss surrounding the hole. The model is analogous to the one proposed for the shear, but with a difference. The difference regards the location of the truss chords around the hole that needs to be addressed in the case of the moment to calculate the tensile force.

Different locations for the truss nodes were assumed around the hole. The smaller truss size yields higher tensile load and the larger truss size yields a lower effect. In this work, the smaller truss size around the hole was not used because it overestimated the tensile forces compared to the numerical results. The truss was assumed to be formed at the centroid of the stresses due to the bending moment above the hole as presented in Figure 7.6. As demonstrated later, the assumption yields good predictions.

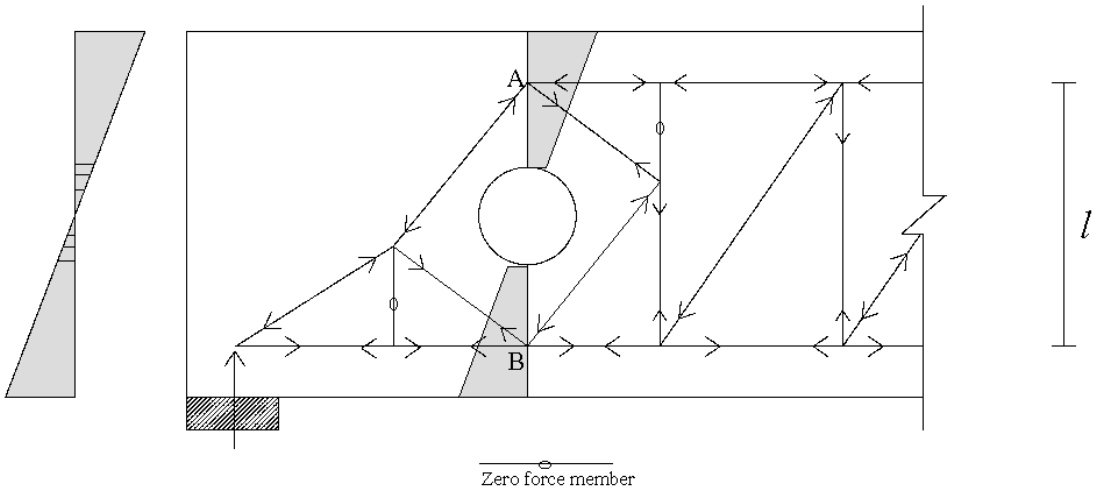

Figure 7.6. Truss model around a hole in a beam shows load path

From beam theory, the stresses due to the moment in the section of the beam are calculated as:

$$\sigma = \frac{My}{I} \tag{7.9}$$

Assuming a plane stress case, by integration of the normal stresses over the hole area, and then by calculating the corresponding moment, the local moment is given by:

$$M_L = \frac{Mh_d^3}{h^3} \tag{7.10}$$

where σ denotes the stress in the section due to bending moment M, y the distance of the fibre from the horizontal mid-depth axis, I the second moment of area of the section without the hole, and M_L the local bending moment due to the hole in the beam.

The couple of horizontal forces (F_L) equivalent to the local bending moment M_L in the section not transferred due to the hole is calculated by dividing the moment (Equation (7.10)) by the chord length (l) as shown in Figure 7.6. The chord length (l) is lever arm calculated assuming a linear stress distribution from the centre of the hole and is the distance between the centroids of the upper and lower stress trapezoid. l is calculated as:

$$l = \frac{2}{3}\left(\frac{h \cdot h_d + h^2 + h_d^2}{h_d + h}\right) \tag{7.11}$$

Using the equilibrium of the upper node in Figure 7.6, the horizontal force is calculated as Equation (7.12):

$$F_L = \frac{3}{2}\frac{M h_d^3 (h_d + h)}{h^3 (h \cdot h_d + h^2 + h_d^2)} \tag{7.12}$$

By applying the equilibrium equation at the upper node, the tensile force (T) due to the bending moment in the inclined member is calculated as:

$$T = \frac{3\sqrt{2}}{4}\frac{M h_d^3 (h_d + h)}{h^3 (h \cdot h_d + h^2 + h_d^2)} \tag{7.13}$$

The vertical component of the force ($F_{t,M}$) is calculated by multiplying the inclined force by $\sqrt{2}/2$.

$$F_{t,M} = \frac{3}{4}\frac{M\, h_d^3 (h_d + h)}{h^3 (h \cdot h_d + h^2 + h_d^2)} \tag{7.14}$$

The design tensile force in the section is the sum of the above values of tensile forces due to the shear force and the bending moment as stated in the DIN 1052 (2008).

$$F_{t,d} = F_{t,V} + F_{t,M} \tag{7.15}$$

Therefore, the formulation could be summarized as:

$$F_{t,d} = \frac{\sqrt{2} V\, h_d (3h^2 - h_d^2)}{8\, h^3} + \frac{3}{4}\frac{M\, h_d^3 (h_d + h)}{h^3 (h \cdot h_d + h^2 + h_d^2)} \tag{7.16}$$

Equation (7.16) is used for the design of reinforcements such as screws and plywood in the beams with holes. The design force $F_{t,d}$ is then used to calculate the reinforcement ignoring the tensile strength of the wood and assuming a cracked section. There are also

other criteria for the design of the reinforcement like a minimum distance of the screw from the hole edge, and a minimum embedment length.

7.5 Experimental program

An experimental program was performed to verify the accuracy of the proposed formulation. The target was the measurement of tensile load in the screw reinforcement due to the hole. Table 7.1 presents the geometrical properties of the beams with the holes tested in the experimental program. For three-point bending, the load was applied at the mid-span of the beam, whereas for four-point bending, the two point loads were applied at a distance 'S' between them.

Table 7.1. Geometrical properties of the beams with holes that were tested

Beam No.	Beam dimension (mm)	Hole diameter (mm)	Lc (mm)	Dc (mm)	Reinforcement distance from hole edge (mm)	Loading configuration	S (mm)
1	1500×200×45	80	400	100	30	3 point	-
2	1500×200×45	80	400	100	30	3 point	-
3	1500×200×45	80	400	100	30	3 point	-
4	2000×190×45	82	400	95	30	4 point	500
5	2000×200×45	82	400	100	30	4 point	500
6	2100×300×45	120	550	150	30	3 point	-
7	2100×300×45	120	550	150	30	3 point	-
8	2800×300×45	95	575	150	30	4 point	500
9	2800×300×45	120	575	150	30	4 point	500
10	2100×300×45	154	575	150	30	3 point	-
11	2100×300×45	154	575	150	30	3 point	-

To measure the strain in a screw due to the tensile load, a strain gauge was used. Installing the strain gauge on a self-tapping screw is normally difficult because the screw has to be driven into the wood, and may tear off the strain gauge. It was also not possible to install the strain gauge inside the self-tapping screw. Therefore, a procedure for inserting a screw in the beam with the strain gauges attached to the screw was devised. First, two cylindrical holes of 11 mm diameter (one each side of the main hole) were drilled through the beam breadth at a distance of 30 mm from the hole edge to avoid wood splitting (Figure 7.7). Then a 5.7 mm diameter normal threaded screw with

a strain gauge installed on its surface was embedded in the cylindrical hole by means of epoxy resin. The screw diameter of 5.7 mm was selected because larger screws require larger holes and are not appropriate for testing samples that had a breadth of only 45 mm. Smaller fully threaded screws were also avoided since the gluing of the strain gauges on the surface of a tiny screw is not feasible. HILTI HIT-RE 500-SD epoxy was used to connect the screws to the beam. The final diameter of the screws with the surrounding epoxy was about 11 mm.

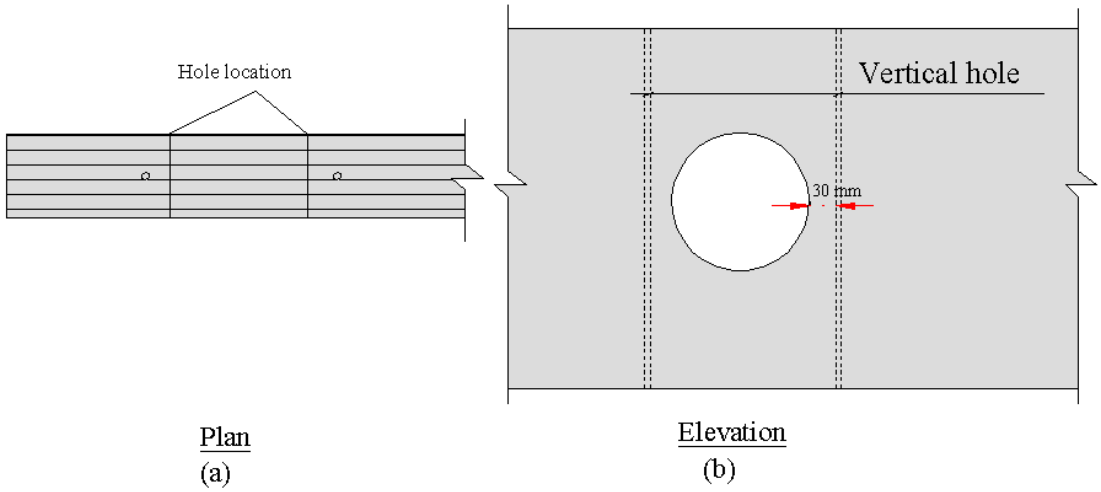

Figure 7.7. Beam with vertical holes: (a) plan, (b) elevation

The total length of the screws was dependent on the beam depth. At the onset of the experiments, the screws were inserted throughout the entire depth of the beam (Figure 7.8 (a)). Some preliminary experiments demonstrated that a failure mechanism during testing occurred at the tensile edge of the beam, and this was not desirable. The failure was initiated by separation of the glue from the wood in the lower edge of the beam leading to complete fracture as shown in Figure 7.8 (b).

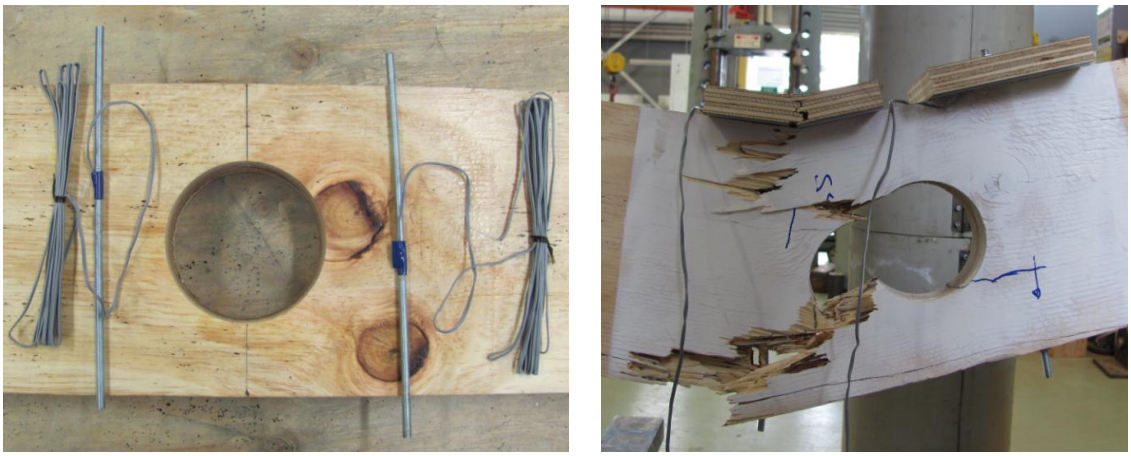

(a) (b)

Figure 7.8. (a) Full-length screw reinforcement around the hole prior insertion in the LVL, (b) failure mechanism of reinforced LVL beams with hole in shear-dominated region

To prevent the separation of the glue from wood due to the tensile stresses, the length of screws was reduced to the beam depth minus 50 mm (Figure 7.9 (a)). This prevented protrusion of one of the screws from the tensile edge of beam. For the other screw that was protruding from the tensile edge of the beam, a steel plate of 100×45×1 mm dimension was used to transfer the tensile stress (left screw in Figure 7.9 (b)). The plate was glued to the beam by epoxy.

In the experiments, a commonly available fully threaded screw with a tensile strength of 440 MPa was used. The threads of the screws were removed by sand paper to provide a smooth surface at the strain gauge location. The strain gauge was installed as close as possible to the most probable location of the crack surface to give measurements that are more accurate. The strain gauge location was calculated as a plane at an angle of 45 degrees from the hole axis. Epoxy glue was injected in the gap between the screw and the LVL, with help of a special gun, to provide appropriate bond with the timber. The epoxy covers the screw and provides a uniform resisting area. The experimental setup followed the mechanical configuration for simply supported beam testing, according to AS/NZS1720-1 (2003) as explained in chapter 3.

The loading history of a beam with a hole and reinforcement was compared with that of a beam with a hole but without reinforcement. In the latter situation, as the beam is

loaded, tensile strains accumulate at the hole edge. Further loading will cause a crack to be formed where the tensile stresses induced by the load exceeds the tensile strength of timber perpendicular to grain. The crack formation causes the beam to deflect more. The crack starts to propagate in the grain direction due to the natural low tensile strength perpendicular to grain of the wood. Since there is no obstacle to stop the crack from propagating, after propagation for a few millimetres up to centimetres depending on the geometry of the beam, the crack reaches a critical value and fracture of the beam with a very loud noise occurs. In the case of the beam with reinforcement, a similar situation is repeated but with an exception. As the crack reaches the reinforcement, it cannot propagate further. Stopping the crack causes more tensile stress concentration in the reinforcement. For certain hole diameter to beam depth ratios, say up to 30 % according to DIN 1052 and 40 % according to the Swedish glulam handbook (Carling 2001) failure due to the attainment of the maximum bending moment in the section of the beam will be possible.

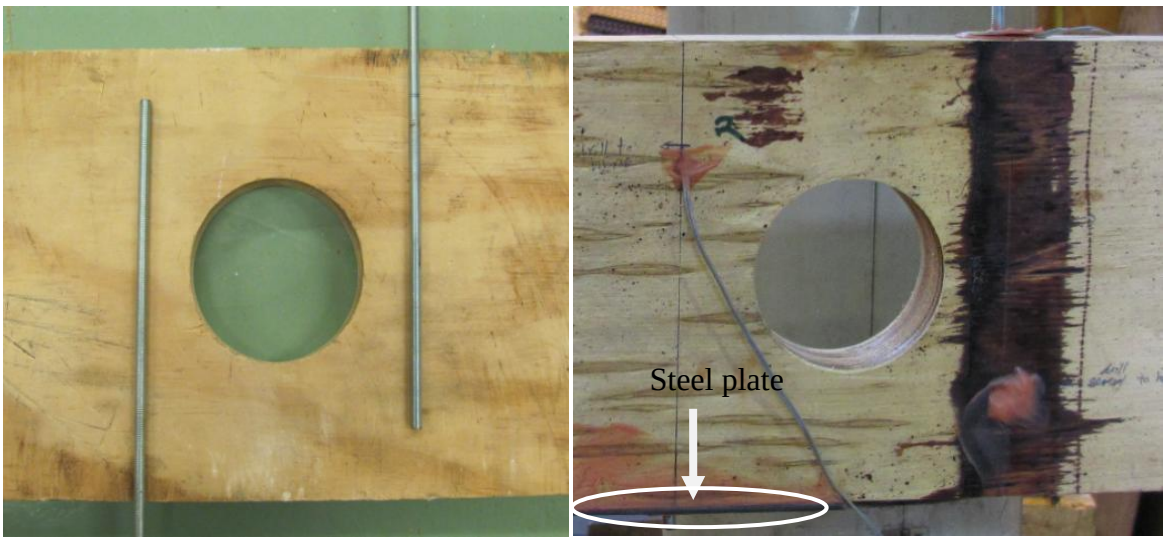

(a) (b)

Figure 7.9. (a) LVL beam specimens with reduced-length screw reinforcement around hole, (b) steel plate reinforcement in the outermost lower fibre

Figure 7.10 shows the external load applied to the beam versus strain for a LVL beam. The beam had a dimension of 2100×300×45 mm and a hole diameter of 150 mm at the mid-depth of the beam at a distance Lc of 550 mm from the support. The reinforcement

was made of two screws with a strain gauges installed on each. The cracking load associated with crack initiation was about 34 kN and when the crack reached the screw, the load was slightly larger (about 36 kN). The strain-load curve up to this step was relatively linear. When the crack approached the screw, it increased the strain in the screw. The screws (left and right) were both carrying the tensile strain due to the external load. By increasing the load of the system, finally, the screws yielded (the strain in the screw increased without much increase in the load of the beam) and the last part of the curve approached a plateau. At this step, brittle failure of the beam due to sudden shear fracture of the beam occurred (Figure 7.11).

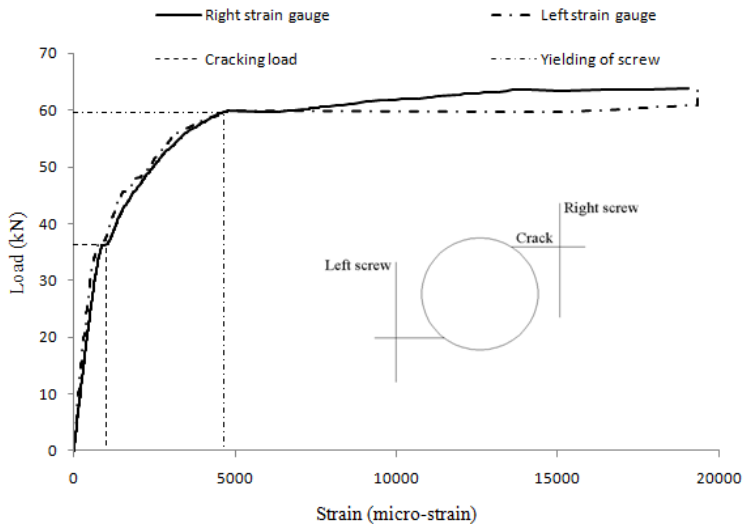

Figure 7.10. Typical load-strain curve in the screw for a reinforced LVL beam with hole

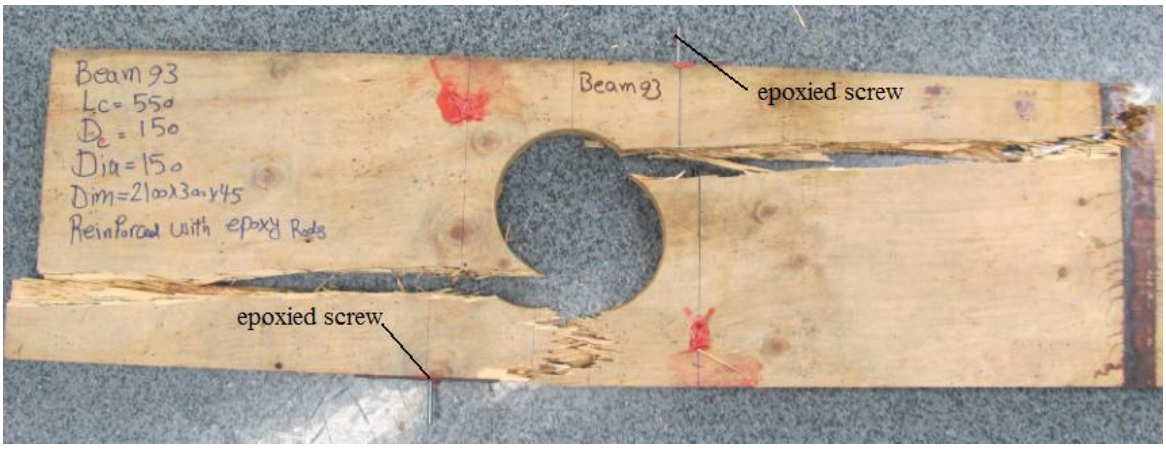

Figure 7.11 Brittle fracture of the beam with hole reinforced with epoxied rod

For a number of the tested beams, the tensile load produced did not yield the screws, which remained in the elastic phase. At the end of the bending test, a part of these beams in the proximity of the hole with the epoxy-grouted rod inside was cut off. This part was then connected to the universal loading machine using a steel plate screwed on the lower side, and the screw itself protruding from upper side, and pulled from both ends (Figure 7.12 (a) and (b)). This yielded the exact strain-tensile load relationship in the screw.

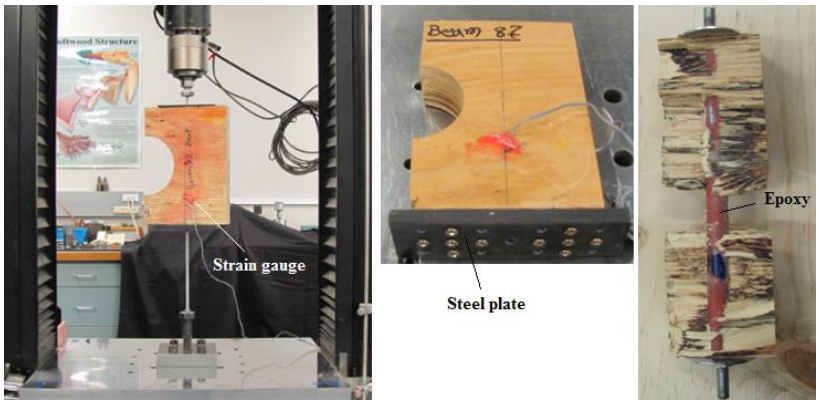

(a) (b) (c)

Figure 7.12 (a) Tensile test configuration for the epoxy grouted rods, (b) lower steel plate screwed to the LVL, (c) epoxy-grouted rod at the end of the test

Figure 7.13 presents the strain-tensile load relationship for a typical epoxy-grouted rod screw. As expected, the behaviour at the start of loading is linear followed by a nonlinear part.

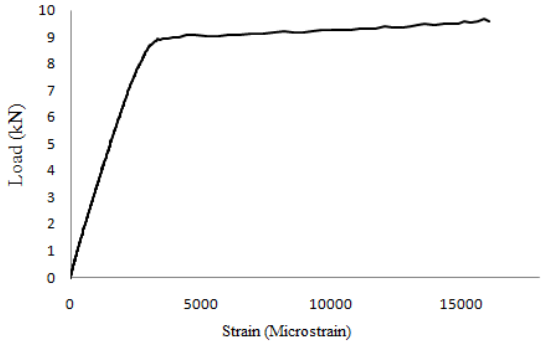

Figure 7.13. A typical tensile load-strain behaviour in epoxy grouted rod

In the experiments, yielding of the screws were not desirable as it caused a rapid increase in strain with eventually a failure due to crack propagation under a collapse load lower than in the case of a beam without hole. Furthermore, yielding of screws causes unrealistic predictions of the tensile load using the proposed approach. However, in the experiments, yielding of the screws only occurred for large hole sizes ($h_d/h \geq 0.5$). Therefore, the experimental strain and corresponding load results before the screw yielding were used for the calculation of the tensile loads in the screws at the beam failure and shown in Figure 7.14 (a).

The analytical predictions using Equation (7.16) are generally slightly higher than the experimental values. If the average values of the experimental results for the beams with the same geometry are plotted against predictions from the Equation (7.16) (Figure 7.14 (b)), it can be concluded that the predictions of the load for all of the beams are higher than experimental results.

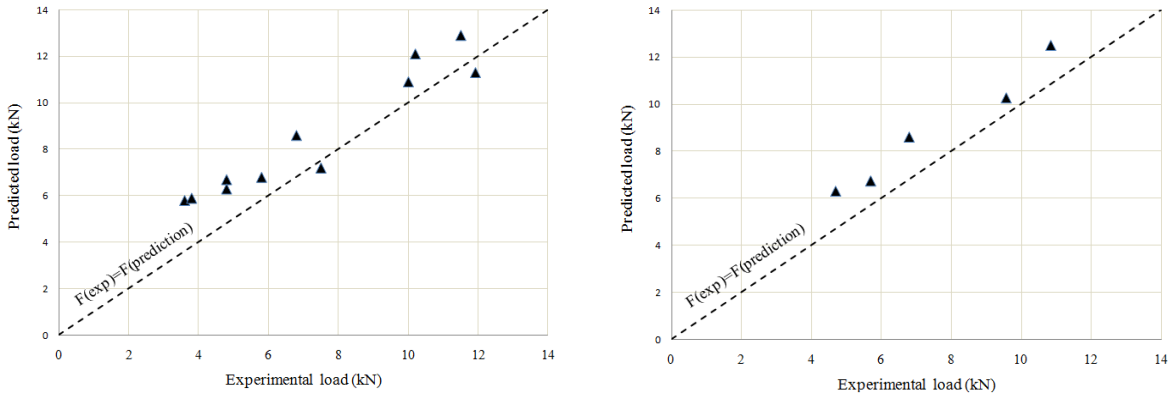

Figure 7.14. Experimental-analytical comparison of the tensile load in the screw reinforcement at the beam failure: (a) individual results, (b) average results

Use of epoxy for the connection between LVL and screw may change the strain in the screw; however, after testing the beam with a hole, a part of a beam with screw was cut off and subjected to a pull-out test. By comparing the strain measured during the beam test with the load versus strain from the pull-out test, this effect is automatically removed from the determination of the force in the screw.

7.6 Finite element model

A numerical analysis was performed to check the accuracy of Equation (7.16) for tensile force prediction in the reinforced beams. The modelling was performed in two steps viz.: (i) modelling of the experimental beams and (ii) modelling of beams with different geometrical and mechanical properties (parametric study).

Three dimensional (3D) linear finite element models were used to replicate the results predicted by Equation (7.16). Material properties of LVL and steel for 3D modelling were discussed in chapter 5. Screws were modelled as steel rods assembled using tie elements that assume full bond exists between timber and steel screws. The use of full bond between screws and timber is realistic, provided that enough embedment length is provided for the screw to avoid screw withdrawal due to the tensile force. 10-node quadratic tetrahedron solid elements (type C3D10) were used as they allow automatic meshing of complex geometries; however, they are also computationally more demanding. The mesh size was 5 to 10 mm around the steel bar, and 2 mm for the steel bar.

In the experiments, prior to beam failure at mid-span, cracks propagated from the hole edge towards the screw. The splitting of the beam stopped at the screw location. In the model, two cracks were introduced to the beam to model this behaviour. The seam option available in the ABAQUS (Habbitt et al. 2010b) was used to introduce the cracks in the model. A seam is a crack that can open if loaded. The location of the crack was assumed to be at the perimeter of the hole at the point where the elastic model predicted the maximum normal stress.

To check the accuracy of the model, load-deflection predictions from the model were compared with experimental results for beam specimen No 7 (Table 7.1) in Figure 7.15. The results are in good agreement.

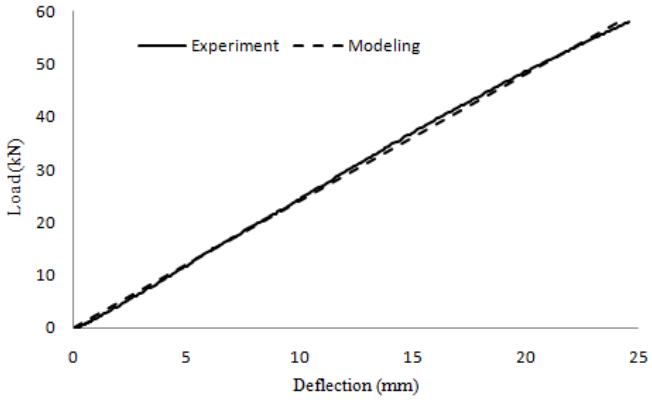

Figure 7.15. Experimental-numerical load-deflection comparison for beam specimen No. 7

A comparison among the average results of the FE model, the average experimental results, and the average analytical results predicted by Equation (7.16) is presented in Figure 7.16 (b) while a more detailed comparison for the experimental beams is presented in Figure 7.16 (a).

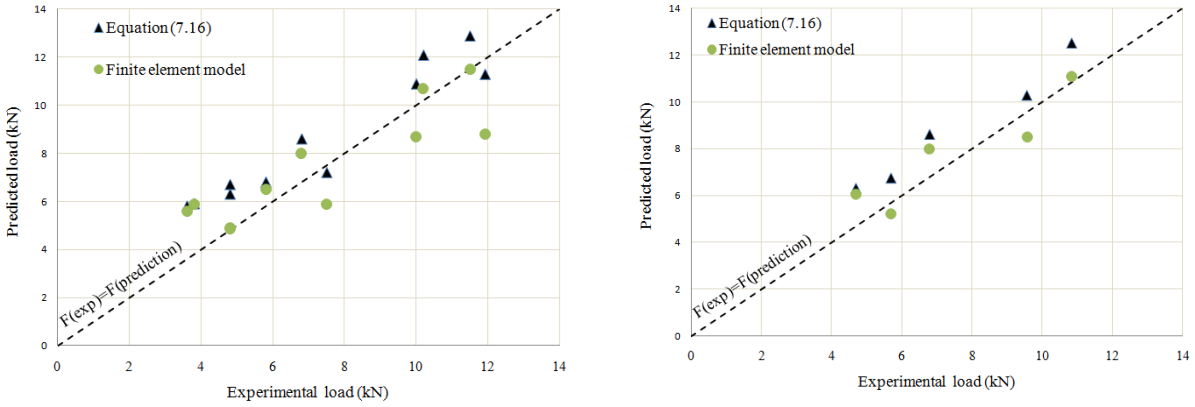

(a) (b)

Figure 7.16. Comparison of the values from experiments, analytical formulation (Equation (7.16)), and finite element results: (a) individual beams, (b) average values

The predicted tensile force from Equation (7.16) in most cases yielded predictions higher than the experimental and numerical finite element results. The maximum error in numerical prediction relative to the average experimental result is about ± 15 %.

To demonstrate the accuracy of Equation (7.16) on a larger number of cases, numerical analysis was used to carry out a parametric study where the tensile load was predicted for a number of cases. Table 7.2 summarizes the beam sizes, screw dimensions, and distance of the screws from hole edge analyzed in the parametric study. The applied load to the beam was obtained assuming a bending strength of the LVL equal to 48 MPa (Buchanan 2007).

Table 7.2. Dimensions of the beams used in the FE parametric study

Beam No.	Beam dimensions (mm)	L_c (mm)	D_c (mm)	Hole diameter (mm)	Screw length (mm)	Failure load of the beam (N)
1	1500×200×45	400	100	60	200	38400
2	1500×200×45	400	100	80	200	38400
3	1500×200×45	400	100	100	200	38400
4	2100×300×45	600	150	60	300	61714
5	2100×300×45	600	150	90	300	61714
6	2100×300×45	600	150	120	300	61714
7	2100×300×45	600	150	150	300	61714
8	3000×400×45	800	200	80	400	76800
9	3000×400×45	800	200	120	400	76800
10	3000×400×45	800	200	160	400	76800
11	3000×400×45	800	200	200	400	76800

Figure 7.17 displays a screen shot of the model and its meshing. The load was applied to a steel plate attached to the beam at mid-span; the supports also had steel plates fixed to them. Two screws were placed in the beam at a distance of 30 mm from the hole nearest edge. Finally, the vertical component of the load in the screws was calculated automatically by using a program that integrates the stresses over the cross-sectional area of the screw.

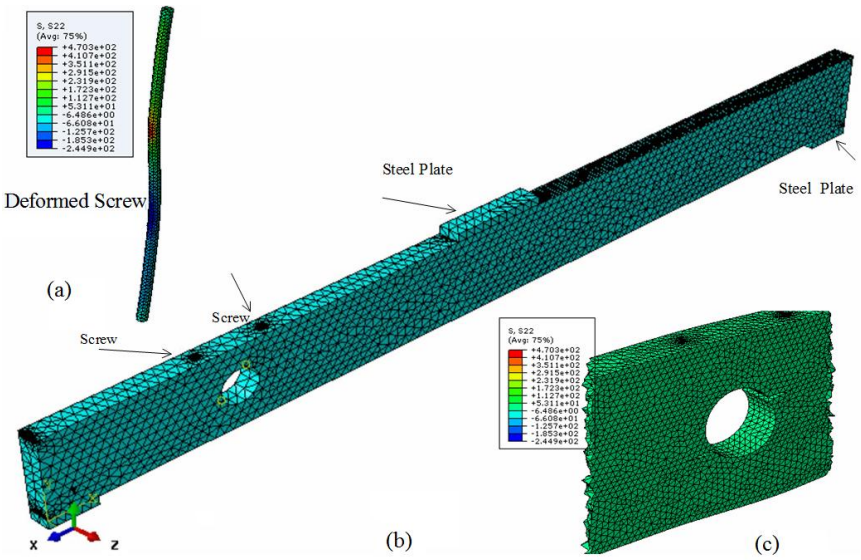

Figure 7.17. Finite element analysis: (a) deformed screw, (b) beam with hole reinforced with screws, (c) crack around the hole

Figure 7.18 presents a graphical comparison of the predictions from finite element modelling and the predictions through Equation (7.16) in terms of tensile load in the screw reinforcement. The predictions from the finite element modelling and the analytical formulations are in good agreement, with the latter being slightly higher, which is beneficial from the design point of view. Larger differences between predictions and finite element results were found for larger h_d/h values.

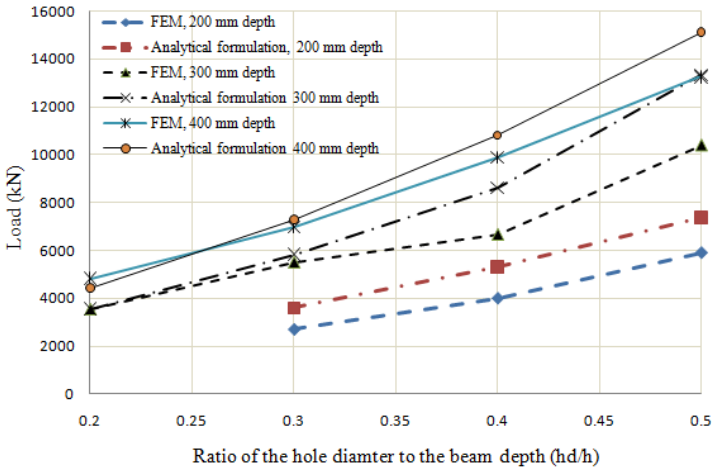

Figure 7.18. Comparison between numerical approach and analytical formulation in terms of tensile load in the screw reinforcement

7.7 Sensitivity analysis

Since wood has a relatively high coefficient of variation (COV) in material properties, the load predictions in a screw could be affected by this variation in material properties. The prediction of the load in the screw for different COVs of the LVL material properties was therefore investigated. 5^{th} and 95^{th} percentiles of the LVL material properties were then calculated for different COV's: 8, 20, and 30 percent using a normal distribution. The Young's and shear moduli were assumed to be fully correlated, namely to have the same distribution functions. The normal distribution formulation can be expressed as Equation (7.17).

$$f(x) = \frac{1}{\sigma\sqrt{2\pi}} e^{-\frac{(x-\mu)^2}{2\sigma^2}} \tag{7.17}$$

where σ denotes the standard deviation of the data set, μ the average of the data set, x a data point, and $f(x)$ denotes the normal distribution function of the data set. Table 7.3 presents the reproduced values of the material properties.

Table 7.3. Material properties of LVL

COV (%)	Percentile	E_x (MPa)	E_y (MPa)	E_z (MPa)	G_{xy} (MPa)	G_{yz} (MPa)	G_{xz} (MPa)	ν_{xy}	ν_{yz}	ν_{xz}
8	5th	10420	421	243	521	21	521	0.3	0.3	0.3
8	95th	13579	548	317	678	27	678	0.3	0.3	0.3
20	5th	8052	325	188	402	16	402	0.3	0.3	0.3
20	95th	15947	644	372	797	31	797	0.3	0.3	0.3
30	5th	6078	246	141	303	12	303	0.3	0.3	0.3
30	95th	17921	724	418	896	36	896	0.3	0.3	0.3

In total, 77 models with different material properties as summarized in Table 7.3 were analyzed to predict the load in the screw at the beam failure. Different hole diameters, ranging from 0.2 to 0.5 of the beam depth, and different beam depths of 200 mm, 300 mm, and 400 mm were analyzed. Table 7.4 presents the results of the analyses.

Table 7.4. Numerical predictions for different material properties

Beam depth (mm)	$h_{d/h}$ ratio	Average of analyses (kN)	COV of the results (%)	COV 8%	COV 8%	COV 20%	COV 20%	COV 30%	COV 30%
				5th percentile (kN)	95th percentile (kN)	5th percentile (kN)	95th percentile (kN)	5th percentile (kN)	95th percentile (kN)
200	0.3	2.52	1.43	2.52	2.50	2.55	2.48	2.56	2.46
200	0.4	3.72	1.09	3.74	3.71	3.76	3.68	3.77	3.66
200	0.5	5.1	1.13	5.11	5.13	5.14	5.04	5.16	5
300	0.2	3.2	2.18	3.22	3.17	3.27	3.13	3.29	3.1
300	0.3	4.84	1.88	4.92	4.84	4.92	4.77	5.03	4.78
300	0.4	5.94	1.98	5.98	5.90	6.04	5.83	6.12	5.78
300	0.5	9.31	1.85	9.38	9.24	9.17	9.13	9.56	9.05
400	0.2	4.3	3.89	4.36	4.24	4.45	4.15	4.53	4.05
400	0.3	6.11	3.35	6.19	6.03	6.31	5.92	6.41	5.84
400	0.4	8.92	3.06	9.01	8.81	9.18	8.67	9.32	8.55
400	0.5	12.2	2.92	12.28	12.00	12.50	11.83	12.67	11.68

Two main results could be inferred from Table 7.4. First, the predicted values are not very sensitive to the change in material properties. It implies that for normal change in material properties of the LVL, the tensile load in the screw varies far less. This result could be due to the high stiffness of a screw relative to the LVL. Another valuable result can be obtained if the tensile load in the screws predicted using average LVL properties is plotted versus the hole diameter to depth ratios for different beam depths (Figure 7.19). The figure shows that the force in the reinforcement increases as the beam size and hole size increase.

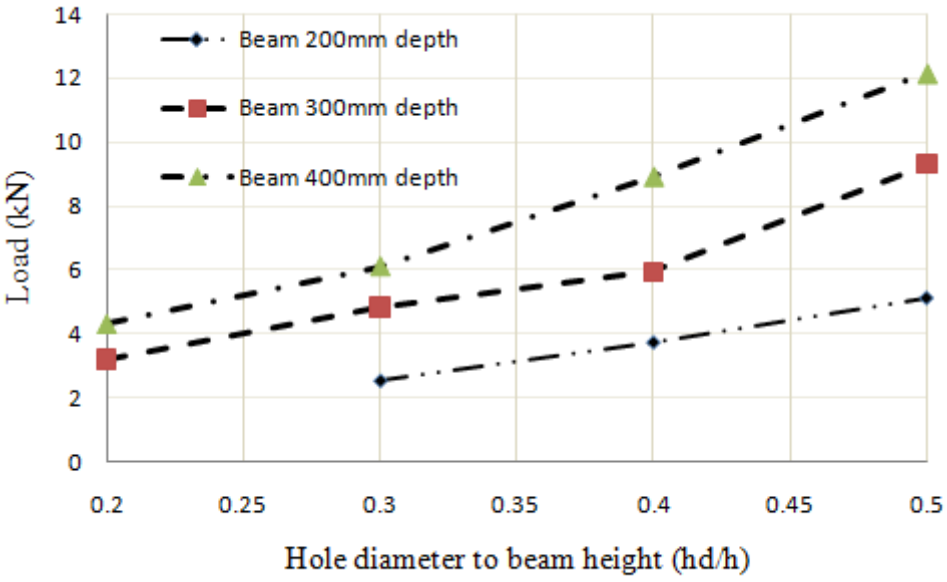

Figure 7.19. Predictions of the tensile force in the reinforcement for different beam depths and hole diameter to beam depth ratios.

7.8 Square holes

A circular hole was the basis for the development of the Equation (7.16). Since square or rectangular holes are also common options for holes, a finite element study with square holes was performed to check the accuracy of the formulations also for this case. Elastic models such as the procedure mentioned above were developed for different sizes of the holes in LVL beams. As in the previous sections, three main beam depths with different hole diameter to depth ratios were considered for the analysis. Table 7.5 summarizes the beam geometries of the finite element analysis. In addition, Figure 7.20 presents a close up picture of beam No. 5 in Table 7.5

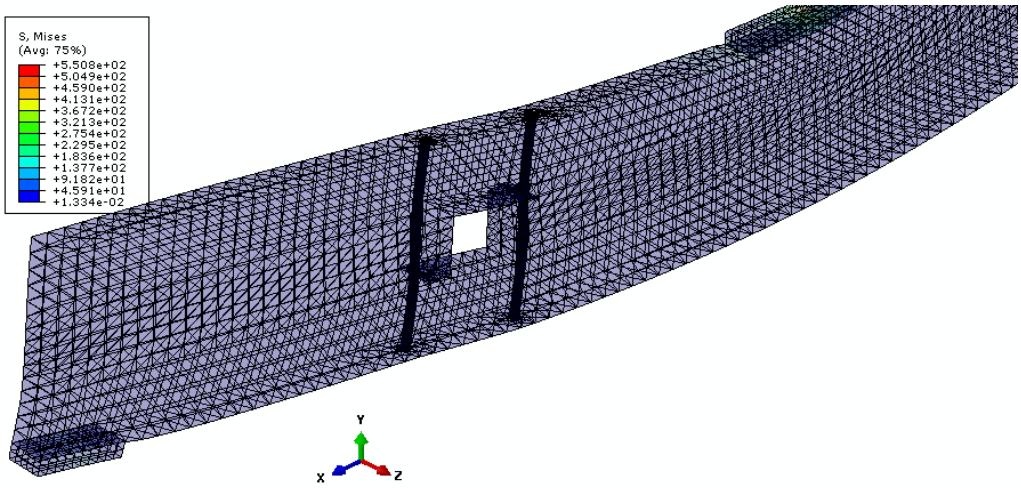

Figure 7.20. Deformed shape of the finite element beam model

Table 7.5. Dimensions of the beams used in the FE parametric study

Beam No.	Beam dimensions (mm)	Lc (mm)	Dc (mm)	Square side (mm)	Screw length (mm)	Mid-span point load (N)	Load in screw from FE analysis (N)
1	1500×200×45	400	100	60	200	38400	4500
2	1500×200×45	400	100	80	200	38400	6500
3	1500×200×45	400	100	100	200	38400	7600
4	2100×300×45	600	150	60	300	61714	7300
5	2100×300×45	600	150	90	300	61714	8200
6	2100×300×45	600	150	120	300	61714	11600
7	2100×300×45	600	150	150	300	61714	15300
8	3000×400×45	800	200	80	400	76800	6540
9	3000×400×45	800	200	120	400	76800	9940
10	3000×400×45	800	200	160	400	76800	14000
11	3000×400×45	800	200	200	400	76800	18800

The best match with numerical results of the tensile force with analytical predictions in the screw (Equation (7.16)) was found when the force in the screw was calculated assuming a circular hole surrounding the square hole (hole circumscribing the square). Therefore, the diameter of the hole was selected as $\sqrt{2}$ times the side length of the square. Figure 7.21 presents a comparison between the results from finite element

analysis and the analytical approach (Equation (7.19)) based on the assumption presented above.

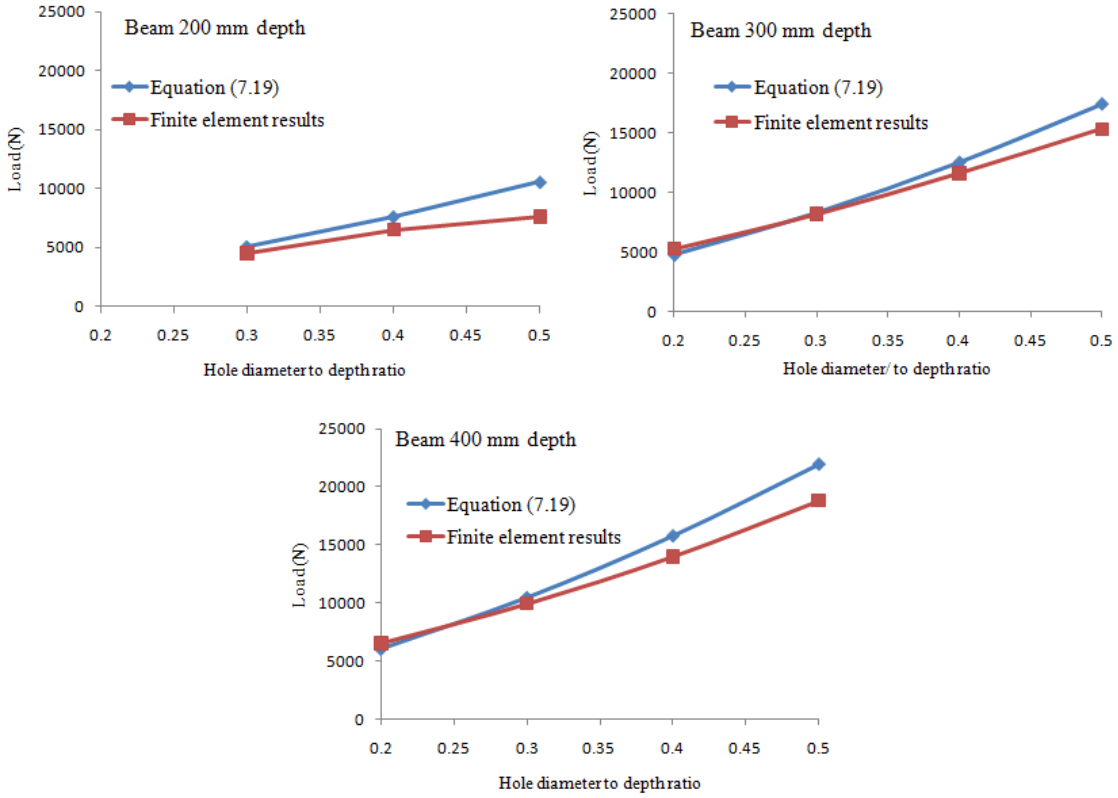

Figure 7.21. Analytical-numerical comparison of the screw load using the proposed formulation for 200 mm, 300 mm, and 400 mm depth beams with square holes

Equation (7.16) overestimates the tensile force for larger h_d/h ratios ($h_d/h \rightarrow 0.5$) while it is closer to the numerically predicted values for the smaller values ($h_d/h \rightarrow 0.2$). A calibration of the analytical model with the finite element was carried out to obtain better estimation of the tensile load predictions. Different options for calibration of the model were noticed. The total moment that could not be transferred due to the hole in the section (Equation (7.10)) for the moment effect was divided by the chord length of AB in Figure 7.6. This could be written as Equation (7.18).

$$F_{t,M} = \xi M \frac{h_d^2}{h^3} \tag{7.18}$$

where ξ is a calibration factor and obtained through calibration of the numerical results with the analytical formulation. The best match between experimental and numerical values was obtained assuming $\xi = 0.7$. Therefore, the total tensile load for the case of square holes could be re-written as:

$$F_{t,d} = \frac{\sqrt{2}}{8h^3} V\, h_d(3h^2 - h_d^2) + 0.7M\frac{h_d^2}{h^3} \qquad (7.19)$$

Comparison between the numerical and the results from Equation (7.16) for beam geometries presented in Table 7.5 is shown in Figure 7.22.

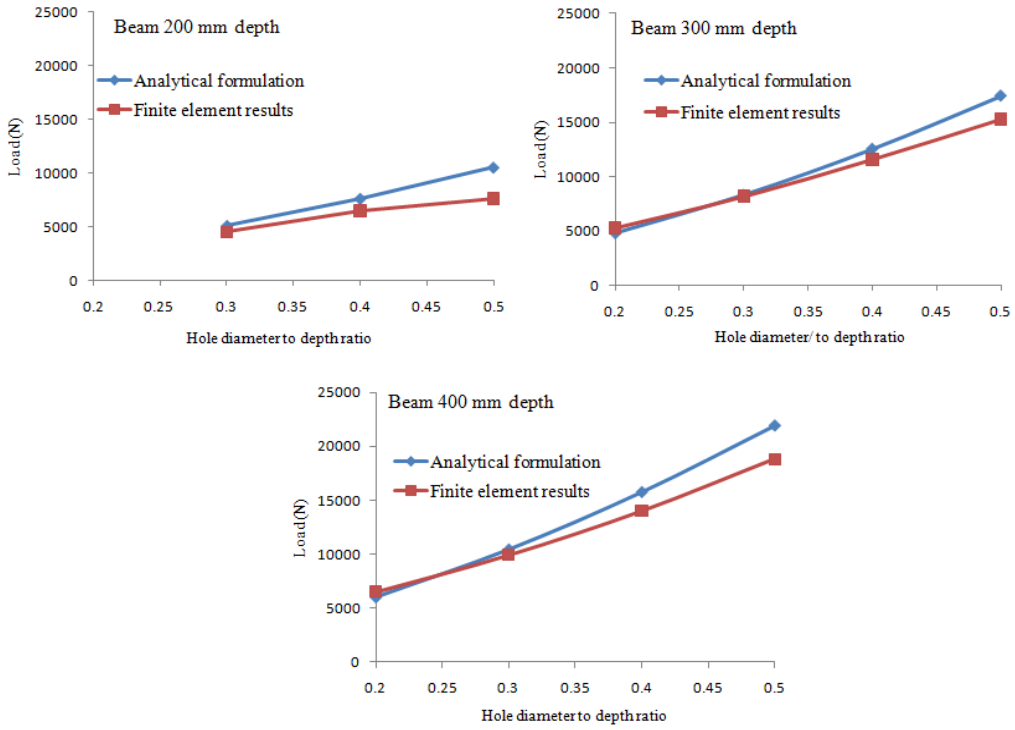

Figure 7.22. Comparison between numerical results and the predicted values from Equation (7.19) for 200 mm, 300 mm, and 400 mm depth beams

7.9 Rectangular holes

Extension of the Equation (7.19) for rectangular holes can be performed for the tensile load predictions in the reinforcement around the rectangular holes. Figure 7.23 shows a

beam with a rectangular hole of dimension b_h by h_d placed at a distance of Lc from the end of the beam.

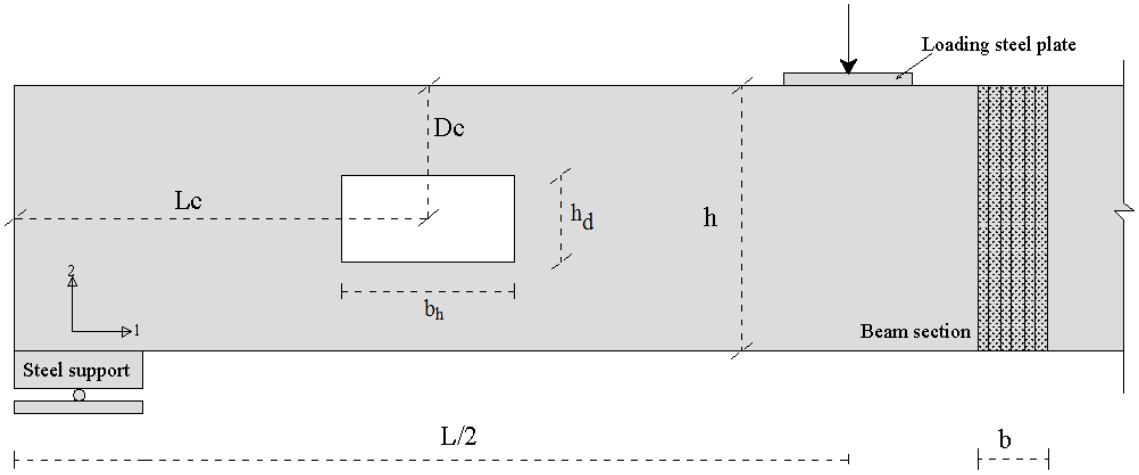

Figure 7.23. Beam with rectangular hole

According to the truss model, passing a circular/square hole through the beam cuts a strut and tie where the produced tensile force around the hole is assumed to be formed at an angle of 45 degrees around the hole for circular/square holes. However, for the rectangular hole, the angle of the load can be different from 45 degrees (Figure 7.24). The produced angle of the tensile force around the hole can be larger or smaller than 45 degrees. Indication of the exact angle is difficult; however, a good match of the numerical values with the analytical was found when the produced tensile load was multiplied by β where β is calculated as:

$$\beta = Max\left(\frac{b_h}{\sqrt{h_d^2 + b_h^2}}, \frac{h_d}{\sqrt{h_d^2 + b_h^2}}\right) \tag{7.20}$$

The factor of β in Equation (7.20) corresponds with the maximum values of $\cos(\theta)$ as shown in Figure 7.24.

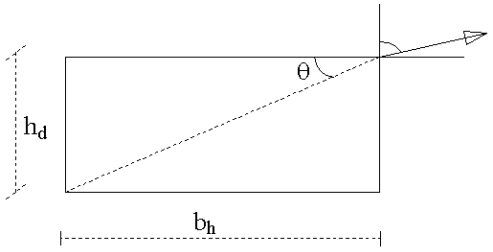

Figure 7.24. Produced tensile force around the hole

Therefore, Equation (7.19) can be re-written as Equation (7.21) for rectangular holes.

$$F_{t,d} = (\frac{\beta}{4h^3})V\ h_d(3h^2 - h_d^2\ ) + 0.7M\frac{h_d^2}{h^3} \qquad (7.21)$$

Equation (7.21) is valid for squares holes too because in square holes $b_h = h_d$ and it leads to Equation (7.19). Accuracy of the Equation (7.21) for rectangular holes was also investigated using the finite element analysis. Models of the beams with the rectangular holes of $b_h = 2h_d$ were made and analyzed. A sketch of the analyzed beams with rectangular hole parameters in Figure 7.25, the dimensions of the beams in Table 7.6, and the results are presented in Figure 7.26.

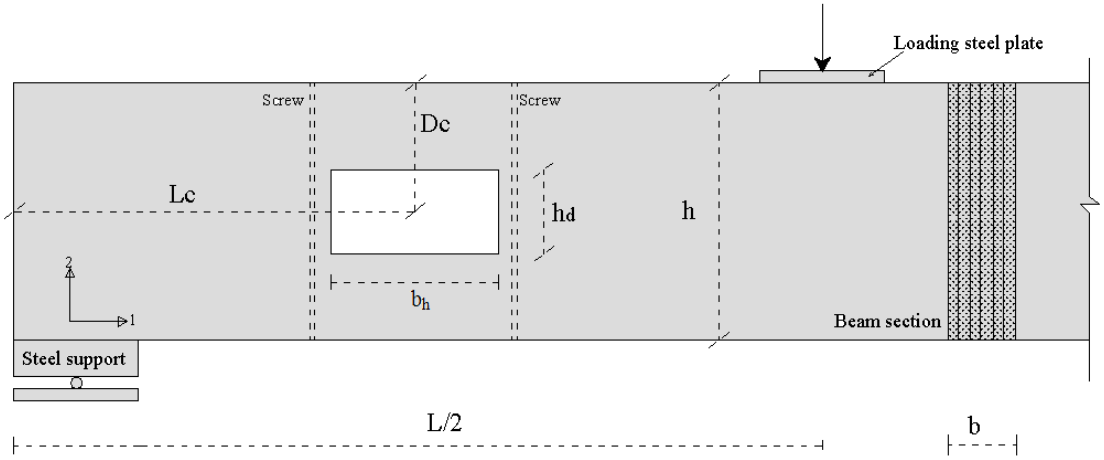

Figure 7.25. Beam with rectangular hole

Table 7.6. Beam dimensions used for finite element modelling

Beam No.	Beam dimensions (mm)	Lc (mm)	Dc (mm)	Small hole side (mm)	Large hole side (mm)	Screw length (mm)	Mid-span point load (N)
1	1500×200×45	400	100	60	120	200	38400
2	1500×200×45	400	100	80	160	200	38400
3	1500×200×45	400	100	100	200	200	38400
4	2100×300×45	600	150	60	120	300	61714
5	2100×300×45	600	150	90	180	300	61714
6	2100×300×45	600	150	120	240	300	61714
7	2100×300×45	600	150	150	300	300	61714
8	3000×400×45	800	200	80	160	400	76800
9	3000×400×45	800	200	120	240	400	76800
10	3000×400×45	800	200	160	320	400	76800
11	3000×400×45	800	200	200	400	400	76800

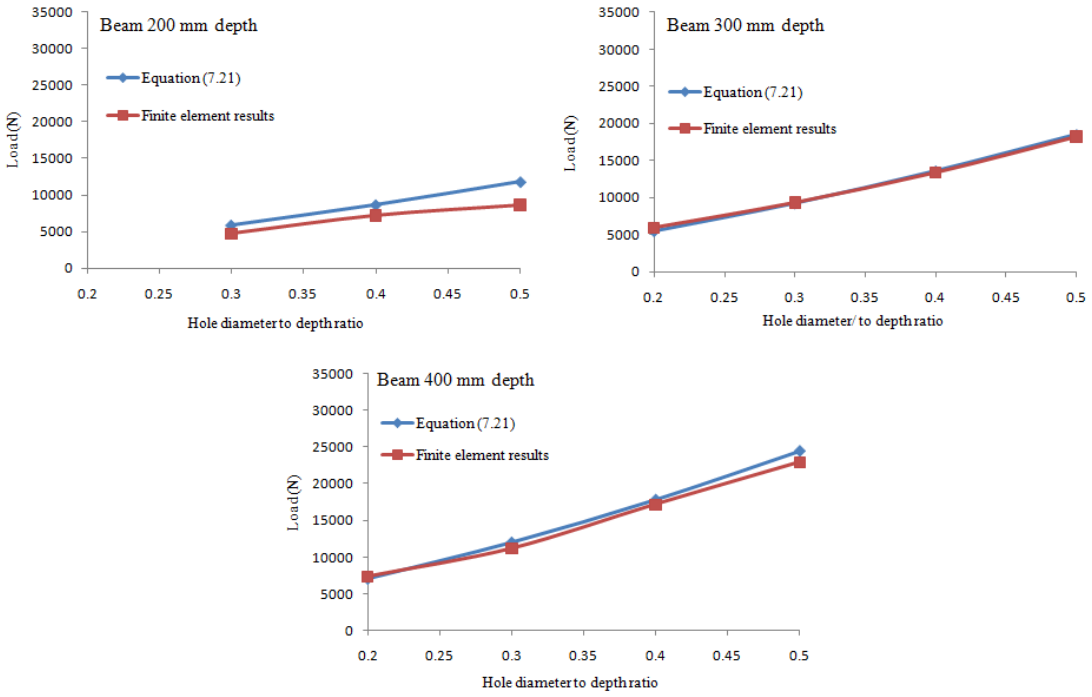

Figure 7.26. Comparison of the predicted values from Equation (7.21) and finite element analysis for rectangular holes with $b_h = 2h_d$

Also, another finite element analysis for the rectangular holes of Table 7.6 assuming that $b_h = 1.5\ h_d$ is presented in Figure 7.27.

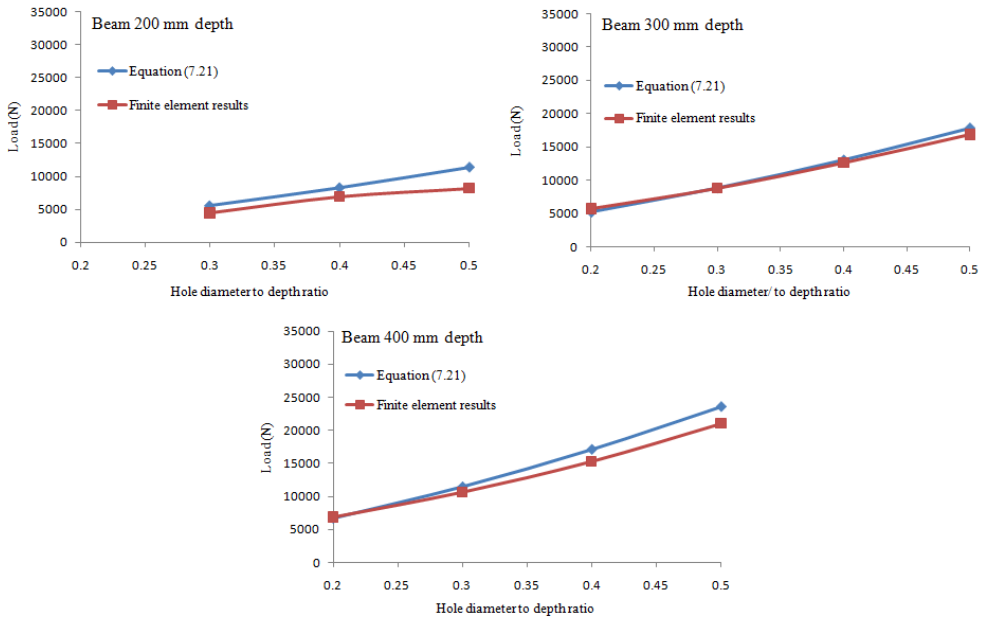

Figure 7.27. Comparison of the predicted values from Equation (7.21) and finite element analysis for rectangular holes with $b_h = 1.5\ h_d$

Finally, another comparison of the numerically predicted values for the case of $b_h = 0.5\ h_d$ is presented in Figure 7.28.

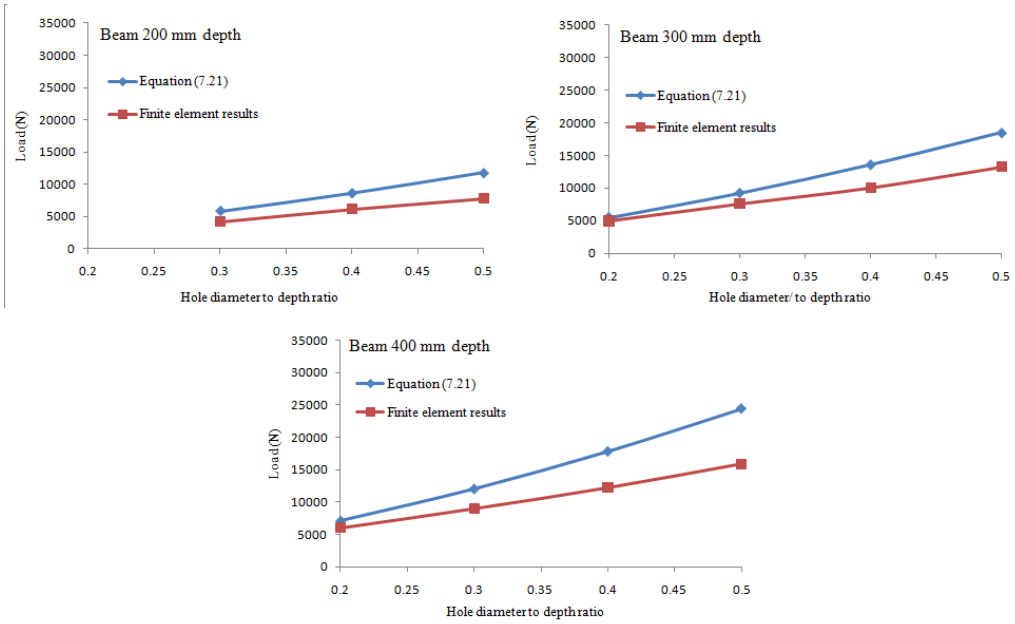

Figure 7.28. Comparison of the predicted values from Equation (7.21) with finite element analysis for rectangular hole with $b_h = 0.5\ h_d$

While Equation (7.21) over estimated the produced tensile load for $b_h < h_d$, the predicted values for $b_h \geq h_d$ are close to the numerical values for rectangular holes.

7.10 Comparison with DIN 1052

As stated previously, DIN 1052 (2008) proposes a formulation for the calculation of the load in the beam reinforcement for circular holes as:

$$F_{t,d} = \frac{V(0.7h_d)}{4h}[3 - \frac{(0.7h_d)^2}{h^2}] + \frac{0.008\,M}{h_r} \qquad (7.22)$$

The parameters were defined in the previous sections. The formulation includes both the effects of the shear and the moment. The shear contribution (first part in Equation (7.22)) is similar to the formulation derived in this paper using the truss model. Although the German design code limits the ratio of the hole diameter to the beam depth to 0.4 for reinforcement with plywood, and to 0.3 for reinforcement with screws, the comparison with the proposed analytical formulation was performed up to the ratio of 0.5. A comparison of the results predicted based on the two analytical methods is presented for the beams listed in Table 7.7, is given in Figure 7.29.

Table 7.7. Beam dimensions used for the comparisons between DIN 1052 approach and Equation (7.16)

Beam No.	Beam dimensions (mm)	Lc (mm)	Dc (mm)	Hole Diameter (mm)
1	3000×200×45	400	100	40
2	3000×200×45	400	100	50
3	3000×200×45	400	100	60
4	3000×200×45	400	100	70
5	3000×200×45	400	100	80
6	3000×200×45	400	100	90
7	3000×200×45	400	100	100
8	4000×300×45	600	150	60
9	4000×300×45	600	150	75
10	4000×300×45	600	150	90
11	4000×300×45	600	150	105
12	4000×300×45	600	150	120
13	4000×300×45	600	150	135
14	4000×300×45	600	150	150
15	5000×400×45	800	200	80
16	5000×400×45	800	200	100
17	5000×400×45	800	200	120
18	5000×400×45	800	200	140
19	5000×400×45	800	200	160
20	5000×400×45	800	200	180
21	5000×400×45	800	200	200
22	6000×600×45	1200	300	120
23	6000×600×45	1200	300	150
24	6000×600×45	1200	300	180
25	6000×600×45	1200	300	210
26	6000×600×45	1200	300	240
27	6000×600×45	1200	300	270
28	6000×600×45	1200	300	300

Figure 7.29 shows that predictions according to DIN 1052 for hole diameter to depth ratios less than 0.30 are more conservative than the proposed approach, whereas they are less conservative for ratios equal to or larger than 0.30.

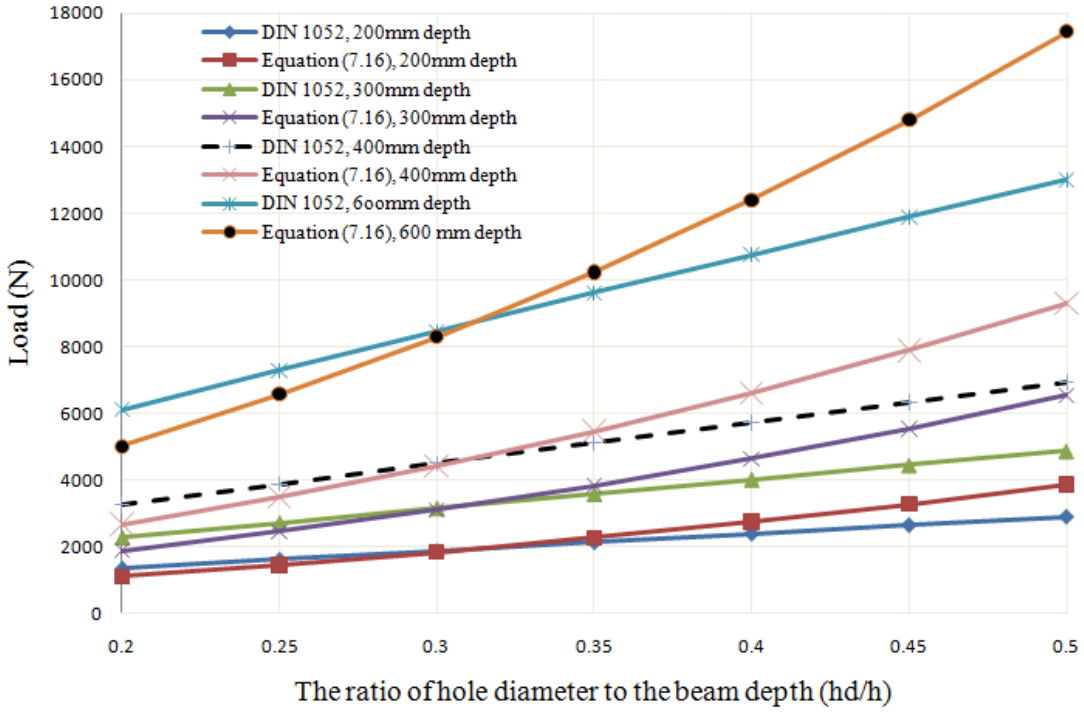

Figure 7.29. Comparison between DIN 1052 and proposed analytical formulation (Equation (7.16)) for the calculation of the tensile load in the screw reinforcement

Recently, the second part of the above formulation has been revised (Aicher 2011). The research has been performed based on the material properties of glulam through a finite element analysis carried out using the ANSYS software package. The new revised form of the above formulation for circular holes is as below:

$$F_{t,d} = \frac{V(0.7h_d)}{4h}\left(3 - \frac{(0.7h_d)^2}{h^2}\right) + \frac{0.084\,M}{h}\left(\frac{h_d}{h}\right)^2 \qquad (7.23)$$

The new format incorporates the h_d/h term. Figure 7.30 presents a comparison of the experimental results and the predictions using the truss model and Equation (7.23). Equation (7.23) for $h_d/h \geq 0.4$ (beam 300 mm and 400 mm depth) yields results lower than experimental values, as presented in Figure 7.30.

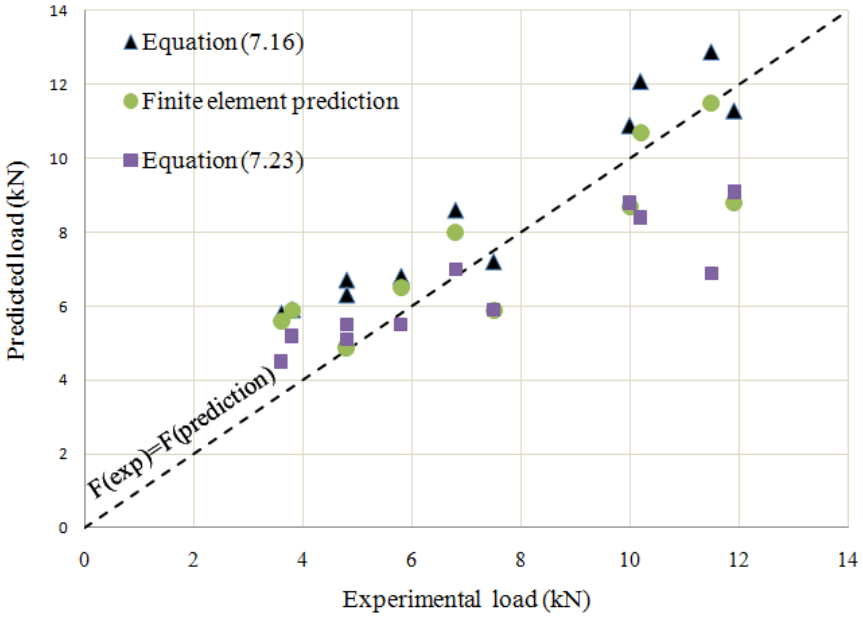

Figure 7.30. Comparison of the tension load in the screw reinforcement among experimental data and predictions using the Equations (7.16) and (7.23)

7.11 Correction factor for larger depths

The maximum length of 450 mm is suggested for screws used as reinforcement. This limit is adopted because for larger lengths the screws would limit the possibility of wood to move due to shrinkage and swelling. Limiting shrinkage and swelling of the wood may cause cracking in wood in the long term. On the other hand, the limitation of the analytical approach for larger depths should be investigated, as the derived formulation was a simplification of a complicated stress field in timber beams with holes.

Since in the previous sections the analysis was performed for beams up to 400 mm depth, a FE analysis was performed on LVL beams with larger depths of 500 mm, 600 mm, and 800 mm. The same type of model as discussed before was used. Table 7.8 summarizes the beam dimensions that were used in the FE analysis.

Table 7.8. Dimensions of the beams used in the FE parametric study

Beam No.	Beam dimensions (mm)	Lc (mm)	Dc (mm)	Hole diameter (mm)	Mid-span point load (N)
1	5000×500×50	1000	250	100	80000
2	5000×500×50	1000	250	150	80000
3	5000×500×50	1000	250	200	80000
4	5000×500×50	1000	250	250	80000
5	6000×600×60	1200	300	120	115200
6	6000×600×60	1200	300	180	115200
7	6000×600×60	1200	300	240	115200
8	6000×600×60	1200	300	300	115200

Although for the beams smaller than 400 mm, predictions using Equation (7.16) yielded good results; the FE analysis shows that the predicted load in the screws for 500 and 600 mm deep beams are lower than the numerical values. Figure 7.31 (a) presents a comparison of the numerical results with the values predicted using Equation (7.16). Different correction factors were considered to take into account this effect. An empirical modification factor of $\sqrt{h/400}$ seems to give the best results if it is applied to the final tensile load in the screw due to the shear and the moment (Figure 7.31 (b)). This will increase the load in the screws for larger depths. The correction factor increases the tensile load in the screw by about 11 percent for 500 mm, and 12 percent for 600 mm depth. Another finite element analysis was performed on a beam of 8000×800×80 mm size with the centre loading of 253.6 kN showing that the load from a finite element analysis in the screw was 33.2 kN, which is very close to the 35.7 kN predicted by the revised formulation. Empirical modification factor of $\sqrt{h/400}$ seems to be significant and its experimental verification is out of the scope of this thesis.

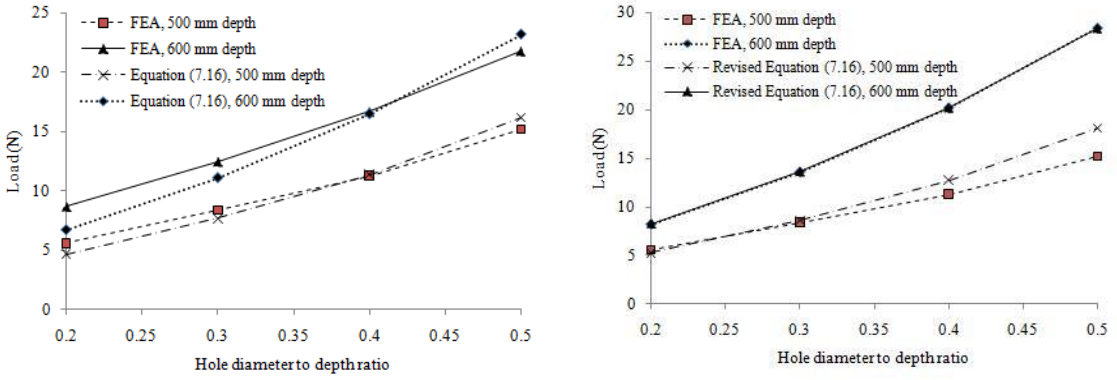

(a) (b)

Figure 7.31. Comparison between FE model and Equation (7.16) in terms of tensile load in the screw reinforcement for different hole diameter to beam depth ratios, and for deeper beam: (a) without correction factor, (b) with empirical modification factor of $\sqrt{h/400}$

7.12 Eccentricity of hole relative to neutral axis

Effect of hole eccentricity relative to neutral axis of beam on the tensile load in screw reinforcement was also investigated by numerical analyses. An eccentricity of 10 % of beam depth was used for a series of numerical analyses on beams with holes. Three different cases of hole placement relative to neutral axis were regarded for numerical modelling viz.: (i) above neutral axis (ii) at neutral axis and (iii) below neutral axis as shown in Figure 7.32. The holes were reinforced with two vertical screws on both sides similar to previous cases.

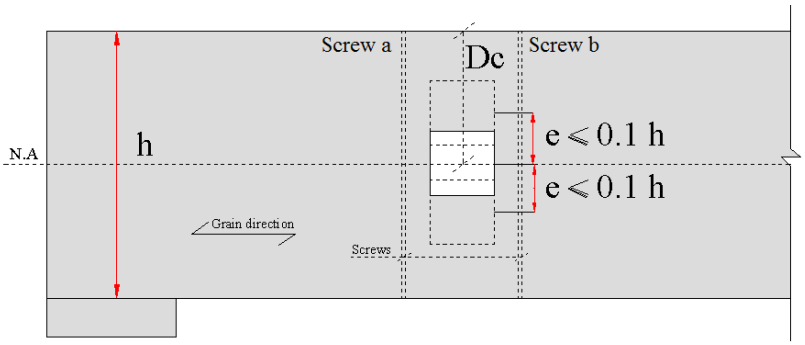

Figure 7.32. Eccentricity of the hole relative to neutral axis of beam

Three-dimensional analyses were performed on beams with holes reinforced with two screws; the results are presented in Figure 7.33. The figures show the ratio of the tensile load for holes above/below the neutral axis to the tensile load for the hole at the neutral axis for different h_d/h ratios. The plots are presented for beam 200 mm, 300 mm, and 400 mm depths. The modelling results show that as the hole shifts upward, the tensile load in the screw (b) (shown in Figure 7.32) increases, and simultaneously decreasing the tensile load in screw (a). Although not presented in the graphs, the produced tensile load in screw (b) is higher than screw (a) and the ratio varies from 20 to 50 percent depending on the hole diameter to depth ratio varying from 0.2 to 0.5 beam depth.

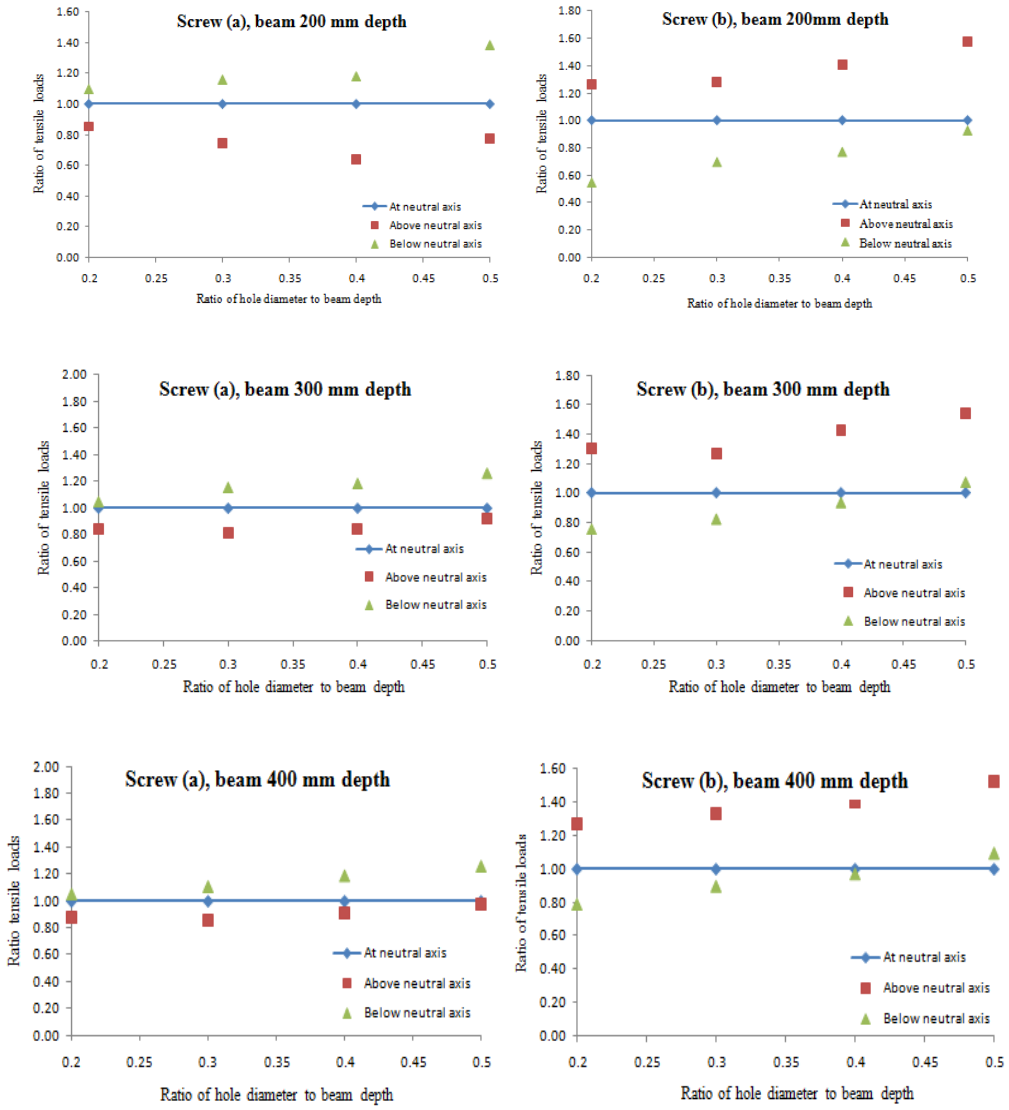

Figure 7.33. Ratio of tensile loads for different h_d/h ratios

Considering only the maximum produced tensile load in the screw for different hole diameters to beam depth ratios, leads to the graph presented in Figure 7.34. The figure shows that the increase in the tensile load for varying $h_d/h = 0.2 \sim 0.5$ is about 25%, 30%, 40%, and 50% respectively. A factor of $(1 + h_d/h)$ seems a reasonable correction factor if it is applied to the final tensile load predicted for the hole at the neutral axis.

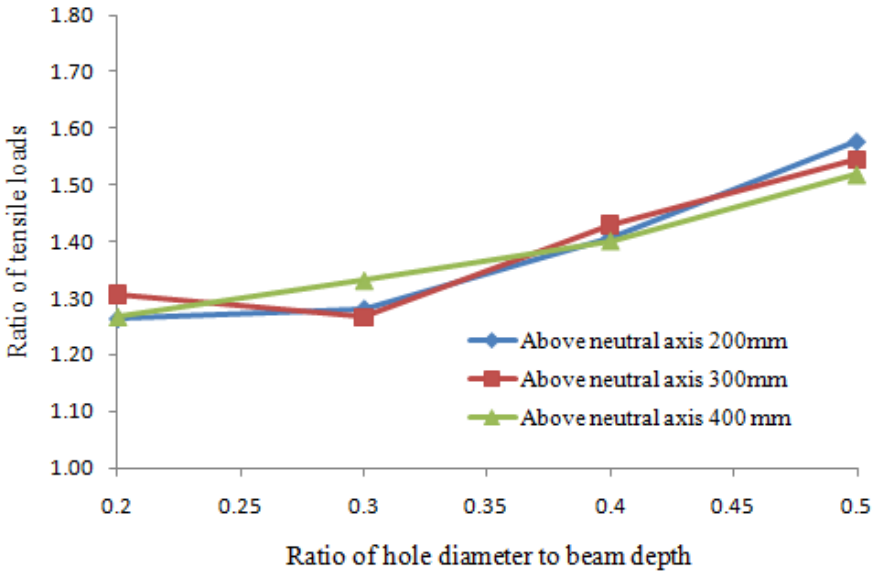

Figure 7.34. Maximum tensile load ratios for different hole diameter to beam depth ratios

7.13 Interaction of the holes

Interaction of holes in LVL beams can affect the load carrying capacity of the beams with the holes. In APA (The Engineered Wood Association), a series of the tests was performed on LVL beams with two holes to investigate effects of the holes on strength reduction of the beams. A sketch of the experimental set up and the results are presented in Figure 7.35 and Table 7.9 while Figure 7.36 presents different failure modes of the beams. The crack propagation from one hole to another hole considerably decreases the capacity of the beam. The results indicate that for double hole specimens, the failure of the beam with two holes was governed through crack initiation at the edges of the hole followed by joining to the other hole in the beam. The shear capacity of the double hole

specimens with a hole diameter of 1/3 of the LVL depth in comparison with the beam without hole, reduced about 50% (APA Report T2009L-30 2009).

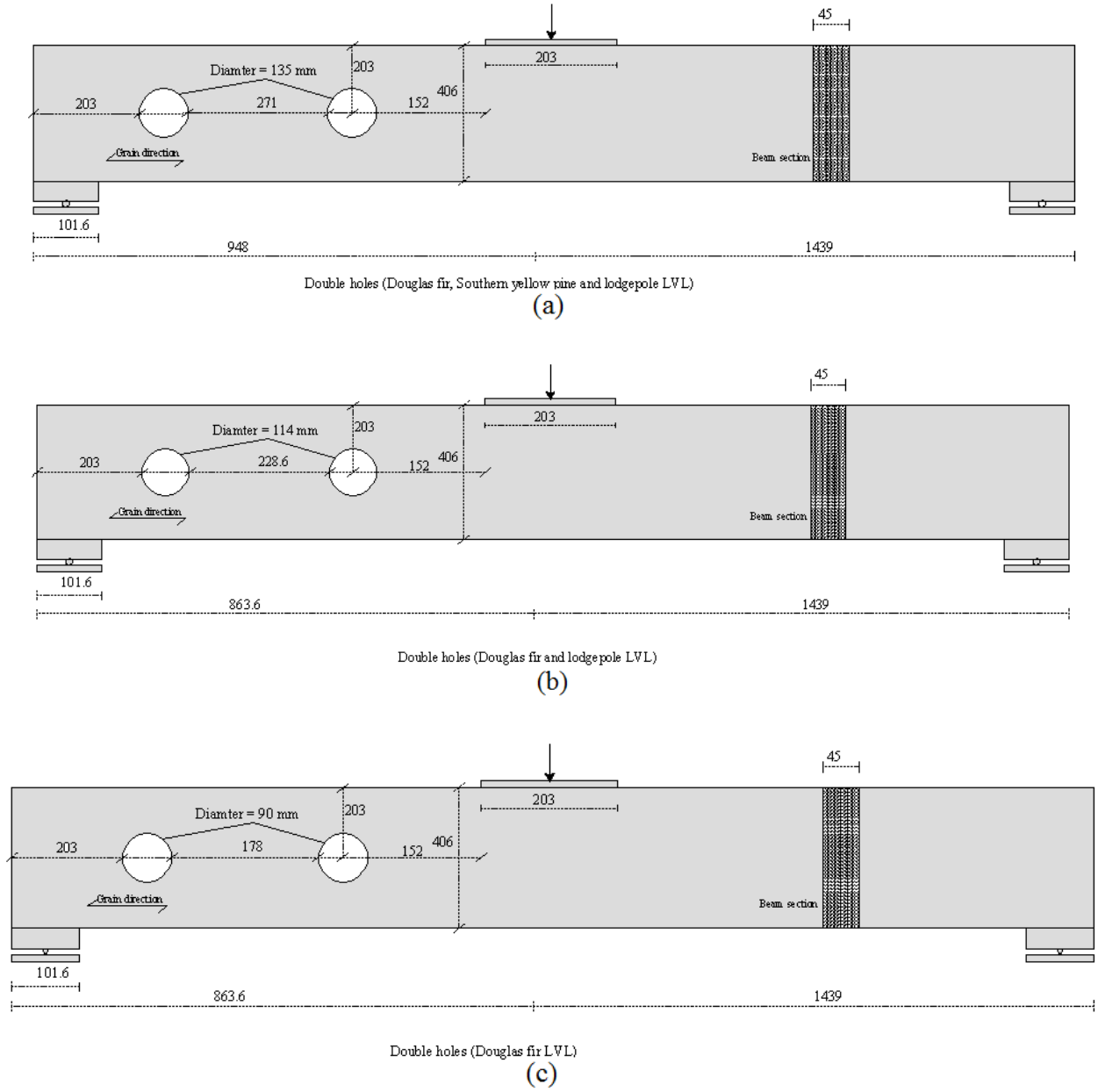

(Dimensions in mm)

Figure 7.35. Three different experimental set up on LVL beams with two holes (APA Report T2009L-30 2009): (a) Douglas fir, southern yellow pine, and lodge pole species, (b) Douglas fir and lodge pole species, (c) Douglas fir species

Table 7.9. Experiments on the beams with holes (APA Report T2009L-30 2009)

Wood type	Lodge pole pine (kN)		Douglas-fir (kN)				Southern yellow pine (kN)	
Hole diameter	135	no hole	135	115	90	Without hole	135	no hole
Number of holes	2	-	2	2	2	-	2	2
Beam 1	38.0	80.0	42.7	53.9	69.9	84.5	48.3	102.6
Beam 2	38.2	72.1	46.0	50.4	72.9	94.1	45.4	83.0
Beam 3	36.4	73.6	48.5	56.3	69.3	93.2	47.2	104.5
Beam 4	32.0	72.0	47.3	57.3	65.9	97.7	46.5	110.0
Beam 5	31.6	70.2	44.7	59.0	74.6	95.6	52.6	97.5
Mean	35.2	73.6	45.8	55.4	70.5	93.0	48.0	99.5
COV (%)	9	5.1	5	6	4.8	5.4	5.8	10.3

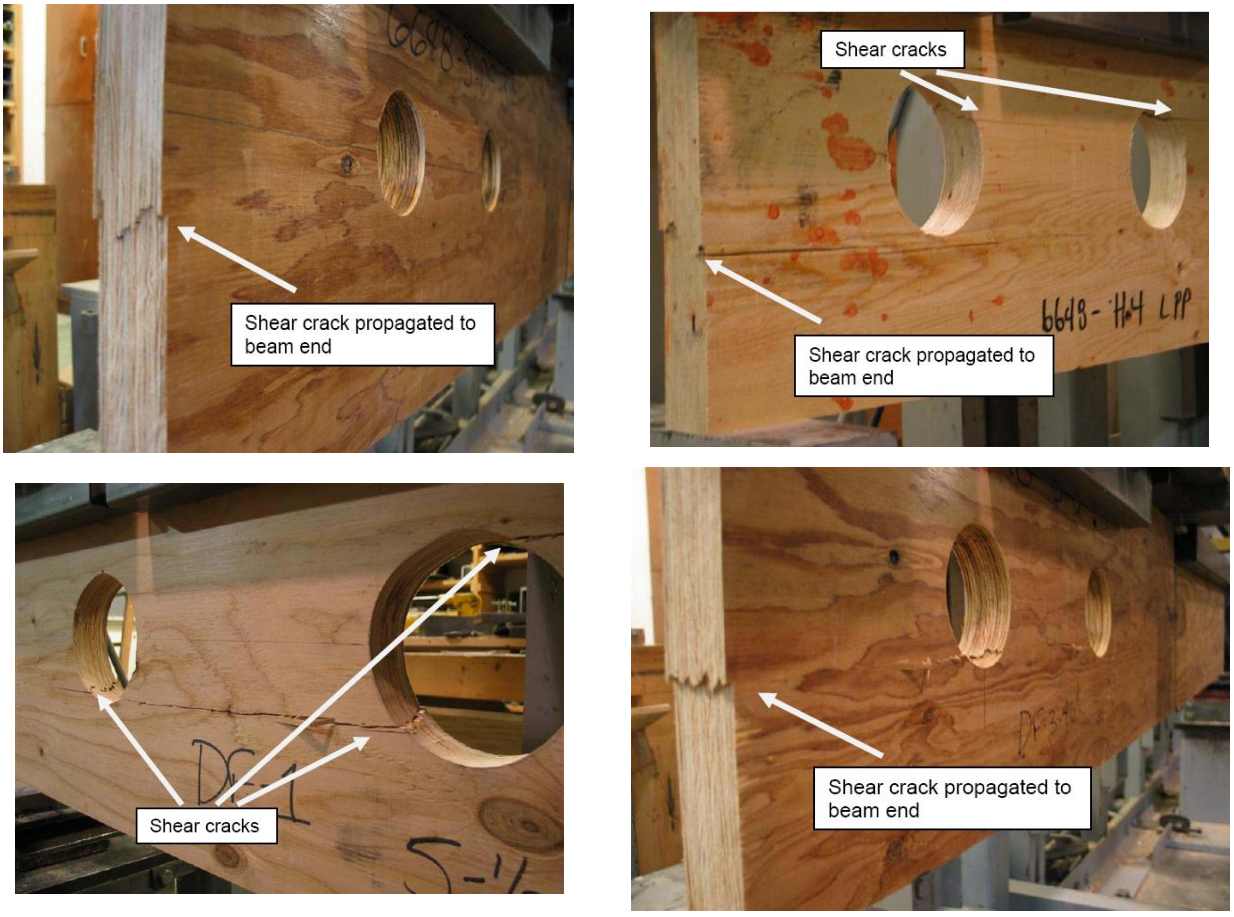

Figure 7.36. Interaction of the holes in LVL beams with the holes (APA Report T2009L-30 2009)

In reinforced beams, interaction between the holes can lead to undesirable failure modes such as beam failure at the edge of the hole because of high stress concentration in a

limited area of the beam. Another effect can be increasing the tensile load in reinforcement around the holes. This could be due to increasing the tensile strains around the hole that in turn affects the reinforcement.

Interaction of the holes should be avoided in reinforced beams to avoid over complex stress fields around the holes because of the closeness of the reinforcements in that section of the beam. To obtain the minimum distance between the holes, a finite element analysis was performed on beams of 200 mm, 300 mm, and 400 mm depth. The dimensions of the studied beams are summarized in Table 7.10.

Table 7.10. Dimensions of the modelled beams

Dimension (mm)	Hole Diameter (mm)	Lc of first hole (mm)	Lc of second hole (mm)	Load (N)
2000×200×45	80	300	470	28800
2000×200×45	80	300	500	28800
2000×200×45	80	300	600	28800
2000×200×45	80	300	700	28800
3000×300×45	120	400	600	43200
3000×300×45	120	400	700	43200
3000×300×45	120	400	800	43200
3000×300×45	120	400	900	43200
3000×300×45	120	400	1000	43200
4000×400×45	160	500	750	57600
4000×400×45	160	500	850	57600
4000×400×45	160	500	950	57600
4000×400×45	160	500	1050	57600
4000×400×45	160	500	1150	57600
4000×400×45	160	500	1250	57600

The modelling procedure is the same as previously discussed. Simply supported boundary conditions were assumed for the modelling. The modelling was performed in two phases as illustrated in Figure 7.37 viz.: (i) the maximum load in reinforcement was calculated by modelling the beam with one hole and (ii) second hole of the same size with reinforcement was added to the beam. Finally, the maximum load in the screw was calculated for different distances.

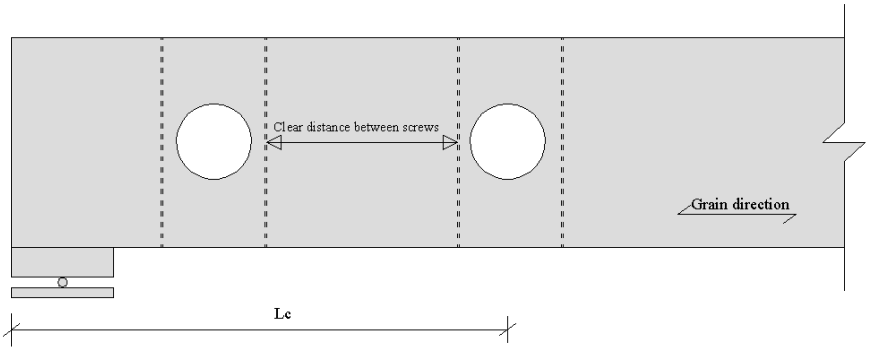

Figure 7.37. sketch of model

A graph of the predicted load in the screw for different clear distances between reinforcements is presented in Figure 7.38. The graph shows that for a beam of 200 mm depth with a clear distance between screws of about 260 mm, the interaction of holes does not affect the tensile load in the screw. The clear distance for a 300 mm depth beam is about 420 mm and for 400 mm depth of beam is 530 mm. The graphs show the dependency of the size of interaction length to the depth of the beam. Clearly, the interaction of the holes does not appear for hole spacing of more than $1.5h$. Therefore, a clear distance of $1.5h$ could be used for reinforced beams with holes.

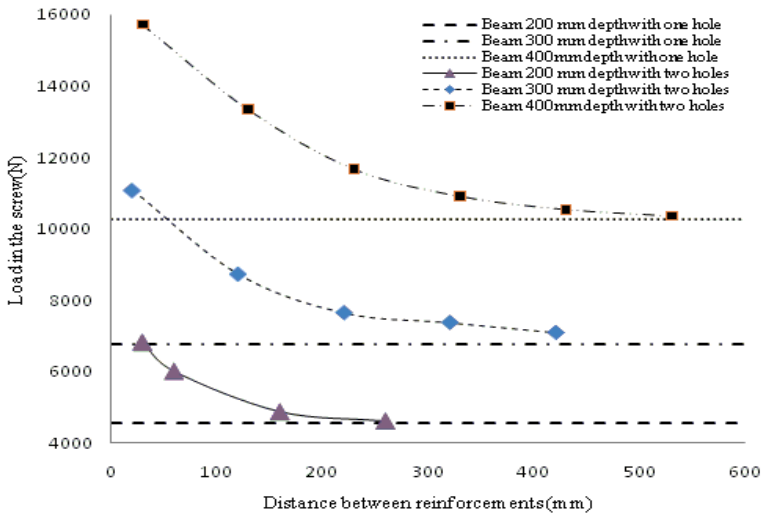

Figure 7.38. graph of the load produced in screw

7.14 Discussion

Prediction of the tensile load produced in the reinforcement around the holes in timber beams is a rather complicated problem, mostly due to the complex stress field that varies from tension to compression around the hole, together with the anisotropy of timber. In this chapter, a formulation is proposed that is based on a truss model. The truss mechanism is assumed to develop at an angle of 45 degrees around the hole. Such a truss mechanism transfers the shear and the moment that could not be resisted due to the hole.

The chosen value of 45 degrees for the angle of the equivalent truss member around the hole is not necessary realistic. Many factors such as the hole location along the beam and the variation in tensile strength perpendicular to the grain can affect the angle of the equivalent truss member and location of the crack. However, in the absence of a robust formulation for the crack initiation angle, it is logical to assume it at an angle of 45 degrees.

The proposed formulation (Equation (7.16)) contains two main contributions: the tensile force due to (i) shear and (ii) moment in the section. The derived formulation for the tensile force due to shear for circular holes matches well with DIN 1052 (2008) that was developed by integrating the shear stresses over a portion of the cross-section limited by the fibres at plus 45 degree inclination from the centre of the hole (Figure 7.1).

The effect of the moment on the tensile load was previously found through a finite element analysis for glulam material properties (DIN 1052 2008). Such a formulation does not include any dependency upon the hole diameter to beam depth ratio (h_d/h). This formulation was recently revised again based on the outcomes of a finite element analysis (Aicher 2011) and the influence of the hole diameter to beam depth ratio was added to it. Again, it is not self evident that the background assumptions and its validity hold for other materials like LVL.

The advantage of the truss model as presented herein is that it gives a simple model based on engineering mechanics rules for the tensile load due to the shear and the moment that could not be transferred in the section of the beam. The first formulation is similar to the formulation of the DIN 1052 standard for circular holes, and using the

same model the second formulation for the moment was obtained with small differences.

Extension of the model led to two more formulations for square and rectangular holes. Again, the shear effect on tensile force is similar to DIN 1052 with a small difference reflecting the size of the rectangular holes and the moment effect has been calibrated with the numerical results of finite element analyses. The extended formulation for a rectangular hole of $b_h \geq h_d$ predicted the tensile load well and for $b_h < h_d$ it overestimated the load.

The analytical prediction of the tensile load in the screw for beam depths up to 400 mm was found to be in good agreement with experimental results and numerical analyses. However, for larger beam depths, the finite element analyses showed that the predicted loads are lower than the numerical ones. This may be due to some assumptions of the model, for example a constant angle of 45 degrees for the crack plane or some other simplifications of the model. However, the finite element analysis of 500, 600, and 800 mm deep beams shows that a empirical modification factor of $\sqrt{h/400}$ if applied to the total tensile load in the screw would yield the best match with experimental values.

Eccentricity of hole relative to the neutral axis of beam and its effect on the induced tensile load in the screws was also investigated through a numerical analysis on beams with holes. The numerical analysis with 10 % of beam depth eccentricity showed that the tensile load in screw increased from 25 to 50% for different hole diameters to beam depth ratios ranging from 0.2 to 0.5. Therefore, a correction factor of $(1 + h_d/h)$ applied to the predicted tensile load in the screw is proposed for taking into account the tensile load increments in a screw due to eccentricity from the neutral axis.

Interaction of the holes also affects the produced tensile load in the reinforcement as shown in the numerical analysis. Interaction between reinforcement could be avoided if the clear distance between holes is greater than $1.5h$.

7.15 Summary

In this chapter, three design formulations were derived for the tensile load prediction in screw reinforcement around circular and rectangular holes in LVL beams. The truss was assumed to be formed around a hole that transfers stresses due to shear and moment in a section of a beam. The formulation is composed of two parts, one part for the tensile force due to the shear, and the other part for the tensile load produced by bending moment.

- The formulations gave good prediction for the tensile force in the screw for the beam depths up to 400 mm, which is the normal beam size for buildings. Both an experimental program and a parametric study carried out using an advanced FE model confirmed the results.

- For larger depths of the beam (>400 mm), an empirical modification factor is required as the numerical analysis shows that the derived formulation underestimates the tensile load in the screw. An empirical modification factor of $\sqrt{h/400}$ for the deeper beams shows that the predicted values are in good agreement with the numerical values.

- Shifting of the hole to the compressive part of beam (above neutral axis) increases the produced tensile load in the reinforcement. A correction factor of $(1 + h_d/h)$ is proposed to increase the produced tensile load in the reinforcement for eccentricity of 10 % of beam depth of the hole centre relative to the neutral axis. Such a correction factor could be applied to the predicted tensile load of a beam with a hole at the neutral axis.

- The numerical results show that variation of the material properties of the LVL does not affect the load in the screws considerably, perhaps due to the high stiffness of the screws relative to that of the surrounding wood material.

- Finally, interaction of the holes decreases the load carrying capacity of the beam through joining the cracks to each other. Numerical analysis shows interaction between the holes increases the produced tensile force in the reinforcement around the holes. A clear distance of $1.5h$ of the screws removes the additional produced tensile force in the reinforcement.

The next chapter presents design of LVL beams with holes and reinforcement around the holes.

8 Design of beams with holes and reinforcement around the hole

This chapter presents a design method for LVL beams with holes. Design of screws, epoxied rod, and plywood is a part of this chapter. Recommendation regarding maximum and minimum hole size, hole location along beam, and hole location in depth of beams is also included. Finally, the chapter also includes some worked examples on reinforcement design around the holes. This chapter uses the results of other chapters.

The majority of this chapter has been presented from the following paper (Ardalany et al. 2012b):

Ardalany, M., Fragiacomo, M., Deam, B. and Buchanan, A. (2012). "Design of reinforcement around holes in Laminated Veneer Lumber (LVL) beams." World Conference on Timber Engineering (WCTE 2012). P. Quenneville. Auckland, New Zealand 1: 539-547.

8.1 Introduction

This chapter provides a design method for LVL beams with holes reinforced with fully threaded screws, epoxied fully threaded rods, and plywood in shear dominant areas of the beam. Also, the chapter includes worked examples of beams with circular and rectangular holes. To simplify, the terms screws and epoxied rods refer to fully threaded screws and epoxied fully threaded rods respectively.

Previously, material properties of LVL were presented in Chapter 2. The experimental program in chapter 3 showed the effectiveness of reinforcement such as screws, epoxied

rods, and plywood for the design. Chapter 4 and 5 addressed issues such as hole distance of the supports, hole in depth of LVL beams, and the working mechanism of reinforcement around holes. In Chapter 6, a series of formulations were expanded for estimation of cracking load of beams with holes. Also, a series of formulations for tensile load prediction in the reinforcement around the holes in LVL beams were expanded in chapter 7.

8.2 General notes

The following section presents general notes regarding design of LVL beams with holes. More details/ worked examples are forming the later parts of this chapter.

8.2.1 Section design

Design of a LVL beam without a hole is the first step in designing LVL beams with holes. The designed section is controlled for hole size, hole location in depth and length of LVL beams, and possible reinforcement methods. Recovering of full beam capacity by reinforcement is the goal of the design method. This means that design engineer in the design of a reinforced LVL beam with hole can ignore the effect of the hole provided that the hole is properly reinforced. In other words, the section of the beam with a hole should be able to carry the shear and moment produced by the external applied load. A sketch showing the geometry of a beam with a circular and a rectangular hole is shown in Figure 8.1 (a) and (b) respectively. The figure shows parameters that will be used in the next parts.

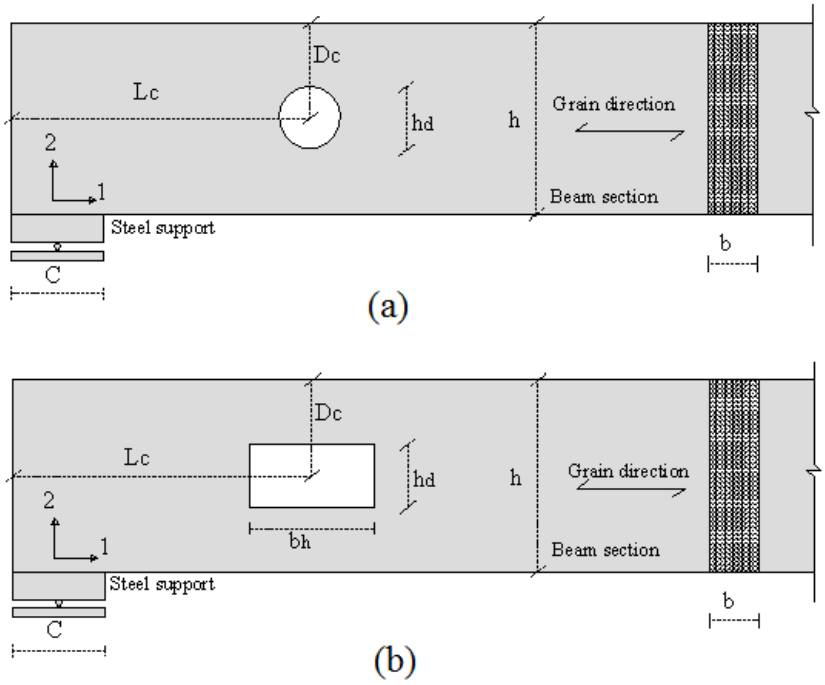

Figure 8.1. Sketch of the beam with hole: (a) circular hole, (b) rectangular hole

8.2.2 Hole location along an LVL beam

The hole should not be placed close to the supports and concentrated load in order to avoid wood crushing in the long term as described in chapter 4, and its centre should have a distance equal to beam depth from the support. In other words, the distance of the support from the centre of the hole should be selected larger than depth of the beam (h) to avoid crushing of wood in long term loading.

$$L_c \geq h + \frac{c}{2} \tag{8.1}$$

8.2.3 Eccentricity of the hole relative to neutral axis

Hole location in the depth is at the neutral axis of the beam. However, as demonstrated in chapter 4 for unreinforced beams and for reinforced beams in chapter 7, for eccentricities of less than 15 % of the beam depth, the load carrying capacity of the beam did not change greatly. Therefore, the hole can have a maximum eccentricity of

15 % of the beam depth relative to the neutral axis of the beam. To be slightly conservative, especially for large hole sizes where the size of the portion above the hole $(h/2 - D_c/2)$ is small; an eccentricity of 10 % seems a reasonable allowable eccentricity to match with other codes of practice.

$$D_c = (\frac{h}{2} \pm 0.10h) \tag{8.2}$$

A sketch of eccentricity of the holes relative to the neutral axis in beams with the holes is shown in Figure 8.2.

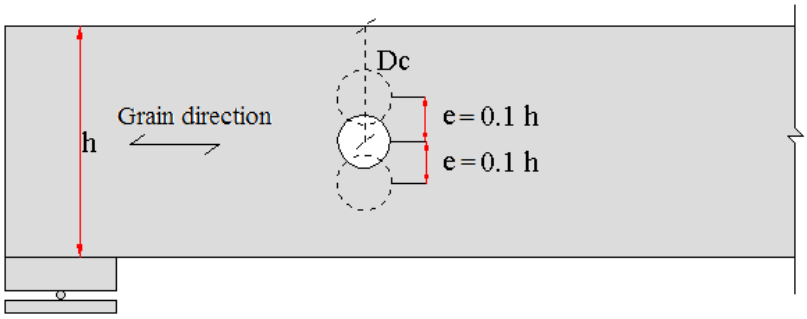

Figure 8.2. Eccentricity of the hole relative to the neutral axis

8.3 Hole size with no reinforcing

As shown in the experimental program in chapter 3 for beams of 200 mm, 300 mm and 400 mm depth, a hole of the size of 50 mm does not affect the behaviour of the beam and the failure of the beam occurs at mid-span due to the bending moment. However, it is logical that the section of the beam with a hole should be designed for a revised section taking into account the hole diameter.

The moment and shear in the section of a beam with a hole are not always problematic for crack propagation. For small hole sizes, research by APA (APA Report T2009L-30 2009; APA Report EWS-G535A 2010) shows that the effect of the hole could be ignored because it does not affect the failure of the beam by crack initiation and propagation. Figure 8.3 and Figure 8.4 show the recommendations from APA. The permitted small hole size is defined as:

$$h_d = \begin{cases} \leq 20\ mm \\ \leq 30\ mm \\ \leq 40\ mm \\ \leq 50\ mm \end{cases} \qquad \begin{array}{l} \text{for } h \leq 90 \text{ mm} \\ \text{for } h \leq 140 \text{ mm} \\ \text{for } h \leq 190 \text{ mm} \\ \text{for } h \leq 190 \text{ mm} \end{array} \qquad (8.3)$$

The above-mentioned hole should only be placed as shown in Figure 8.3.

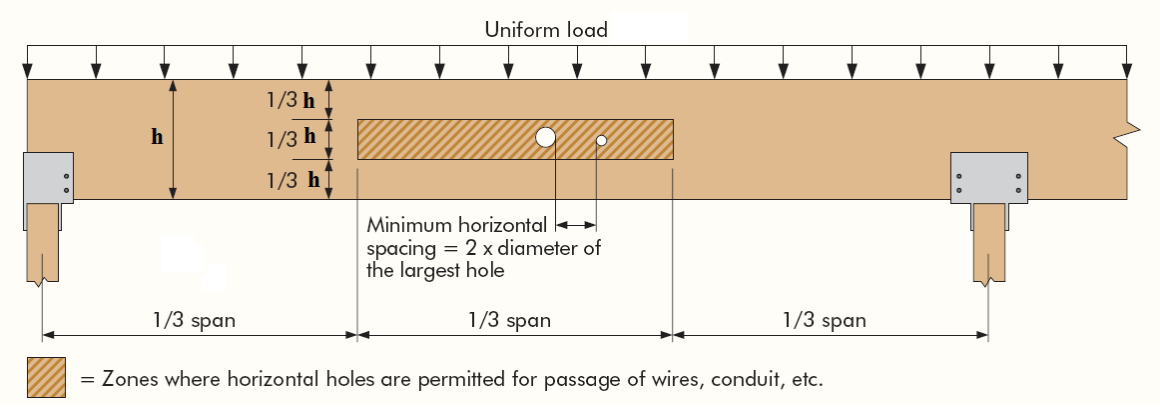

Figure 8.3. Permitted hole placement in LVL beams (APA Report EWS-G535A 2010)

In addition, hole sizes up to 25 mm diameter or smaller may be placed at the middle 1/3 of the beam span anywhere along the span except for the areas that are within 150 mm of clear distance between the support and the nearest edge of the hole provided that following conditions are met (Figure 8.4):

1. The depth of beam is at least 180 mm

2. Beam is subject to uniform load only

3. The span to depth ratio is at least 11

4. There are no more than 3 holes

5. The horizontal spacing must be a minimum of two diameters clear distance between adjacent hole

6. No holes in cantilever beams

For the case that the span-to-depth ratio is less than 11, 25 mm diameter hole or smaller holes may be placed in accordance with the provisions listed above except that the

location of the hole must maintain a clear distance of between the face of the support and the nearest edge of hole of at least 1/6 of the span.

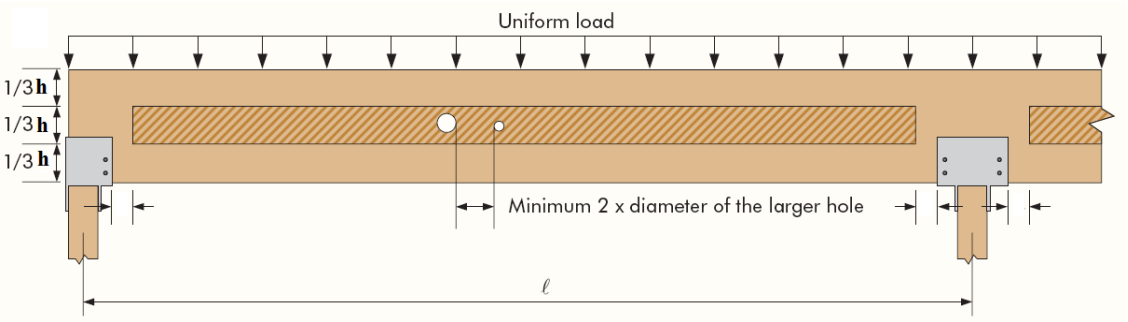

Figure 8.4. Zones where 25 mm or smaller hole sizes may be placed for beam depth greater than 180 mm (APA Report EWS-G535A 2010)

8.4 Large hole check for no reinforcing

According to the above, for larger hole sizes beams should be reinforced. Therefore, for the shear dominant area of a beam (first 1/3rd of the beam) the maximum hole size is limited to 25 mm, and for larger hole sizes, the beam should be reinforced.

Before of going any further for reinforcement of the holes, it is necessary to check to see if reinforcement is necessary because for some cases where the applied load is small, no reinforcement will be needed. As mentioned in chapter 6, the cracking load of the LVL beam with a hole could be reasonably obtained through the following formulations:

$$\frac{P}{P_t} + (\frac{M}{M_t})^2 = 1 \tag{8.4}$$

where P and M are shear and moment in the section of the beam respectively. P_t and M_t are total resisting shear and moment capacity in section of the beam defined as:

$$P_t = 2P_{cr} \tag{8.5}$$

$$M_t = 2M_{cr} + b\sigma_M(h_{cr} + h_d \cos(45))(h - h_{cr}) \text{ for circular holes} \tag{8.6}$$

$$M_t = 2M_{cr} + b\sigma_M(h_{cr} + h_d)(h - h_{cr}) \text{ for rectangular holes} \quad (8.7)$$

where σ_M is the tensile stress due to the bending moment M_{cr}, h_{cr} is the height of the cracked section. P_{cr} and M_{cr} are shear capacity and moment capacity of the section of the beam with the hole defined as:

$$P_{cr} = \frac{bf_{t,d}}{\sqrt{4\lambda^2 + \frac{6}{5}\frac{Kb}{GA}}} \quad (8.8)$$

$$M_{cr} = \frac{f_{t,d}b}{2\lambda^2} \quad (8.9)$$

where K as defined before is:

$$K = \frac{f_{t,d}^2}{2G_{If,d}} \quad (8.10)$$

and the factor λ is defined as below:

$$\lambda^4 = \frac{Kb}{4EI} \quad (8.11)$$

where $f_{t,d}$ is the design tensile stress perpendicular to the grain for the LVL. The value is presented in chapter 2 as:

$f_{t,k} = 1.4\ MPa$

According to EUROCODE 5:

$f_{t,d} = k_{mod}\frac{f_{t,k}}{\gamma_m} = 0.6 \times \frac{1.4}{1.2} = 0.7$ MPa

where $\gamma_m = 1.2$ for LVL and k_{mod} is a factor taking into account load duration and moisture that for the case of permanent load is 0.6. The characteristic fracture energy for LVL ($G_{If,k}$) from chapter 2 is defined:

$G_{If,k} = 0.7$ N/mm

and same as above, the design action is defined as below:

$$G_{If,d} = k_{mod}\frac{G_{Ic,k}}{\gamma_m} = 0.6 \times \frac{0.7}{1.2} = 0.35 \text{ N/mm}$$

Therefore, if load applied to the beam is smaller than the load that is obtained through Equation (8.4**)**, it may not cause crack formation. For other cases, the beam should be reinforced.

Although previously in chapter 6 a factor of $K_s = K(\frac{1-\alpha}{\alpha})^m$ was used for artificially increasing the stiffness of the springs for small holes in beams ($h_d/h \leq 0.4$), the factor for design purposes may be ignored. Ignoring the factor makes predictions more conservative and under-estimates the shear capacity of the section.

The unreinforced holes for service class 1 and 2 can be used while for service class 3 the holes should be reinforced because the drying of timber may cause crack initiation. Service class 1 relates to an indoor heated condition. Service class 2 is mainly characterized by indoor unheated conditions with no direct contact with water and service class 3 refers to outdoor conditions with possible contact with water.

8.5 Reinforcement design load

Reinforcement should control tensile stresses raised by hole. Controlling the tensile stresses stops crack propagation in LVL beams and restores the capacity of the beam. The tensile force necessary for design of the reinforcement was discussed in chapter 7. Three main formulations were derived to predict the tensile load due to openings in LVL beams for beam depths up to 400 mm. The formulations are:

$$F_{t,d} = \frac{\sqrt{2}V\ h_d(3h^2-h_d^2)}{8\ h^3} + \frac{3}{4}\frac{M\ h_d^3(h_d+h)}{h^3(h\ .h_d+h^2+h_d^2)} \text{ (Circular holes)} \quad (8.12)$$

$$F_{t,d} = \frac{\sqrt{2}}{8h^3}V\ h_d(3h^2 - h_d^2) + 0.7M\frac{h_d^2}{h^3} \text{ (Square holes)} \quad (8.13)$$

$$F_{t,d} = (\frac{\beta}{4h^3})V\ h_d(3h^2 - h_d^2) + 0.7M\frac{h_d^2}{h^3} \text{ (Rectangular holes)} \quad (8.14)$$

$$\beta = \text{Max}\ (\frac{b_h}{\sqrt{h_d^2+b_h^2}} \text{ and } \frac{h_d}{\sqrt{h_d^2+b_h^2}}) \quad (8.15)$$

Equations (8.12**)** to (8.15**)** are valid for $h \leq 400$ mm as shown in chapter 7. The formulation for larger depth ($h \geq 400$ mm) is multiplied by $\sqrt{h/400}$. This increases the

produced tensile load by 11 % for 500 mm and 22 % for 600 mm and finally 41 % for 800 mm depth specimens.

Equations (8.12**)** to (8.15**)** should be revised for the cases that the hole is not at the neutral axis of the beam as shown in chapter 7. For an eccentricity of the hole equal to 10 % of beam depth, a correction factor of (1+h_d/h) can be used as shown in chapter 7. This increases the produced tensile load by 20 %, 30 %, and 40 % for h_d/h values of 0.2, 0.3, and 0.4 respectively.

As shown in chapter 3, through the experimental program on LVL beams with holes, screws, epoxied rods, and plywood are reliable options for reinforcing holes in LVL beams. Another option like a thin steel plate (bracket) is not suggested for reinforcing because it has no continuous connection with the beam. Screws and plywood should be designed for the tensile load predicted through Equations (8.12**)** to (8.15**)** depending on the type of the hole.

8.6 Hole diameter limitation for reinforcing

The limitation of maximum hole diameter to beam depth for reinforcing by screws and plywood is different. Plywood somehow increases the shear strength of the material in the reinforced section while screws do not increase the shear capacity of the beam significantly; therefore, the limiting h_d/h ratio for reinforcing with plywood should be larger than the reinforcing by screws.

As shown in the experimental program, fully threaded self-tapping SPAX screws and epoxied in rods recovered full capacity of the tested beams. The limitation is presented in Equation (8.16**)**.

$$h_d \leq 0.4h \tag{8.16}$$

However, this limit is slightly higher than DIN 1052 and Swedish glulam handbook recommendation for designing of glulam, which are 0.3 and 0.35 respectively. The difference in the h_d/h ratios relative to DIN 1052 may be attributed to the method of the reinforcing. DIN 1052 presents the screw driven in a beam just from one side of beam (compressive edge); however, in the experimental program the screws were

driven from both sides of the beam (tensile and compressive edges). This provided enough embedment length for the screw and improved its behaviour.

Chapter 3 also included experiments on LVL beams with the holes reinforced with plywood. The plywood restored the beam capacity for hole diameter to beam depth up to 0.5; however, for $h_d = 0.5\ h$ some small cracks were observed at the mid-breadth of the beam. Having this observation in mind, in order to be slightly conservative the following limitation is assumed for plywood reinforcing:

$$h_d \leq 0.45h \tag{8.17}$$

Chapter 3 comprised some tests on LVL beams with square holes reinforced with SPAX screws. Maximum size of the square hole was 0.4 of the beam depth reinforced with SPAX screws. The reinforcement restored the capacity of the beam. Having in mind that due to the corners in rectangular holes, stress concentration occurs, hence the limitation for screw reinforcement is selected a little conservative as:

$$h_d \leq 0.35h \tag{8.18}$$

For plywood reinforcement of a rectangular hole, the following limitation can be used (adopted from DIN 1052):

$$h_d \leq 0.4h \tag{8.19}$$

The experiments in chapter 3 were focused on square and circular holes. Since rectangular holes are also common forms of hole, the dimensions that are advised for glulam in DIN 1052, is adopted for LVL. The limitation of the dimension is:

$$b_h < 2.5h_d \tag{8.20}$$

8.7 Screw reinforcement design

As demonstrated in chapter 3, screws can be used for the reinforcement around the holes in LVL beams. The main types of screws used in the experiments were self-tapping fully threaded SPAX screws. The design of epoxied rods is similar. Figure 8.5 shows a sketch of screw reinforcement around a hole with their appropriate parameters.

The screws are driven in the beam from both sides of the hole having a distance of $a_{1,c}$ and $a_{2,c}$ from the edges of the beam to avoid splitting of wood and a distance of a_2 from each other.

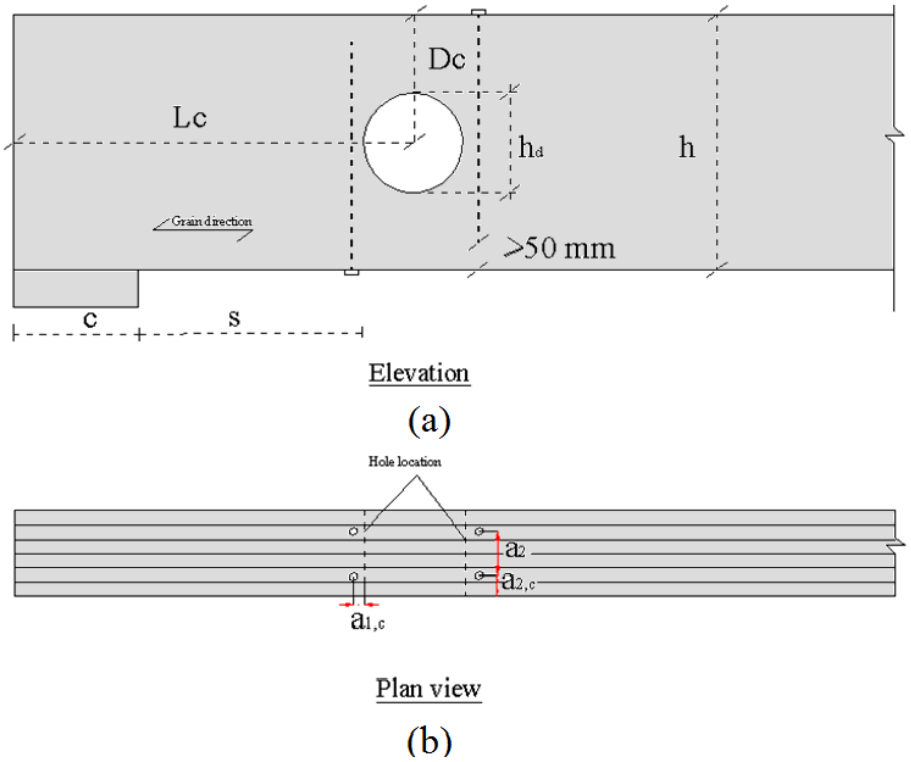

Figure 8.5. Sketch of reinforcement with screws and parameters: (a) elevation, (b) plan view

8.7.1 Controlling the splitting of wood

In designing the screw reinforcement, the screw should have enough distance from the edges of the beam to avoid splitting of the wood. According to DIN 1052 (2008) and SPAX recommendation for using screws, the following values are recommended for the edge distance:

$$2.5d_r \leq a_{1,c} \leq 4d_r \text{ with and without pre-drilling} \quad (8.21)$$

$$a_2 \geq 3d_r \text{ with and without pre-drilling} \quad (8.22)$$

$$a_{2,c} \geq 2.5d_r \text{ with and without pre-drilling} \quad (8.23)$$

where d_r is the outer diameter of the screw, and $a_{1,c}$ is the distance of the screw from the edge of the hole, $a_{2,c}$ is the distance of the screw from the outer edge of the beam. The parameters are shown in Figure 8.5.

In the experimental program, screw core diameter of 6 mm without pre-drilling was used for 45 mm breadth specimens with the edge distance ($a_{1,c}$) of 30 mm which for epoxied rods two vertical holes of 11 mm were drilled in the beam.

8.7.2 Controlling the screw yielding and withdrawal

The tensile force predicted using Equations (8.12**)** to (8.15**)** should be carried by the reinforcement. Such an assumption is equal to ignoring the tensile strength of LVL in perpendicular to grain direction or assuming a cracked section. The reinforcement should not yield or withdraw, so the following relationships should be controlled:

$$F_{t,d} \leq R_{ax,d} \tag{8.24}$$

$$R_{ax,d} = k_{mod} \frac{R_{ax,k}}{\gamma_M} \tag{8.25}$$

$$R_{ax,k} = \text{Min}\,(R_{t,k}, f_{1,k} L_{bd} d_r\,) \tag{8.26}$$

where $R_{ax,d}$ is the design tensile strength of the screw, $R_{ax,k}$ is the characteristic tensile strength, k_{mod} is the modification factor taking into account the effect of the load duration and moisture content, γ_M is the partial safety factor for steel 1.3 and for LVL 1.2 according to Eurocode 5 (2004), $R_{t,k}$ is the characteristic tensile strength of the steel and k_{mod} for LVL could be calculated from the Table 8.1, L_{bd} is embedment length of the screw and d_r is the outer diameter of the screw.

Table 8.1 Partial safety factor (k_{mod}) taking into account load duration and moisture content (Eurocode 5 2004)

Material	Service class	Permanent action	Long term action	Mid-term action	Short term action	Instantaneous action
LVL	1	0.60	0.70	0.80	0.90	1.10
LVL	2	0.60	0.70	0.80	0.90	1.10
LVL	3	0.50	0.55	0.65	0.70	0.90

Also, $f_{1,k}$ is the withdrawal strength of a screw in LVL in the perpendicular to grain direction. The screw in the LVL should not withdraw, so, the tension force calculated from the above formulation should be less than withdrawal capacity of the LVL. According to the experiments on the LVL with SPAX screws with outer diameter of 8 mm the following formulation was obtained for the withdrawal strength of LVL with density of $550\ \mathrm{kg/m^3}$ (refer to chapter 2).

$$f_{1,k} = 81 \times 10^{-6} \times \rho^2 \tag{8.27}$$

In the above formulation ρ is density of the LVL in $\mathrm{kg/m^3}$. The withdrawal strength for LVL in the perpendicular to grain direction is 24.5 MPa.

The screw must pass the crack surface to control the cracking of a timber beam with a hole. The screw should continue after passing through possible crack surface to avoid screw withdrawal. $\mathrm{L_{ad}}$ and $\mathrm{L_{bd}}$ are the embedment lengths, these should provide enough strength to avoid screw withdrawal.

$$\mathrm{L_{ad}} = 0.5h - 0.354h_d \text{ for circular holes} \tag{8.28}$$

$$\mathrm{L_{ad}} = 0.5h - 0.5h_d \text{ for rectangular holes} \tag{8.29}$$

$$\mathrm{L_{bd}} \geq \mathrm{Max}\,(12d_r\,, L_{ad}) \tag{8.30}$$

The embedment parameters of $\mathrm{L_{ad}}$ and $\mathrm{L_{bd}}$ are shown in Figure 8.6.

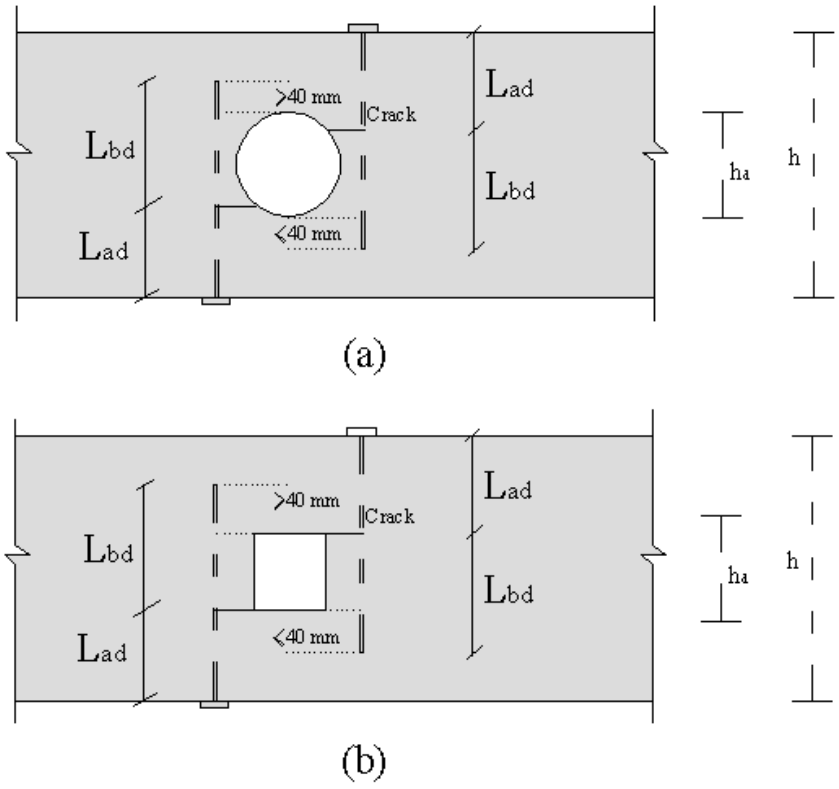

Figure 8.6. Embedment parameters: (a) circular hole, (b) rectangular hole

The Swedish glulam handbook recommends the screw to continue more than 40 mm above the highest edge of the hole as shown in Figure 8.6 (a) and (b) for providing sufficient bond with the surrounding LVL.

The screw length should also be smaller than the beam depth minus 50 mm to avoid failure due to a vertical hole created by the screw as shown in experiments in chapter 3. Therefore, the length of the screw can be calculated as:

$$\text{Screw length} = \text{Max}\,(L_{ad} + L_{bd}, D_c + \frac{h_d}{2} + 40) \leq (h - 50)$$

Also for yielding of the screw, Equation (8.31**)** should be controlled:

$$\frac{F_{t,d}}{(\frac{\pi d_r^2}{4})} \leq f_{y,d,screw} \tag{8.31}$$

where $f_{y,d,screw}$ is the design yielding tensile strength of SPAX screw. According to Eurocode 5:

$$f_{y,d,screw} = k_{mod} \frac{f_{y,k}}{\gamma_m} \tag{8.32}$$

where $f_{y,k}$ is the characteristic yielding strength of the screw. k_{mod} for steel should be taken as 1, and γ_m for connections should be assumed as 1.3.

8.7.3 Worked example for design of screw reinforcement

A beam of dimension 3000×300×45 mm has been loaded at mid-span. A hole of diameter 90 mm is introduced into the beam at the distance of 600 mm from one support. The beam is for use in the roof of a house subjected to permanent roof loads. Determine the reinforcement that should be used for design. Fully threaded SPAX screws of 6 mm core diameter with the thread of 2 mm are used (Figure 8.7).

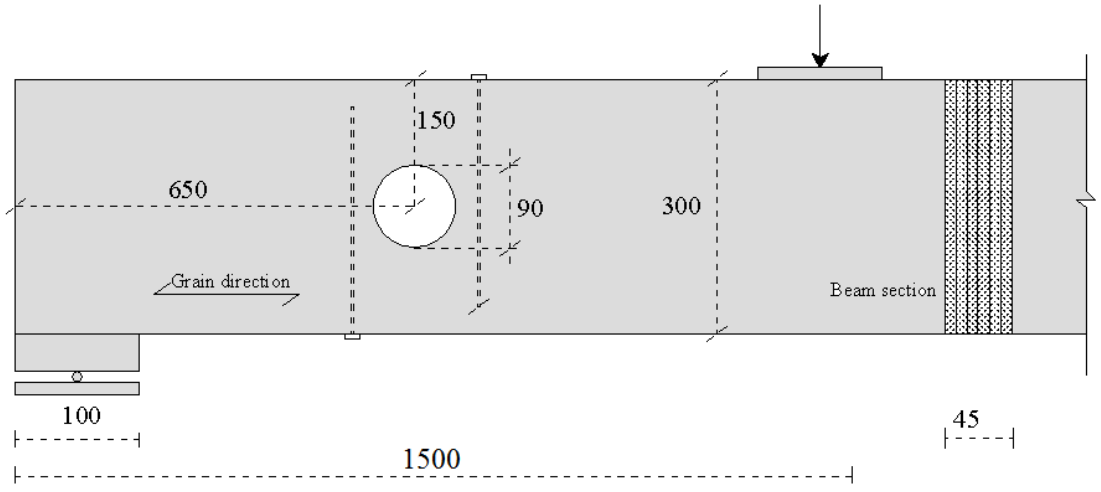

(dimensions in mm)

Figure 8.7. Sketch of the beam with hole reinforced with screw

Shear capacity of the section:

The shear capacity of the section for the case of no reinforcement can be calculated as:

$$h_{cr} = \left(\frac{H}{2} - \frac{h_d}{2} \times \cos(45)\right) = (\frac{300}{2} - \frac{90}{2} \times \cos(45)) = 126.36 \text{ mm}$$

$$A = b \times h_{cr} = 126.36 \times 45 = 5686.22 \text{ mm}^2$$

$$I = \frac{b \times h_{cr}^3}{12} = \frac{45 \times 126.36^3}{12} = 7565983 \text{ mm}^4$$

$$K = \frac{f_{t,d}^2}{2G_{If,d}} = \frac{0.7^2}{2 \times 0.35} = 0.7 \text{ N/mm}^3$$

$$\lambda = \frac{Kb}{4EI} = \frac{0.7 \times 45}{4 \times 10700 \times 7565983} = 0.0031$$

$$P_{cr} = \frac{bf_{t,d}}{\sqrt{4\lambda^2 + \frac{6}{5}\frac{Kb}{GA}}} = \frac{45 \times 0.7}{\sqrt{4 \times 0.0031^2 + \frac{6}{5} \times \frac{0.7 \times 45}{750 \times 5686.22}}} = 8.5 \text{ kN}$$

$$M_{cr} = \frac{f_{t,d}b}{2\lambda^2} = 1596908 \text{ N. mm}$$

$$P_t = 2P_{cr} = 2 \times 9063.6 = 18.1 \text{ kN}$$

$$\sigma_M = \frac{M_{cr}}{\frac{(b \times h_{cr}{}^2)}{6}} = \frac{1672918}{\frac{(45 \times 126.36^2)}{6}} = 13.34 \text{ N/mm}^2$$

$$M_t = 2M_{cr} + b\sigma_M(h_{cr} + h_d\, cos(45))(h - h_{cr})$$

$$= 2 \times 18127.2 + 45 \times 13.96\left(126.36 + 90 \times \sqrt{\frac{2}{2}}\right)(300 - 126.36)$$

$$= 21.3 \text{ kN. m}$$

$$M = P \times Lc = 600 \times L_c$$

$$\frac{P}{P_t} + (\frac{M}{M_t})^2 = 1$$

By solving the above equation, the shear in the section of the beam can be calculated as 8.7 kN. Therefore, the external loads of 17.3 kN at mid-span cause crack formation around the hole. As it was stated, the calculated shear underestimated the capacity of the

beam. However, in chapter 6, a modification factor of$(1/(1-h_{cr}/h))^m$ with $m=2$ applied to the fracture energy to take into account the effect of small hole size. Applying this coefficient to the fracture energy, the resulting shear force capacity of the section is calculated as 11.9 kN and the external force that causes crack formation is about 23.8 kN.

For the shear forces larger than 8.7 kN in the section of the beam with a hole, the section needs to be reinforced. Assuming that the section is designed for maxim shear capacity of the section, the following steps are followed for designing the reinforcement around the hole by screws.

Controlling hole diameter:

The ratio of the hole diameter (h_d) to beam dept (h) is 0.3, that is smaller than the limitation for fully threaded SPAX screw of 0.4. Reinforcement by screws can be followed.

Tensile load perpendicular to grain in screw:

Assuming the section of the beam is designed for full shear capacity of the section, the following steps should be performed.

The characteristics shear capacity of LVL in the grain direction is (Buchanan 2007):

$f_{v,k} = 6.0$ MPa

$$f_{v,d} = \frac{f_{v,k} \times k_{mod}}{\gamma_m} = \frac{6 \times 0.6}{1.2} = 3.0 \text{ MPa}$$

The maximum shear force capacity of the section according to Eurocode 5 can be calculated as:

$$V_d = \frac{2}{3} f_{v,d} bd = \frac{2}{3} \times 3.0 \times 45 \times 300 = 27 \text{ kN}$$

and the moment for the beam shown in Figure 8.7 is:

$$M_d = V_d \times L_c = 27000 \times 600 = 16.2 \text{ kN.m}$$

So the tension force in the screw can be calculated as:

$$F_{t,d} = F_{t,V,d} + F_{t,M,d} = \frac{\sqrt{2}}{8h^3} V_d h_d \left(3h^2 - h_d^2\right) + \frac{3}{4}\left(\frac{M h_d^3 (h+h_d)}{h^3 (h.h_d + h^2 + h_d^2)}\right)$$

$$F_{t,d} = \frac{\sqrt{2}}{8 \times 300^3} \times 27000 \times 90 \times (3 \times 300^2 - 90^2) + \frac{3}{4} \times \frac{16200000 \times 90^3 \times (300+90)}{300^3 (300 \times 90 + 300^2 + 90^2)}$$
$$= 5.2 \text{ kN}$$

Since the section of the beam is smaller than 400 mm, no increment of the tensile load due to a hole is required.

Design of screw reinforcement:

With the assumption of using fully threaded SPAX screws for the reinforcement, the withdrawal strength can be calculated as below:

$$f_{1,k} = 81 \times 10^{-6} \times \rho^2 = 81 \times 10^{-6} \times 550^2 = 24.5 \text{ MPa}$$

The embedment length of the screw for a circular hole can be calculated as:

$$\mathrm{L_{ad}} = 0.5h - 0.354h_d = 0.5 \times 300 - 0.354 \times 90 = 118 \text{ mm}$$

$$\mathrm{L_{bd}} = \text{Max}\,(L_{ad}, 12d_r) = \text{Max}\,(118, 12 \times 8) = \text{Max}\,(118, 96) = 118 \text{ mm}$$

The embedment length of 118 mm with 8 mm diameter can carry the following tensile load:

$$R_{ax,k} = L_{bd} f_{1,k} d_r$$

$$R_{ax,k} = 118 \times (81 \times 10^{-6}) \times 550^2 \times 8 = 23.2 \text{ kN}$$

$$R_{ax,d} = \frac{R_{ax,k} K_{mod}}{\gamma_m} = \frac{23208 \times 0.6}{1.2} = 11.6 \text{ kN}$$

The embedment length of 118 mm provides 11.6 kN resistance for the withdrawal. The above force is higher than the design force of 5.2 kN in the screw. Therefore, that embedment length is sufficient.

According to the Swedish glulam handbook (Carling 2001), the screw should continue at least 40 mm after the hole level as shown in Figure 8.6 (a) for circular holes. The following equation should be satisfied:

$$\text{Screw length} = \text{Max}\,(\mathrm{L_{ad}} + \mathrm{L_{bd}}, D_c + \frac{h_d}{2} + 40) \leq (h - 50)$$

$$\text{Screw length} = \text{Max}\left(118 + 118, 118 + \frac{90}{2} + 40\right) \leq (300 - 50)$$

$$\text{Screw length} = 236 \text{ mm} \leq 250 \text{ ok}$$

So, the screw length of 236 mm can be used.

The screw also should not yield. Assuming the characteristic yielding strength of the SPAX about 400 MPa, the following force derived as the yielding force of the screw.

$$f_{y,k,screw} = \frac{400 \times \pi \times 6^2}{4} = 11.3 \text{ kN}$$

$$f_{y,d,screw} = k_{mod}\frac{f_{y,k}}{\gamma_m} = 1 \times \frac{11.3}{1.3} = 8.7 \text{ kN}$$

So the force of 8.7 kN is bigger than the design axial force of 5.2 kN in the screw. The tensile force due to the hole is smaller than resisting tensile force by the screw.

Controlling of distance of screw from edges:

Distance of the screw from edge of the hole and surface of the beam should be controlled. To control distance of the screw from edge of the hole ($a_{1,c}$) following relationship should be satisfied:

$$3d_r \leq a_{1,c} \leq 4d_r$$

The outer diameter of the screw is 8 mm, therefore we have:

$$3 \times 8 \leq a_{1,c} \leq 4 \times 8$$

$$24 \leq 30 \leq 32 \text{ ok}$$

The distance of the screw from the other surface of the beam ($a_{2,c}$) is:

$$a_{2,c} \geq 2.5d_r$$

The distance of the screw from the surface of the beam is:

$$a_{2,c} \geq 2.5d_r = 2.5 \times 8 = 20 \text{ mm}$$

$a_{2,c} = \frac{45}{2} = 22.5 \text{ mm} \geq 20 \text{ mm}$ ok

The distance of the hole from the support is controlled through the following equation:

$$L_c \geq h + \frac{c}{2}$$

$650 \geq 350$ ok

The design is now complete for self-tapping screws. In the following part, design of the epoxied rod will be discussed.

Design of epoxied rod:

Design of epoxied rods is similar to the design of the fully threaded screw. Driving the screw from the tension side of the beam (below the neutral axis) is beneficial from embedment length perspective, but cutting the tensile edge of a beam can develop an undesirable failure mode such as what observed through the experimental program for vertical holes that caused fracture of the beam starting from tensile edge of the beam (Figure 8.8)

Figure 8.8. Fracture at the hole edge

Such a failure mechanism was prevented in the experimental program by using a steel plate glued to the beam in the experimental program; however, it can also be prevented

by using the sketch as shown in Figure 8.9 so that the epoxied rods have a distance from the edge of the tensile stress.

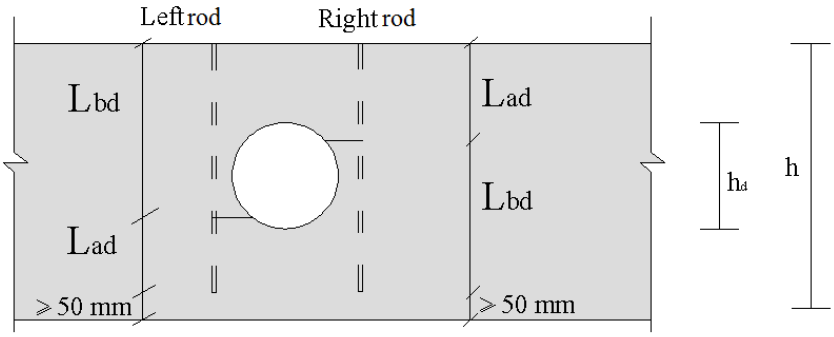

Figure 8.9. The format of inserting epoxied rod in LVL

Control of the right screw:

For the case mentioned in Figure 8.9, the embedment length should be controlled:

$L_{ad} = 0.5h - 0.354h_d = 0.5 \times 300 - 0.354 \times 90 = 118$ mm

and L_{bd} is:

$L_{bd} = 300 - 50 - 118 = 132 \text{ mm} > \text{Max}\,(12 \times 8 = 96, 118)$ mm

The load associated with this embedment length of L_{ad} is:

$R_{ax,k} = 118 \times 8 \times 81 \times 10^{-6} \times 550^2 = 23.1$ kN

$R_{ax,d} = \frac{R_{ax,k} K_{mod}}{\gamma_m} = \frac{23130 \times .06}{1.2} = 11.8$ kN ≥ 5.2 kN ok

The produced load by the embedment length is higher than the load in the screw. Assuming that the epoxied rod has strength of 400 MPa, control of the yielding was performed previously.

Control of the left rod:

For the left rod in Figure 8.9, L_{ad} is calculated as:

$L_{ad} = 0.5h - 0.354h_d - 50 = 0.5 \times 300 - 0.354 \times 90 - 50 = 69$ mm

The embedment length of 69 mm provides the following tensile load:

$R_{ax,k} = 69 \times 8 \times 81 \times 10^{-6} \times 550^2 = 13.5$ kN

$R_{ax,d} = \frac{R_{ax,k} K_{mod}}{\gamma_m} = \frac{13525 \times .06}{1.2} = 6.8$ kN ≥ 5.2 kN ok

Therefore, the embedment length of 69 mm here can resist the applied tensile force. The rods should be also controlled for the yielding.

8.8 Plywood reinforcement design

Plywood, as demonstrated in chapter 3 through the experimental program is a viable option for reinforcement around the holes. Plywood is glued and nailed to the outer surface of the beam. Nailing of the plywood to a glued beam applies a uniform pressure and creates full bond with the beam. In the experimental program, gluing plywood on both sides of the beams recovered full beam capacity while one side gluing improved the behaviour but did not recover the capacity of the beam fully. Figure 8.10 shows a sketch of a beam with plywood attached to the beam.

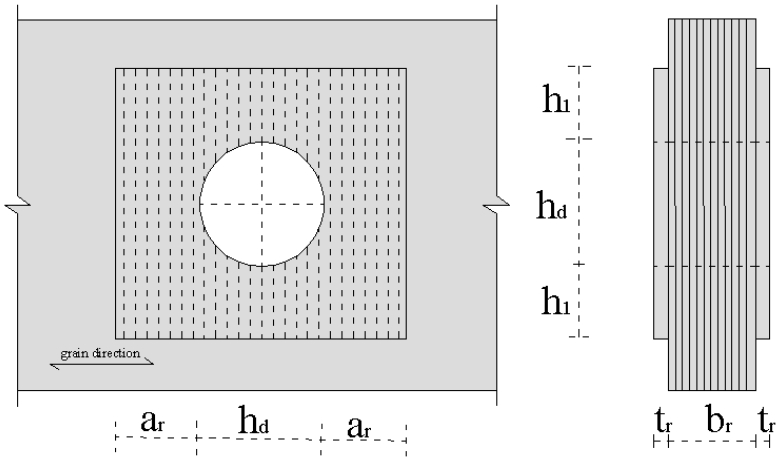

Figure 8.10. Plywood as reinforcement around the hole

8.8.1 **Plywood design**

The plywood should cover the area where the normal stresses go beyond the tensile strength of LVL in the perpendicular to the grain direction. According to Aicher (2011), the following limitation is recommended for the dimensions of the plywood plates:

$$0.25h_d \leq a_r \leq 0.3(h + h_d) \tag{8.33}$$

$$h_1 \geq 0.25h_d \tag{8.34}$$

Also for design of the LVL beams with holes:

$$\sigma_{t,90,d} \leq f_{d,ply} \tag{8.35}$$

$$f_{d,ply} = k_{mod} \frac{f_{t,90,k}}{\gamma_m} \tag{8.36}$$

$$\sigma_{t,90,d} = \frac{K \times F_{t,d}}{2 \times a_r \times t_r} \tag{8.37}$$

where $F_{t,d}$ is the tensile force due to the shear and moment in the section, t_r is the thickness of plywood, k_{mod} is a factor taking into account the duration of load and moisture content selected as 0.6 for permanent load, and γ_m is a partial material factor for LVL and plywood selected as 1.2 (Eurocode 5 2004). K is a magnifying factor for stress concentration, the factor is advised as equal to 2. A magnifying factor is applied because the distribution of the tensile stresses around the hole is not uniform and the tensile stresses decrease exponentially away from the hole (Figure 8.11 (a)). A triangular tensile stress distribution is assumed (Figure 8.11 (b)).

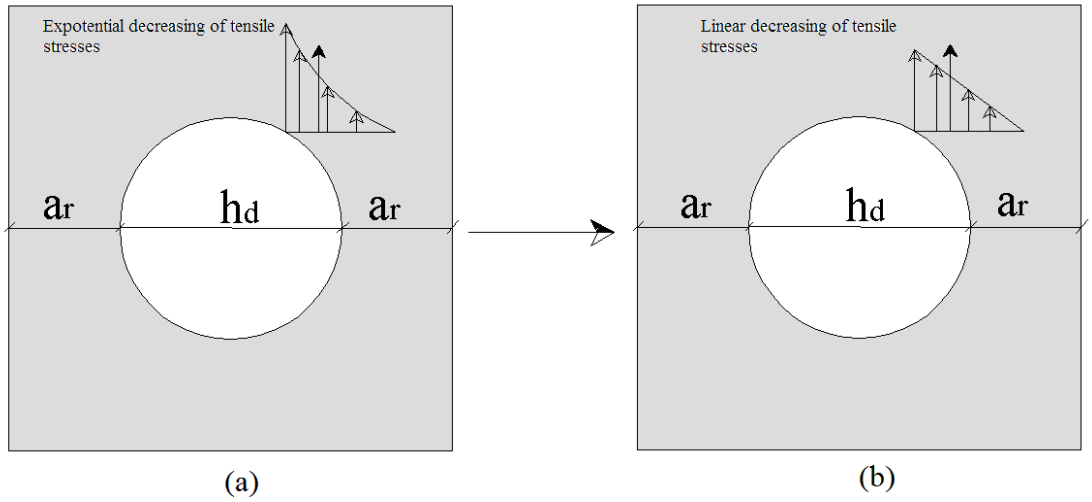

Figure 8.11. Stress distribution around the hole stresses are decreasing: (a) exponential decrease, (b) triangular decrease

The tensile strength of the New Zealand plywood can be obtained from NZS 3603 (1993). The characteristic tensile strengths of different classes of plywood are presented in Table 8.2.

Table 8.2. Characteristics tensile strength of New Zealand plywood (NZS 3603 1993)

Class of plywood	Characteristics tensile strength $f_{pt,k}$ (MPa)
F22	34.6
F17	26.7
F14	22
F11	17.3
F8	13.5

where F22, F17, F14, F11 and F8 represent the class of the plywood.

The shear stress between the plywood and the LVL beam should be transferred by the glue line. Assuming that glue line is strong enough to transfer the shear stresses, Figure 8.12 shows sketches of the tensile stress field around rectangular and circular holes in LVL beams. The tensile force due to the hole causes shear stress in the plywood. Depending on the orientation of the first veneer of the plywood, rolling shear may develop at the second veneer of the plywood.

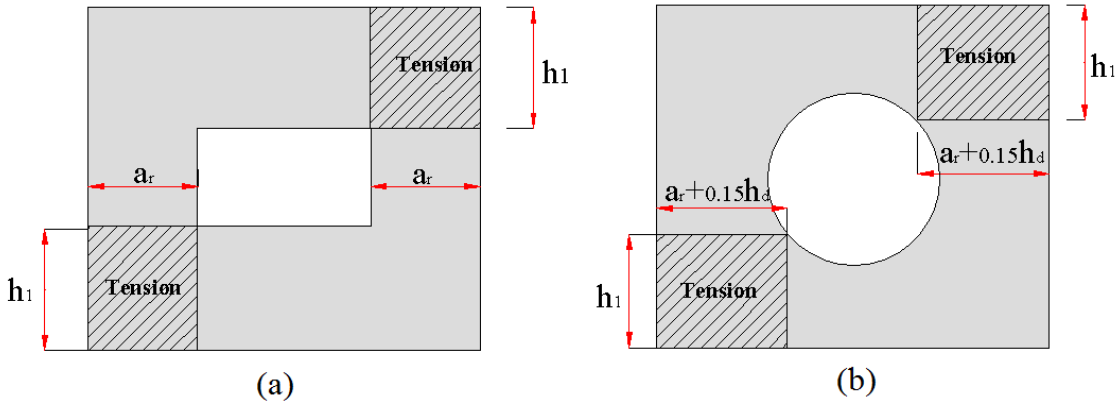

Figure 8.12 Tensile stress field plywood, rectangular hole (a), and circular hole (b)

The tensile force in the beam due to the hole may cause rolling shear stresses. If the design shear strength of the glue line is $\tau_{pr,d}$, the following equations should be satisfied:

$$\frac{F_{t,d}}{2\times(a_r+0.15h_d)\times h_1} \leq \tau_{pr,d} \text{ For circular holes} \quad (8.38)$$

$$\frac{F_{t,d}}{2\times a_r\times h_1} \leq \tau_{pr,d} \text{ For rectangular holes} \quad (8.39)$$

where $\tau_{pr,d}$ is calculated as:

$$\tau_{pr,d} = k_{mod}\frac{\tau_{pr,k}}{\gamma_m} \quad (8.40)$$

$\tau_{pr,k}$ is characteristic rolling shear strength of the glue line. The characteristic rolling shear for plywood of class F8 according to NZS 3603 (1993) is 1.7 MPa.

A recommendation through discussion with a specialist in design of connections was made to minimize the probability of that failure. The recommendation was to glue the first veneer of plywood perpendicular to the grain direction of the LVL (Figure 8.13). It is believed that continuity of the grains in the LVL beam mitigate the probability of rolling shear failure. However, this suggestion contradicts with Kolb et al. (1977)

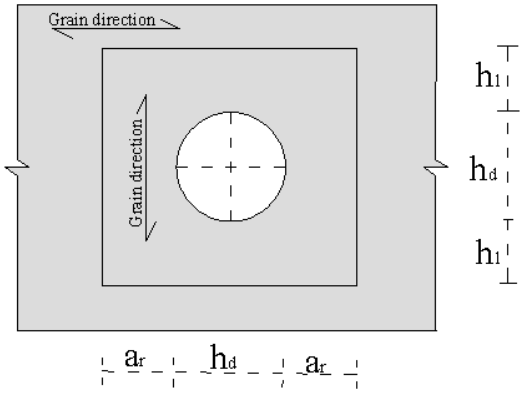

Figure 8.13. grain direction layout

In the experimental program, first veneer of plywood was glued perpendicular to grain direction and no rolling shear failure was observed.

8.8.2 Worked example of design of LVL beam with hole reinforced with plywood

A beam of dimension 3000×300×45 mm has been loaded at mid-span. A hole of 90 mm diameter is introduced into the beam at the distance of 650 mm from the nearest end of the beam. The beam has been used in the roof of a house subjected to permanent roof loads (Figure 8.14).

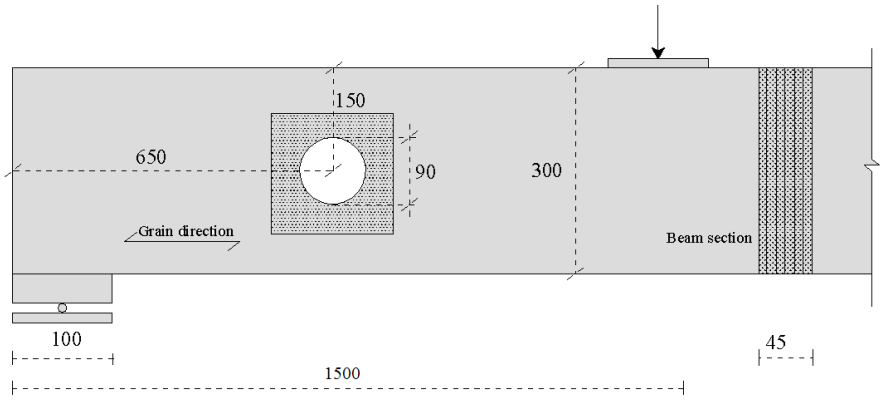

Figure 8.14. Sketch of the beam reinforced with plywood

Shear capacity of the section:

The geometry, hole size, dimension of the beam, and material properties are similar to the worked example as presented in part 8.7.3, therefore the capacity of the section before cracking was estimated 8.7 kN. Assuming using full capacity of the section, reinforcement is necessary.

Controlling hole diameter:

The ratio of the hole diameter to beam depth is 0.3 smaller than the limitation of 0.45 for plywood reinforcement. Reinforcing by plywood can be performed.

Controlling hole distance from the support:

Distance of the hole centre from the support of the beam should be performed:

$$L_c \geq h + \frac{c}{2}$$

$650 \geq 300 + 50 = 350$ mm ok

Tensile load perpendicular to grain in plywood:

The design is performed for the recovering the maximum shear capacity of the section. The maximum shear force capacity of the section according to Eurocode 5 is:

$$f_{v,d} = \frac{f_{v,k}\, k_{mod}}{\gamma_m} = \frac{6 \times 0.6}{1.2} = 3 \text{ MPa}$$

$$V_d = \frac{2}{3} f_{v,d} bd = \frac{2}{3} \times 3.0 \times 45 \times 300 = 27 \text{ kN}$$

$$M_d = V_d \times L_c = 27000 \times 600 = 16.2 \text{ kN.m}$$

The tensile force perpendicular to grain is calculated as:

$$F_{t,d} = F_{t,V,d} + F_{t,M.d} = \frac{\sqrt{2}}{8h^3} V_d h_d \left(3h^2 - h_d^2\right) + \frac{3}{4} \frac{M_d h_d^3 (h + h_d)}{(h.h_d + h_d^2 + h^2)}$$

$$F_{t,d} = \frac{\sqrt{2}}{8 \times 300^3} \times 27000 \times 90 \times (3 \times 300^2 - 90^2) + \frac{3}{4} \times \frac{16200000 \times 90^3 (300 + 90)}{300^3 (300 \times 90 + 300^2 + 90^2)} = 5.2 \text{ kN}$$

Plywood Dimensions:

The horizontal dimension of the plywood should be limited to:

$0.25h_d \leq a_r \leq 0.3(h + h_d)$, and

$22.5 \leq a_r \leq 117$

The plywood should carry tensile forces due to the hole in the section of the beam.

$\sigma_{t,90,d} \leq f_{d,ply}$

$f_{d,ply} = k_{mod}\frac{f_{t,k}}{\gamma_m} = 0.6 \times \frac{15}{1.2} = 7.5$ MPa

Assuming the use of 9 mm plywood, the length of the coverage area is defined as below:

$\sigma_{t,90,d} = \frac{K \times F_{t,d}}{2 \times a_r \times t} = \frac{2 \times 5200}{2 \times a_r \times 9} = \frac{577}{a_r}$

$a_r \geq 77$ mm then we select $a_r = 100$ mm

h_1 should be:

$h_1 \geq 0.25h_d = 0.25 \times 90 = 22.5$ mm, assuming it as $h_1 = 50$ mm

The actual dimension would be 290×190×9 mm.

Controlling rolling shear:

The rolling shear stress should be controlled. The characteristic rolling shear strength of plywood is 1.7 MPa.

$\tau_{pr,d} = k_{mod}\frac{\tau_{pr,k}}{\gamma_m}$

$\tau_{pr,d=} 0.6 \times \frac{1.7}{1.2} = 0.85$ MPa

$\frac{F_{t,d}}{2(a_r + 0.15h_d) \times h_1} \leq \tau_{pr,d}$

$\frac{5200}{2\times(100+0.15\times90)\times50} = 0.46 \leq 0.85$ ok

Therefore, the final dimension of the plywood is selected 290×190×9 mm.

8.9 Rectangular holes

Design of the beams with rectangular holes reinforced with screws and plywood is similar to the design of beams with circular holes reinforced with screws and plywood respectively. However due to stress concentration at the corners of the square/rectangular hole, special controls should be performed viz.: (i) controlling of shear raised by the corners and (ii) increased tensile and compressive stresses due to holes. The first control is to prevent crack propagation due to the shear and the latter avoids failure mechanisms of fracture formation at the edge of the hole.

8.9.1 LVL beams with square/rectangular holes and plywood reinforcement

As demonstrated in the experimental program, square holes also can be reinforced to recover the capacity of the beam. In the experimental program, the maximum size of the square hole was limited to 0.4 of the depth of beam; however, the limit of $0.35h_d$ was advised in section (8.6) due to stress concentrations at the corners for screw reinforcing and following the other codes of practice a limitation of $0.4h_d$ for reinforcing with plywood. Although the experimental program was limited to reinforcement of circular holes with plywood, the design procedure was extended to the use of plywood for square/rectangular holes too. Figure 8.15 shows a sketch of a beam with a square hole reinforced with plywood with definition of the parameters that will be used in the latter sections. To avoid of the stress concentration at the sharp edge of the hole, a radius of 15 mm is recommended by DIN 1052.

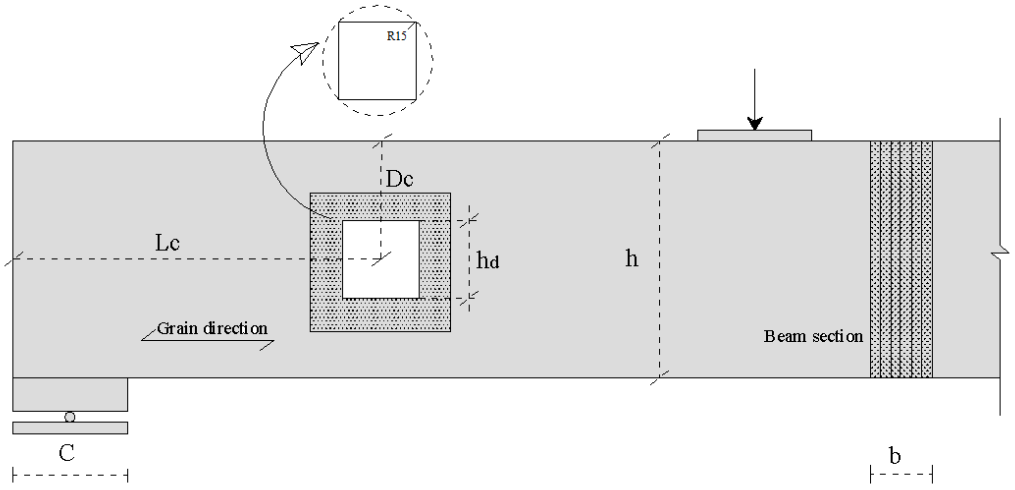

Figure 8.15. Sketch of the beam with square hole

8.9.2 Shear stress concentration at corners for rectangular holes

Design of a beam with square/rectangular hole reinforced with a screw is a little different compared with a circular hole. Due to the corners of the square, the distribution of the shear stresses near the corners of the hole deviates considerably from beam theory. For an example, a schematic representation of the shear stresses for a rectangular hole is shown in Figure 8.16 where τ_1, τ_2, τ_3 and τ_4 are shear stresses at different sections of the hole. In general, $\tau_2 > \tau_3 > \tau_1 > \tau_4$ (Blass et al. 2004).

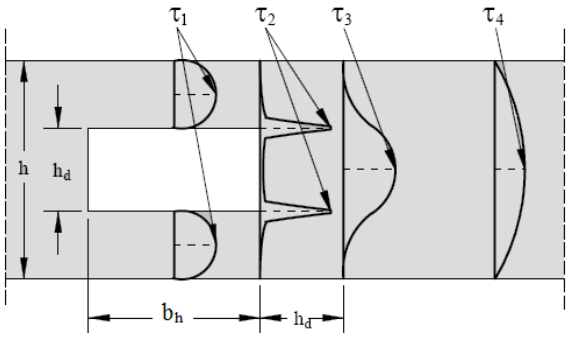

Figure 8.16. Distribution of shear stresses in a beam with a rectangular hole (Blass et al. 2004)

To estimate the shear stress at the corner of the hole, Blass et al. (2004) through extensive finite element analysis suggested Equations (8.41) and (8.42):

$$\tau_2 = \kappa_2 \times 1.5 \frac{V_d}{b(h - h_d)} \tag{8.41}$$

$$\kappa_2 = 1.84 \left(1 + \frac{b_h}{\mathrm{h}}\right) \times \left(\frac{\mathrm{h_d}}{\mathrm{h}}\right)^{0.2} \tag{8.42}$$

Equation (8.41) and Equation (8.42) apply for $0.1 \leq b_h/h \leq 1$ and $0.1 \leq h_d/h \leq 0.4$. The shear stresses above were presented for holes with sharp corners and the effect of the curved corners was not taken into account. It is not clear that how the effect of the radius of the corner could be addressed. This has been discussed in Aicher (2011). In the absence of a formulation to address this problem correctly, a possible solution is accepting Equations (8.41) and (8.42) as state of the art and controlling the shear stresses for only screw reinforcement because in the case of plywood, the shear is increased considerably in a reinforced section. Therefore, Equation (8.43) control could be applied.

$$\tau_2 \leq f_{v,d} \tag{8.43}$$

$f_{v,d}$ is design shear capacity of the section defined as:

$$f_{v,d} = k_{mod} \frac{f_{v,k}}{\gamma_m} \tag{8.44}$$

$f_{v,k}$ is characteristics shear strength of LVL should be taken as 6.0 MPa for LVL (Buchanan 2007).

8.9.3 Increased tensile and compressive stresses for rectangular holes

At a section of a beam with a rectangular hole, tensile and compressive stresses in the grain direction are increased due to the hole. The results of an analysis on an LVL beam of 2200×200×45 mm with a rectangular hole of 60×120 mm with centre loading of 10 kN is shown in Figure 8.17 (a), where the rectangular hole is 400 mm from the end

distance of the beam. The figure shows the variation of tensile stress and compressive stresses in the grain direction. The maximum calculated tensile stress produced in point 'a' is about 8.8 MPa, that is about 30 % larger than 6.7 MPa for the same section of the beam without a hole; therefore, controlling the maximum tensile stresses and maximum compressive is necessary to avoid local failure of the beam.

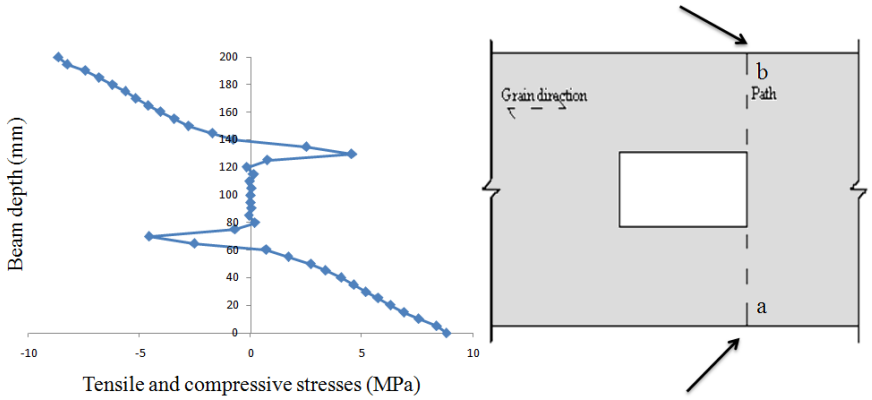

(a) (b)

Figure 8.17. Tensile/compressive stress distribution in the grain direction: (a) along beam depth, (b) beam portion

Figure 8.18 shows a portion of a beam with a rectangular hole. Increased compressive and tensile stresses in grain direction can be calculated from Equations (8.45) and (8.46) respectively as presented by Yong et al (2001).

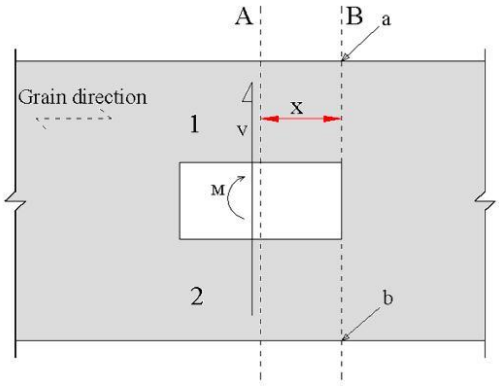

Figure 8.18. beam with rectangular hole

$$\sigma_a = -\frac{M}{(I/C)} - \frac{V_A x\ I_1/(I_1+I_2)}{I_1/C_1} \tag{8.45}$$

$$\sigma_b = +\frac{M}{(I/C)} + \frac{V_A x\ I_2/(I_1+I_2)}{I_2/C_2} \tag{8.46}$$

where V_A and M_A denote shear and moment in section 'A', σ_a compressive stresses, σ_b tensile stresses, I_1 and I_2 moment of inertia for upper and lower portion of the beam about their own axes, moment of inertia about net beam section is denoted by I. C_1, C_2 and C are the distances of the farthest edges of the beam from their respective neutral axes. Parameter x is shown in Figure 8.18. The preceding equations are derived by replacing all forces acting on the beam to the right of section A. The couple produces bending stress given by the first term and the shear divides between part 1 and 2 according to their moments of inertias and produces an additional bending moment in each part. The stresses due to the moment are reflected in the second part of Equations (8.45) and (8.46). Therefore, the beam section should be controlled for the following limitations:

$$\sigma_a \leq f_{c,0,LVL} \tag{8.47}$$

$$\sigma_b \leq f_{t,0,LVL} \tag{8.48}$$

where σ_a and σ_b are stresses defined in Equations (8.45) and (8.46). $f_{c,0,LVL}$ and $f_{t,0,LVL}$ are compressive and tensile strength of LVL obtained according to Eurocode 5 (2004) as:

$$f_{c,0,LVL} = k_{mod}\left(\frac{f_{c,0,k}}{\gamma_m}\right) \tag{8.49}$$

$$f_{t,0,LVL} = k_{mod}\left(\frac{f_{t,0,k}}{\gamma_m}\right) \tag{8.50}$$

$f_{c,0,k}$ and $f_{t,0,k}$ are characteristic compressive and tensile strength of LVL in the grain direction. $f_{c,0,k}$ and $f_{t,0,k}$ for LVL in New Zealand are about 45 MPa and 33 MPa respectively (Buchanan 2007).

8.9.4 Stress concentration at the corners of the plywood reinforcement

Shear stress concentration at the corners of the plywood reinforcement was considered. Numerical analysis on LVL beams with holes shows the concentration of the shear stresses at the outer corner of the plywood. Figure 8.19 shows the results of finite element analysis on a beam of 1500×200×45 mm with hole of 90 mm reinforced with two plywood sheets of 200×200×9 mm. The modelling procedure is the same as mentioned in chapter 5 using cohesive elements.

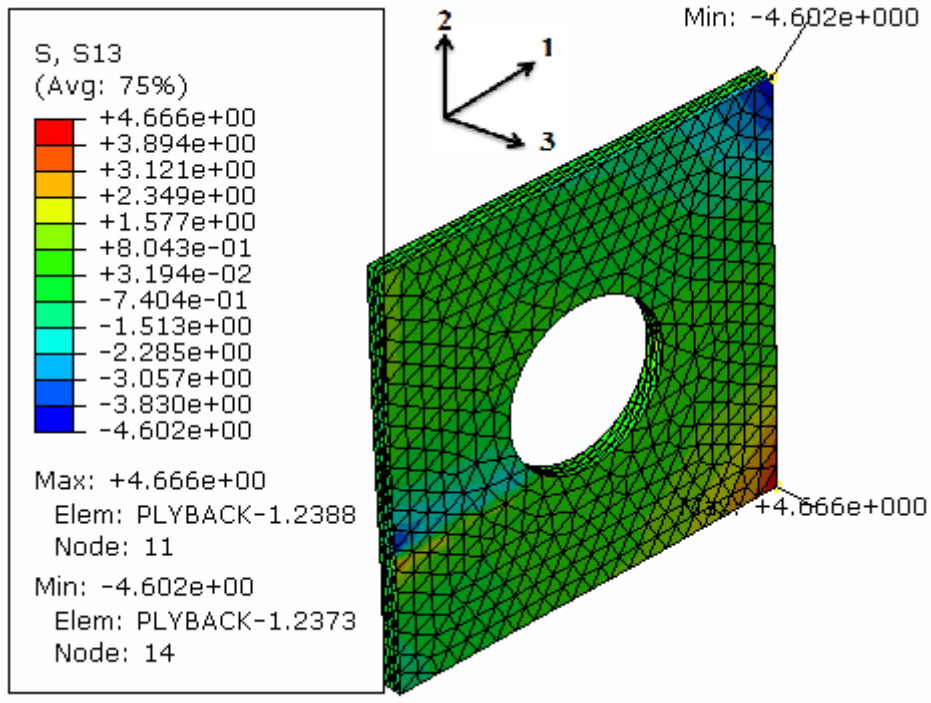

Figure 8.19. Shear stress concentration at the corners of plywood

Cutting of the corners of the plywood was noticed to decrease the shear stress concentration at the corners of the plywood. Triangular cuts with dimension of 20×20×28.3 mm and 40×40×56.6 mm were cut around the plywood as shown in the Figure 8.20. The model shows that the maximum shear stress at the top corner falls from 4.602 MPa to 4.277 MPa for the first cut and falls about 3.834 MPa for the latter cut. The shear stress at the lower right corner of plywood is 4.666 MPa that decreases to

3.859 MPa for the cut of 20×20×28.3 mm at the corner, and for the cut of 40×40×56.6 mm, the shear stress decreases to 3.441 MPa.

The cutting of the corner of plywood decreases the maximum shear stresses considerably, while it distributes the decreased shear stresses over a larger area of the plywood as shown in Figure 8.20.

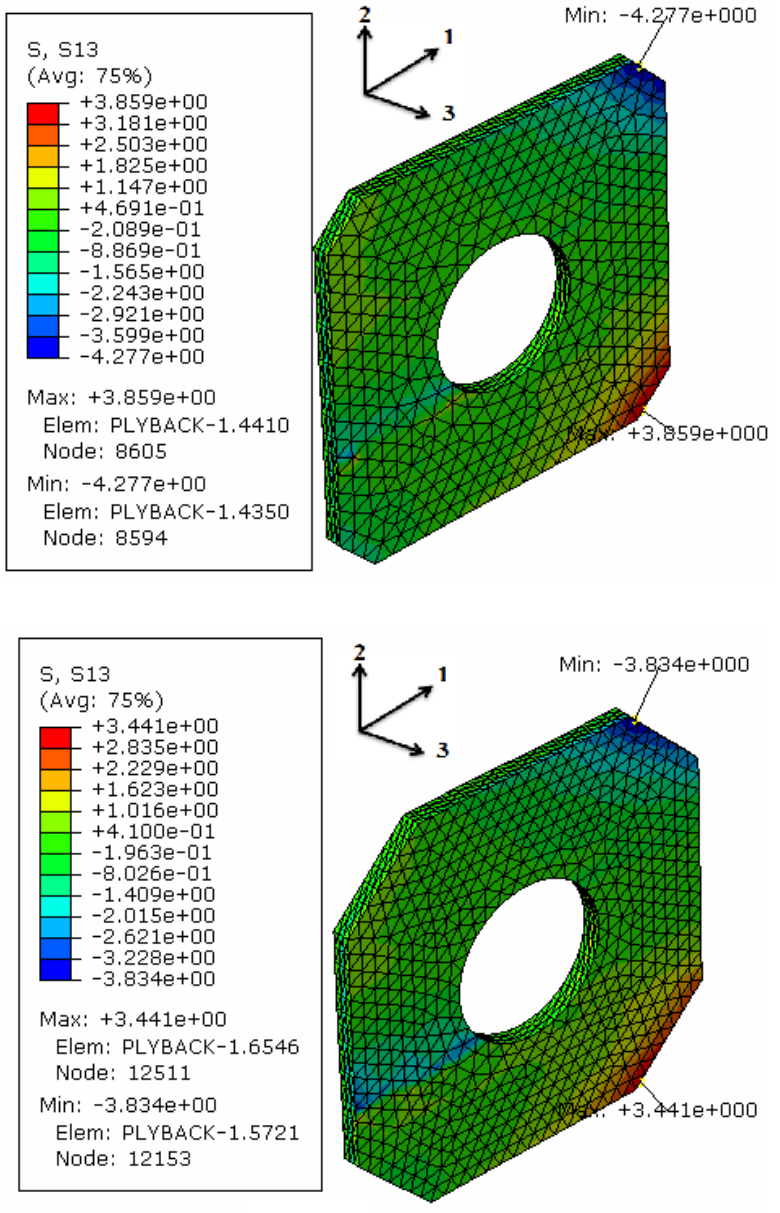

Figure 8.20 Shear stress concentration at the corners of the plywood: (a) cut of 20×20×28.3 mm, (b) cut of 40×40×56.6 mm

8.9.5 Worked example of design of LVL beam with square hole reinforced with plywood

A beam of dimension 3000×300×45 mm has been loaded at mid-span. A hole of dimension equal to the 90×90 mm at a distance of 600 mm from the end is introduced into the beam. The beam has been used in the roof of a house subjected to permanent roof loads (Figure 8.21).

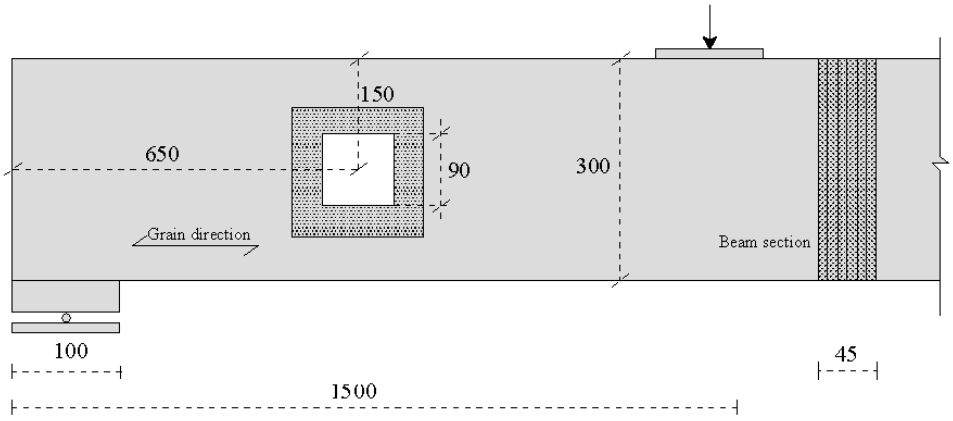

Figure 8.21. Sketch of the beam with square hole reinforced with plywood

Shear capacity of the section:

The shear capacity of the section for the case of no reinforcement can be calculated as:

$$h_{cr} = \left(\frac{H}{2} - \frac{h_d}{2} \times \cos(45)\right) = \left(\frac{300}{2} - \frac{90}{2}\right) = 105 \text{ mm}$$

$$A = b \times h_{cr} = 126.36 \times 45 = 4725\ mm^2$$

$$I = \frac{b \times h_{cr}^3}{12} = \frac{45 \times 126.36^3}{12} = 4341093 \text{ mm}^4$$

$$K = \frac{f_{t,d}^2}{2G_{If,d}} = \frac{0.7^2}{2 \times 0.35} = 0.7 \text{ N/mm}^3$$

$$\lambda^4 = \frac{Kb}{4EI} = \frac{0.7 \times 45}{4 \times 10700 \times 4341093} = 0.0036$$

$$P_{cr} = \frac{bf_{t,d}}{\sqrt{4\lambda^2 + \frac{6}{5}\frac{Kb}{GA}}} = \frac{45 \times 0.7}{\sqrt{4 \times 0.0036^2 + \frac{6}{5} \times \frac{0.7 \times 45}{5 \times 750 \times 4725}}} = 7953 \text{ N}$$

$$M_{cr} = \frac{f_{t,d} b}{2\lambda^2} = 1290613 \text{ N.mm}$$

$$P_t = 2P_{cr} = 2 \times 7953 = 15906\ N$$

$$\sigma_M = \frac{M_{cr}}{\frac{(b \times {h_{cr}}^2)}{6}} = \frac{1290613}{\frac{(45 \times 126.36^2)}{6}} = 14.62 \text{ N/mm}^2$$

$$M_t = 2M_{cr} + b\sigma_M(h_{cr} + h_d\, cos(45))(h - h_{cr})$$

$$= 2 \times 1290613 + 45 \times 14.62\left(105 + 90 \times \sqrt{\frac{2}{2}}\right)(300 - 105)$$

$$= 2745082 \text{ N.mm}$$

$$M = P \times Lc = 600 \times L_c$$

$$\frac{P}{P_t} + (\frac{M}{M_t})^2 = 1$$

The calculated shear force capacity of the section without applying the correction factor is 7709 N and with applying revision factor of $m = 2$ to the results is 9952 N.

Controlling hole diameter:

The ratio of the hole diameter (90 mm) to the beam depth (300 mm) is 0.3; that is lower than the recommended ratio for the of 0.4 for plywood reinforcement. The design can be followed for reinforcement design around the holes with plywood.

Controlling distance of the hole from the support:

The distance of the hole from the support is controlled as:

$$L_c \geq h + \frac{c}{2}$$

$650 \geq 300 + 50 = 350$ mm ok

Tensile load perpendicular to grain in screw:

The design is similar to the previous example with a few modifications. The maximum shear force capacity is adopted from Eurocode 5:

$$f_{v,d} = \frac{f_{v,k} k_{mod}}{\gamma_m} = \frac{6 \times 0.6}{1.2} = 3.0\ MPa$$

$$V_d = \frac{2}{3} f_{v,k} bd = \frac{2}{3} \times 3.0 \times 45 \times 300 = 27\ \text{kN}$$

$$M_d = V_d L_c = 54000 \times 600 = 16.2\ \text{kN.m}$$

The tensile force due to the hole location could be calculated as below:

$$F_{t,d} = F_{t,V,d} + F_{t,M.d} = \frac{\sqrt{2}}{8h^3} V_d h_d \left(3h^2 - h_d^2\right) + 0.7 M_d \left(\frac{{h_d}^2}{h^3}\right)$$

$$F_{t,d} = \frac{\sqrt{2}}{8 \times 300^3} \times 27000 \times 90 \times (3 \times 300^2 - 90^2) + 0.7 \times 16200000 \times \left(\frac{90^2}{300^3}\right) = 7.6\ \text{kN}$$

Dimensions of plywood:

The horizontal dimension of the plywood should be limited with the following equations:

$$0.25 h_d \leq a_r \leq 0.3(h + h_d)$$

$$22.5 \leq a_r \leq 117$$

The plywood should carry tensile forces due to the hole in the section of the beam.

$$\sigma_{t,90,d} \leq f_{d,ply}$$

$$f_{d,ply} = k_{mod} \times \frac{f_{t,k}}{\gamma_m} = 0.6 \times \frac{15}{1.2} = 7.5\ \text{MPa}$$

Assuming the use of plywood with 12 mm thickness, the length of the coverage area is defined as:

$$\sigma_{t,90,d} = \frac{K \times F_{t,90,d}}{2 \times a_r \times t_r} = \frac{2 \times 7600}{2 \times a_r \times 12} = \frac{633}{a_r}$$

$a_r \geq 84.4$ mm then we select $a_r = 100$ mm

and h_1 should be:

$h_1 \geq 0.25 h_d = 0.25 \times 90 = 22.5$ mm, assuming it as $h_1 = 50$ mm

The actual dimension would be 290×190×12 mm.

As stated before, corners of the hole should have a radius of the 15 mm to mitigate the stress concentration at the edges of the hole.

Controlling of rolling shear stresses at the corners of the hole:

The shear stress should be carried by the plywood reinforcement.

$$\tau_{pr,d} = k_{mod} \frac{\tau_{pr,k}}{\gamma_m}$$

$$\tau_{pr,d=} 0.6 \times \frac{1.7}{1.2} = 0.85 \text{ MPa}$$

$$\frac{F_{t,d}}{2a_r \times h_1} \leq \tau_{pr,d}$$

$$\frac{7600}{2\times100\times50} = 0.76 \leq 0.85 \text{ ok}$$

Controlling of increased tensile and compressive stresses in the grain direction:

Characteristic bending strength of LVL is 48 MPa (Buchanan 2007). The design bending strength is 24 MPa. The design load at the mid-span can be calculated as 21.6 kN; therefore, the shear in the section of the beam is equal to 10.8 kN and corresponding moment is 6.48 kN.m. The maximum tensile stress produced in the grain direction is:

$$\sigma_b \leq f_{t,0,LVL}$$

$$f_{t,0,LVL} = k_{mod}\left(\frac{f_{t,0,k}}{\gamma_m}\right) = 0.6 \times \frac{33}{1.2} = 16.5 \text{ MPa}$$

$$\sigma_b = \frac{M}{(I/C)} + \frac{V_A X\, I_2/(I_1+I_2)}{I_2/C_2} = \frac{6480000}{(\frac{45\times300^3}{12})/150} + \frac{10800\times45\times(\frac{45\times105^3}{12})/(\frac{2\times45\times105^3}{12})}{(\frac{45\times105^3}{12})/(\frac{105}{2})} = 12.53 \text{ MPa}$$

The calculated tensile stress of 12.53 MPa is lower than 16.5 MPa for LVL. Controlling the compressive strength of LVL is not necessary because the hole is in the mid-depth of the beam and is much higher than the tensile strength.

Controlling of the shear stresses at the corners of the hole:

The shear stresses at the corners of the hole should be controlled.

$$\kappa_2 = 1.84\left(1+\frac{b_h}{h}\right)\times\left(\frac{h_d}{h}\right)^{0.2} = 1.84\left(1+\frac{90}{300}\right)\times\left(\frac{90}{300}\right)^{0.2} = 1.88$$

$$\tau_2 = \kappa_2 \times 1.5\frac{V_d}{b(h-h_d)} = 1.88\times 1.5\frac{10800}{45(300-90)} = 3.22 \text{ MPa}$$

The shear stress of 3.22 MPa should be carried by the plywood reinforcement and LVL. However, if only LVL is assumed to control the shear we will have:

$\tau_2 \leq f_{v,d}$

3.22 ≤ 6.0 ok

8.10 Interaction of the holes

Interaction of the holes was addressed in chapter 7. The Interaction can increase the tensile load produced in the reinforcement around the holes. The interaction could be avoided through assuming a critical distance between reinforcements in LVL beams.

$$l_{cr} \geq 1.5\, h \qquad (8.51)$$

where l_{cr} is the distance between two closest reinforcements.

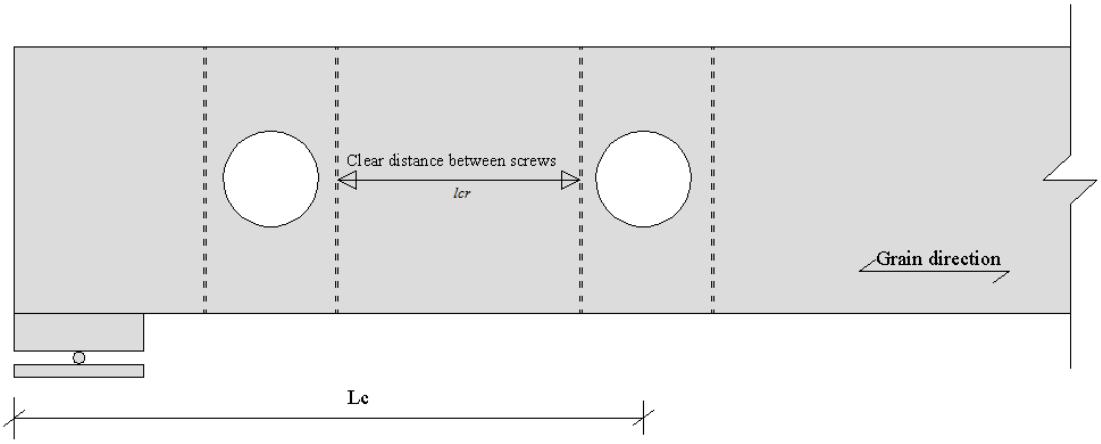

Figure 8.22. Interaction of the holes

8.11 Installation of pipes

Proper installation of the pipes is necessary. Installation of the pipe at the lower edge of the beam can increase the tensile strains locally around the hole. However, if the pipe is installed above the hole, the weight of the pipe also helps to create a local compression around the hole; therefore, following format of the installation as sketched in Figure 8.23 (a) is suggested. The figure shows a reinforced beam that a pipe is passing through. The size of the hole is larger than the pipe. The pipe is tied to the steel angle. The angle is above the top edge of the hole. Figure 8.23 (b) shows an example of the pipe installation. The Angle needs to move a little more above to ensure that the location of the pipe is above a possible crack surface.

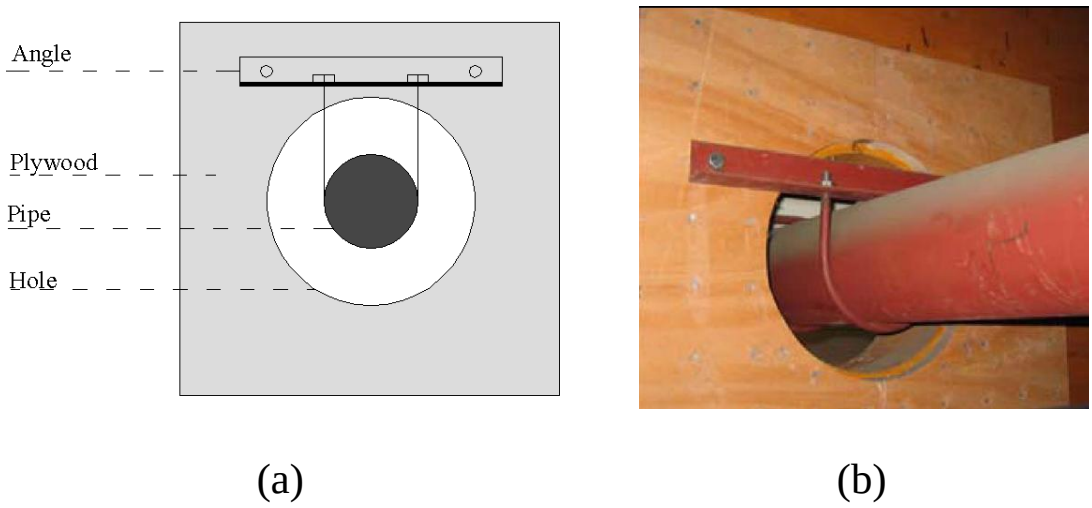

(a) (b)

Figure 8.23 (a) Sketch of proper installation of pipe,(b) an example of the pipe installation

8.12 **Summary**

This chapter presented a design method for reinforcement of LVL beams with holes. Design of screws, epoxied rods, and plywood were discussed and worked examples were presented.

9 Conclusion and future work

This chapter presents conclusions of the study and recommendations for future works.

9.1 Introduction

This thesis explored analysis and design of Laminated Veneer Lumber (LVL) beams with holes, and methods of reinforcement around the holes. Experiments were performed on LVL specimens to obtain material properties such as mode I fracture energy, fracture toughness, tensile strength perpendicular to the grain, modulus of elasticity in different directions, and screw withdrawal strength. The later experimental program included several experiments on reinforced and unreinforced LVL beams with holes to determine effectiveness of different reinforcement types for the holes. The analytical part was developed using Linear Elastic Fracture Mechanics (LEFM), and Nonlinear Fracture Mechanics (NLFM). LEFM was used for failure load prediction of LVL beams with holes. LEFM guided the analysis to NLFM analyses using cohesive elements to understand the behaviour of the fracture layer before and after reinforcement. Analytical formulations were derived by using a beam on an elastic foundation theory for the cracking load predictions of LVL beams with holes. Tensile load prediction in the reinforcement was the target of a later series of analytical formulations, and finally a design method was proposed for LVL beams with holes reinforced with screws, glued in rods, and plywood.

This thesis provides a sound basis for the design of LVL beams with holes. Screws and plywood have been introduced as reliable reinforcement options. However, Plywood

can be used for larger hole diameters in comparison to screws as it is the preferable reinforcement option in this case.

9.2 Conclusions

Chapter 2 presented material properties of LVL obtained through experiments. Tensile perpendicular to the grain experiments on LVL specimens showed that the tensile strength of LVL is lower than tensile strength of sawn timber. Low tensile strength perpendicular to the grain makes LVL susceptible to cracking due to perpendicular to the grain tensile stresses increased by the holes.

Fracture tests on LVL in mode I showed that fracture energy of LVL in opening mode in the grain direction is considerably higher than for sawn timber, which indicates that the energy required for propagating a crack in LVL is higher than for sawn timber. Therefore in comparison, LVL cracks at lower stresses than sawn timber, but more energy is required for a crack in LVL to propagate in the grain direction.

Chapter 3 presented experiments on LVL beams with the holes and possible reinforcement around the holes. The results can be categorized in two main groups, viz.: (i) no reinforcement around the holes, and (ii) reinforcement around the hole.

No reinforcement around the hole:

Holes smaller than 50 mm diameter for beams 200 mm, 300 mm, and 400 mm depth did not change the behaviour of the beam, and mid-span failure occurred. Holes larger than 50 mm diameter (with diameter of 0.3 to 0.6 of the beam depth) in shear dominant areas of LVL beams reduced the load carrying capacity of the beam from 10 to 52%. In the experimental program, the failure load of LVL beams with holes (final load carrying capacity) was 8 to 46 % higher than the load corresponding with crack initiation.

Reinforcement around the hole:

The aim of reinforcement was to recover the full capacity of a beam with a hole so that the effect of the hole can be ignored. Different options for reinforcement of holes in LVL beams were used: (i) fully threaded self-tapping SPAX screws, (ii) epoxied in rods, (iii) plywood, and (iv) steel brackets. In general, reinforcement with continuous

connection like plywood sheets worked better than reinforcement with discrete connection like steel brackets.

Fully threaded screws and epoxied rods could not prevent crack initiation at the edges of the hole but were effective at limiting crack propagation.

While fully threaded screws and epoxied rods were two effective means of reinforcement for LVL beams with holes having a diameter to beam depth ratio equal or less than 0.4, plywood glued and nailed/screwed on both sides of a beam were promising ways of reinforcing LVL beams for a larger hole diameter up to beam depth ratio of 0.5. Nailing/screwing of plywood on both sides of holes ensures uniform pressure on connection hence best results. Bonding between plywood and LVL makes it possible for internal forces to flow around holes by alternate routes.

Although a steel bracket can be an alternative reinforcement method for holes, it suffers a few shortcomings viz.: (i) the steel bracket may buckle due to compressive stress field around holes; and (ii) the steel plate may limit free shrinkage of wood.

Chapter 4 presented numerical analyses using Linear Elastic Fracture Mechanics (LEFM) for failure load predictions of LVL beams with holes.

LEFM can be used for failure load prediction of LVL beams with holes if appropriate crack length (pre-cracking) is introduced in the modelling. Crack lengths of 2 to 3 mm provided reasonable predictions of the failure load for the range of experimental LVL beams with the length to depth ratio less than 10. Initial crack criterion as proposed by Gustafsson (1993b) for LVL provided conservative estimation of the failure load.

LEFM analysis showed that a distance of at least the beam depth should be adopted from the hole centre to the support of the beam in order to mitigate the probability of crushing above the support. This minimum distance was obtained based on considerations on the change in the Stress Intensity Factors (SIFs).

Studying SIFs shows that a concentrated load tends to close cracks around the holes; Decreasing SIFs for Uniformly Distributed Loading (UDL) towards the mid-span of a beam indicates that the maximum capacity for unreinforced beam could be obtained by moving the hole towards the mid-span of beams.

LEFM and experiments showed that for a small shifting of hole relative to the neutral axis (17.5 % of beam depth), the capacity of the beam increased by about 10 % when the hole was above the neutral axis and remained almost constant when the hole was below the neutral axis.

Chapter 5 presented the use of the cohesive crack model for failure load predictions of LVL beams with holes. The model was then extended to investigate the behaviour of the fracture layer.

Cohesive elements with traction-separation law behaviour can be used for failure load predictions of LVL beams with holes. The material properties of the cohesive layer are important for the failure load predictions and needs calibration with experimental results.

Analyses using cohesive elements showed that the cracking in LVL beams starts when the elements surrounding the crack tip attain their maximum tensile strength and this is followed by crack propagation due to the shear stresses in the section.

Screw reinforcement around the holes helped to control the tensile stress raised by the hole itself. It also caused shear stress concentration at the screw location that should be carried by LVL. The shear stress concentration causes brittle failure of the beam if the screw has yielded. Since plywood locally increased the shear capacity of the beam, it is more effective than screws.

Chapter 6 derived a series of formulations for predicting cracking load of LVL beams with holes. The theory of a beam on an elastic foundation was applied to the beams with holes to estimate the cracking load.

A portion of a beam with hole at the time of crack initiation ($t = 0$) can be assumed as a beam resting on Winkler springs with stiffness corresponding to the fracture properties of LVL in opening mode. This requires that the lower beam be assumed as an infinitely stiff beam. The assumption works well for large hole diameters. For small hole diameters, the stiffness of the lower beam contributes to the deflection of the beam and under-estimates the cracking load.

The beam on elastic foundation schematization to predict the cracking load of the beam works well for hole diameters equal or larger than 0.4 of the beam depth. For hole

diameters smaller than 0.4 of the beam depth, the results of the model for cracking load predictions are mostly conservative. For small hole sizes, the cracking load may be predicted by artificially increasing the stiffness of the Winkler springs. A modification factor can be applied that accounts for the stiffness of lower beam.

A beam with a hole needs to be reinforced if the shear in the section of the beam is larger than the shear predicted through the cracking load formulations.

The formulation was applied to the tests performed on glulam beams and effectively predicted the cracking load of glulam beams with holes.

Chapter 7 derived a series of formulations for tensile load predictions in the reinforcement near holes. The formulations were derived based on a truss model assumed to be formed around holes in LVL beams.

The analytical formulation considers the contribution of shear and moment on the tensile load predictions around the holes in LVL beams. A truss model is proposed to obtain the tensile load due to shear and moment in the section of a beam. The predicted tensile load through proposed analytical formulations is in good agreement with experimental and numerical values for beam depths up to 400 mm. For larger depth beams ($h > 400$ mm), the formulation underestimates the tensile load. A modification factor of $\sqrt{h/400}$ may be used to adjust the tensile load with numerically predicted values.

Using numerical analysis the formulation for the tensile load predictions was revised for square and rectangular holes considering the dimensions of rectangular holes relative to each other. The predicted tensile loads through analytical and numerical analysis are in good agreement for rectangular holes.

Another numerical analysis of beams with holes showed that by shifting the hole above the neutral axis (eccentricity of 10 % of beam depth) the maximum tensile force in the reinforcement increases. A correction factor of $(1 + h_d/h)$ is proposed to increase the tensile load in the reinforcement around the holes.

Interaction of holes (two holes in a beam) was investigated for a series of numerical analyses on LVL beams with holes. A clear distance of $1.5h_d$ between reinforcements minimized the effect on the tensile load in the reinforcement around the holes.

Chapter 8 presented a design method for reinforcement around the holes in LVL beams. Three main reinforcement types were considered for design purposes: (i) screw, (ii) epoxied rods, and (iii) plywood.

9.3 Specific conclusions

Conclusions of the thesis from numerical, analytical, experimental and design perspectives are presented as follows:

9.3.1 Numerical

Numerical modelling techniques were devised to capture the cracking, and failure load of LVL beams with holes. Key outcomes from this research are as follows:

- Linear Elastic Fracture Mechanics (LEFM) can predict the failure load of LVL beams with holes provided that an accurate prediction of the crack length could be made. For the range of experimental beams, a crack length of 2 to 3 mm provided good predictions of the failure load.
- Cohesive elements (interface element) with traction-separation law behaviour in ABAQUS predicted the failure load of LVL beams with holes very well.

9.3.2 Analytical

Analytical modelling techniques were used to capture the cracking, and failure load of LVL beams with holes. Key outcomes from this research are as follows:

- The beam on an elastic foundation theory can be applied to LVL beams for cracking load prediction. A portion of a beam with a hole can be regarded as a beam resting on Winkler elastic springs with spring stiffness adopted from fracture properties of LVL. Limitations in terms of hole diameters to beam depth should be applied to the method to predict the cracking load effectively.
- The truss model as presented can predict the tensile force produced in the reinforcement around circular holes. Modifications of the truss model to

accommodate rectangular holes using finite element results were performed, and demonstrated the good potential of the model.

9.3.3 Experimental

Experimental testing was carried on LVL beams for indication of material properties of LVL. Different reinforcement methods were used around the holes. Key outcomes from this research are as follows:

- Reinforcement of Laminated Veneer Lumber can recover the capacity of the beam with hole to a beam without hole. Three methods of reinforcement viz.: (i) using self-tapping SPAX screws, (ii) epoxied in rods and (iii) plywood glued and nailed on both sides of the beam are suggested for reinforcement of the holes.
- Plywood glued and nailed on both sides of LVL beam is the preferable reinforcement method because it prevents tensile stresses raised by the hole and distributes the load over a large area of the beam. Applicability of plywood for beams up to 90 mm breadth was experimentally verified.

9.3.4 Design

Taking into account conclusions from experimental testing, numerical analysis, and analysis on LVL beams with holes and reinforcement, design methods for LVL beams with holes were developed. Key outcomes from this work are given below:

- A design method is proposed for beams with holes reinforced with plywood, self-tapping screws and epoxied in rods. Step-by-step procedures are presented.
- A number of minor changes to the DIN 1052 procedure were shown to give much better production of the results. The changes viz.: (i) basic equations for tensile load predictions around the holes were changed, (ii) a new series of formulations were added to predict the cracking load of LVL beams with holes, (iii) hole diameter to beam depth ratio was revised, (iv) increased

tensile and compressive stress verification was added to the verifications for rectangular holes, (v) verification of the shear stresses (adopted from (Blass et al. 2004)) were added to the design, and (vi) the distance of the hole from concentrated load was revised.

- Limited test results of tension perpendicular to grain show that cross-banded LVL will have much greater resistance to failure than normal LVL.

9.4 Future work

While this thesis attempted to lay a sound basis for the analysis of LVL beams with holes and of design reinforcement around the holes, as for any relatively new structural system, there is a significant amount of further research required. Some specific aspects that have been identified from this thesis are listed below:

Efficiency of plywood for thick beams:

An experimental program on wider LVL beams is necessary to address the effectiveness of plywood as a reinforcement of wider LVL beam. Experimental programs were limited to 90 mm breadth. More research should be performed to verify the results for wider LVL beams.

Holes in post-tensioned timber structures:

The current study focused on holes in normal beams; the study needs to be expanded for the post-tensioned timber beams that have been recently developed at the University of Canterbury, New Zealand. The post-tensioning force can potentially increase the tensile stresses around the holes. A revision of the truss model is required to account for the tensile stresses raised by the holes.

Holes in cantilever beams:

The study mainly focused on simply supported beams, and it did not address holes in cantilever beams. The stress field around a hole in a cantilever beam is different. A new research topic could be the reinforcement of cantilever beams.

Holes in curved beams:

The current study was performed on the straight beams. Curved beams present special problem because perpendicular to grain tensile stress concentration occurs at mid-span of the beam. The tensile stress can be increased by introducing holes. Figure 9.1 shows a curved beam with the tensile stress concentrations at the middle of the beam. The truss model as suggested maybe revised for the curved beams. The validity of the model could be verified through experimental and numerical analysis.

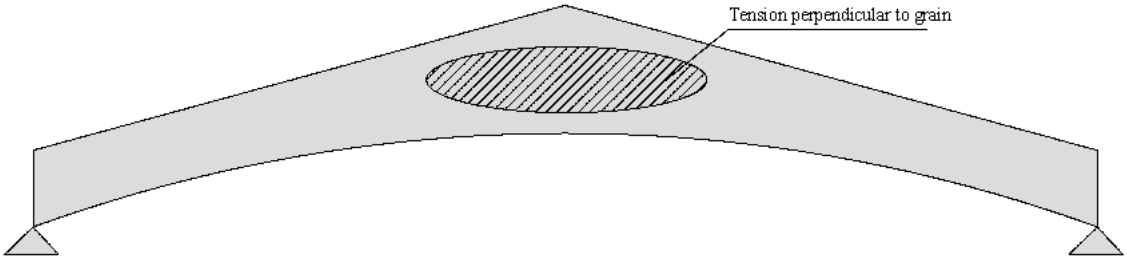

Figure 9.1 curved beam with stress concentration at the mid-span

Holes in cross - banded LVL:

Another alternative for design is the use of cross-banded LVL. Cross-banded LVL has higher tensile strength perpendicular to the grain directions. Cross-banded LVL is somewhat similar to a beam reinforced with plywood. It would be interesting to investigate the effect of holes on cross-banded LVL through an experimental programme.

Vertical holes:

It was found that vertical holes in LVL beams can cause a reduction of the strength. The failure due to vertical holes needs experimental and numerical analysis. Vertical holes may result from drilling holes self tapping screws. The effects of the vertical holes should be addressed properly to avoid undesirable failure modes.

Long term behaviour of the LVL beam with reinforced hole

This thesis was concentrated on short-term behaviour of LVL beams with holes and reinforcement around holes. The effect of the holes in the long term still needs to be

addressed. Continuous shrinkage and swelling cycles of the wood may have potential for crack formation/propagation around reinforced holes. This needs an experimental and numerical study.

Size effect in reinforced LVL beam with hole

Experimental tests on LVL beams with holes and reinforcement were carried out for beams up to 400 mm depth. A size effect may exist for larger depth. This requires an experimental program to be addressed.

Fire resistance of beams with holes:

Fire resistance of beams with holes needs an experimental and numerical analysis. Although the scope of this thesis did not include fire in beams with holes, it is believed that appropriate design of beams can be made by accounting for the effect of the fire. A research area can be considering of fire effects in the design of beams with holes.

10 References

Aicher, S. (1996). "Fracture mechanics models for strength analysis of timber beam with a hole or a notch: Part 2. Stress intensity factor approch." In Rhilem Report**:** 1-31.

Aicher, S. (2011). "Glulam beams with internally and externally reinforced holes - tests, detailing and design." Proceedings of CIB-W18 Meeting 44, Paper 44-12-4, Alghero, Italy, University of Karlsruhe.

Aicher, S. and Hofflin, L. (2000). "A contribution to the analysis of glulam beams with round holes." Otto-Graf-Journal2, Stuttgart, Germany **11**: 167-188.

Aicher, S. and Hofflin, L. (2001). "Round holes in glulam members: Part I Analysis." Journal of Bautechnik **78**(10): 706-7014.

Aicher, S. and Hofflin, L. (2002). "Glulam beams with round holes: A comparison of different approaches vs. test data." Proceedings of CIB-W18, Meeting 35, Paper 35-12-1, Kyoto, Japan, University of Karlsruhe.

Aicher, S. and Hofflin, L. (2004). "New design model for round holes in glulam beams." Proceeding of 8th World Conference on Timber Engineering. Lahti, Finland. **1:** 67-72.

Aicher, S. and Hofflin, L. (2009). "Glulam beams with holes reinforced with steel bars." Proceedings of CIB-W18, Meeting 42, Paper 42-12-1, Duebendorf, Switzland, University of Karlsruhe.

Aicher, S., Hofflin, L. and Reinhardt, H. W. (2007). "Round holes in glued laminated timber: Part 2 load capacity and design " Journal of Bautechnik **84**(12): 867-880.

Aicher, S., Schmidt, J. and Brunold, S. (1995). "Design of timber beams with holes by means of fracture mechanics." Proceedings of CIB-W18, Meeting 28, Paper 28-19-4, Copenhagen, Denmark, University of Karlsruhe.

APA Report EWS-G535A (2010). "Field notching and drilling of Laminated Veneer Lumber." Washington, USA, The Engineered Wood Association (EWA)**:** 1-6.

APA Report T2009L-30 (2009). "Allowable holes in LVL ". Washington, USA, The Engineered Wood Association (EWA)**:** 1-21.

Ardalany, M., Deam, B. and Fragiacomo, M. (2010a). "Numerical investigation of the load carrying capacity of Laminated Veneer Lumber (LVL) joists with holes." World Conference on Timber Engineering (WCTE 2010). Riva del Garda, Italy

Ardalany, M., Deam, B. and Fragiacomo, M. (2012a). "Experimental results of fracture energy and fracture toughness evaluation of Radiata Pine Laminated Veneer Lumber (LVL) in mode I (opening)." Journal of Materials and Structures RILEM **45**(8): 1189-1205.

Ardalany, M., Deam, B., Fragiacomo, M. and Crews, K. (2010b). "Tension perpendicular to grain strength of wood, Laminated Veneer Lumber (LVL) and Cross banded LVL (LVL-C)." 21st Australasian Conference on the Mechanics of Structures and Materials. S. Fragomeni , S. Venkatesan, N. Lam and S. Setunge. Melbourne, Victoria, Australia, CRC Press**:** 891- 896.

Ardalany, M., Fragiacomo, M., Deam, B. and Buchanan, A. (2012b). "Design of reinforcement around holes in Laminated Veneer Lumber (LVL) beams." World Conference on Timber Engineering (WCTE 2012). P. Quenneville. Auckland, New Zealand **1:** 539-547.

AS/NZ 2269 (2004). "Plywood Structural Standard." New Zealand, Standards New Zealand.

AS/NZS1720-1 (2003). "Timber structures." Part 1: Design Methods. Australia, Standards Australia**:** 1-188.

AS/NZS 4063 Part.2 (2010). "Characterization of structural timber Part 2: Determination of characteristic values." Australia, Standards Australia**:** 1-54.

ASTM D143-94 (2000). "Standard test method for small clear specimens of timber." West Conshohocken, USA, ASTM International.

ASTM D4442-92 (2000). "Standard test methods for direct moisture content measurement of wood and wood-based materials." West Conshohocken, USA, ASTM International.

Ballerini, M. and Bezzi, R. (2001). "Numerical LEFM analyses for the evaluation of failure loads of beams loaded perpendicular to grain by single dowel connections." Proceedings of CIB-W18, Meeting 34, Paper 34-7-2, Venice, Italy, University of Karlsruhe.

Ballerini, M. and Bezzi, R. (2007). "Numerical LEFM analyses for the prediction of the splitting strength of beams loaded perpendicular-to-grain by dowel-type connections." Journal of Materials and Structures, RILEM **40**(1): 139-149.

Barsoum, R. S. (1976). "On the use of isoparametric finite elements in linear fracture mechanics." International Journal for Numerical Methods in Engineering, WILEY **10**(1): 25-37.

Blass, H. and Bejtka, I. (2004). "Reinforcements perpendicular to the grain using self-tapping screws." World Conference on Timber Engineering (WCTE 2004). Lahti, Finland. **1:** 233.

Bostrom, L. (1992). "Method of determination of the softening behaviour of wood and the applicability of a nonlinear fracture mechanics model." Sweden, Lund. **PhD thesis:** 1-148.

Buchanan, A. (2007). "Timber design guide." Wellington, New Zealand, Timber Industry Federation.

Carling, O. (2001). "Swedish glulam handbook (online http://www.svensktlimtra.se/en/limHTML/)." Stockholm, Sweden, Svenskt Limträ.

Chan, P. W. and Redwood, R. G. (1974). "Stresses in beams with circular eccentric web hole." Journal of Structural Devision, ASCE **100**(1): 231-248.

Chen, L. S. and Kuang, J. H. (1993). "A displacement extrapolation method for two dimensional mixed mode crack problems." Journal of Engineering Fracture Mechanics, ELSEVIER **46**(5): 735-741.

Christopher, E. (2006). "Digital image correlation and tracking ". http://www.mathworks.com/matlabcentral/fileexchange/12413.

Cook, R. D. (2002). "Concepts and applications of finite element analysis." Wiley, New York, USA.

Danielsson, H. (2007). "The strength of glulam beams with holes: A survey of tests and calculation methods." Sweden, LUND University**:** 1-91.

Danielsson, H. (2009). "The strength of glulam beams with holes: A probabilistic fracture mechanics method and experimental tests." Lund, Sweden, LUND University. **Licentiate Degree:** 75.

Dassault-Systemes-Simulia-Corp. (2006). "Selecting Material Parameters in Abaqus for Cohesive Elements Defined in Terms Of Traction-Separation."

Davies, M. (2006). "Long term behaviour of Laminated Veneer Lumber (LVL) members prestressed with unbounded tendons." Department of Architecture and Planning. Sassari, University of Sassari, Italy. **Master thesis:** 59.

Dias, A. M. P. G., Van de Kuilen, J. W., Lopes, S. and Cruz, H. (2007). "A non-linear 3D FEM model to simulate timber-concrete joints." Journal of Advances in Engineering Software, ELSEVIER: 522-530.

DIN 1052 (2008). "Design of timber structures - General rules and rules for buildings (In German)." Berlin, Germany, Construction Standards Committee (NABau) at DIN**:** 239.

Dugdale, D. S. (1960). "Yielding of steel sheets containing slits." Journal of the Mechanics and Physics of Solids **8**(2): 100-104.

Eurocode 5 (2004). "Eurpoean Committee for Standardization CEN, EN 1995-1-1. Design of timber structures-part 1-1: General-common rules for buildings.". Bruxelles, Belgium.

European Committee for Standardization EN 789 (2004). "Timber structures-test methods- Determination of mechanical properties of wood based panels."

Franke, B. and Quenneville, P. (2011). "Numerical Modeling of the Failure Behavior of Dowel Connections in Wood." Journal of Engineering Mechanics, ASCE **137**(3): 186-195.

Green, D. W. (2001). "Wood: strength and stiffness." Encyclopaedia of Materials: Science and Technology**:** 9732-9736.

Griffith, A. A. (1921). "The phenomena of rupture and flow in solids." Philosophical Transactions of the Royal Society of London. Series A, Containing Papers of a Mathematical or Physical Character **221**(ArticleType: research-article / Full publication date: 1921 / Copyright © 1921 The Royal Society): 163-198.

Guan, Z. W. and Zhu, E. C. (2004). "Nonlinear finite element modelling of crack behaviour in oriented strand board webbed wood I-beams with openings." Journal of Structural Engineering ASCE **130**(10): 1562-1569.

Guan, Z. W. and Zhu, E. C. (2009). "Finite element modelling of anisotropic elasto-plastic timber composite beams with openings." Journal of Engineering Structures, ELSEVIER **31**: 394-403.

Guinea, G. V., Planas, J. and Elices, M. (2000). "KI evaluation by the displacement extrapolation technique." Journal of Engineering Fracture Mechanics, ELSEVIER **66**(3): 243-255.

Gustafsson, P. (1993a). "Mean stress approch and initial crack approach." Sweden, Lund University. **Report TVSM-7134** 1-15.

Gustafsson, P. J. (1985). "Fracture mechanics studies of non-yielding materials like concrete: Modeling of tensile fracture and applied strength analyses, Report TVBM-1007." Lund, Sweden, Institute of Technology

Gustafsson, P. J. (1993b). "Fracture mechanics models for strength analysis of timber beams with a hole or a notch - A Report of RILEM TC-133 : mean stress approach and initial crack approach (paper in report)." P. Gustafsson. Sweden, Lund University. **Report TVSM-7134** 1-15.

Gustafsson, P. J. and Serrano, E. (1999). "Fracture mechanics in timber engineering - some methods and applications." 1st International RILEM Symposium on Timber Engineering. L. Bostrom. Stockholm, Sweden, RILEM Publications**:** 141-150.

Habbitt, Karlsson and Sorensen (2010a). "ABAQUS, Theory Manual, Version 6.10 - EF1." USA, ABAQUS Inc. Dessault Systemes.

Habbitt, Karlsson and Sorensen (2010b). "ABAQUS, User Manual, Version 6.10-EF1." USA, ABAQUS Inc. Dessault Systemes.

Hallström, S. (1996). "Glass fibre reinforced holes in laminated timber beams." Journal of Wood Science and Technology **30**(5): 323-338.

Harper, P. W. and Hallett, S. R. (2008). "Cohesive zone length in numerical simulations of composite delamination." Journal of Engineering Fracture Mechanics, ELSEVIER **75**(16): 4774-4792.

Henshell, R. D. and Shaw, K. G. (1975). "Crack tip finite elements are unnecessary." International Journal for Numerical Methods in Engineering, WILEY **9**(3): 495-507.

Hillerborg, A. (1991). "Application of the fictitious crack model to different types of materials." International Journal of Fracture, SpringerLink **51**(2): 95-102.

Hillerborg, A., Modéer, M. and Petersson, P. E. (1976). "Analysis of crack formation and crack growth in concrete by means of fracture mechanics and finite elements." Journal of Cement and Concrete Research **6**(6): 773-781.

Hofflin, L. (2005). "Round holes in glulam beams: Experimental and theoretical analyses." Stuttgart, Germany, MPA University. **PhD Thesis**.

Hummer, T., Dolan, D. and Wolcott, M. (2006). "Tension perpendicular to grain of wood, Lamianted Veneer Lumber, and a Wood Plastic Composite." World Conference on Timber Engineering (WCTE 2006). D. Rosowsky. Portland, D. Rosowsky.

Irwin, G. R. (1958). "Analysis of stresses and strains near the end of a crack traversing a plate." Journal of Applied Mechanics(24): 361-364.

Jensen, J. L. (2005). "Quasi-non-linear fracture mechanics analysis of splitting failure in simply supported beams loaded perpendicular to grain by dowel joints." Journal of Wood Science **51**(6): 577-582.

Jensen, J. L. and Gustafsson, P. J. (2004). "Shear strength of beam splice joints with glued-in rods." Journal of Wood Science **50**(2): 123-129.

Jernkvist, L. O. (2001a). "Fracture of wood under mixed mode loading I. Derivation of fracture criteria." Journal of Engineering Fracture Mechanics, ELSEVIER **68**(5): 549-563.

Jernkvist, L. O. (2001b). "Fracture of wood under mixed mode loading II. Experimental investigation of Picea Abies." Journal of Engineering Fracture Mechanics, ELSEVIER **68**(5): 565-576.

Johannesson, B. (1983). "Design problems for glulam beams with holes." Division of Steel and Timber structures. Göteborg, Sweden, Chalmers University of Technology. **PhD thesis:** 1-74.

Kanninen, M. F. (1973). "An augmented double cantilever beam model for studying crack propagation and arrest." International Journal of Fracture, SpringerLink **9**(1): 83-92.

Kolb, H. and Frech, P. (1977). "Instruction for the reinforcement of apertures in glulam beams." Proceedings of CIB-W18, Meeting 8, Paper 8-12-2, Bruxelles, Germany, University of Karlsruhe.

Kollmann, F. F. P. (1951). "Technologie des Holzes und der Holzwerkstoffe." Springer.

Larsen, H. J. and Gustafsson, P. J. (1990). "Determination of fracture energy of wood for tension perpendicular to grain." Proceedings of CIB-W18, Meeting 23, Paper 23-10-12, Lisbon, Portugal, University of Karlsruhe.

Leicester, R. H. (1971). "Some aspects of stress fields at sharp notches in orthotropic materials: I. Plane stress." Division of Forest Products technological paper ; no. 57. Melbourne, Australia Commonwealth Scientific and Industrial Research Organization.

Leicester, R. H. (2006). "Application of linear fracture mechanics to notched timber elements." Journal of Progress in Structural Engineering and Materials **8**(1): 29-37.

Leicester, R. H. and Bunker, P. C. (1968). "Fracture at butt-joints in laminated pine." Journal of Forest Product **19**(2): 59-60.

Lekhnitskii, S. G. (1963). "Theory of Elasticity of an Anisotropic Elastic Body." San Francsisco, Holden-Day Inc.

Lin, X. B. and Smith, R. A. (1999). "Finite element modelling of fatigue crack growth of surface cracked plates: Part III: Stress intensity factor and fatigue crack growth life." Journal of Engineering Fracture Mechanics, ELSEVIER **63**(5): 541-556.

Madsen, B. and Fuglsang Nielsen, L. (1992). "Structural behaviour of timber." North Vancouver, B.C, Timber Engineering Ltd.

Norman, D. E. (2009). "Mechanical behavior of materials:International edition." Prentice Hall.

Norris, C. B. (1962). "Strength of orthotropic materials subjected to combined stresses (Report)."**:** 40.

NZS 3603 (1993). "Timber Structures Standard." New Zealand, Standards New Zealand, Wellington.

Patton-Mallory, M. and Cramer, S. M. (1987). "Fracture mechanics - a tool for predicting wood component strength." Forest Products Journal **37**(7-8): 39-47.

Pirzada, G. B., Chui, Y. H. and Lai, S. (2008). "Predicting Strength of Wood I-Joist with a Circular Web Hole." Journal of Structural Engineering, ASCE **134**(7): 1229-1234.

Pizio, S. (1991). "The use of fracture mechanics in design of timber structures, analysed on beams with holes and notched beams (in German)." Zurich, ETH.

Ranta-Maunus, A. (1990). "Application of fracture mechanics to timber structures." Proceedings of CIB-W18, Meeting 23, Paper 23-19-3, Lisbon, Portugal, University of Karlsruhe.

Riipola, K. (1995). "Timber beams with holes: fracture mechanics approach." Journal of Structural Engineering, ASCE **121**(2): 225-240.

Romanowicz, M. and Seweryn, A. (2008). "Verification of a non-local stress criterion for mixed mode fracture in wood." Journal of Engineering Fracture Mechanics, ELSEVIER **75**(10): 3141-3160.

Schoenmakers, D. (2010). "Fracture and failure mechanisms in timber loaded perpendicular to grain by mechanical connections." Civil engineering. Netherlands, University of Eindhoven. **Doctorate thesis:** 318.

Sih, G. C., Paris, P. C. and Irwin, G. R. (1965). "On cracks in rectilinearly anisotropic bodies." International Journal of Fracture, SpringerLink **1**(3): 189-203.

Smith, I., Landis, E. and Gong, M. (2003a). "Fracture and fatigue in wood." Chichester, West Sussex, England ; Hoboken, NJ, John Wiley amd Sons Ltd.

Smith, I. and Vasic, S. (2003b). "Fracture behaviour of softwood." Journal of Mechanics of Materials **35**(8): 803-815.

SPAX (2007). "General Building Authority Approval, Number Z-9.1-499." ABC Verbindungestechnik GmbH & Co. KG

Stanzl-Tschegg, S. E., Tan, D.-M. and Tschegg, E. K. (1995). "New splitting method for wood fracture characterization." Journal of Wood Science and Technology **29**(1): 31-50.

Szabo, T. (1977). "Plywood reinforcement for structural wood members with Internal defects." Bulletin of the Association for Preservation Technology **9**(1): 11-15.

Van Der Put T.A.C (2011). "A new fracture mechanics theory of wood." New York, Nova Science Publishers Inc.

Vasic, S. and Smith, I. (2002a). "Bridging crack model for fracture of wood." Journal of Engineering Fracture Mechanics, ELSEVIER **69**: 745-760.

Vasic, S., Smith, I. and Landis, E. (2002b). "Fracture zone Characterization—Micro-Mechanical Study." Journal of Wood and Fiber Science **34**(1): 42-56.

Wittmann, F. H. and Hu, X. (1991). "Fracture process zone in cementitious materials." International Journal of Fracture, SpringerLink **51**(1): 3-18.

Wu, E. M. (1967). "Application of fracture mechanics to anisotropic plates." Journal of Applied Mechanics **34**(4): 967-974.

Young, W. C. and Budynas, R. G. (2001). "Roark's Formulas for Stress and Strain (7th Edition)." McGraw-Hill.

Zhu, E. C., Guan, Z. W., Rodd, P. D. and Pope, D. J. (2005). "A constitutive model for OSB and its application in finite element analysis." Journal of Holz als Roh-und Werkstoff **63**(2): 87-93.

Appendix 1

Experimental results of fracture energy and fracture toughness of Radiata Pine Laminated Veneer Lumber (LVL) in mode I (opening) is the subject of this appendix. Extensive experimental tests on LVL and Radiata Pine were performed to obtain the fracture properties of LVL in opening mode of fracture. Experimental testing machine was also revised to facilitate the testing of wood specimens.

Materials and Structures (2012) 45:1189–1205
DOI 10.1617/s11527-012-9826-1

ORIGINAL ARTICLE

Experimental results of fracture energy and fracture toughness of Radiata Pine laminated veneer lumber (LVL) in mode I (opening)

Manoochehr Ardalany · Bruce Deam · Massimo Fragiacomo

Received: 29 September 2010 / Accepted: 4 January 2012 / Published online: 26 January 2012

Abstract The load-carrying capacity of notched timber beams can be predicted using linear elastic fracture mechanics (LEFM). Material properties such as fracture toughness and energy are needed for the analysis. The micro and macroscopic complexity of wood and its anisotropic nature give different fracture properties in the longitudinal, radial and tangential grain directions. This complexity and the infrequent use of LEFM mean there is little data available. While wood is highly anisotropic, fracture analysis can use a subset of the possible material properties because wood normally cracks parallel to its grain due to its low tensile strength perpendicular to grain. This allows a significant reduction in the number of tests required to measure fracture properties, with considerable saving of resources. This paper presents the results of an experimental study investigating the fracture energy and fracture toughness of Radiata Pine laminated veneer lumber in mode I (opening). A more efficient test apparatus is proposed and shown to produce identical results to the test apparatus used by others. Results are presented for the fracture toughness properties in the grain direction, and include fifth percentiles and coefficients of variation. The influence that the specimen size has on the fracture toughness is also presented. Numerical analyses using the ABAQUS software package show good agreement with the experimental test results. The experimental results are within the range of experimental values reported in the literature for solid wood.

Keywords Fracture toughness _ Fracture energy _ Laminated veneer lumber _ LVL _ Moisture content _ Size effect _ Timber _ Wood _ LEFM _ Numerical analyses

M. Ardalany (&) _ B. Deam
Department of Civil and Natural Resources Engineering, University of Canterbury, Christchurch, New Zealand
e-mail: manoochehr.ardalany@pg.canterbury.ac.nz
B. Deam
e-mail: Bruce.deam@canterbury.ac.nz
M. Fragiacomo
Department of Architecture, Design and Urban Planning, University of Sassari, Sassari, Italy
e-mail: fragiacomo@uniss.it

Appendix 2

Tension perpendicular to grain strength of LVL, Sawn timber and cross-banded LVL is the subject of this appendix. Experimental tests on the materials are included for further reference.

Tension Perpendicular to Grain Strength of Wood, Laminated Veneer Lumber (LVL), and Cross-Banded LVL (LVL-C)

M. Ardalany
PhD candidate, Department of Civil and Natural Resources Engineering, University of Canterbury, Christchurch, New Zealand, Email: mar149@canterbury.ac.n

B. Deam
Senior Lecturer, Department of Civil and Natural Resources Engineering, University of Canterbury, Christchurch, New Zealand, Email: Bruce.deam@canterbury.ac.nz

M. Fragiacomo
Associate Professor, Department of Architecture, Design and Urban Planning, University of Sassari, Italy, Email: fragiacomo@uniss.it

K.I. Crews
Professor of Structural Engineering, Centre for Built Infrastructure Research, University of Technology, Sydney, Australia, Email: keith.crews@uts.edu.au

ABSTRACT: Recent experimental tests carried out on structural timber members have highlighted the importance of tension perpendicular to grain strength, particularly in beams with holes and notches, in connection regions, in curved beams, and in post-tensioned timber frames. Innovative engineered wood products such as Cross Banded Laminated Veneer Lumber (LVL-C) have been introduced into the market specifically to improve the perpendicular to grain properties of normal Laminated Veneer Lumber (LVL).

This paper reports the results for a series of perpendicular to grain tension tests that were performed at the University of Canterbury using specimens of sawn timber Radiata Pine, LVL and LVL-C. The perpendicular to grain tension strengths of LVL were generally lower than those for sawn timber, but the LVL-C showed a significantly improved perpendicular to grain tensile strength. The paper also compares the experimental results with strengths predicted using both coupled elastic Finite Element Method (FEM) and Linear Elastic Fracture Mechanics (LEFM) models. These models were found to predict the average strength with reasonable accuracy.

KEYWORDS:Timber, Wood, LVL, LVL-C, perpendicular to grain, FEM, LEFM, strength.

1 INTRODUCTION

Wood as an orthotropic material has different material properties in different directions. The best material properties of wood are those stressing the material in the grain direction while the perpendicular properties are remarkable weaker. The low perpendicular to grain strength and stiffness of wood provides the potential for failure if not properly accounted for in design.

The low tensile strength of wood in perpendicular to grain direction may be reduced even further by introducing holes, notches and other stress concentrators, which cause a significant increase in tension stresses perpendicular to grain.

Many procedures in the design of wood members avoid high stresses in perpendicular to grain direction, however, sometimes it becomes inevitable. Two methods of mitigating this deficiency in wood products are reinforcing locally using screws and rotating some of the laminates so they are perpendicular to their original direction (e.g. like plywood).

Engineered wood products such as Laminated Veneer Lumber (LVL) and Cross Banded Laminated Veneer Lumber (LVL-C) have been introduced into market to improve consistency and other material properties of sawn timber. LVL is made of nominally 3 mm thick Radiata pine veneers that are glued and pressed together. The 3 mm veneer thickness was chosen to avoid crack propagation from one veneer to adjacent veneers(Dean et al. 1982). In LVL all of the veneers are aligned in one direction while in LVL-C a small portion of the longitudinal veneers are perpendicular to the others to improve the tension perpendicular to grain strength. The production is similar to plywood except normally only two of the laminates are rotated (the third laminate from each surface to maintain symmetry) to improve the perpendicular properties, without reducing the parallel to grain strength and stiffness too significantly.

2 EXPERIMENTS

An experimental program was developed to provide a qualitative comparison of the perpendicular to grain strength of the Radiata pine used for construction in New Zealand. The experiments evaluated the approximate strength and its coefficient of variation (COV) for sawn timber, LVL and LVL-C. A total of 117 samples were tested. Important sample properties are summarized in Table 1. The specimens were prepared according to ASTM D143-94 standard (ASTM D143-94 2000).

Table 1. Radiata pine specimens.

Material (Radiata pine)	Number	Thickness (mm)	Moisture content (%)	Number of veneers	
				Perp*	Para**
LVL	57	50	9.3	0	16
LVL-C	30	35	11.7	2	8
Sawn timber	30	50	11.0	-	-

* Perpendicular, ** Parallel

2.1 *Specimen preparation and testing*

The sawn timber was purchased from a local supplier with samples cut from randomly selected sticks. All of the LVL-C was cut from a single billet. A more extensive sampling strategy was employed for the LVL to provide better material statistics. Samples of LVL were selected from a single production run from one manufacturer and from different production runs from the other manufacturer.

The specimens were cut to size using an electric saw and drilled with a low speed drill to avoid forming additional cracks around the hole edges. The specimen shape and dimensions are shown in Figure 1. After cutting, the specimens were measured using a micrometer with accuracy of 0.01 mm. The moisture content of specimens was measured by oven drying randomly selected specimens after they had been tested. The moisture content was measured in accordance with ASTM D4442-92 (ASTM D4442-92 2000).

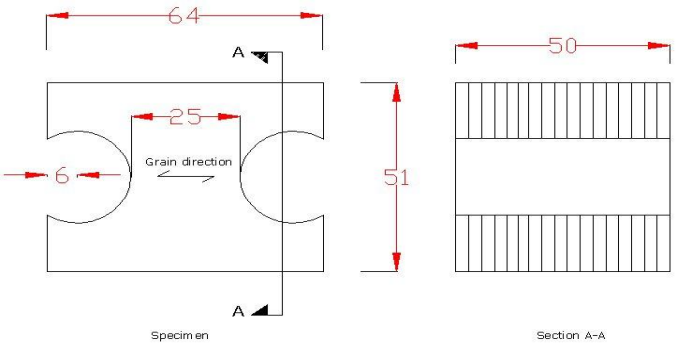

Figure 1. Geometry of specimens (dimensions in mm)

A universal testing machine was used for the testing. The specimens were inserted into steel jaws of the universal testing machine (see Figure 2), which were pulled apart at a rate of 2 mm/min. Universal joints were provided above and below the jaws, and load was measured using a 10kN load cell calibrated to class 1 of BS1610[4]. The force measurements were acquired at 10 Hz during the test.

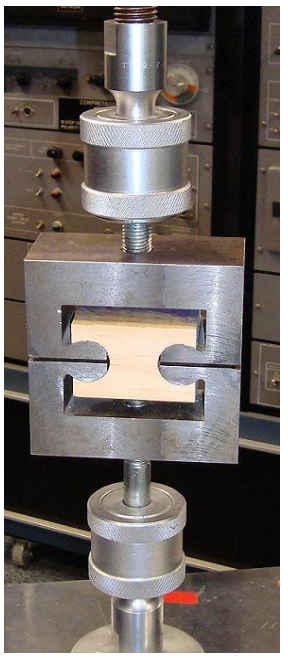

Figure 2. Set-up of experiments

2.2 *Experimental observations*

The crack surfaces within the sawn timber specimens mostly followed the growth rings, with occasional steps through the rings. The fracture surfaces were smooth in comparison to those for LVL where they were very jagged as the cracks propagated between laminates.

A range of fracture mechanisms were observed. The crack surface profiles are summarized in Figure 3. The sawn timber was vey brittle when it fractured whereas the LVL was less brittle.

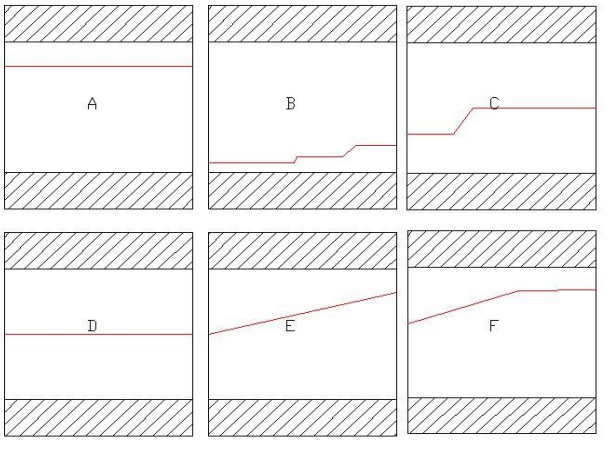

Figure 3. Crack surface profiles for sawn timber (section A-A of Figure 1)

Figure 4. Glue shearing separation (up) and normal LVL fracture (Bottom)

Cracks developed in the middle of the LVL specimens and propagated in reasonably straight lines except some cases where the LVL crack approached a knot in one veneer. Knots and other defects appeared to slightly increase the tension perpendicular to grain strength.

The specimens of LVL tended to start crack initiation and propagation from one edge to other edge. The crack surfaces within LVL-C were relatively similar to those in LVL except the veneers loaded parallel to grain either fractured (3 specimens) or remained intact but separated from their adjacent laminates (X specimens) as shown in Figure 4, with as many specimens shearing along the glue line as along the grain).

There were no fractures of the type shown in Figure 5 and reported by Hummer et al. (Hummer et al. 2006), where the top right portion of the specimen broke off due to a form of flexural cracking. This could be due to the higher shear and tensile strengths of the New Zealand pine used to manufacture the LVL.

Figure 5 Failure of specimens in upper right part (Hummer et al. 2006)

2.3 *Tensile strengths*

The calculation of the tension strength of the material was performed by dividing the load by the measured surface area of the fracture before testing. Table 2 summarizes the results of the strength calculations for three sets of experiments. The results of the experiments show higher strength values for sawn timber in comparison to LVL. This could be due to either twisting of the fibers in the sawn timber or micro-cracking of the LVL veneers during the production process. This is in good match with the (Hummer et al. 2006).

Table 2 also shows that like all other material strength properties, the COV of LVL is lower than it is for the original material. However, it is not as significantly lower as the typical modulus of elasticity and modulus of rupture for LVL.

A comparison between LVL and Glulam, which has strength about 3MPa (Gustafsson 1993), shows better properties for Glulam but when LVL-C is used the situation changes markedly due to the rotated veneers, with the strength of the material increasing about 2.5 times than Glulam. This will make LVL-C a very good option for the cases where there are hole and notches in the member.

Table 2. Calculated tensile strength of the material

Specimen	Selecting process	Average tensile strength (MPa)	Minimum tensile strength (MPa)	Coefficient of variation (%)	5^{th} percentile of the values (MPa)
LVL	Random	2.021	1.152	18	1.434
LVL-C	Cut from 1 billet	7.540	5.827	10	6.495
Sawn timber	Random	3.887	2.662	23	3.018

3 PREDICTING TENSILE FAILURE LOAD

The Finite Element Method (FEM), Linear Elastic Fracture Mechanics (LEFM), and the initial crack method were all used to predict the tension perpendicular to grain strength of LVL specimens.

The procedure for modeling and predicting the failure load is summarized as:

1. Finite element modeling of the specimens using shell elements to estimate the most likely location of crack initiation and propagation.

2. Cracks were introduced into model using 'seam' elements; where the seam is a crack that opens when loaded.

3. The length of the crack was calculated using the initial crack method (Gustafsson 1993)

4. The crack tip was modeled using special elements (Ardalany et al. 2010)

5. The stress intensity factors were calculated using ABAQUS software (Habbitt et al. 2007)

6. The failure load was calculated using Wu's mixed mode fracture criterion (Wu 1967; Wu 1968).

The LVL specimens in the ABAQUS software package were modeled using 50 mm thick planner shell elements. LVL was assumed to be elastic orthotropic with material properties given in Table 3 (Ardalany et al. 2010).

Table 3: Material properties of LVL

E_x (MPa)	E_y(MPa)	G_{xy}(MPa)	ϑ_{xy}
12000	600	1000	0.3

E_x and E_y are the elastic moduli parallel and perpendicular to grain, respectively, G_{xy} is the shear strength, and ϑ_{xy} signifies the Poisson's ratio.
The element mesh was created with emphasis on minimizing both the mesh distortion and transition. Quad elements (S8R) were used for the meshing. The resulting mesh and the principal stress contours are displayed in Figure 6. The 1kN uniformly distributed load was applied over the middle upper curved edges of the model and lower curved edges were also used for the supports.

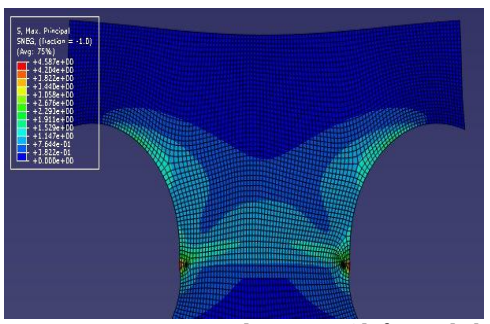

Figure 6. Maximum Principal stresses (deformed shape)

As expected, Figure 6 shows the greatest stress intensities at the specimen centerline. However, there are also significant stresses closer to the jaw contact positions which accounts for secondary fracture illustrated in Figure 6.

For step 2, modeling the fracture, seam elements were introduced into the high stressed area to model the crack opening as the seam elements are separated. Very fine meshing was used at the crack tip. The tip itself was modeled with a ring of triangular elements type S8R5, which are 8-node doubly curved thin shells with reduced integration, and five degrees of freedom per node. The rest of the model was meshed with the S8R 8-node doubly curved thick shells, also with reduced integration. The option to minimize mesh transition was selected to avoid extra mesh deformation.

In order to improve accuracy of the calculations, the middle node closest to the crack tip was moved to the half length to create singularity of $1/\sqrt{r}$ (Ardalany et al. 2010), where $\sqrt{r}$ is the distance from crack tip (see Figure 7).

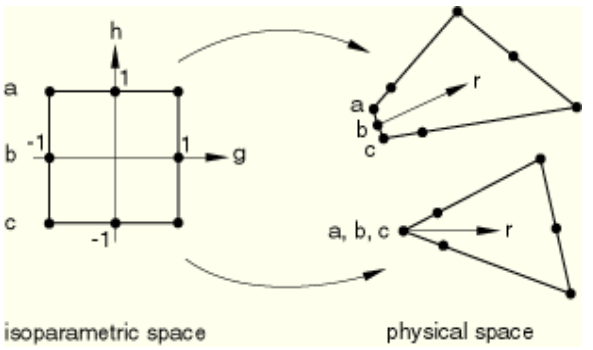

Figure 7:Meshing for modeling of singularity (Habbitt et al. 2007)

The elastic model was then analyzed and the stress intensity factors in mode I and II calculated.

The crack length was calculated using the initial crack approach. In this method, a crack with finite length is introduced into the model. The length is calculated using the formulas recommended by Gustafsson (Gustafsson 1993).

$$2x_0 = \frac{2}{\pi}\frac{E_I G_{Ic}}{{f_t}^2}\frac{E_x}{E_y}\left(\frac{G_{IIc}}{G_{Ic}}\right)^2\frac{1}{4k^4}\left\{\sqrt{1+4k^2\sqrt{\frac{E_y}{E_x}}\frac{G_{Ic}}{G_{IIc}}} - 1\right\}^2\left\{1+\frac{k^2}{\left(\frac{f_v}{f_t}\right)^2}\right\} \quad (1)$$

$$\frac{1}{E_I} = \frac{1}{E_x}\sqrt{\frac{E_x}{2E_y}\sqrt{\sqrt{\frac{E_x}{E_y}}+\frac{E_x}{2G_{xy}}-\vartheta_{yx}\frac{E_x}{E_y}}} \quad (2)$$

$$\frac{1}{E_{II}} = \frac{1}{E_x}\sqrt{\frac{1}{2}\sqrt{\sqrt{\frac{E_x}{E_y}}+\frac{E_x}{2G_{xy}}-\vartheta_{yx}\frac{E_x}{E_y}}} \quad (3)$$

In this formulation, x_0 is the crack length which is twice the crack length obtained using the mean stress criterion method, x_0 is the shear strength of the material in the crack plane, f_t is the tensile strength of the LVL experimentally obtained, G_{Ic} and G_{IIc} are the critical energy release rate values in mode I and II respectively, k is the mixed mode ratio defined as K_{II}/K_I and finally E_I and E_{II} are the equivalent modulus of elasticity for orthotropic materials calculated from above formulas. The stress intensity factors can be obtained from the energy release rate values using the following equations:

$$K_I = \sqrt{E_I G_I} \tag{4}$$

$$K_{II} = \sqrt{E_{II} G_{II}} \tag{5}$$

For pure mode I ($k \to 0$) the crack length formulation can be simplified as follows:

$$2x_0 = \frac{2}{\pi} \frac{E_I G_{Ic}}{f_t^2} \tag{6}$$

Similarly, for pure mode II ($k \to \infty$) can be simplifies to:

$$2x_0 = \frac{2}{\pi} \frac{E_{II} G_{IIc}}{f_v^2} \tag{7}$$

For the experimentally measured mode I of fracture $K_{Ic} = 0.354\ \mathrm{MPa}\sqrt{\mathrm{m}}$ (Ardalany et al. 2010; Ardalany et al. 2010) and the tensile strength calculated from current experiments, the crack length was estimated to be 9.4mm.
By introducing the crack length in the model and obtaining the stress intensities at the crack tip, the failure load can be calculated using the Wu's mixed mode fracture criterion (Ballerini & Rezzi 2001; Ballerini & Rizzi 2007).

$$\frac{K_I}{K_{IC}} + \left(\frac{K_{II}}{K_{IIc}}\right)^2 = 1 \tag{8}$$

In the above formulation K_{IC} and K_{IIC} are the fracture toughness of LVL in mode I and II, respectively. For pure mode I and mode II the equation (8) becomes:

$$K_I = K_{Ic} \tag{9}$$

$$K_{II} = K_{IIc} \tag{10}$$

Figure 8 shows the deformed model with the cracks. Around the crack, a half circle partition was considered to avoid using of very fine elements for other parts of the specimen and speeding up the analysis.

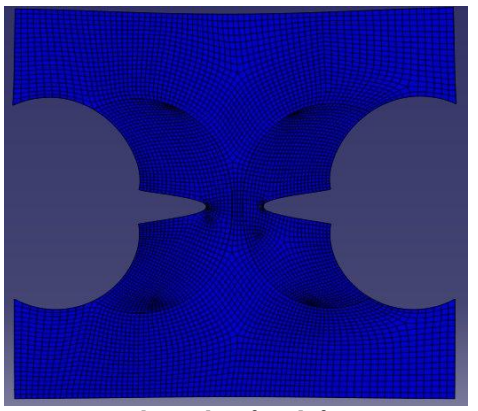

Figure 8: Specimen with cracks after deformation

ABAQUS calculations of stress intensity factors make use of the contour integrals. The software automatically detects the mesh around the crack tip and calculates the stress intensities from the deformations with the adjoining elements using the displacement extrapolation method(Ballerini & Rezzi 2001). However, additionally layers of elements are used to calculate the stress intensity factors.

ABAQUS calculates the stress intensities factors from the deformations of rings of elements using an appropriate formulation, based on displacements, the so-called displacement extrapolation technique(Chen & Kuang 1992; Guinea et al. 2000). However, other energy based methods can be used to calculate the energy required to close the crack.

The calculated stress intensity factors using the first five contour integrals are presented in Table 4. As expected, mode II had little influence on the results because opening is the dominating mode of deformation.

Table 4. Calculated stress intensity factor × (10^{-3})

Contour	1	2	3	4	5
Mode I	5.630	5.696	5.605	5.572	5.614
Mode II	0.4590	0.3597	0.3645	0.4622	0.4739

The calculated failure loads using different contour integrals are shown in Table 5.

Table 5. Predicted failure load for LVL using different contours

Contours	1	2	3	4	5
Load (kN)	2.66	2.63	2.68	2.69	2.67

The first few contour integrals are usually ignored because they are very close to the crack tip and may give quite unrealistic values (Habbitt et al. 2007). The third contours predicted load is 2.68kN which was quite close to the average experimental load for the LVL which was 2.53kN.

4 DISCUSSION

The tension perpendicular to grain strength of LVL, LVL-C and Sawn timber radiata pine was measured

experimentally and predicted using coupled numerical analysis.

Experiments showed better tension perpendicular to grain strength for sawn timber than LVL, however LVL-C exhibited significantly higher tensile strength perpendicular to grain.

The low tension perpendicular to grain makes LVL susceptible to crack initiation and propagation around holes, notches, splits and joints. Special care should therefore be given to the design of these members. A good solution could be to use LVL-C when there are notches and other stress concentrators. The rotated grain of the LVL-C, in fact, significantly increases the strength of the material in the perpendicular to the grain direction.

Numerical analyses were found to be in good agreement with the experiments. The initial crack method appears to provide the best approach for estimating the crack length for calculation of stress intensities used in fracture mechanics to predict the failure load.

5 ACKNOWLEDGMENTS

The Authors would like to extend their gratitude to the Department of Civil and Natural Resources Engineering of University of Canterbury, New Zealand, for providing the PhD scholarship to support the first author; Warwick Banks and Andrew Vanhoutte for providing material; Dr. David Carradine for the useful comments; and the technical support of laboratory technicians from the University of Canterbury, especially Alan Poynter.

6 REFERENCES

Ardalany, M., Deam, B. & Fragiacomo, M. (2010). Numerical investigation of the load carrying capacity of laminated veneer lumber joists with holes. World Conference WCTE2010. Trentino, Italy

Ardalany, M., Deam, B., Fragiacomo, M. & Crews, K. (2010). "Experimental results of fracture toughness evaluation of radiata pine laminated veneer lumber (LVL) in mode II (shearing)." Journal of Structural Engineering (unpubl.).

Ardalany, M., Deam, B., Fragiacomo, M. & Crews, K. (2010). "Experimental results of fracture energy and fracture toughness evaluation of radiata pine laminated veneer lumber (LVL) in mode I (opening)." Journal of materials and structures RILEM (TO BE PUBLISHED).

ASTM D143-94 (2000). Standard test method for small clear specimens of timber West Conshohocken, ASTM International.

ASTM D4442-92 (2000). Standard test methods for direct moisture content measurement of wood and wood-based materials. West Conshohocken, ASTM International.

Ballerini, M. & Rezzi, R. (2001). Numerical LEFM analyses for the evaluation of failure loads of beams loaded perpendicular to grain by single dowel connections. CIB-W18 conference. Venice, Italy: Paper 34-7-2.

Ballerini, M. & Rizzi, M. (2007). "Numerical LEFM analyses for the prediction of the splitting strength of beams loaded perpendicular-to-grain by dowel-type connections." Journal of Materials and Structures 40(1): 139-149.

Chen, L. S. & Kuang, J. H. (1992). "A displacement extrapolation method for determining the stress intensity factors along flaw border." International Journal of Fracture 57(4): R51-R58.

Dean, J., Gibson, J. A. & Moss, P. J. (1982). The fracture properties of timber. Timber Engineering. University of Canterbury, Christchurch, New Zealand: 97-115.

Guinea, G. V., Planas, J. & Elices, M. (2000). "KI evaluation by the displacement extrapolation technique." Journal of Engineering fracture mechanics 66(3): 243-255.

Gustafsson, P. (1993). Fracture Mechanics Models for Strength Analysis of Timber Beams with a Hole or a Notch - A Report of RILEM TC-133 : Mean stress approach and initial crack approach (paper in report). Sweden, Lund University. Report TVSM-7134 1-15.

Habbitt, Karlsson & Sorensen (2007). ABAQUS, Theory Manual, Version 6.7-1, ABAQUS Inc.

Habbitt, Karlsson & Sorensen (2007). ABAQUS, User Manual, Version 6.7, ABAQUS Inc.

Hummer, T., Dolan, D. & Wolcott, M. (2006). Tension perpendicular to grain of wood, Lamianted Veneer Lumber, and a Wood Plastic Composite. 9th world conference on timber engineering (WCTE2006). Portland.

Wu, E. M. (1967). "Application of fracture mechanics to anisotropic plates." Journal of Applied Mechanics 34(4): 967-&.

Wu, E. M. (1968). "Application of fracture mechanics to anisotropic plates." Journal of Mechanical Engineering 90(4): 134-&.

Appendix 3

The classical approach in analyzing cracks can be referred to as the stress intensity factor approach and is based on the solution of the Airy stress function that can be expressed in terms of two analytical functions of a complex variable.

Crack tip stress field

The appendix is adopted from Schoenmakers (2010). The classical approach in analyzing cracks can be referred to as the stress intensity factor approach and is based on the Airy stress function, which can be expressed in terms of two analytical functions of a complex variable.

In the absence of body forces in studying the case of a two-dimensional elastic body, the equilibrium equations are (see Figure 1):

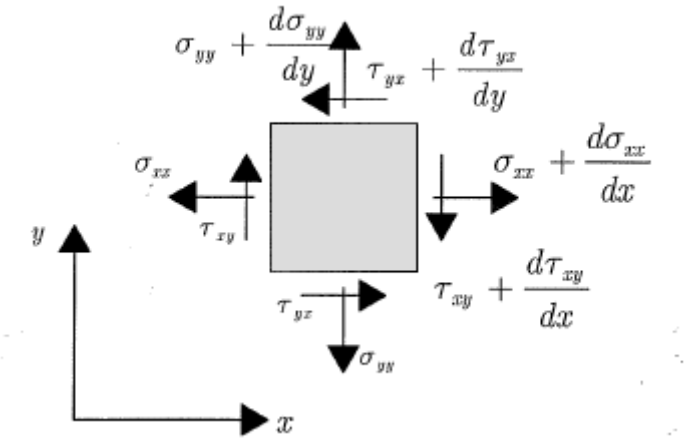

Figure 1 Stress components acting on an elastic plane body

$$\frac{\partial \sigma_{xx}}{\partial x} + \frac{\partial \tau_{xy}}{\partial y} = 0 \qquad \frac{\partial \tau_{xy}}{\partial x} + \frac{\partial \sigma_{yy}}{\partial y} = 0 \qquad (1)$$

with $\tau_{xy} = \tau_{yx}$

The compatibility equilibrium equation representing the strain-displacement relationship is given by Equation (2):

$$\frac{\partial^2 \varepsilon_{xx}}{\partial y^2} + \frac{\partial^2 \varepsilon_{yy}}{\partial x^2} + \frac{\partial^2 \gamma_{xy}}{\partial x \partial y} = 0 \qquad (2)$$

In satisfying both equilibrium and compatibility equations exactly, an Airy stress function Ω can be introduced of which the second order derivatives represent the stresses. Under assumption that the Cartesian and orthotropic material coordinate systems coincide, it follows $\sigma_{11} = \frac{\partial^2 \Omega}{\partial y^2}$, $\sigma_{22} = \frac{\partial^2 \Omega}{\partial x^2}$ and $\sigma_{12} = \frac{\partial^2 \Omega}{\partial x \, \partial y}$. The governing equation can be given as Equation (3).

$$c_{22} \frac{\partial^4 \Omega}{\partial x^4} + (2c_{12} + c_{66}) \frac{\partial^4 \Omega}{\partial x^2 \partial y^2} + c_{11} \frac{\partial^4 \Omega}{\partial y^4} = 0 \qquad (3)$$

In this equation c_{ij} are components of the orthotropic compliance matrix$[C]$. Integration of this partial differential equation yields:

$$\left(\mu_1 \frac{\partial}{\partial x} - \frac{\partial}{\partial y}\right)\left(\mu_2 \frac{\partial}{\partial x} - \frac{\partial}{\partial y}\right)\left(\mu_3 \frac{\partial}{\partial x} - \frac{\partial}{\partial y}\right)\left(\mu_4 \frac{\partial}{\partial x} - \frac{\partial}{\partial y}\right)\Omega = 0 \qquad (4)$$

The parameter μ_i $(i = 1,2,3)$ are the roots of the characteristic auxiliary equation resulting from Equation (4).

$$c_{11}\mu^4 + (2c_{12} + c_{66})\mu^2 + c_{22} = 0 \qquad (5)$$

The roots of this equation, being either complex or purely imaginary, occur in conjugate pairs and are found to be:

$$\mu_{1,2} = \sqrt{\frac{-(c_{66} + 2c_{12}) \pm \sqrt{(c_{66} + 2c_{12})^2 - 4c_{11}c_{22}}}{2c_{11}}} \tag{6}$$

The solution of the equation (4) in terms of Ω allows expressing the stress field in the crack tip vicinity expressed by Sih et al. (1965) and is obtained by determining two complex functions satisfying the boundary conditions and by transformation of the global Cartesian coordinate system to polar coordinate system.

$$\begin{aligned}
\sigma_{11} &= \frac{K_I}{\sqrt{2\pi r}} \Re \left[\frac{\mu_1 \mu_2}{\mu_1 - \mu_2} \left(\frac{\mu_2}{\sqrt{cos\theta + \mu_2 sin\theta}} - \frac{\mu_1}{\sqrt{cos\theta + \mu_1 sin\theta}} \right) \right] \\
&\quad + \frac{K_{II}}{\sqrt{2\pi r}} \Re \left[\frac{1}{\mu_1 - \mu_2} \left(\frac{{\mu_2}^2}{\sqrt{cos\theta + \mu_2 sin\theta}} - \frac{{\mu_1}^2}{\sqrt{cos\theta + \mu_1 sin\theta}} \right) \right] \\
\sigma_{22} &= \frac{K_I}{\sqrt{2\pi r}} \Re \left[\frac{1}{\mu_1 - \mu_2} \left(\frac{\mu_1}{\sqrt{cos\theta + \mu_2 sin\theta}} - \frac{\mu_2}{\sqrt{cos\theta + \mu_1 sin\theta}} \right) \right] \\
&\quad + \frac{K_{II}}{\sqrt{2\pi r}} \Re \left[\frac{1}{\mu_1 - \mu_2} \left(\frac{1}{\sqrt{cos\theta + \mu_2 sin\theta}} - \frac{1}{\sqrt{cos\theta + \mu_1 sin\theta}} \right) \right] \\
\sigma_{12} &= \frac{K_I}{\sqrt{2\pi r}} \Re \left[\frac{\mu_1 \mu_2}{\mu_1 - \mu_2} \left(\frac{1}{\sqrt{cos\theta + \mu_1 sin\theta}} - \frac{1}{\sqrt{cos\theta + \mu_2 sin\theta}} \right) \right] \\
&\quad + \frac{K_{II}}{\sqrt{2\pi r}} \Re \left[\frac{1}{\mu_1 - \mu_2} \left(\frac{\mu_1}{\sqrt{cos\theta + \mu_1 sin\theta}} - \frac{\mu_2}{\sqrt{cos\theta + \mu_2 sin\theta}} \right) \right]
\end{aligned} \tag{7}$$

In these expressions r denotes the radial distance from the crack tip to the material point of interest, θ the inclination angle with the future crack path and $\Re$ denotes the real part of a function. The parameters K_i $(i = I, II)$ are the stress intensity factors corresponding to mode I and II, respectively.

In addition, analytical expressions of displacements fields in the crack tip vicinity can be derived and determined. The difference between the isotropic and orthotropic solution of the Airy stress function and its resulting Equation (5) lies in the roots μ_i $(i = 1,2,3,4)$. In the

isotropic case the equilibrium and compatibility equations yield the bi-harmonic equation $\nabla^2(\nabla^2\Omega)$ with roots $\mu_1 = \mu_2 = i$, indicating that equation (7) is only valid in the case of most orthotropic materials.

The stress components thus can be expressed in a more general format shown by Equation (8), with $f_{ij}(\theta)$ functions dependent upon the angle θ and elastic constants.

$$\sigma_{ij} = \frac{K_i}{\sqrt{2\pi r}} f_{ij}(\theta) \tag{8}$$

References

Schoenmakers D (2010) Fracture and failure mechanisms in timber loaded perpendicular to grain by mechanical connections. University of Eindhoven, Netherlands

Sih GC, Paris PC, Irwin GR (1965) On cracks in rectilinearly anisotropic bodies. International Journal of Fracture 1 (3):189-203. doi:10.1007/bf00186854